Tearing of rubber

Kartpan Sakulkaew

**A thesis submitted to the University of London
for the degree of Doctor of Philosophy**

**Department of Materials
Queen Mary, University of London**

October 2012

Abstract

There have been several studies on the tearing of rubber materials since the seminal paper on rupture of rubber was published by Rivlin and Thomas (1953).The behaviour is typically characterised using a fracture mechanics approach whereby the rubber has a geometrically independent relationship between crack growth rate during tearing versus strain energy release rate. This approach works well under conditions of steady tearing as the crack growth rate is easy to measure. However, this approach is much harder to interpret under the condition where the rubber exhibits discontinuous crack growth behaviour such as knotty tearing or stick slip tearing.

Unfortunately, these are common tearing conditions observed in practice for filled rubbers as well as for some unfilled rubbers, especially those such as natural rubber that are capable of strain-induced crystallisation. Under these conditions it is not clear what the actual crack growth rate is as the value typically given results from the average of a very rapid tearing rate and a zero velocity tearing rate.

The aim of this work is to develop a new approach to characterise the unsteady tearing behaviour of rubber in terms of the relationship between the rate of increase in the strain energy at the crack tip just immediately prior to the onset of the tearing which is quantified directly as the time derivative of the strain energy release rate $\dot{T}$, and the critical strain energy release rate T^* required to propagate the crack. The approach adopted in this study is then evaluated using a range of different crystallising and non-crystallising rubbers as well as crystallising rubbers that have been modified to alter their crystallisation over a range of different test temperatures. Additionally, a new elastic-viscous transition diagram in association with the rate of change in the strain energy release rate at the tip of the crack is presented.

Declaration

I hereby declare that the work carried out and presented in this thesis submitted for the degree of Doctor of Philosophy is original and my own. Any literature or figures not emerged from this original piece of work are referenced as such.

Kartpan Sakulkaew

Acknowledgements

I would like to express my sincere gratitude to my supervisor Dr. James Busfield for his continual guidance, tremendous help, and encouragement throughout this work.

I also would like to thank Prof. Alan Thomas for his guidance and a valuable source of ideas. I wish to thank Prof. Yoshihide Fukahori for valuable discussion and help in some aspects of this work.

I also wish to express my gratitude to my colleagues in the QMUL Rubber Research Group, both former and current, for all the support and encouragement, especially, Dr. Philip Gabriel; Dr. Nutthanun Suphadon; Dr. David Lowe, Thomas Baumard, and Lewis Tunnicliffe.

I would like to thank Bill Godwind (now at University of Manchester), Vince Ford, Danny Neighbour, and all technical staffs for technical supports.

I also wish to thank TARRC for the rubber materials and EPSRC Engineering Instrument Pool for the loan of a high speed video camera and an IR thermal imaging camera for the experiment.

Financial support from the Royal Thai Government is gratefully acknowledged.

Finally, I express my deep thankfulness to my family for emotional support and encouragement throughout this study.

Table of contents

Abbreviations

ACM	polyacrylate rubber
AEM	ethylene-acrylic rubber
ASTM	American Society for Testing Material
AU	polyester urethane
BR	butadiene rubber
CBS	N-Cyclohexyl-2-benzothiazole sulfenamide
CR	chloroprene rubber
CSM	chlorosulphonated polyethylene rubber
CV	constant viscosity (rubber)
DMA	dynamic mechanical analysis
DPG	diphenyl guanidine
ECO	epichlorohydrin rubber
ENR	epoxidised natural rubber
EPDM	ethylene-propylene-diene rubber
EPM	ethylene-propylene rubber
EU	polyether urethane
FPM	fluorocarbon rubber
FFKM	perfluorocarbon rubber
FMQ	fluorosilicone rubber
HAF	high Abrasive Furnace (carbon black)
HNBR	hydrogenated nitrile rubber
IIR	isobutene-isoprene rubber
IR	isoprene rubber (synthetic)
ISO	Organization for Standardization
NBR	acrylonitrile-butadiene rubber
NR	natural rubber
OENR	oil-extended natural rubber
phr	parts by weight per hundred parts of rubber
6PPD	N-(1,3-Dimethylbutyl)-N'-phenyl-p-phenylenediamine
RSS	ribbed smoked sheet (rubber)
SBR	styrene-butadiene rubber
TARRC	Tan Abdul Razak Research Rubber
TSR	technically specified rubber

VMQ	vinyl-methyl silicone rubber
YBPO	thermoplastic polyether-esters

Symbols

a	arbitrary constant
A	area of one fracture surface of the crack
A_c	total area of the mould cavities
A_0	cross-sectional area of the specimen in the undeformed state
A_p	area of press piston head
ΔA	Helmholtz free energy
b	number per unit volume of single carbon-carbon bonds
c	crack length
C_1,C_2	material constant
d	tip diameter in unstrained state
d_0	minimum diameter of the crack tip
e_b	elongation at break
E	elastic modulus
E_b	strain energy at break
E_0	minimum elastic strain energy
E_t	elastic strain energy at the tip of the crack
F	force
F_b	force at break
F_E	elastic force in energetic term
F_{fric}	frictional force
F_{static}	static frictional force
F_S	elastic force in entropic term
F_t	tangential force
G	shear modulus
h	specimen thickness
I	strain invariant
J_b	elastic strain energy of each single bond
k	elastic constant
k_B	Boltzmann constant
k_s	slowly varying function of strain
l	overall length
l_{or}	original distance between the bench marks

L	distance between adjacent crosslinks in determination of threshold tearing energy
l_0	original distance between the bench marks
l_b	distance between the bench marks at the point of the specimen rupture
m_1	mass of rubber in air
m_2	mass of rubber determined by weighing in water
M_c	number average molar mass of the chain length between crosslinks
M_L	minimum torque
M_H	maximum torque
n	number of monomer unit
N	number of chain segment
N_A	Avogadro constant
P_m	moulding pressure
P_0	oil pressure
r	radius
r_c	crack growth rate
R	gas constant
s	second
S	entropy
S_c	crosshead speed of the test machine
t	time
T	tearing energy
T_c	critical tearing energy
T_g	glass transition temperature
T_0	threshold tearing energy
TS_b	tensile strength
t_s2	time till two torque unit rise above the minimum
t(90)	time required for the rubber compound to reach 90% of the total state of cure
T_1	tearing energy derived from the strain distribution at the crack tip
T_2	tearing energy derived from the overall force
U	internal energy
v_c	crack tip velocity
V	volume
w	specimen width
w_n	specimen width (tensile test)

W	total elastic strain energy
W_f	weight of the filler in the specimen
W_r	weight of dry rubber
W_s	weight of solvent absorbed by the rubber specimen
β	parameter pertaining to the characteristic of a particular chain
δ	phase angle
ε_0	overall state of strain
θ	angular distance
λ	extension ratio
ξ	length of monomer unit
ρ	density
ρ_r	density of rubber compound
ρ_s	density of solvent
σ_{eng}	engineering tensile stress
σ_t	theoretical breaking stress
σ_{true}	true tensile stress
τ	temperature
Φ	loss function
Ω	number of chain conformation

List of figures

List of tables

Chapter 1: General introduction

Rubber is one of the most fascinating materials in regular use. It possesses a remarkable molecular architecture that renders it to be elastic, soft, and also to exhibit damping. These properties have made it useful in many engineering applications. Like other engineering materials, rubber components can fail in service under a critical applied stresses resulting in a catastrophic tear. The durability of rubber to resist the failure has been assessed in many ways. One of the most practical methods is to examine the tearing behaviour of rubber using fracture mechanics.

Tearing fracture in rubber is known to initiate from an inherent flaw present in the rubber (Gent 2005). When the rubber is stretched, the local stress in the vicinity of flaw is amplified. Once the local stress reaches a critical level, the rubber tears by the extension of the crack. It has been widely reported that the energy used to propagate the crack in a rubber is determined by a characteristic energy per unit area of the fracture surface created, often known as the tearing energy or the strain energy release rate (Rivlin and Thomas 1953; Tsunoda et al. 2000; Busfield et al. 2005; Papadopoulos et al. 2008). The relationship between the rate of tearing and the strain energy release rate is a material characteristic that is independent of test piece geometry (Greensmith and Thomas 1955; Thomas 1960). The relationship can therefore be characterised using any suitable test specimen.

The tearing behaviour of rubber can either assume steady tearing and unsteady or stick slip tearing. Steady tearing can easily be interpreted using the framework based on the rate of separation of the clamps as the tear rate hardly changes and the relationship between the strain energy release rate and the crack growth rate can be evaluated to characterise the behaviour (Greensmith and Thomas 1955). However, for a lot of rubber materials the behaviour can be stick slip in nature. Under these conditions the tearing is not steady and the characteristic rate of crack growth is much harder to determine as it fluctuates between a very rapid rate and a zero rate of crack growth. Measurements of the crosshead speed can not therefore be easily used to characterise the rate of crack growth, and the resulting average rate derived from the crosshead speed is not very meaningful. Thus, the aim of this

study is to introduce a novel approach, for the first time, based on a measure of the rate of change of the strain energy release rate which relates to the strain rate at the tip of the crack just prior to the crack extending.

Structure of this thesis

This thesis is separated into a number of distinct chapters. The three primary chapters, namely chapter 4, chapter 5, and chapter 6 are based around the author's journal papers.

Chapter 2 gives a literature review starting from a brief history of rubber and then basic rubber elasticity follows. Next, the general overview of the tearing fracture is introduced including the type of tearing typically found in rubber materials. Many factors affecting the tearing behaviour of rubber, for example, rate of tearing, temperature, crosslink systems, and strain crystallisation are also addressed. Finally, the different types of experimental techniques used by many investigators to study the rapid tearing of rubber are described and explained.

Chapter 3 presents the detailed experimental techniques used in this work including the detailed explanation of specimen preparation, material characterisation and equipment setup to carry out the test.

Chapter 4 shows the effect of the rate of strain on tearing in rubber which is characterised based on the relation between the critical strain energy release rate and the time derivative of the strain energy release rate using non-strain crystallising and strain crystallising rubber vulcanisates.

Chapter 5 extends work from Chapter 4 to examine the tearing behaviour of rubber, especially the strain crystallising rubbers, at elevated temperatures.

Chapter 6 proposes a new generalised concept of the tearing behaviour of rubber in terms of the elastic-viscous transition diagram. This diagram is generated primarily based on the data obtained from Chapter 4.

In chapter 7, the key findings in this thesis are summarised and the suggestions of the future work are described.

Chapter 2: Literature review

2.1 Rubber—General history

Everyone living today is familiar with rubber and its behaviour. Rubber can be regarded as one of the most indispensible materials available and it has a significant impact on our daily life. Rubber possesses the characteristic properties and holds an outstanding place in a wide range of applications ranging from the implant materials inside the human body to the sealing materials used in the international space station travelling in outer space. The word 'rubber' was coined by Joseph Priestly in 1770 when he noted that a half-inch cube of material available from an artist's material shop in London could erase the marks of a black lead pencil from paper (Loadman 2005).

The utilisation of rubber from nature dated as early as 1600 BC in the Mesoamerica era in Central America. The oldest archaeological rubber specimens are solid rubber balls excavated from the Manati site in Veracruz, Mexico. Several rubber artefacts recovered from other Mesoamerican sites include small nodules, small solid rubber balls, wooden tool handles wrapped in rubber, human figurines, human hands, a hollow human head, and a stone tool hafted with a rubber band. Early Mesoamerica rubber artefacts were made from latex collected from the *Castilla elastica* tree, native to the tropical lowlands of Mexico and Central America. Latex from *Castilla elastica* tree is too brittle to retain its shape when it is dried. Thus, Mesoamerica people improved the qualities of this latex by mixing it with juice from a morning glory vine (*Ipomoea alba*) which was believed to contain some chemicals that cured the rubber (Hosler et al. 1999). Nowadays nearly all commercial natural rubber is obtained from the latex of the *Hevea brasiliensis* tree commercially grown in a number of tropical countries including Thailand, Malaysia, and India. Smaller quantities are produced in Central and South America (Ownby 2002). The recovery of rubber artefacts from several archaeological sites in Central America suggests that the Mesoamerican communities had known about the basic techniques of manufacturing articles from rubber for at least three thousand years before the first Europeans saw natural rubber (Loadman 2005). In 1736 rubber was introduced to Europe by Charles Marie de la Condamine from The French Academy of Sciences

in Paris. He sent a package of rubber from Quito in Peru to France with a long report concerning many aspects of its origin and production. In his report to the Royal Academy of Sciences published in 1751, he described how the natives collected the latex from the rubber tree and how they used the hardened sediment to waterproof fabrics, shoes and elastic water bottles. By the end of the eighteenth century and the early nineteenth century, the rubber was utilised to produce a variety of articles. For example, in France in 1783, Jacques Alexander Cesar Charles launched the first hydrogen balloon (Figure 2.1) which was coated with a rubber solution in turpentine to render it impermeable to hydrogen and in 1823 Charles Macintosh invented waterproof cloth using rubber as a layer to bound two layers of fabric (Morawezt 2000). However, its utility was rather limited initially because of its propensity to be sticky when hot and brittle when cold. Thus behaviour was improved significantly though after the discovery of vulcanisation in 1839.

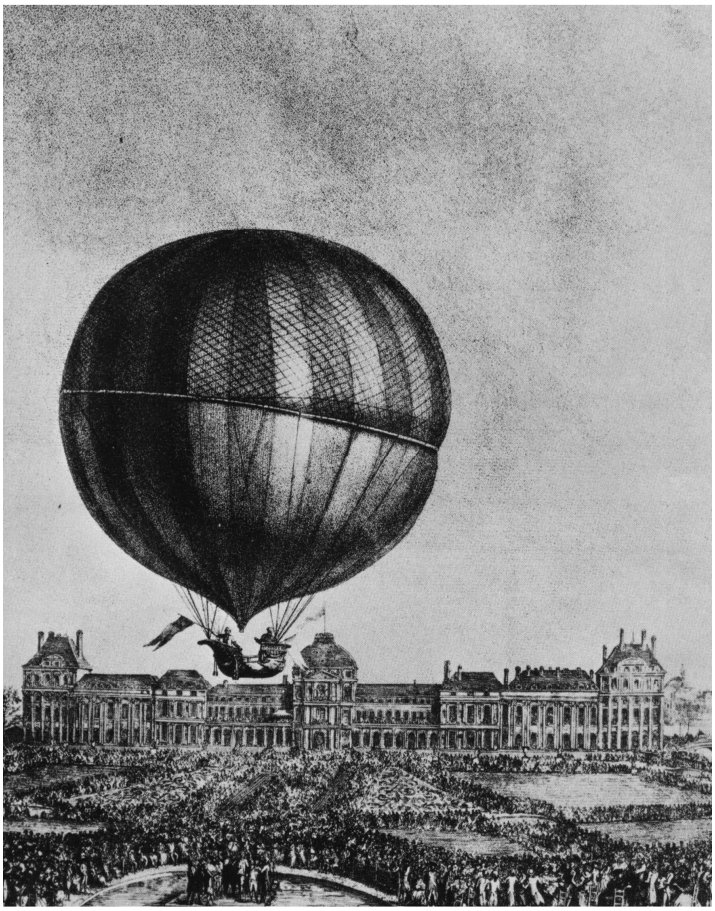

Figure 2.1: A hydrogen-filled balloon which was first launched by Jacques Alexander Cesar Charles[1].

[1] **Image source: http://www.centennialofflight.gov/essay/Dictionary/Charles/DI16G2_hi.JPG**

2.2 Types of rubber

Rubbers are a member of materials classification known as polymers which are characterised by long chain molecules of high molecular weight which are made up of many repeating units called monomers. Basically, there are three primary conditions that must be satisfied to exhibit rubber-like properties (Young and Lovell 2011):

1. The polymer must be above its glass transition temperature, T_g, at ambient temperature;
2. The polymer must not be highly crystalline;
3. The polymer should be lightly crosslinked.

Currently, a lot of rubbers are commercially available. They are typically identified by abbreviations of their chemical structures. Table 2.1 shows the designations given by ISO standard (ISO 1629) and a selection of the most common trade names (Nagdi 1993). In the thesis, the rubbers which are examined experimentally will be detailed next.

2.2.1 Natural rubber (NR)

Natural rubber is an agricultural product and is commonly obtained from the rubber tree called *Hevea Brasiliensis*. Alternatively, natural rubber can also be derived from other plants such as the guayule shrub (*Parthenium argentatum*), the Sapotaceae tree, and a few members of *Ficus* family, for example, *Ficus elastica*. However, none of these alternative plants have been extensively grown on a large scale for use in the rubber industry as yet (Halladay 2003).

The methods of manufacture of natural rubber commences with a collection of a milky sap (latex) extracted from a wound cut into the trunk of the tree. This sap consists of polyisoprene, water, and small amounts of other ingredients including proteins and carbohydrates from a rubber plant. The latex is then chemically coagulated with formic acid to form a processable coagulum. Natural rubber is commercially provided in a variety of different grades that are differentiated by their dirt content and their manufacturing processes (Subramaniam 1987, Mathew 2001).

Table 2.1: Standard abbreviations for commercially available rubbers based on ISO 1629.

Designation (ISO 1629)	Chemical name	Selected tradenames
BR	Butadiene rubber	Buna CB, Budene
CR	Chloroprene rubber	Neoprene, Bayprene
IIR	Isobutene-isoprene rubber (butyl rubber)	Exxon butyl
IR	Isoprene rubber, synthetic	Natsyn
NBR	Acrylonitrile-butadiene rubber (nitrile rubber)	Perbuna, Chemigum
HNBR	Hydrogenated nitrile rubber	Therban
NR	Isoprene rubber, natural	-
SBR	Styrene-butadiene rubber	Buna SE
ACM	Polyacrylate rubber	HyTemp
AEM	Ethylene-acrylic rubber	Vamac
CSM	Chlorosulphonated polyethylene rubber	Hypalon
EPDM	Ethylene-propylene-diene rubber	Keltan, Nordel, Dutral
EPM	Ethylene-propylene rubber	Keltan
FPM	Fluorocarbon rubber	Viton
FFKM	Perfluorocarbon rubber	Kalrez
VMQ	Vinyl-methyl silicone rubber	Siloprene
FMQ	Fluorosilicone rubber	Silastic
ECO	Epichlorohydrin rubber	Hydrin, Epichlomer
AU	Polyester urethane	Urepan, Pelletthane
EU	Polyether urethane	Adiprene
YBPO	Thermoplastic polyether-esters	Hytrel

There are two conventional grades of natural rubber. The first is ribbed smoked sheet (RSS). This grade of natural rubber has the characteristic crisscross rib patterns on the sheet. These patterns are introduced during the manufacturing process to increase the surface area and facilitate drying. Before being packaged into bales, the rubber sheets are dried in the smoke house at the temperature of about 40-60 °C for 4-6 days. There are 5 grades of sheet rubber which are designated as RSS 1 to RSS 5 based on the quality of appearance, namely colour

and transparency, presence of mould, blisters, dirt, etc. RSS 1 is the premium grade and RSS 5 has the worst quality. The second conventional grade is pale crepe which is a light-coloured premium grade of rubber from which the yellow pigments have chemically been removed or bleached. It is produced with intention to be used in products for which a light colour is preferred.

In order to ensure the consistency in quality of rubber to meet the consumer requirements and also to market the rubber in forms that are easier to process or handle, many grades of technically-specified rubbers (TSR) have been introduced. Typically, not graded by visual examination, TSR is classified according to the source of rubber (latex or field coagulum) and its properties.

Viscosity stabilized grades contain a small amount of chemical additives to inhibit an increase of viscosity during storage especially at relatively low humidity. Sekhar (1960) suggested that the storage hardening might be caused by the crosslinking reaction between the carbonyl groups and aldehyde-condensing agent within the rubber molecules. Burfield and Gan (1975) suggested that the change in the properties of NR during storage was resulted from the ring opening of epoxide groups by amino groups resulting in cumulative crosslinking. According to American Society for Testing and Materials (ASTM) D 2227, TSR CV (constant viscosity) can be divided into 3 grades in association with the Mooney viscosity which is obtained by measuring the torque that is required to rotate a disk embedded in rubber specimen: 5CV 50, 5CV 60, and 5CV 70.

TSR 5, TSR 10, and TSR 20 are produced from clean and fresh field coagulum. The designation of 5, 10 or 20 is primarily based on a percent dirt content allowed in each grade. TSR 5 is the lowest dirt content that is less than 0.05% being retained on 45 μm sieve.

Oil-extended natural rubber (OENR) is a type of natural rubber that is a physically modified form derived by incorporating aromatic or naphthenic processing oil. It is normally used in tyre treads as it provides good skid resistance on wet surfaces (Mathew 2001).

Epoxidised natural rubber (ENR) is a chemically modified form of natural rubber with improved resistance to hydrocarbon oils, low gas permeability, increased damping and good bonding properties. It is produced by epoxidising natural rubber latex by

reaction with formic acid and hydrogen peroxide (Gelling 1985). Two grades of ENR are commercially available, namely ENR 25 and ENR 50 with 25 mole% and 50 mole% of epoxide groups, respectively. Although its molecular structure has been chemically modified, ENR with peroxide groups up to 50 mole% is still capable of some strain-induced crystallisation (Davies et al. 1983).

2.2.2 Styrene-butadiene rubber (SBR)

SBR, which is the most widely used synthetic rubber, is a copolymer of butadiene and styrene. The regular grade contains about 23% styrene and the remainder is butadiene. An increase of styrene content leads to loss of resilience. In contrast to NR, the tensile strength of unfilled SBR is very poor. This is because of the absence of crystallisation on stretching the gum rubber. Consequently, this rubber does not develop high tensile strength without the aid of reinforcing fillers. SBR was manufactured during Second World War as a substitute for NR.

SBR is produced by the free-radical polymerisation as an emulsion in water, or anionically in solution (Hamed 2001). In emulsion polymerisation, the emulsifying agents are soaps and synthetic emulsifiers. The molecular weight of SBR is controlled by the use of mercaptan as a chain transfer agent. When the polymerisation is complete, coagulation of the emulsion is carried out with dilute sulfuric acid or aluminum sulfate. When the emulsion polymerisation is carried out at an elevated temperature, about 50°C, the rate of the polymerisation is high, and the polymer formed is highly branched. To overcome this, the polymerisation is carried out at low temperature, about 5°C, producing ‘cold’ emulsion SBR, with less branching which produces stronger vulcanisates. Solution SBR is produced by alkyl lithium-based catalyst systems. In comparison with emulsion polymers, the molecular weight distribution of anionically prepared SBR is narrow, and because the chain ends remain reactive after polymerisation, the molecules can be functionalized or coupled. For example, SBR macromolecules can be amine-terminated to provide the increased interaction with carbon black. Solution SBR is purer than emulsion SBR, because of the absence of emulsion residues.

2.2.3 Butadiene rubber (BR)

BR primarily consists of 1,3 butadiene monomer with a chemical double bond being an active site for polymerisation. It is mainly produced by a solution process using Ziegler-Natta catalysts or by anionic catalyst system. With Ziegler-Natta catalysts, the product contains a relatively high *cis* content more than 95% resulting in an ability to strain crystallise. BR which is anionically produced contains a mixture of *cis*, *trans*, and vinyl contents. High *cis* BR has a lower glass transition temperature than anionically based BR. Low vinyl BR are often blended with SBR and NR to produce tyre tread compounds with good abrasion resistance (Datta 2001, Hamed 2001).

2.3 Rubber elasticity

Rubber has the striking characteristics in being soft, highly extensible, and highly elastic. These behaviours are contrary to those of crystalline solids and glasses, which can only be elastically strained to a very small fraction of their original dimensions. Additionally, the behaviour is different to ductile materials which can withstand a large deformation without rupture but which exhibit a large amount of plastic strain (Shaw and McKnight 2004).

The elastic behaviour of rubber has been extensively investigated due to its technological importance in terms of being uniquely suited in a large number of applications such as sealing, vibration and shock absorption, and load bearing applications.

The theoretical concepts of rubber elasticity were reviewed by a number of investigators (Flory 1953; Treloar 1975; Rubinstein and Colby 2003; Sperling 2006; Young and Lovell 2011; Painter and Coleman 2009). The remarkable concepts, developed to elucidate the elastic behaviour of rubber, will be highlighted. The thermodynamic approach, dealing with the relationship between the macroscopic properties of the system regardless of molecular structure, will be discussed first, Next, the statistical treatment regarding the analysis of the molecular chain configurations in response to the elastic deformation will be examined. A phenomenological treatment, which is based on continuum mechanics, to extend the

concept of the rubber elasticity to three dimensions and large deformations then follows.

2.3.1 Thermodynamic treatment

The thermoelastic behaviour of rubber was reported for the first time by Gough in 1805. He described his experimental results on a rubber band as follows:

1. The rubber which is maintained in a given strain shrinks on heating;

2. The heat is released when the rubber is elongated and is absorbed when the rubber is retracted to its original shape.

Gough's discoveries were quantitatively reexamined by Joule (1859). These two thermodynamic effects are usually known as the Gough-Joule effects. This characteristic phenomenon was considered by a number of investigators in an attempt to establish the relationship between force, length, and temperature of the rubber specimen in terms of the thermodynamic quantities: internal energy and entropy.

Based on the first and second laws of thermodynamics, the deformation of an elastic system (at constant volume) is concerned with changes in both the internal energy and the entropy which is given by

$$F = \left(\frac{\partial U}{\partial L}\right)_{T,V} - \tau\left(\frac{\partial S}{\partial L}\right)_{\tau,V} \qquad \text{Equation 2.1}$$

where F is an elastic force exerted by rubber, U is the internal energy which is the sum of the potential and kinetic energies of all particles in the system, L is the length of the rubber specimen, τ is the temperature, V is the volume of the rubber specimen and S is the entropy associated with the changes in the distribution of chain conformations.

The two contributions to the elastic force of rubber are an energetic term F_E that is the change of the internal energy with respect to the length of the rubber

$$F_E = \left(\frac{\partial U}{\partial L}\right)_{\tau,V}$$ Equation 2.2

and entropic term F_s that is the product of temperature and the change of entropy with respect to the specimen length

$$F_s = -\tau\left(\frac{\partial S}{\partial L}\right)_{\tau,V}$$ Equation 2.3

In typical crystalline solids, such as metals, the internal energy-driven elastic force is dominant because the internal energy, essentially the potential energy, increases when the crystalline lattice spacing is forced apart from their equilibrium positions. In rubber, the entropic contribution, which is related to the changes in the distribution of chain conformation, to the elastic force is more important than the energetic effect. Therefore, for an ideal rubber which is analogous to an ideal gas (its molecules have neither geometry nor intermolecular interactions), $F_E = 0$. In reality, of course, for the real rubber, its molecular chains are not completely free to rotate around the bonds resulting in a higher energy of some local conformations, which is associated with the energetic contribution to the elastic force upon stretching.

The relationship between the partial differentiation of the entropy and that of the elastic force is given by

$$-\left(\frac{\partial S}{\partial L}\right)_{\tau,V} = \left(\frac{\partial F}{\partial \tau}\right)_{L,V}$$ Equation 2.4

Using the relationship given by Equation 2.4, Equation 2.1 can be rewritten in the form

$$F = \left(\frac{\partial U}{\partial L}\right)_{\tau,V} + \tau\left(\frac{\partial F}{\partial \tau}\right)_{L,V}$$ Equation 2.5

which is sometimes called the thermodynamic equation of state for rubber elasticity. Flory (1953) provided a simple approach to analyse Equation 2.5 by establishing a plot of the elastic force against the temperature as shown in Figure 2.2. The slope of the curve at any temperature τ is $\left(\frac{\partial F}{\partial \tau}\right)_{L,V}$ or $-\left(\frac{\partial S}{\partial L}\right)_{\tau,V}$. The change in the ordinate

from the point on the curve to the intercept of the tangent line with the *y*-axis (the elastic force) is the entropic contribution. The value at the intercept of the tangent line to the curve with the *y*-axis is the energetic contribution.

The thermodynamic treatment of rubber elasticity discussed previously is associated with the macroscopic properties of the system without taking into account the effect of the geometry and molecular structure. It considers the behaviour of rubber as that of an ideal gas in the sense that the stress in a deformed rubber increases with increasing temperature, which is similar to an increase of the pressure in a compressed gas with increasing temperature. This gas-like behaviour, in fact, implies that the elastic force (the retractive force) is entropic in origin.

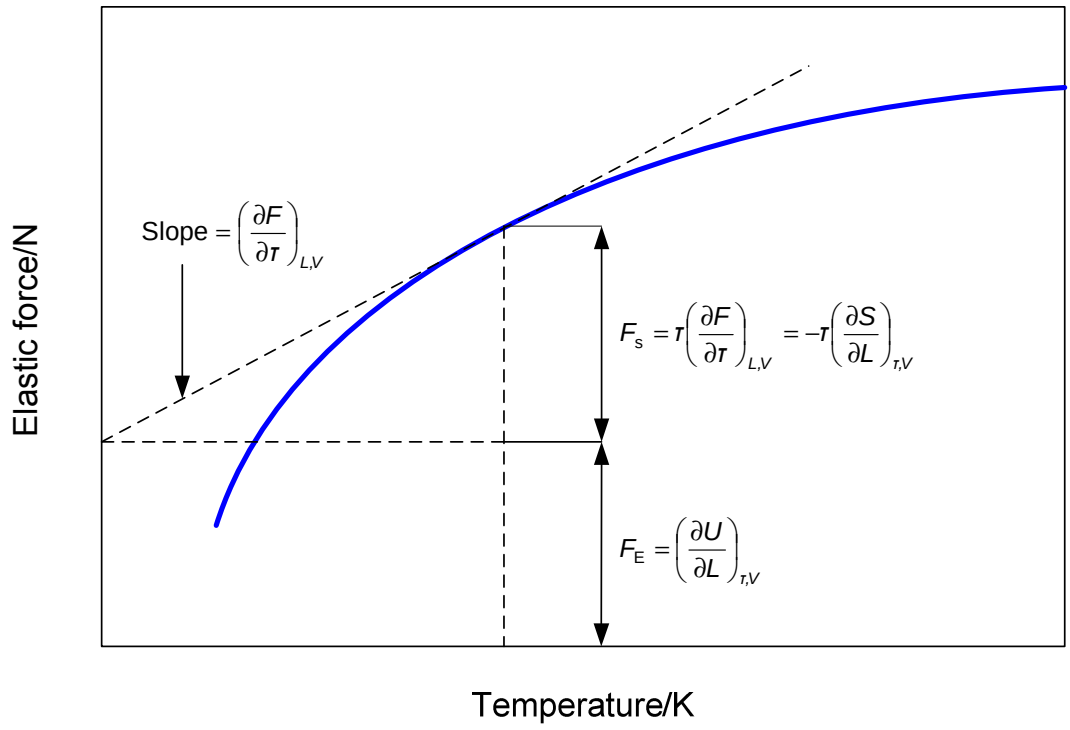

Figure 2.2: Determination of the energetic and entropic contributions to the elastic force of the rubber under constant length at various temperatures. (Adapted from Flory 1953).

2.3.2 Statistical treatment

This approach considers the change in molecular conformation of the rubber during deformation in relation to the change in entropy. It also allows the elastic force of rubber when strained to be related directly to the change in entropy (the entropy is decreased when the molecular chains are elongated resulting in a reduction in the coiling of the molecules).

With regard to the statistical thermodynamics which is associated with thermodynamic entropy and the probability of a thermodynamic state (molecular conformations), the entropy of a single chain of molecule is given by

$$S = k_B \ln \Omega \qquad \text{Equation 2.6}$$

where k_B is the Boltzmann constant which is a function of the gas constant R and the Avogadro constant N_A and Ω is the number of possible chain conformations which is proportional to the probability per unit volume W(x, y, z) of finding one end of a freely-jointed chain at a point (x, y, z) at a distance r from the other end which is fixed at the origin as shown in Figure 2.3. W(x, y, z) is inversely proportional to r in that W(x, y, z) drops as r is increased resulting in the reduced number of conformations. In relation to W(x, y, z), the entropy of a single chain is defined by

$$S = a - k_B \beta^2 r^2 = a - k_B \beta^2 (x^2 + y^2 + z^2) \qquad \text{Equation 2.7}$$

where a is an arbitrary constant and β is a parameter pertaining to the characteristic of a particular chain which is a function of a freely-jointed chain of n segments of length l.

For the molecular network of rubber under an affine deformation, where it is assumed that every part of the rubber deforms as does the whole, the strained state, with reference to Figure 2.4, is given by

$$x' = \lambda_1 x, \; y' = \lambda_2 y, \; z' = \lambda_3 z \qquad \text{Equation 2.8}$$

where λ is the extension ratio in a particular direction which is defined by the strained length of the molecular chain divided by the original length in the same direction.

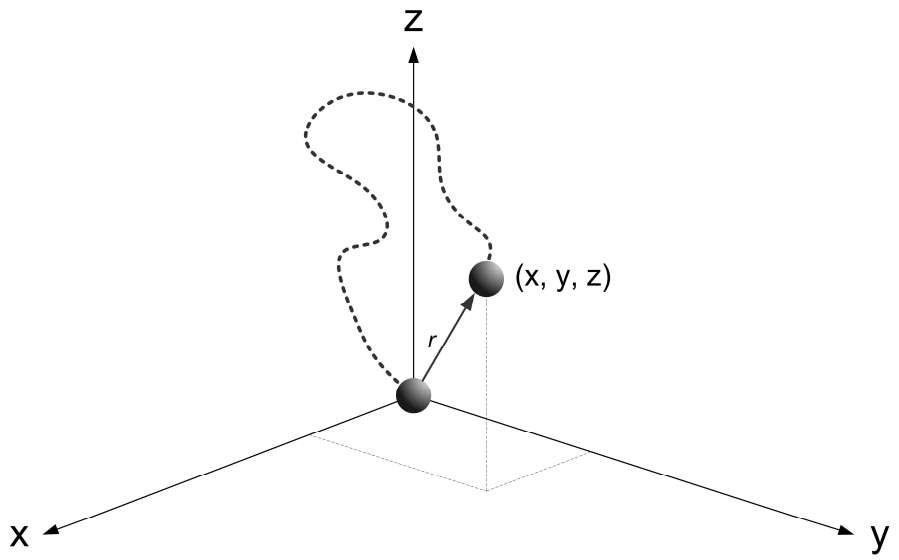

Figure 2.3: Single molecular chain, which is detached from the molecular network, is located by the principal directions x, y, z. '●' represents the point of crosslink (tie point). '----' represents the rubber molecular chain. *r* is the end-to-end distance.

The entropy of a chain in the undeformed state and after deformation is given by Equation 2.9 and 2.10:

$$S = a - k_B \beta^2 (x^2 + y^2 + z^2) \qquad \text{Equation 2.9}$$

$$S' = a - k_B \beta^2 (\lambda_1^2 x^2 + \lambda_2^2 y^2 + \lambda_3^2 z^2) \qquad \text{Equation 2.10}$$

Therefore, the change in entropy of an individual chain is

$$\Delta S = S' - S = -k_B \beta^2 [(\lambda_1^2 - 1)x^2 + (\lambda_2^2 - 1)y^2 + (\lambda_3^2 - 1)z^2] \qquad \text{Equation 2.11}$$

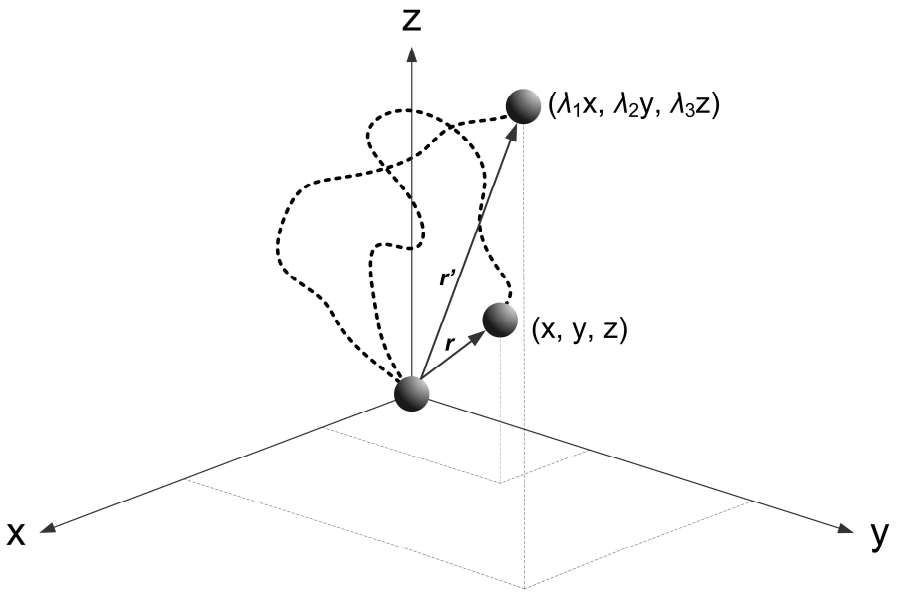

Figure 2.4: Schematic drawing shows the undeformed (x, y, z) and deformed (λ_1x, λ_2y, λ_3z) states of a single chain.

The total change in the entropy of the whole network is

$$\Delta S = \sum_{1}^{N} \Delta s = -\frac{1}{2} N k_B (\lambda_1^2 + \lambda_2^2 + \lambda_3^2 - 3) \qquad \text{Equation 2.12}$$

where N is the number of chains per unit volume in the rubber network and Δs is the entropy change of an individual chain.

Obviously, the change in entropy of the molecular network, with reference to Equation 2.12, is a function of the extension ratio λ and the number of molecular chains between crosslinks per unit volume. If it is assumed that there is no change in the internal energy U on deformation at constant volume, then the change in free energy (Helmholtz free energy) ΔA per unit volume is

$$\Delta A = -T\Delta S = \frac{1}{2} N k_B T (\lambda_1^2 + \lambda_2^2 + \lambda_3^2 - 3) \qquad \text{Equation 2.13}$$

Equation 2.13, which relates the work done by the retractive force (internal force) in relation to the change in entropy, is identical to the work done by the counterbalance

force (external force) to create the deformation per unit volume W, which is commonly known as the strain energy function, therefore

$$W = \frac{1}{2} N k_B T (\lambda_1^2 + \lambda_2^2 + \lambda_3^2 - 3) \qquad \text{Equation 2.14}$$

Referring to the density ρ of the rubber material which is defined as

$$\rho = \frac{N M_c}{N_A} \qquad \text{Equation 2.15}$$

where M_c is the number-average molar mass of the chain length between crosslinks, N_A is Avogadro constant ($=6.022 \times 10^{23}$ mol^{-1}) and N again is the number of chains per unit volume in the rubber network.

Thus, Equation 2.14 becomes

$$W = \frac{\rho R T}{2 M_c} (\lambda_1^2 + \lambda_2^2 + \lambda_3^2 - 3) \qquad \text{Equation 2.16}$$

where R is the gas constant ($=8.314$ J.mol^{-1}.K^{-1}) which is derived from the product of Avogadro constant N_A and Boltzmann constant k_B. Therefore, Equation 2.16 can be simplified to

$$W = \frac{1}{2} G (\lambda_1^2 + \lambda_2^2 + \lambda_3^2 - 3) \qquad \text{Equation 2.17}$$

This equation is very important in that the work of deformation per unit volume or the strain energy function is related to the extension ratio by the parameter G which is referred to as the shear modulus of the rubber. As G is inversely proportional to M_c, it implies that the stiffness of the material is a function of the crosslink density.

Presumably, the rubber is an incompressible solid (Poisson's ratio is very nearly to 0.5) which implies a constancy of the volume on deformation. The product of the extension ratio λ in the three mutually perpendicular axes (the Cartesian coordinate system) is therefore

$$\lambda_1 \lambda_2 \lambda_3 = 1 \qquad \text{Equation 2.18}$$

For the uniaxial deformation at constant volume, the extension ratio under this condition is given by

$$\lambda_1 = \lambda, \quad \lambda_2 = \lambda_3 = \frac{1}{\sqrt{\lambda}} \qquad \text{Equation 2.19}$$

With reference to Equation 2.17 and Equation 2.19, the strain energy function for the uniaxial deformation is defined by

$$W = \frac{1}{2}G\left(\lambda^2 + \frac{2}{\lambda} - 3\right) \qquad \text{Equation 2.20}$$

If F is the force per unit cross-sectional area in the undeformed state which is equivalent to an engineering tensile stress σ_{eng}, the work done on the system to increase the unit length of the rubber by an amount dl is

$$\mathrm{d}W = F\mathrm{d}l = F\mathrm{d}\lambda \qquad \text{Equation 2.21}$$

Thus,

$$F = \sigma_{\text{eng}} = \frac{\mathrm{d}W}{\mathrm{d}\lambda} = G\left(\lambda - \frac{1}{\lambda^2}\right) \qquad \text{Equation 2.22}$$

For the true tensile stress σ_{true}, where $\sigma_{\text{true}} = \lambda\sigma_{\text{eng}}$, therefore

$$\sigma_{\text{true}} = G\left(\lambda^2 - \frac{1}{\lambda}\right) \qquad \text{Equation 2.23}$$

Figure 2.5 shows the comparison of the stress-strain curve of simple extension of natural rubber derived from Equation 2.22, where G = 0.39 MPa, and that obtained from the experiment.

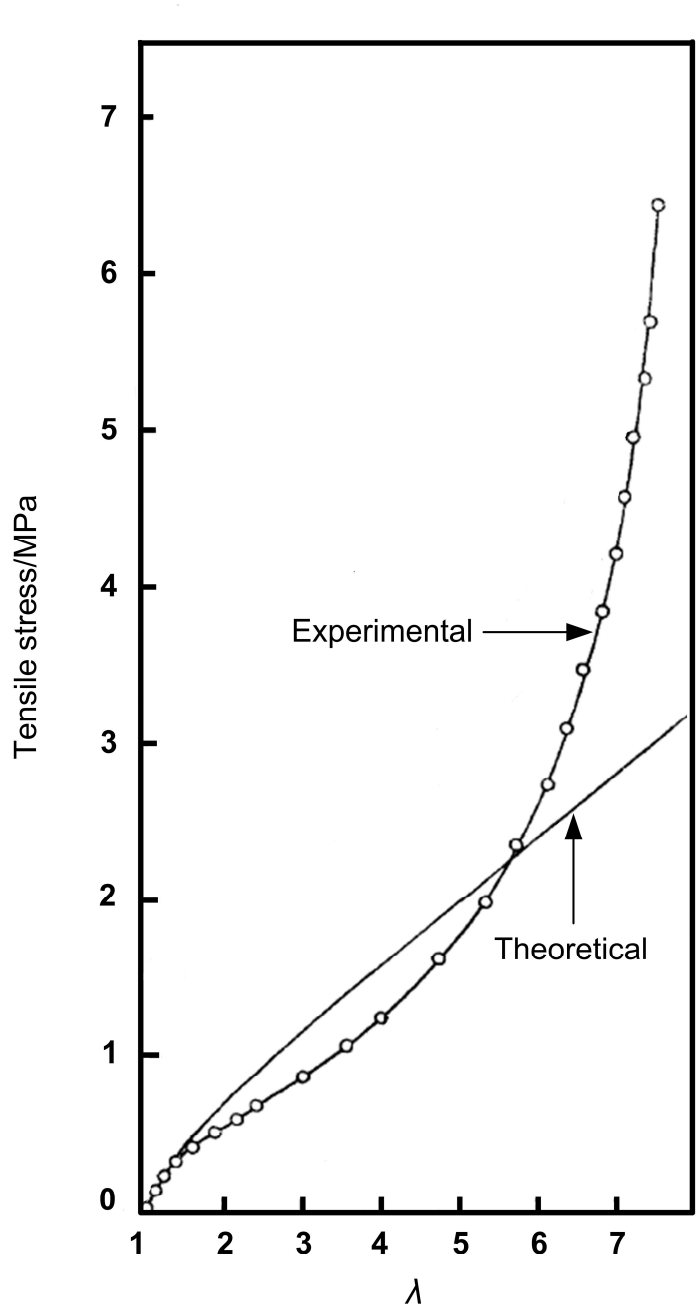

Figure 2.5: Plot of the stress-strain curves of natural rubber which is derived from Equation 2.22 (theoretical) and from an experiment. (Adapted from Treloar 1944).

A good agreement is observed for extension ratios λ below 1.5. However, the deviation is obvious at higher extension ratios. At very large strains this is due to the limited extensibility of the molecular chains in the real molecular networks resulting in an invalidity of the statistical approach which relies on the assumption of an infinite extension of the chain networks. Although the statistical treatment is most effective only at relatively low strains, it is very useful in providing an important insight into the parameters contributing to rubber elasticity.

2.3.3 Phenomenological treatment

This treatment is only concerned with describing observed behaviour of rubber, irrespective of the considerations of the molecular structure of rubber. It utilises continuum mechanics to derive a strain energy function to govern the experimentally determined stress-strain behaviour. Mooney (1940), at nearly the same time as the early development of the statistical approach, was the first to propose the strain energy function W of the rubber material. Based on the assumption of an incompressible elastic solid, isotropic in the unstrained state and conformable to Hooke's law in simple shear that is the shear stress is proportional to shear strain, Mooney showed that the strain energy function can be represented by

$$W = C_1\left(\lambda_1^2 + \lambda_2^2 + \lambda_3^2 - 3\right) + C_2\left(\lambda_1^{-2} + \lambda_2^{-2} + \lambda_3^{-2} - 3\right) \qquad \text{Equation 2.24}$$

where C_1 and C_2 are material constants. For simple extension, Equation 2.24 takes the form which is the well-known stress-strain relation.

$$\sigma = 2\left(C_1 + \frac{C_2}{\lambda}\right)\left(\lambda - \frac{1}{\lambda^2}\right) \qquad \text{Equation 2.25}$$

where σ is the engineering stress. This model is successful at describing the behaviour of a rubber component which deforms at less than 200% elongation (Marckmann and Verron 2006).

Rivlin (1948) generalised an equation of the elastic deformation of a rubber material that is built on the Mooney's approach and showed that the strain energy function can be expressed as an infinite power series

$$W = \sum_{i=0,j=0}^{\infty} C_{ij}\left(I_1 - 3\right)^i \left(I_2 - 3\right)^j \qquad \text{Equation 2.26}$$

where C_{ij} are material constants and I_1 $(= \lambda_1^2 + \lambda_2^2 + \lambda_3^2)$ and I_2 $(= \lambda_1^2\lambda_2^2 + \lambda_2^2\lambda_3^2 + \lambda_1^2\lambda_3^2)$ are the strain invariants which are the function of the extension ratios λ and which are independent of the orientation of the coordinate

system. For simple extension, by differentiation of *W* with respect to *I* in Equation 2.26, the stress-strain relation is given by

$$\sigma = 2\left(\frac{\partial W}{\partial I_1} + \frac{1}{\lambda}\frac{\partial W}{\partial I_2}\right)\left(\lambda - \frac{1}{\lambda^2}\right) \qquad \text{Equation 2.27}$$

Obviously, the partial derivatives $\partial W/\partial I_1$ and $\partial W/\partial I_2$ are equivalent to C_1 and C_2 respectively, as shown in Equation 2.25. For simple shear, according to Rivlin (1956), the stress-strain relation is given by

$$\frac{\tau}{\gamma} = 2\left(\frac{\partial W}{\partial I_1} + \frac{\partial W}{\partial I_2}\right) \qquad \text{Equation 2.28}$$

where τ is the shear stress and γ is the shear strain which is related to I_1 by $\gamma^2 = (I_1 - 3)$.

Referring to Equation 2.26, if only the first term is retained, we obtained

$$W = C_{10}(I_1 - 3) \qquad \text{Equation 2.29}$$

This equation is known as the neo-Hookean model and it is identical to Equation 2.17, $C_{10} = G$, which is derived from the statistical approach. Interestingly, this provides the significant link between the two approaches. Building on the Rivlin's formulation for an incompressible material, $\lambda_1\lambda_2\lambda_3 = 1$, Mooney's equation, Equation 2.24, can be reduced to

$$W = C_{10}(I_1 - 3) + C_{01}(I_2 - 3) \qquad \text{Equation 2.30}$$

This material model becomes popularly known as the Mooney-Rivlin equation.

Figure 2.6 shows the Mooney plot, which is the graph of the reduced stress $\sigma/(\lambda-\lambda^{-2})$ against λ^{-1} for the uniaxial tensile data of four similar rubber materials with different levels of the curatives.

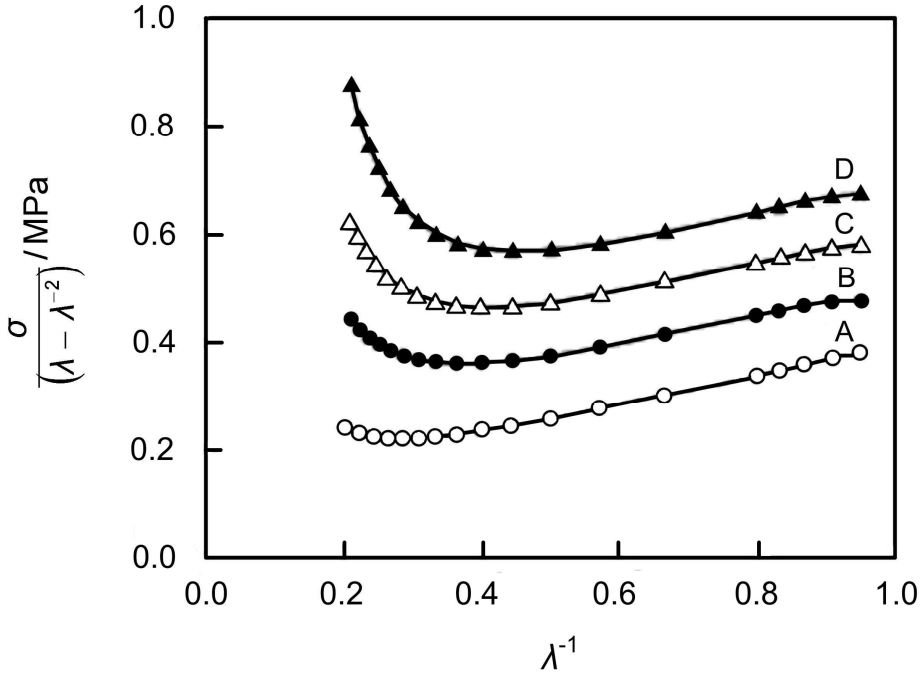

Figure 2.6: Mooney plot of four rubber materials (A-D) with identical 1:1 ratios but with different amounts of accelerator (CBS) and sulphur: A (0.5:0.5); B (1.0:1.0); C (1.5:1.5); D (2.0:2.0). (Yeoh and Fleming 1997).

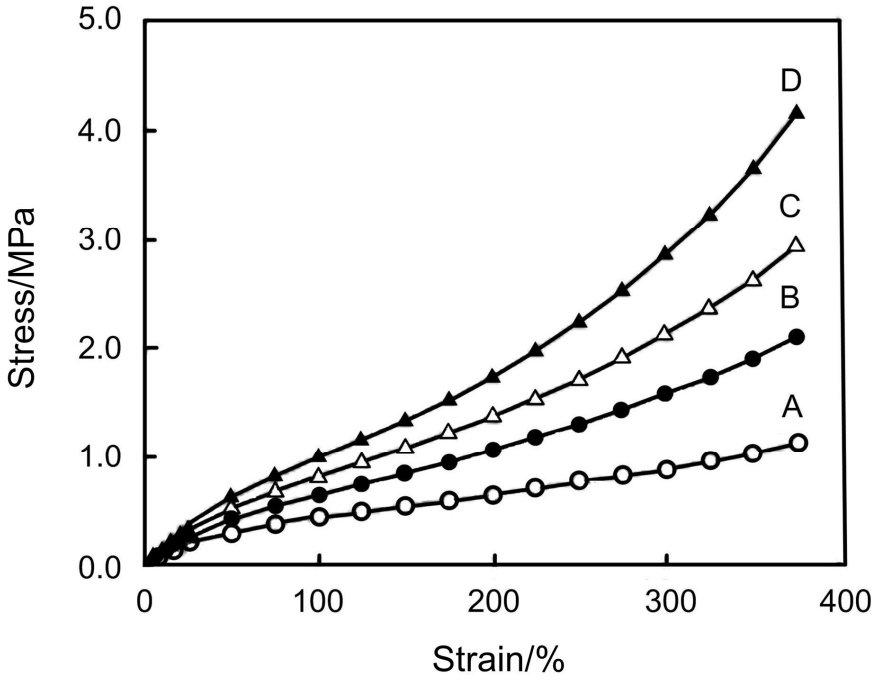

Figure 2.7: Stress-strain curves of rubber materials with different amount of curatives. (Yeoh and Fleming 1997).

Obviously, the linear portion of the curve, with the slope C_2 and intercept C_1, is shorter as the amount of the curatives has been increased. At higher extensions, which is when λ^{-1} becomes smaller, the departures can be observed with a rapid increase in the reduced stress for the material with increased curatives. This effect is related to the crosslink density of the material (Mullins 1959). These trends correspond to those of the conventional stress-strain curves, as shown in Figure 2.7, when the up-turn occurs earlier with higher curative levels.

2.4 General overview of fracture in materials

Fracture is a phenomenon of great scientific interest as well as of practical importance. It is a matter of concern in terms of identifying problems leading to safety issues. This has become more important and has created an increasing demand for advanced materials from which the new products can be created with improvements in our quality of life. In many consumer products, for example, the handles of the carrier bags, toys and so on, fracture may be an annoyance. Fracture in car tires, conveyor belts or the fuselage of the plane, however, can result in catastrophic and often life threatening consequences.

2.4.1 Fracture in polymeric material

Basically, the theoretical strength of a solid material can be simply derived from the basic knowledge of the potential energy of interaction between its constituent atoms (Cottrell 1964). This is defined by

$$\sigma_t = \alpha E \qquad \text{Equation 2.31}$$

where σ_t is the theoretical breaking stress in tension and α is a material constant in association with the interatomic spacing of the atoms in the unstrained condition and a surface free energy which is the work done per unit area of surface in creating the fracture and E is the elastic modulus of the solid material. In practice, the values of α are typically of the order of 10^{-3} for bulk solids.

For polymeric material, the theoretical tensile strength can be obtained from the load to break a carbon-carbon bond of the polymer chain in relation to the molecular cross-sectional area, perpendicular to the molecular chain axis, which depends on

the molecular weight, the density of specimen, and the length of repeat unit (Vincent 1972). Based on Vincent's data which were obtained from thirteen polymers, the values of the theoretical tensile strength of polymeric materials are in the range of 6100 to 30500 MPa. However, these values are about 200 times greater than the experimentally established data.

The large discrepancy between the theoretical and observed tensile strength in a solid was, for the first time, explained by Griffith (1921). Griffith's theory, in its original form, is applicable only to a perfectly brittle material such as glass. It cannot be applied directly to the polymeric material. However, Griffith's concept has provided a basic understanding about the fracture of polymeric material in that it obviously relates the fracture stress to the size of the initial flaw and the energy required to create a new fracture surface. Generally, the fracture energy is defined as the energy required to create unit area of crack surface and must equal the energy supplied by the system as the crack propagates. The energy supplied is usually expressed in terms of 'strain energy release rate', $-(\partial W/\partial A)$ where W is the total elastic strain energy which is stored in the material under strained condition and A is the area of one fracture surface of the crack. The fracture energy T is then equal to the critical value of the strain energy release rate at which the crack propagates

$$-\left(\frac{\partial W}{\partial A}\right)_{\text{crit}} = T \qquad \text{Equation 2.32}$$

The strain energy release rate can be experimentally obtained from the applied stress or strain and the specimen geometry including the crack length.

According to Griffith's criterion for brittle fracture, the crack will spread when the decrease in the total elastic strain energy is at least equal to the surface energy of the solid which is defined as half the energy to break unit area of interatomic bonds. However, a lot of polymeric materials including rubber are not perfectly elastic and the fracture energy greatly exceeds the bond fracture energy. The excess energy is dissipated in irreversible process like viscoelastic and plastic flow throughout the material (Andrews 1979). Therefore, for rubber, a modified version of the Griffith's equation must be utilised.

2.4.2 Fracture in rubber

The original Griffith's criterion (1921) based on an energy balance approach where the energy required to from a new fracture surface (tearing energy) is equivalent to the loss of elastic strain energy in the test piece. This was first adopted to the study of vulcanised rubber by Rivlin and Thomas (1953). The criterion for tearing of rubber states that the amount of work necessary to increase the size of a cut of length *c* by a small amount d*c*, therefore creating an area *t*d*c* of new surface, is equal to *T*td*c*, where *T* is a characteristic of the material and independent of the overall shape of the specimen and *t* is the thickness. If this cut grows without the forces applied on the specimen moving in the quasi-static manner (no external work is done at the system boundaries), the energy is derived only from the elastic strain energy in the specimen. Thus, the energy available for a crack in rubber to be driven called the strain energy release rate or tearing energy, is defined by

$$T = -\frac{1}{h}\left(\frac{\partial W}{\partial c}\right)_l \qquad \text{Equation 2.33}$$

where *W* is the total elastic strain energy stored in the specimen, *h* is the specimen thickness, and *c* is the crack length. The suffix *l* denotes the differentiation with constant displacement of the boundaries over which the forces are applied.

Practically, rubber materials are not perfectly elastic, that is, part of tearing energy is employed to break the chemical bonds to crate a new fracture surface and another is viscoelastically dissipated throughout the material. Thus, the greater the amount of energy dissipated, then the higher the tear strength is.

Several studies have shown that the tearing energy is a characteristic property of the material and independent of the form of test piece (Rivlin and Thomas 1953; Thomas 1960; Lake et al. 1969). Figure 2.8 shows the plot of the tearing energy against the tearing rate for unfilled SBR specimens using various geometrical configurations obtained from Figure 2.9. Obviously, a constant, independent of specimen geometry, between the tearing energy and the tearing rate can be achieved.

The three types of tearing specimen that are most commonly utilised for the study of the tearing behaviour of rubber are a trouser tear specimen or a simple extension

tear test piece (Figure 2.9 a), a simple tension specimen with a single edge cut (Figure 2.13), and a planar tension specimen (Figure 2.9 b) with single edge cut known as the pure shear crack growth specimen in the rubber literature. This type of specimen is relatively short and wide so that the lateral contraction is prohibited. Normally, the clamps are pulled at a constant rate of displacement to cause a crack to grow. Distant from the crack tip, the state of deformation is pure shear, so called as the axes of strain are not rotated. Figure 2.10 illustrates a block of rubber in a state of pure shear.

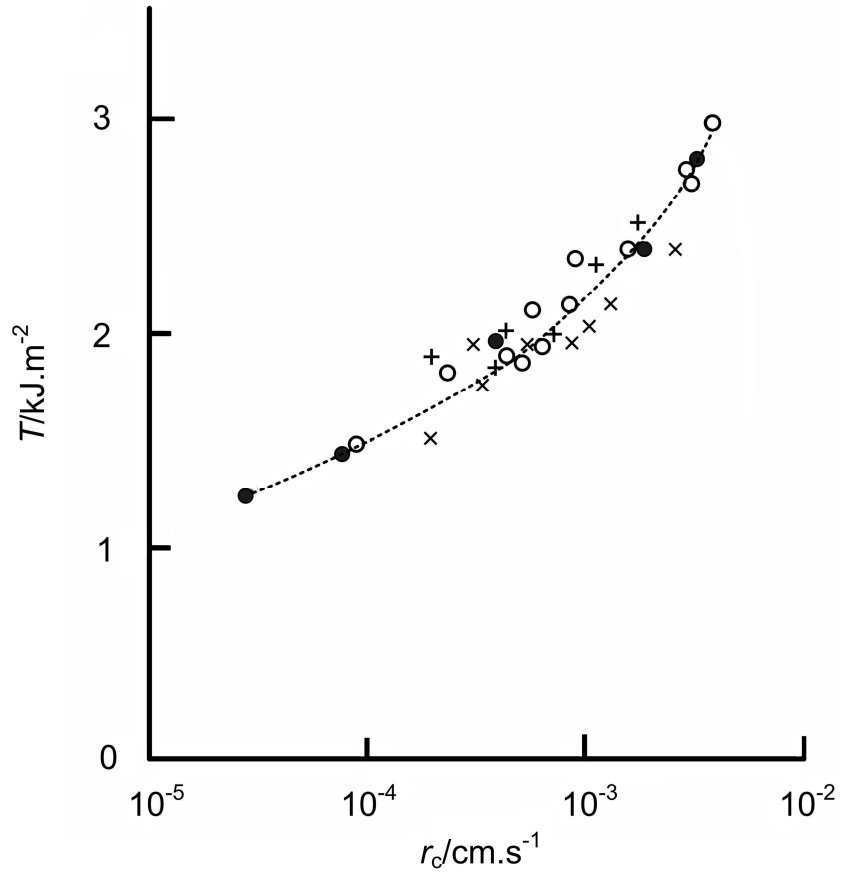

Figure 2.8: The plot of the tearing *T* against the crack growth rate r_c for an SBR vulcanisate using various tearing specimens shown in Figure 2.9: trouser tear, ×; pure shear crack growth, +; angled, •; and split, o (Lake et al. 1969).

For the trouser specimen, the tearing energy was determined based on the energy balance approach (Rivlin and Thomas 1953) by considering the schematic diagram in Figure 2.11.

If the cut length is sufficiently long compared with the half-width of the specimen, when deformed, then region *A* of each of the legs is substantially in simple extension

with the corresponding extension ratio λ. The region *B* is undeformed if the uncut portion of the specimen sufficiently long. The strain distribution in the vicinity of the clamp *C* and in the neighbourhood *D* of the tip of the cut is complicated. When the cut length increases by d*c*, the size of region *A*, which is in simple extension, increases at the expense of the undeformed region *B*. The volume of the region *A* at the expense of region *B* increases by A_0d*c*, where A_0 is the cross-sectional area of the specimen in its undeformed state. Thus, the overall length *l* between the clamps will increase by an amount d*l*, given by 2λd*c*, then

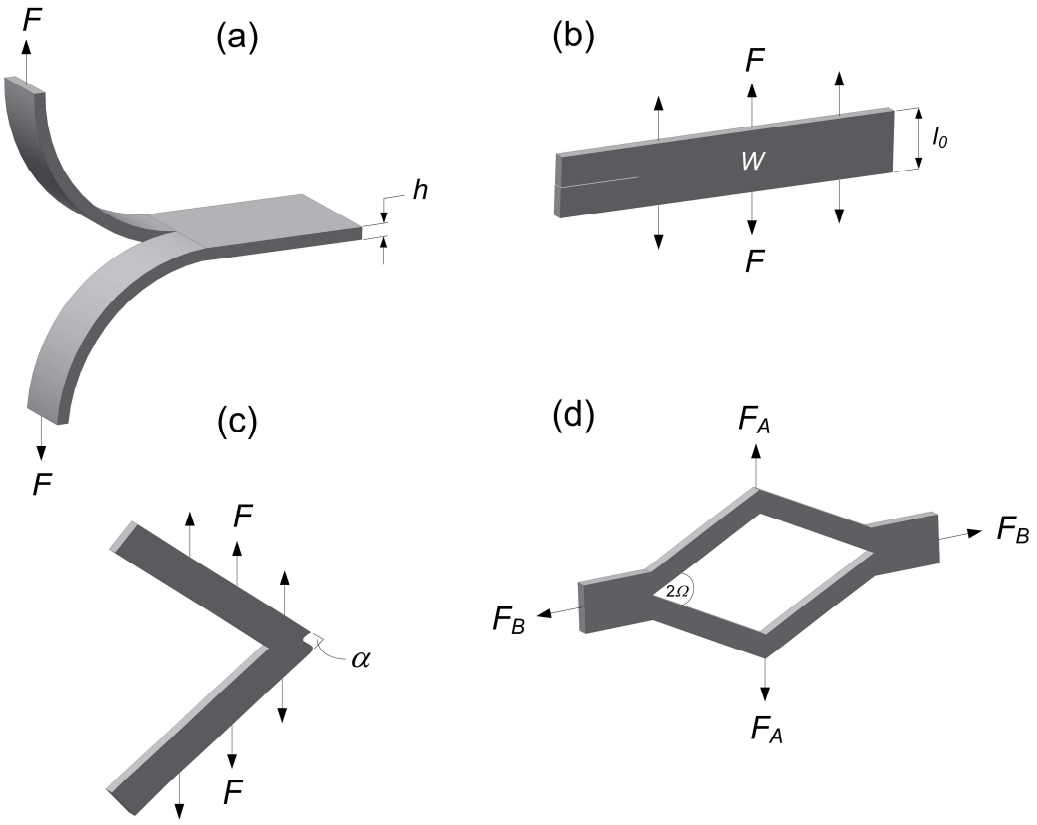

Figure 2.9: Tearing specimens: (a) simple extension or trouser tear, (b) pure shear crack growth, (c) angled and (d) split. (Adapted from Lake 1995).

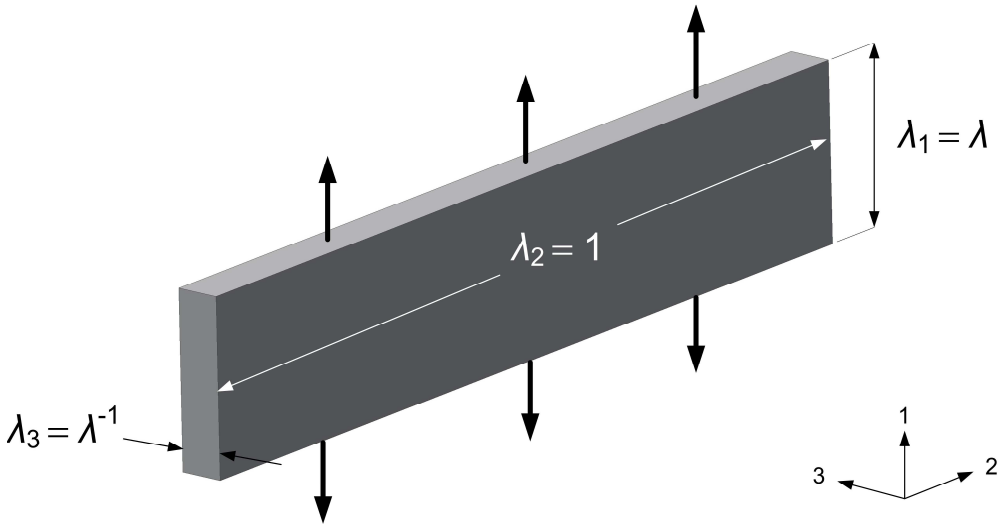

Figure 2.10: Pure shear deformation. It is defined as a tension applied in the 1-direction with the condition that the width in the 2-direction is prevented from altering due to the presence of the test grips ($\lambda_2 = 1$). The term 'shear' means that a deformation in which a line parallel to one of the principal axes undergoes no change in length. The term 'pure' means that the principal axes do not rotate during the deformation (Gent 2001).

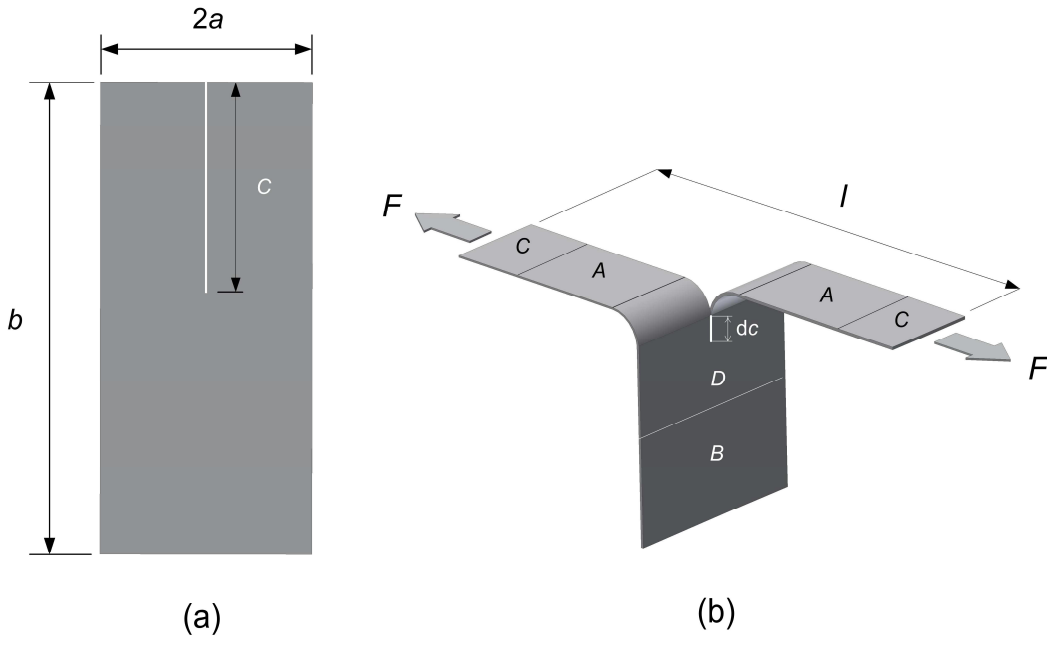

Figure 2.11: Schematic diagram of trouser tear specimen: (a) undeformed, (b) deformed. (Adapted from Rivlin and Thomas 1953).

$$\left(\frac{\partial l}{\partial c}\right)_F = 2\lambda$$ Equation 2.34

The strain energy W in the specimen is a function of c and l and thus the change dW is related to the changes of crack length dc and overall length dl by

$$\mathrm{d}W = \left(\frac{\partial W}{\partial c}\right)_l \mathrm{d}c + \left(\frac{\partial W}{\partial l}\right)_c \mathrm{d}l$$ Equation 2.35

The extended force is defined as $F = \left(\frac{\partial W}{\partial l}\right)_c$

Combining these relations yields

$$\left(\frac{\partial W}{\partial c}\right)_F = \left(\frac{\partial W}{\partial c}\right)_l + F\left(\frac{\partial l}{\partial c}\right)_F$$ Equation 2.36

Equation 2.36 yields, if you assume $\left(\frac{\partial l}{\partial \mathrm{c}}\right)_F = 2\lambda$,

$$\left(\frac{\partial W}{\partial c}\right)_l = \left(\frac{\partial W}{\partial c}\right)_F - 2\lambda F$$ Equation 2.37

Under conditions of a constant applied force F, an increase in cut-length dc transfers a volume A_0dc of rubber from an undeformed state to a state of simple extension, the change in the elastically stored energy dW in the specimen is W_0 A_0dc. Therefore,

$$\left(\frac{\partial W}{\partial c}\right)_F = W_0 A_0$$ Equation 2.38

where A_0 is the cross-sectional area of the undeformed specimen and W_0 is the elastically stored energy per unit of undeformed volume.

Substituting (2.38) into (2.37), we obtain

$$\left(\frac{\partial W}{\partial c}\right)_l = W_0 A_0 - 2\lambda F \qquad \text{Equation 2.39}$$

Introducing (2.33) into (2.39),

$$T = \frac{2\lambda F}{h} - wW_0 \qquad \text{Equation 2.40}$$

where w is the width of the specimen which is equivalent to 2a in Figure 2.11.

For the pure shear crack growth specimen as shown in Figure 2.12, when it is deformed by the clamp separation in the direction parallel to the dimension l_0, the elastic strain energy in the specimen will not be the same in the different regions of the specimen. Region *A* is substantially undeformed and so the elastic strain energy will be zero.

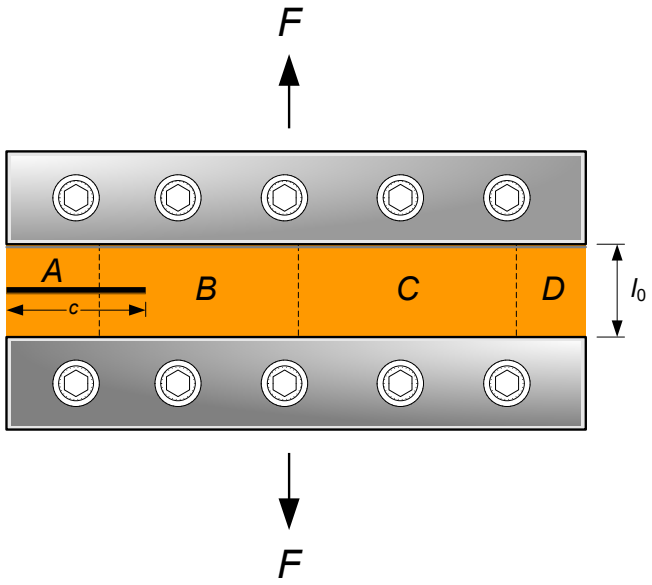

Figure 2.12: Schematic diagram of pure shear crack growth specimen. (Adapted from Rivlin and Thomas 1953).

Region *B*, around the crack tip, is in a complicated state of strain and the elastic strain energy is difficult to determine. Region *C* is in a state of pure shear. Region *D* is the force-free edge region where it is slightly departed from pure shear.

If the overall distance between the clamps is unchanged, in other words, the extension ratio in the pure shear region *C* is unchanged, the propagation of the cut-length dc as measured in the unstrained state does not alter the state of the strain in

the region *B* but only shifts this zone parallel to the direction of the crack, resulting in the propagation of the region *A* at the expense of the region *C*. The change in the elastic strain energy d*W* due to a change in the cut-length d*c* is

$$dW = -Wl_0 h dc \qquad \text{Equation 2.41}$$

where l_0 is the length of the specimen between the clamps measured in the undeformed state, *h* is the specimen thickness, and *W* is the elastic strain energy per unit volume of the material in a state of pure shear at the relevant strain.

Then,

$$\left(\frac{\partial W}{\partial c}\right)_l = Wl_0 h \qquad \text{Equation 2.42}$$

From (2.33), we obtain

$$T = Wl_0 \qquad \text{Equation 2.43}$$

Generally, *W* can be determined from the graphical integration of the stress-strain curve of the pure shear specimen.

In the simple tension specimen with a single edge cut as shown in Figure 2.13, the tearing energy *T* depends on the elastic strain energy *W* in the simple extension region, the crack length *c* and a strain-dependent parameter or a slowly varying function of strain k_s.

$$T = 2k_s Wc \qquad \text{Equation 2.44}$$

The dependence of the parameter k_s on strain is defined approximately by $\pi/(1+\varepsilon)^{\frac{1}{2}}$ where ε is the tensile strain (Greensmith 1963). This parameter, which is dependent on the extension, appears to be directly related to the lateral contraction of the specimen containing a crack in simple extension.

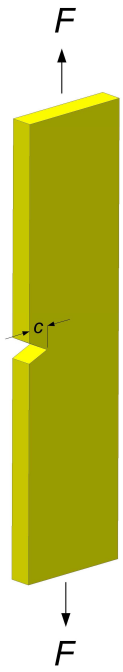

Figure 2.13: Schematic diagram of simple tension specimen with a single edge cut with the cut length *c*.

2.4.3 Relationship between the tearing energy and the localised fracture at the tip

The tearing energy concept for rubber which is based on the energy balance approach was further extended to gain an insight into the highly localised fracture at the tip by examining the relationship between the tearing energy derived from the strain distribution around the crack tip and that found from the overall forces or strains as described previously in section 2.4.2.

With reference to the model crack in the form of a parallel-sided slit terminated as illustrated in Figure 2.14, the shaded area represented the loss of the elastic strain energy per unit volume as the crack c propagates by amount of Δc as referred to the unstrained conditions.

An increase in the crack length by Δc results in the energy loss consisting of two components:

1) The elastic strain energy loss in the excised region;
2) The work done by relaxing the stresses on the new tip surface to zero.

The amount of the elastic strain energy loss in the shaded area in relation to the first term given by

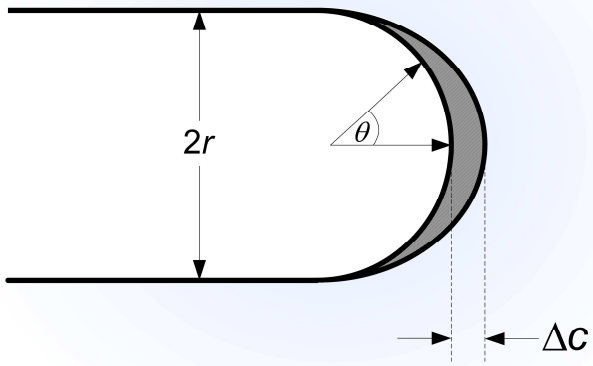

Figure 2.14: Schematic diagram of model crack with a circular tip of unstrained diameter *d*. The shaded area, in which the region ahead of the tip is excised, represents the loss of the elastic strain energy per unit volume as the crack *c* propagates by amount of Δ*c* as referred to the unstrained condition. (Adapted from Thomas 1955).

$$-\Delta W_1 = \int_{-\frac{\pi}{2}}^{+\frac{\pi}{2}} E_t \Delta c t r \cos\theta \mathrm{d}\theta \qquad \text{Equation 2.45}$$

where E_t is the elastic strain energy density per unit volume at the crack tip surface at an angular distance θ form the pole. The second component, $-\Delta W_2$, is the work done by relaxing the stresses on the new crack surface to zero which is a minimum and can be neglected in comparison with $-\Delta W_1$, thus with reference to Equation 2.33, we obtain:

$$T = -\frac{1}{h}\left(\frac{\partial W}{\partial c}\right)_l = r\int_{-\frac{\pi}{2}}^{+\frac{\pi}{2}} E_t \cos\theta \mathrm{d}\theta = r\int_{-1}^{+1} E_t \mathrm{d}(\sin\theta) \qquad \text{Equation 2.46}$$

Thomas (1955) used simple extension and pure shear crack growth test pieces of unfilled natural rubber. For the simple extension, the geometry of the test specimen and the experimental arrangement are illustrated in Figure 2.15 and Figure 2.16 respectively.

With reference to Figure 2.16, the test piece with the reference marks on the semicircular edge of the incision was extended by the horizontal force which is achieved by the application of the various loads *M*. Under this condition, there were regions in the arms in which the rubber specimen was in simple extension, and there was a region beyond the tip of the incision that was in an unstrained state. The lengths of the element around the tip of the incision before and after straining by the application of loads *M* were determined by means of a microscope equipped with an eyepiece scale. The angular distance θ from the pole and the radius *r* of the tip, shown in Figure 2.17, were determined at the central point of each element around the tip in the unstrained state condition. The relationship between the elastic strain energy at the tip of the incision E_t, which is obtained from the strain of each element as a function of the numerically integrated area under the stress-strain curve separately determined using the tensile strip test piece, and the angular distance θ from the pole which is represented in terms of sin θ as shown in Figure 2.18.

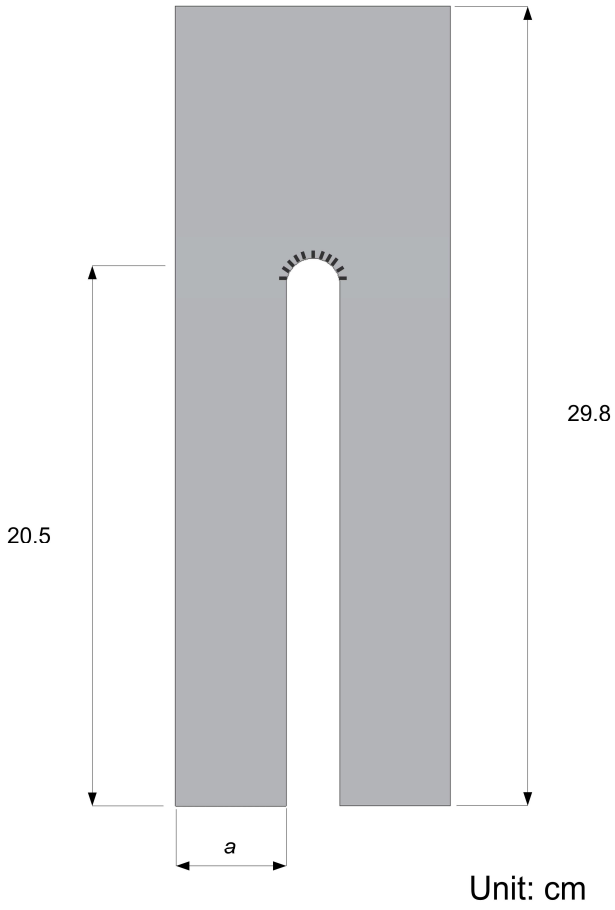

Figure 2.15: Dimensions of the simple extension test piece with the reference marks '-' at the tip of the incision which were made in order to facilitate a measurement of the strain distribution in this region. The letter '*a*' represents the width of the legs (2.0 and 4.9 cm). (Adapted from Thomas 1955).

For the pure shear crack growth test piece, the experimental setup is shown in Figure 2.19. The determination of the tearing energy obtained from the strain energy distribution around the tip of the incision was carried out under the same framework as previously described for the simple extension test piece. Figure 2.20 and 2.21 show the plots of the relation between the tearing energy derived from the strain distribution around the tip of the incision T_1 and that obtained from the overall force T_2 for the simple extension and the pure shear test pieces.

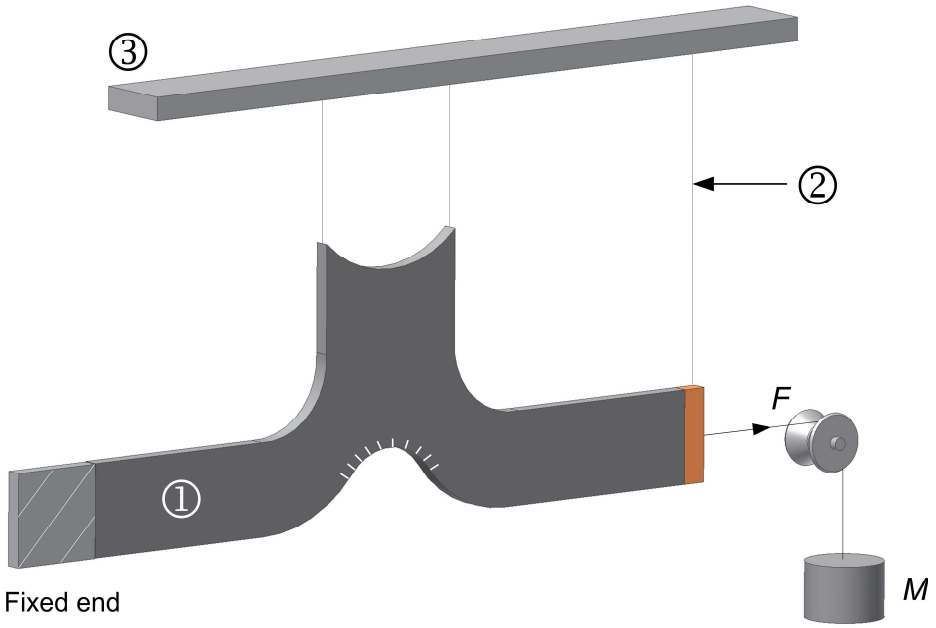

Figure 2.16: Experimental arrangement for the simple extension test piece. The test piece ① is supported by the string ② being attached to the rigid plate ③. (Adapted from Thomas 1955).

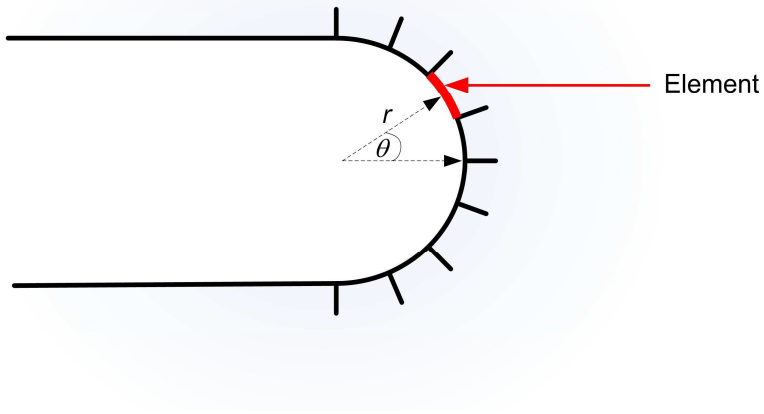

Figure 2.17: Schematic picture illustrating the individual undeformed elements at a model crack tip which are utilised to determine the angular distance θ from the pole.

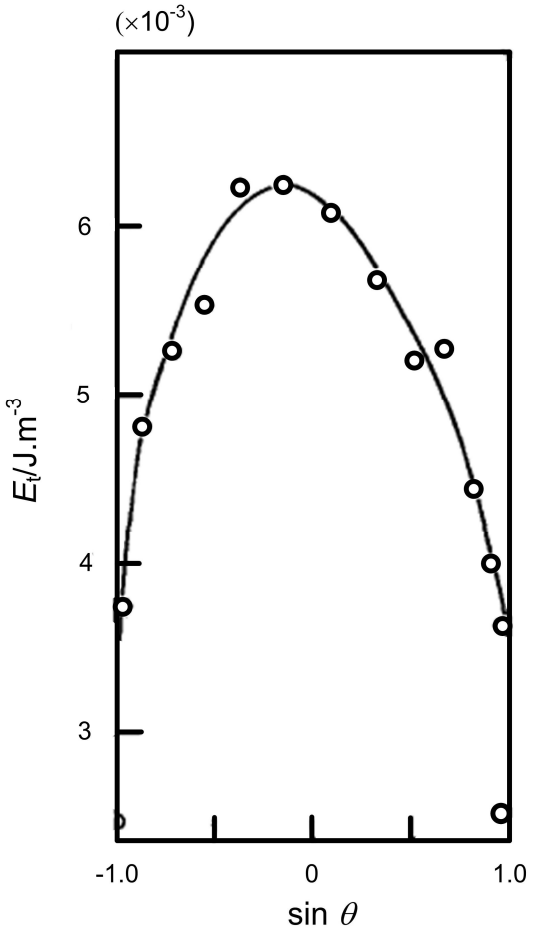

Figure 2.18: The typical relationship between the elastic strain energy at tip of the incision E_t and sin θ obtained from the application of load 1.01 kg (Thomas 1955).

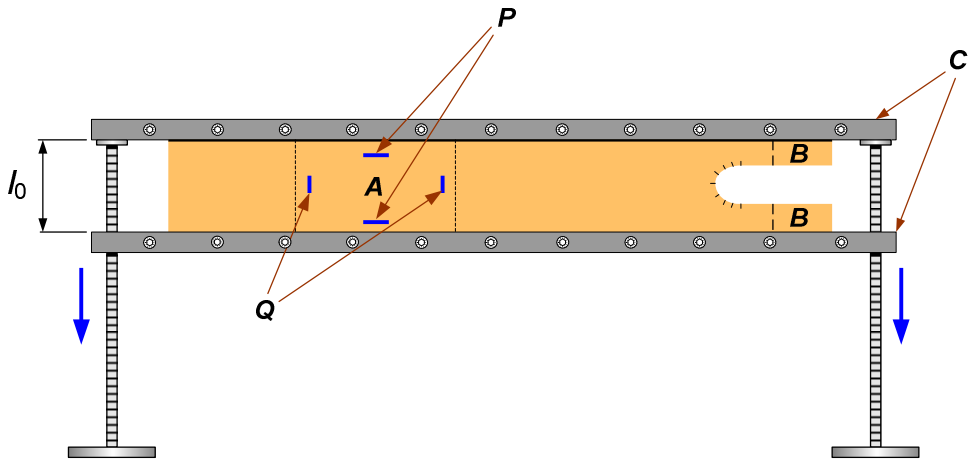

Figure 2.19: The experimental setup for the pure shear crack growth specimen. Region *A* is in the state of pure shear which is checked by a pair of marks *P* and *Q*. Marks *P* were made to monitor the extension ratio λ in region *A* in which is required to be the value of unity as the marks *Q* was extended by the clamps *C*, with an original separation l_0, to generate the strain at the tip of the incision. Regions *B* are unstrained. (Adapted from Thomas 1955).

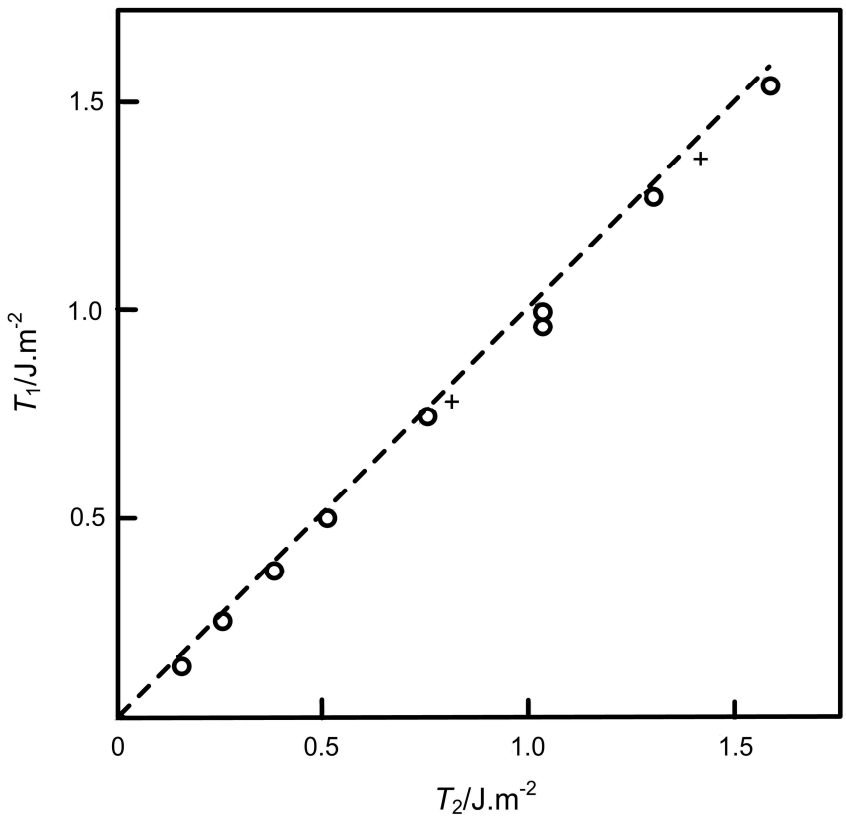

Figure 2.20: The relationship between the tearing energy derived from the strain distribution around the tip of the incision T_1 and that obtained from the overall force T_2 for the simple extension test piece: (o) represents a = 4.9 cm; (+) represents a = 2.0 cm, where a is the width of the legs of the test piece as shown in Figure 2.15 (Thomas 1955).

With reference to the test results as shown in Figure 2.20 and 2.21, the tearing energy T, obviously, can be determined in terms of the shape of the tip of the incision and the strain distribution around it. The magnitude of the tearing energy can be given by the approximation of the product of the diameter of the tip of the incision referred to the unstrained state d and the elastic strain energy of the rubber at the tip E_t. Therefore, at the critical point, this is defined as:

$$T_c \cong dE_b \qquad \text{Equation 2.47}$$

where T_c is the critical tearing energy and E_b is the strain energy density at break of the material. Equation 2.47 is confirmed by the independent experiments which were carried out separately by Thomas (1955) to obtain the value of T_c/d, that should be a constant independent of d, from the trouser test piece with various diameters of tip and the magnitude of the strain energy at break E_b which was derived from the

dumbbell test piece. Thomas (1955) showed that the validity of the Equation 2.47 was satisfactory.

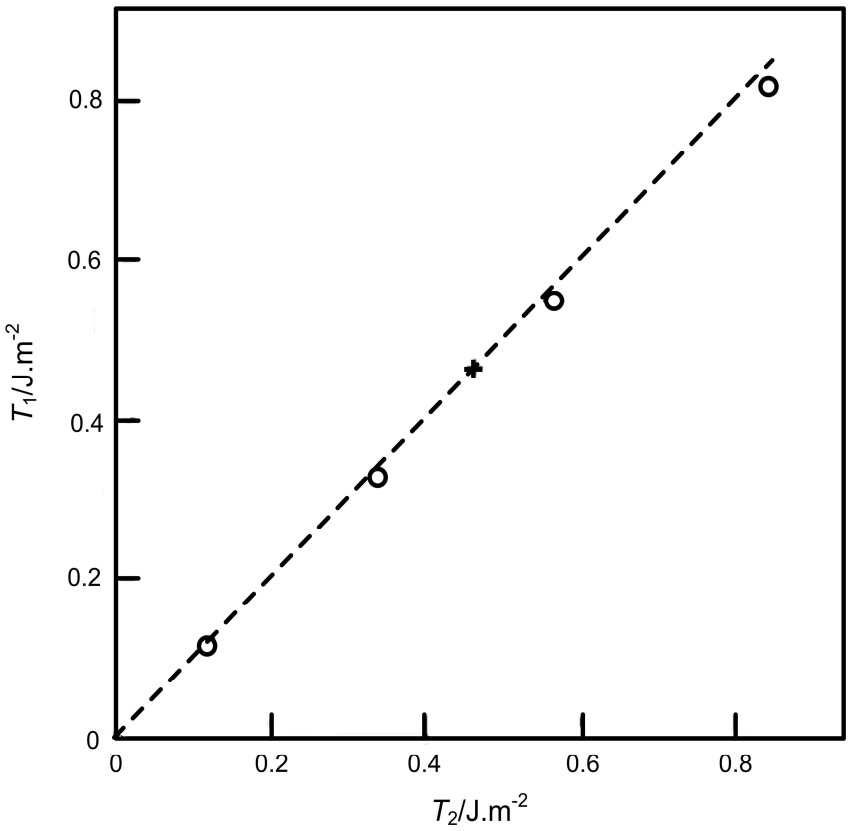

Figure 2.21: The relationship between the tearing energy derived from the strain distribution around the tip of the incision T_1 and that obtained from the overall force T_2 for the pure shear crack growth test piece T: (o) represents the strain increasing; (+) represents the strain decreasing which was taken to detect the effect of the hysteresis (Thomas 1955).

Building on Thomas's work, Greensmith (1960) compared the tearing energy for crack growth from tear measurement, using a trouser tear specimen with a tip diameter of 2 mm, with E_b from tensile measurement done independently at various rates. Plotting T_c/d and E_b against the reciprocal of the time to catastrophic failure $1/t$ as shown in Figure 2.22 (a) and Figure 2.22 (b) for unfilled and black-filled SBR respectively, he found that in both cases T_c/d and E_b were comparable in magnitude and showed a similar dependence with time. However, the values of E_b were consistently lower than those of T/d. This is assumed to be the imperfect elasticity of the material which is ignored in Equation 2.47 and the considerable difference in the dimensions of the specimen. In the tear specimen, the point of catastrophic failure is confined to a relatively small region which is a fraction of a millimetre in size. This

gives rise to an effect of flaw size, orientation, and distribution on this type of the specimen is less significant than that on the tensile specimen (Thomas 1955).

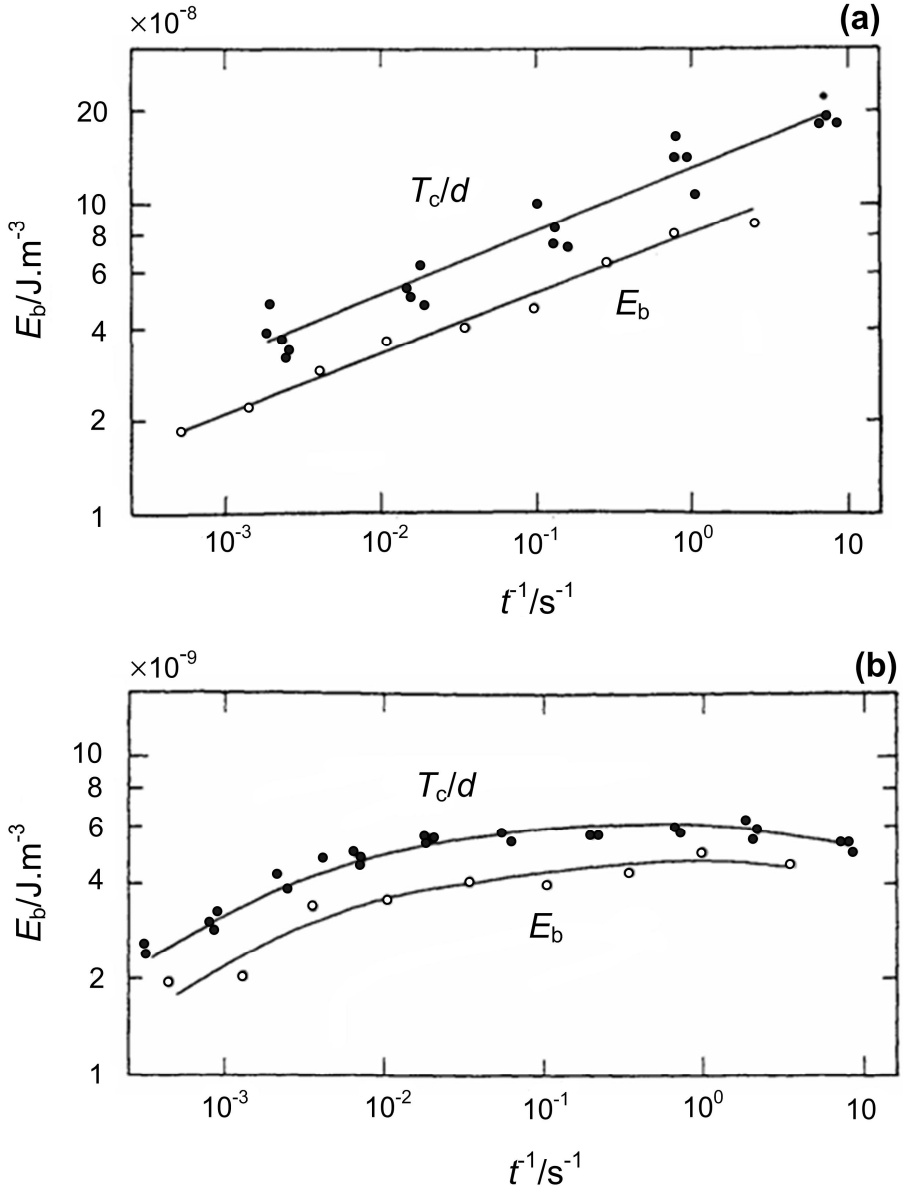

Figure 2.22: Comparison of E_b, against t^{-1} and T_c/d against t^{-1} for (a) an unfilled SBR vulcanisate, (b) a SRF carbon black-filled SBR vulcanisate (Greensmith 1960).

2.4.4 Threshold tearing energy

For a rubber, which is a viscoelastic material, the tearing energy T normally increases as the tearing rate is increased or the temperature is decreased. At sufficiently high temperatures and slow crack growth rates, T achieves a threshold value T_0, which is the minimum limit of the mechanical strength of rubber, in the absence of chemical effects, below which the crack growth is solely attributed to

chemical degradation, for example, by ozone. Under the threshold conditions, the viscous effects in the rubber are minimised resulting in the minimum possible energy dissipation (Lake and Thomas 1967).

For various rubbers, both crystallising and non-crystallising rubbers, the magnitude of T_0 is fairly similar although their other strength properties, tensile and tear strengths, are considerably different. The value of T_0 was derived based on the molecular structure and the strength of the primary chemical bonds. As shown schematically in Figure 2.23, a molecular chain, whose end points (crosslinks) lie on the opposite sides, lying across the plane of crack growth.

In order to propagate the crack, all such chains must be ruptured. It is possible to employ the Equation 2.45 to obtain T_0. Thus, on the molecular scale, Equation 2.47 becomes

$$T_0 = E_0 d_0 \qquad \text{Equation 2.48}$$

where E_0 is the minimum elastic strain energy density at the tip and d_0 is the minimum possible diameter of the crack tip in the unstrained state which is assumed to be as small and therefore as sharp as possible. In the case of rubber, however, it is unlikely for the tip diameter of the crack to be of atomic dimensions because of their long flexible molecular conformation which are crosslinked at relatively random intervals. Therefore, the minimum possible tip diameter in the unstrained condition must be of the order of the distance between adjacent crosslinks in the unstrained state L (Lake and Thomas 2001) and from the statistical theory (Treloar 1975), $L \cong \xi n^{\frac{1}{2}}$. The average value of d_0 is then given as

$$d_0 \cong \xi n^{\frac{1}{2}} \qquad \text{Equation 2.49}$$

where ξ is the length of a monomer unit and n is the average number of monomer units between the crosslinks. Presumably, the chains are essentially straight, just before the rupture, each bond in the carbon backbone chain is subjected to the same force primarily transmitted by the crosslinks. The maximum possible elastic strain energy density will be of the order of bJ_b where b is the number per unit

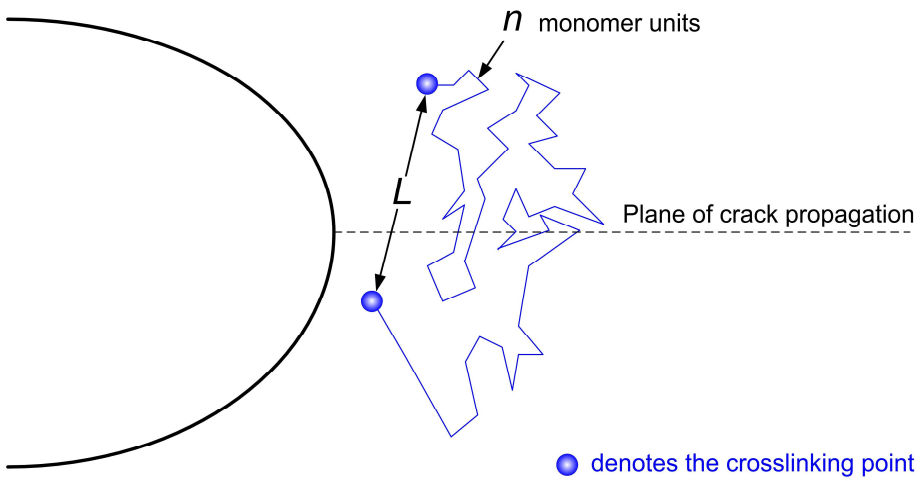

Figure 2.23: Schematic diagram depicting a polymer molecular chain lying across the plane of crack growth. *L* is the distance between adjacent crosslinks which is a function of the length of a monomer unit ξ and the number of monomer units between the crosslinks *n*. (Adapted from Lake and Thomas 1967).

volume of single carbon-carbon bonds under stress regardless of the effects of side groups and J_b is the elastic strain energy stored by each single bond just before rupture. Substituting $E_0 = bJ_b$ and $d_0 \cong \xi n^{\frac{1}{2}}$ into Equation 2.48 yields

$$T_0 \cong bJ_b \xi n^{\frac{1}{2}} \qquad \text{Equation 2.50}$$

Obviously, from Equation 2.50, T_0 is governed by various fundamental parameters in association with the molecular scale. The estimated value of T_0 which is derived from this theory is approximately 25 J.m^{-2} whereas the experimentally obtained result, which was carried out on the swollen specimens at relatively slow rate of tearing and at relatively high temperature in order to suppress the effect of hysteresis, is approximately 50 J.m^{-2}. The difference in T_0 that is derived by the two approaches is a factor of 2. Lake (1995) suggested that the discrepancy might be attributed to the additional elastic energy losses in the chains linked to those which are broken and the effect of type and degree of crosslink. The rubber containing polysulphide crosslinks tends to provide higher T_0 than mono- or di-sulphide ones. This is, perhaps, because the polysulphide crosslinks have their tendency to rupture more easily under stress resulting in a substantial increase in the number of monomer units between the crosslinks *n* which is directly proportional to T_0 as shown in Equation 2.50.

Andrew (1974) proposed the generalised relationship between the tearing energy T and the threshold value T_0 as shown in Equation 2.51.

$$T = T_0 \Phi (r_c, \text{temperature}, \varepsilon_0) \qquad \text{Equation 2.51}$$

where Φ is a loss function whose value depends on the crack growth rate r_c, the temperature, and the overall state of strain ε_0 in the material. The loss function Φ reduces to unity for a perfectly elastic material.

Andrews and Fukahori (1977) experimentally investigated the dependence of tearing energy T on the threshold tearing energy T_0 and the loss function Φ, as given in Equation 2.51, for four highly deformable materials, namely styrene-butadiene rubber, ethylene propylene diene rubber, plasticised polyvinyl chloride, and low density polyethylene. In their study, the tearing energy was determined directly from the crack propagation experiments and the loss function was obtained from the measured strain distribution around the propagating crack. The value of the threshold tearing energy was derived using the microscopic parameters in relation to the molecular structure of the material investigated. They found that the results showed a good agreement between experiment and theory.

2.4.5 Types of tearing

Figure 2.24 shows the typical tearing force-time curves for different types of crack growth. Curve (a) denotes small fluctuations of tearing force with rate. The tearing is generally straight and the fracture surfaces are fairly smooth as shown in Figure 2.25 (a). Curve (b) denotes marked fluctuations of tearing force with rate. The tearing path is tortuous and the torn surfaces are rough and irregular as shown in Figure 2.25 (b). For stick-slip tearing, curve (c), the tearing does not propagate continuously but rather arrests and reinitiates at fairly regular intervals. This would result in a more pronounced fluctuation of the tearing force with the rate of propagation. The torn surface appears to have both smooth and rough regions as shown in Figure 2.25 (c). The rough surface corresponds to the stick period where the force is building up, and the smooth surface corresponds to the propagation of the tearing.

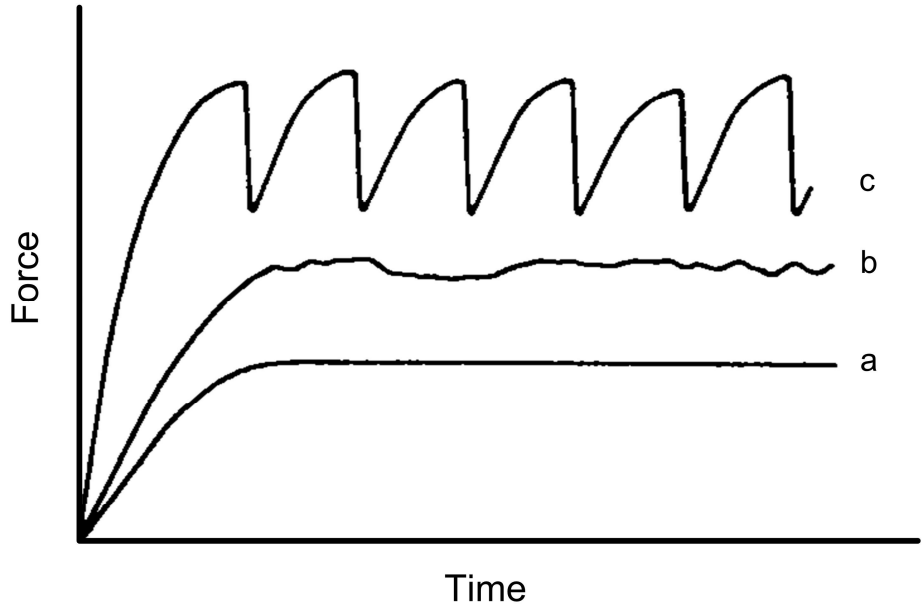

Figure 2.24: Schematic tearing force-time curves for constant rate of extension of the specimen: (a) and (b) steady tearing; (c) stick-slip tearing (Greensmith and Thomas 1955).

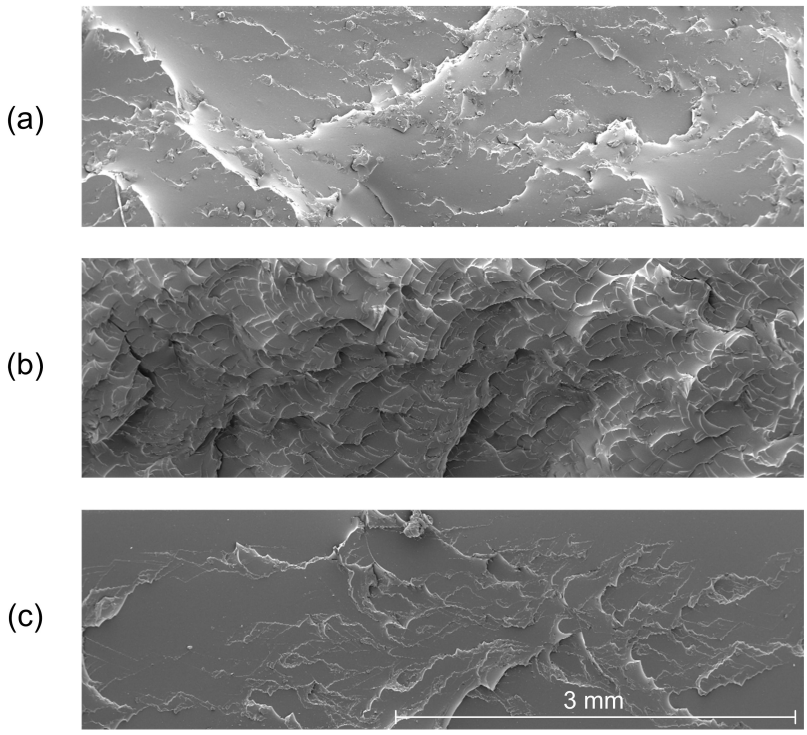

Figure 2.25: Fracture surface of rubber vulcanisates: (a), (b) steady tearing, and (c) stick-slip tearing.

2.4.6 Dependence of tearing energy on crack growth rate

Greensmith and Thomas (1955) provided in-depth analysis of the work of Rivlin and Thomas (1953), that was based on an energetic approach, so as to find a relationship between the tearing energy and the tearing rate. In their analysis, by the selection of a suitable specimen as shown in Figure 2.26, they suggested that if the width of the specimen *w* was sufficiently large relative to the thickness *t*, then an extension in the legs of the specimen could be ignored (an extension ratio $\lambda \approx 1$), the tearing was considered to be continuous with the propagation rate. Thus, if the crack length increases by d*c*, the separation *l* of the clamps is increased by

$$\mathrm{d}l = 2\lambda \mathrm{d}c \qquad \text{Equation 2.52}$$

where λ is the extension ratio in the legs of the test specimen. Equation 2.52 can be related to the rate of separation of the clamps S_c by

$$S_c = \frac{\mathrm{d}l}{\mathrm{d}t} = \frac{2\lambda \mathrm{d}c}{\mathrm{d}t} \qquad \text{Equation 2.53}$$

Equation 2.53 can be simplified as

$$\frac{\mathrm{d}c}{\mathrm{d}t} = \frac{S_c}{2} \qquad \text{Equation 2.54}$$

where d*c*/d*t* is the rate of crack propagation and S_c is the crosshead speed of the test machine. This approach can be used correctly to characterise the tearing of rubber when the rate is steady as is often observed with an unfilled and non-crystallising rubber such as styrene-butadiene rubber (SBR). During steady tearing, the rate of propagation essentially remains constant once the tearing has commenced. Figure 2.27 shows the plot of the crack growth rate d*c*/d*t* which is approximately half of the crosshead speed according to Equation 2.54 against time *t*. Obviously, the d*c*/d*t* remains constant until the rubber has been completely ruptured. However, for a lot of rubber materials such as strain-crystallising rubber like natural rubber (NR) or with rubbers filled with reinforcing fillers such as carbon black the rate of tearing is no longer steady. Although this framework is not quantitatively valid for stick-slip tearing behaviour where the tearing rate is inconsistent with the tearing force in the sense that there are fluctuations between

the zero and rapid rate of tearing, it can still be regarded as a parameter with some indication in association with the dependence of tear energy on the rate of crack propagation.

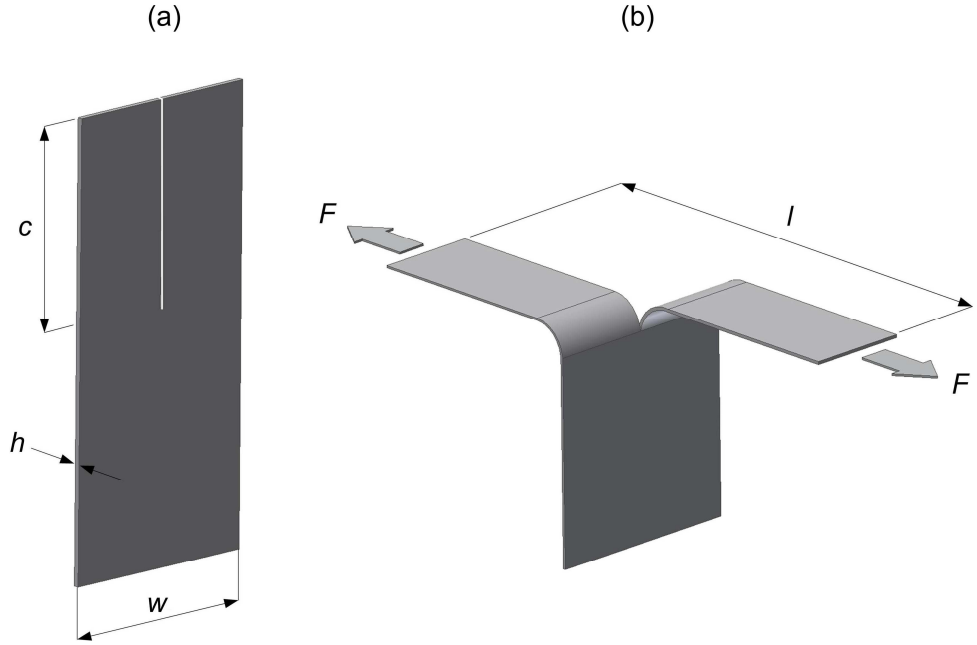

Figure 2.26: Trouser tear specimen: (a) undeformed; (b) extended.

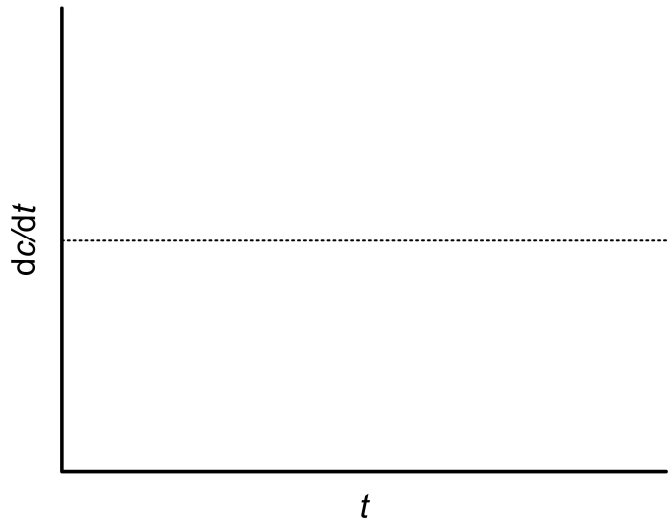

Figure 2.27: A plot of the crack propagation rate d*c*/d*t* against time *t* of the steady tearing behaviour under the framework which is governed by the constant rate of the clamp separation.

Kadir and Thomas (1981) investigated the crack propagation of rubber vulcanisates, namely NR, SBR, BR, and NBR over a wide range of rates using the pure shear

crack growth specimens. The tearing rate was derived from the amount of time that it took for the crack tip to pass the reference marks on the specimen. The data which are the plots of tearing energy as a function of tearing rate are shown in Figure 2.28. Building on the data as derived from Figure 2.28, interestingly, the relationship between the crack growth rate and the tearing rate can be generalised into three distinctive regimes in association with the patterns of fracture surface: rough, stick-slip and smooth tearing as shown schematically in Figure 2.29.

In the low crack growth rate, regime A, with tearing rates of less than 0.1 $mm.s^{-1}$, the cracks propagate in a relatively steady manner where the torn surfaces appear to be very rough. The degree of roughness tends to decrease with increasing rates. In regime B, stick-slip behaviour, the very large changes in instantaneous rate are marked between the stick and slip states. The average value of crack growth rate has little significance to tear energy. Conversely, at fast crack growth rate of more than 10 $mm.s^{-1}$ in regime C, crack growth occurs at a noticeably constant rate. The fracture surface is very smooth, reminiscent of a glassy fracture surface.

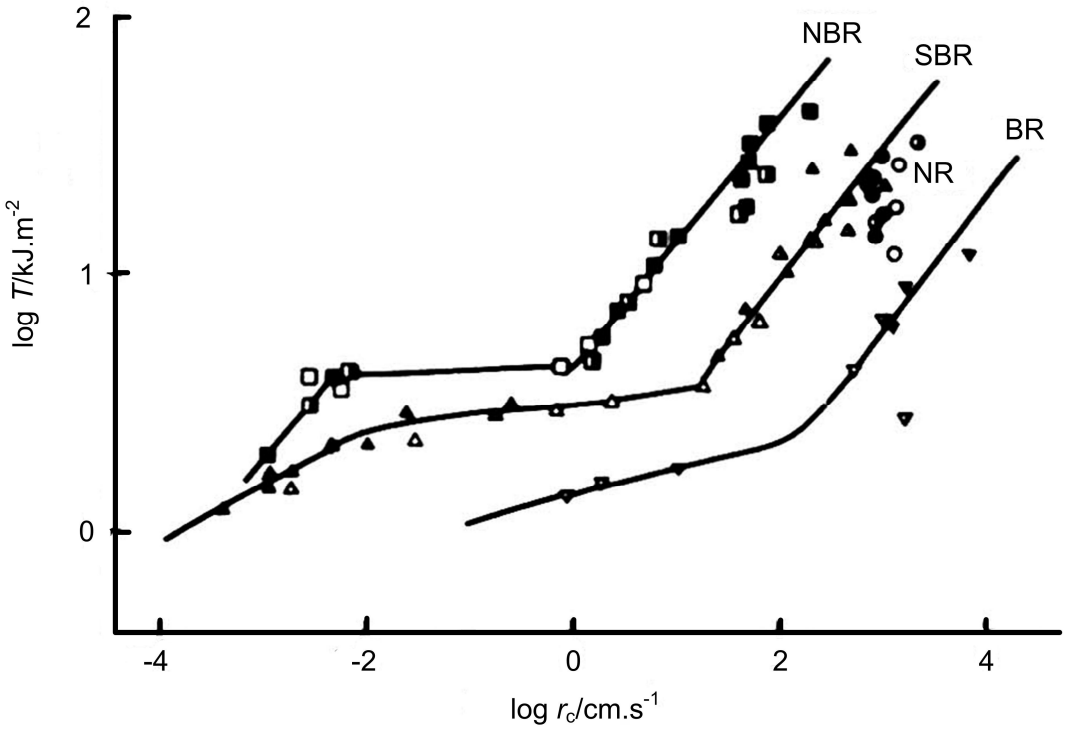

Figure 2.28: Tearing energy is a function of tearing rate for NBR, □, ■; SBR, △, ▲; NR, ○, ●; BR, ▽, ▼. The length of the specimen between the clamps in the undeformed state were 2.0 and 4.0 cm (Kadir and Thomas 1981).

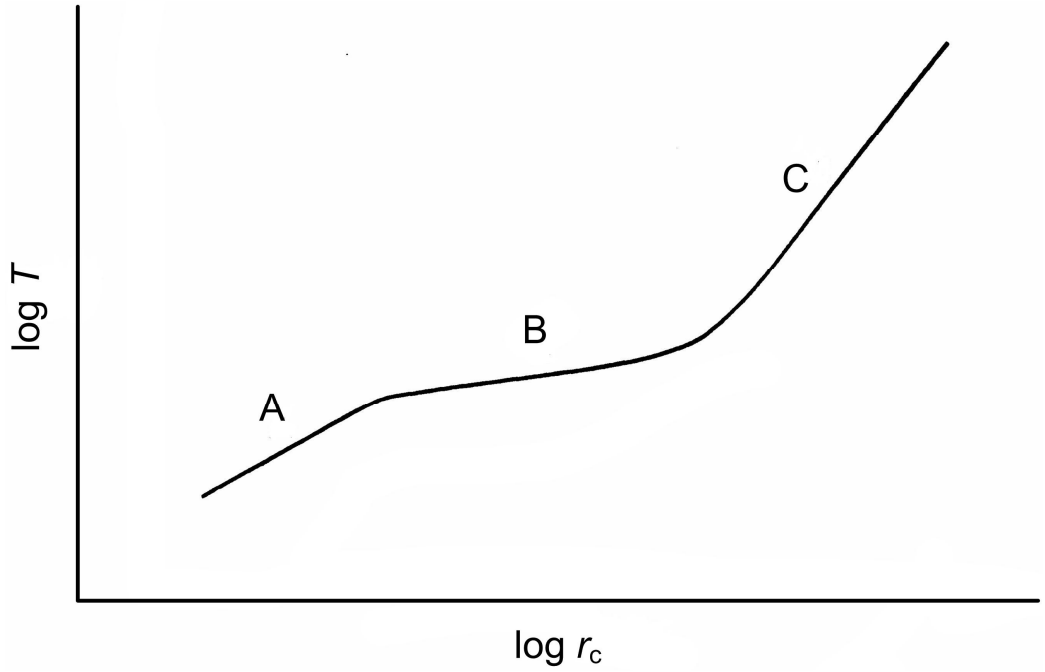

Figure 2.29: Schematic diagram illustrating the relationship between the tearing energy and the tearing rate of rubber vulcanisates in accordance with the profile of the fracture surfaces: A = rough surface; B = stick-slip behaviour; and C = smooth surface (Kadir and Thomas 1981).

Tsunoda et al. (2000) investigated the relationship between the tearing energy and the tearing rate of SBR vulcanisates in more detail using the pure shear crack growth and the trouser tear specimens which were subjected to various testing conditions included: the effect of a swelling liquid; the effect of carbon black content under swollen condition; and the effect of crosslink density. They found that the relationship between the tearing energy and the consequent crack growth rate is of the form illustrated in Figure 2.29 for most of the materials studied.

Hamed and Hiza (2010) studied an effect of tearing rate on a model natural rubber tyre belt vulcanisates using a modified trouser tear specimen with a lengthwise groove on both sides located in the middle of the specimen, as illustrated in Figure 2.30, in order to provide a path for crack growth. Tests were carried out using a tensile testing machine with the crosshead speeds of 5 and 500 mm/min. In this study, the tearing behaviour of the carbon black-filled natural rubber vulcanisate which is stick-slip in nature is subdivided into three distinct types based on the characteristics of tearing force and the patterns of fracture surface, namely I_b, II, and III. For the testing rate at 5 mm/min as shown in Figure 2.31, type III tearing was only found. This type of tearing shows a sideways crack, or so-called ‘knot’, which

does not turn and propagate into a leg. The crack develops in the thin region of the groove for several millimetres before arresting.

Figure 2.32 shows the plot of tearing force as a function of the clamp displacement (equivalent to the crosshead distance) at the speed of clamp separation of 500 mm/min. In this test condition, three types of tearing were observed. With reference to Figure 2.32, type II tearing exhibits sideways crack growth within the leg and then turns to the thin region of the groove as seen by a drop in tearing force. Type I_b is represented by a saw tooth fracture pattern with the development of the crack growth entirely within thin region.

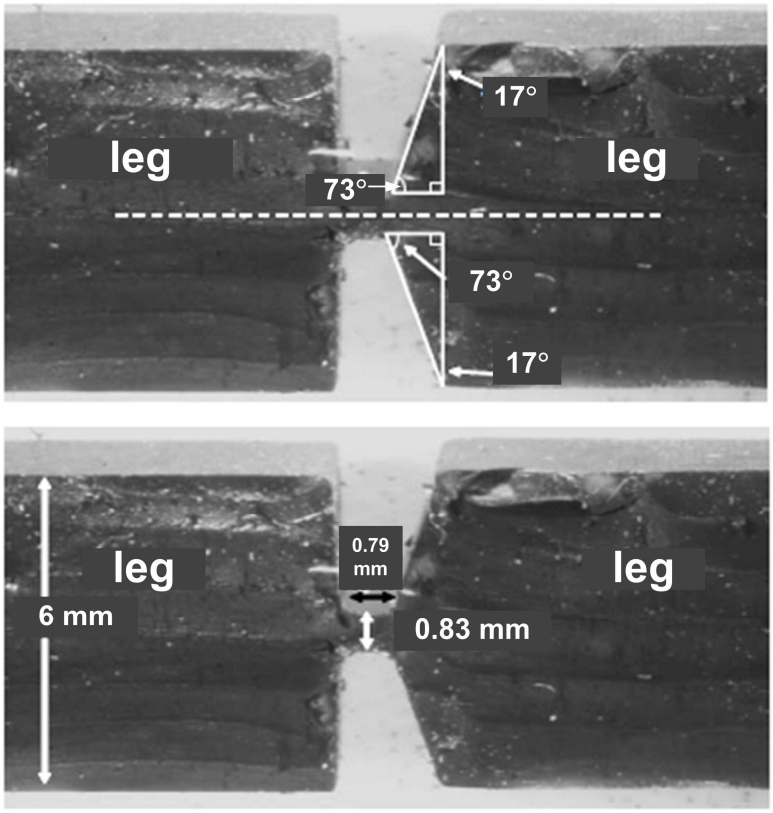

Figure 2.30: Cross-section of a modified trouser tear specimen (Hamed and Hiza 2010).

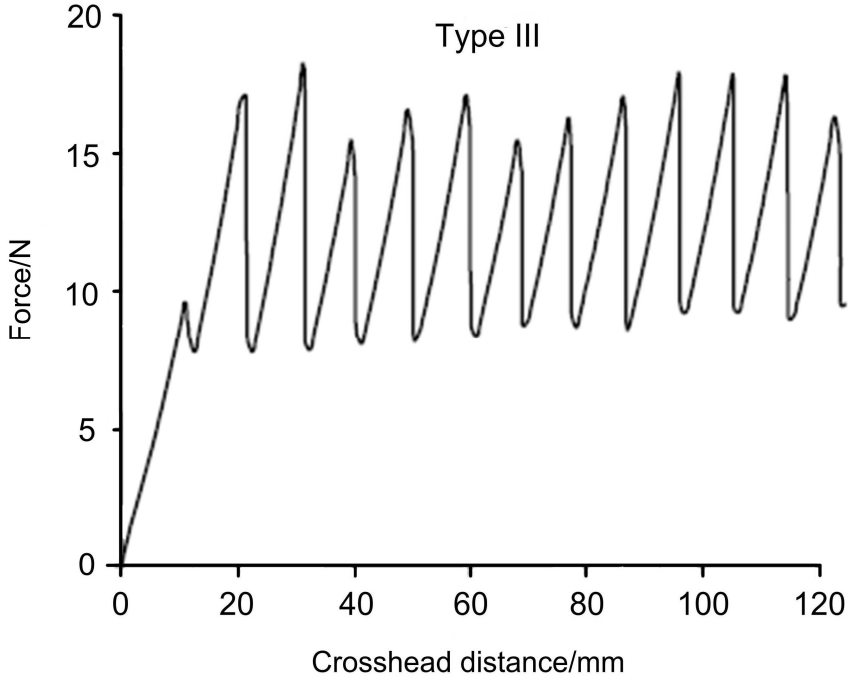

Figure 2.31: Tearing force of a modified trouser tear specimen with type III tearing. The test was carried out at a crosshead speed of 5 mm/min (Hamed and Hiza 2010).

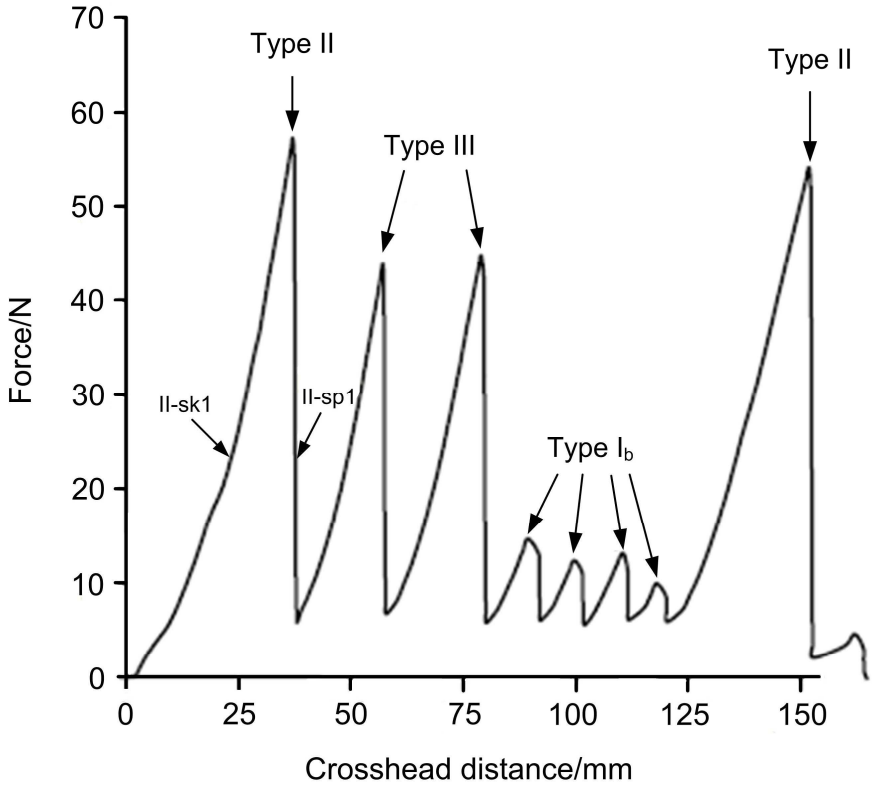

Figure 2.32: Tearing force of a modified trouser tear specimen at a crosshead speed of 500 mm/min. II-sk1 represents an increase in tearing force due to the crack propagation into and within a leg. II-sp1 denotes a decrease in tearing force as the crack returns to the thin region and grows forward (Hamed and Hiza 2010).

2.4.7 Dependence of tearing energy on crack growth rate and temperature

The magnitude of tear energy depends on both the crack growth rate and temperature. These effect are best described by 3-dimensional plots of tearing energy versus tearing rate and temperature (Greensmith et al. 1960) as shown in Figure 2.33 (a) and (b), and Figure 2.34 for unfilled SBR, unfilled NR and carbon black-filled SBR respectively.

In the case of the unfilled SBR, Figure 2.33 (a), the tearing energy increases with increasing crack growth rate and decreasing temperature. This reflects the dominant influence of the viscoelastic energy dissipation. In the case of the strain crystallising rubber NR, Figure 2.33 (b), the dependence of tearing energy on crack growth rate and temperature becomes less observed. This might be associated with strain-induced crystallisation whose effect on crack growth behaviour outweighs the effect of the viscoelastic component. However, a noticeable behaviour appears at relatively low temperatures (about -20 °C) and high speeds that it might be supposed that crystallisation does not develop rapidly enough to exert its full effect. In the case of the carbon black-filled SBR, Figure 2.34, a flat plateau is observed at low crack growth rates and low temperatures. This flat plateau represents a large increase in the tearing energy over the unfilled material and it is associated with knotty crack growth. Outside this range, where knotty crack growth does not exist, the carbon black filler causes a relatively small increase in tearing energy compared to that of unfilled SBR. This suggests that the development of knotty crack growth depends not only on the crack growth rate but also on temperature. This plot also indicates a complex crack growth phenomenon in reinforced rubbers associated with viscoelastic energy dissipation and strength anisotropy at the crack tip.

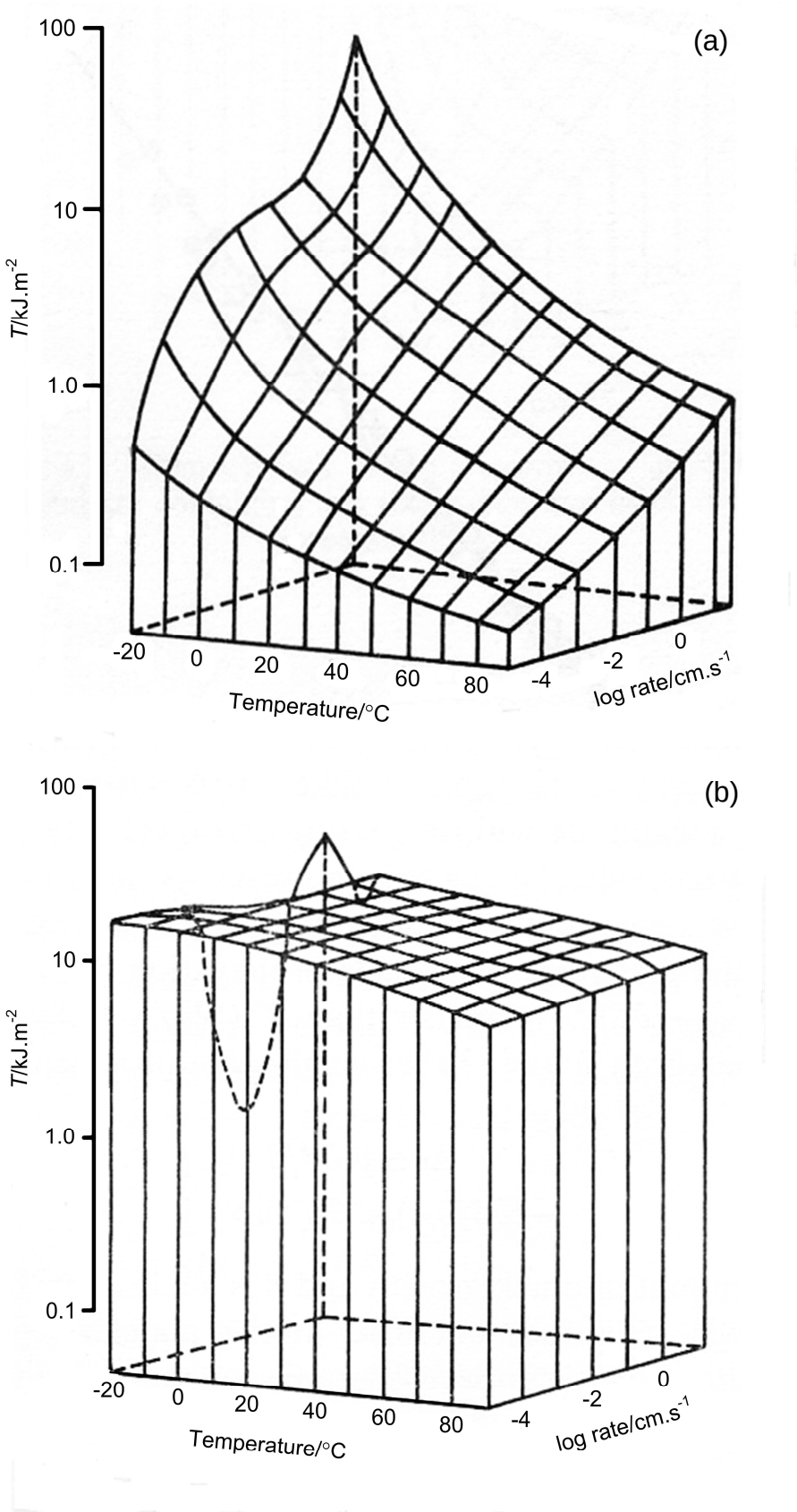

Figure 2.33: The effect of crack growth rate and temperature on tear energy for (a) unfilled SBR, (b) unfilled NR (Greensmith et al. 1960).

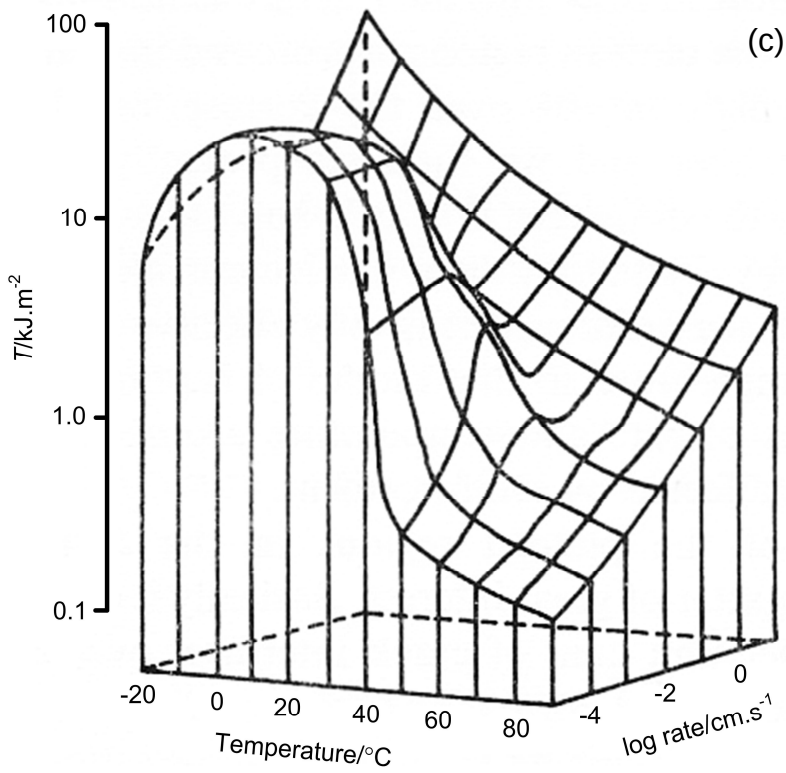

Figure 2.34: The effect of crack growth rate and temperature on tear energy for FT carbon black-filled SBR (Greensmith et al. 1960).

2.4.8 Dependence of tearing energy on crosslink system

The tearing energy of rubber is dependent not only on its molecular structure but also on the concentration and types of crosslink. Brown, Porter and Thomas (1987) investigated the effect of vulcanising system on the tearing energy in natural rubber. In their study, they used the isomerised natural rubbers which were vulcanised with various vulcanising systems to obtain the different types of crosslink, namely monosulfidic, polysulfidic, and carbon-carbon crosslink. The isomerised natural rubber was employed with the intention to avoid the strengthening effect due to strain induced crystallisation typically found in ordinary natural rubber. The results are shown in Figure 2.35 where tearing energy is plotted against shear modulus which represents the stiffness of rubber vulcanisates in relation to the crosslink density. The tearing energy T decreased with increasing G for each of the three vulcanising systems. The observed ranking of the tear strength was polysulfidic > monosulfidic > peroxide curing system. This decreasing order of strength seemed to follow an increase in the bond strength of the crosslink based on chemical evidence (Brown et al. 1987). This is somewhat counter-intuitive at first sight in that

the strongest crosslink creates the weakest vulcanisates. But clearly weak crosslink can yield more readily. In another major study, Yanyo (1989) investigated the effect of the chemical nature of crosslinks on the fatigue crack growth of filled natural rubber. In his experiment, the amount of accelerator to sulphur was adjusted to alter the ratio of monosulfidic to polysulfidic crosslinks. Carbon-carbon crosslinks were generated using a peroxide curing system. It was found that the polysulfidic networks exhibited the slowest crack growth rate at a given tearing energy. The specimen with mainly monosulfidic crosslinks also appeared more resistant to crack growth than the peroxide cured specimen. A possible explanation for this might be that under cyclic deformation the molecular network chains are alternately stretched and relaxed. The degree of free mobility of chain segments depends on the structure of the crosslinks. That is the longer the crosslinks, the easier it is for individual chains to move rather than break when the rubber is subjected to the applied stresses. The polysulfidic crosslinks, a type of crosslink which the number of sulphur atoms for each crosslink formed ranges from 10-15 atoms, may provide this flexibility and hence improve the fatigue life.

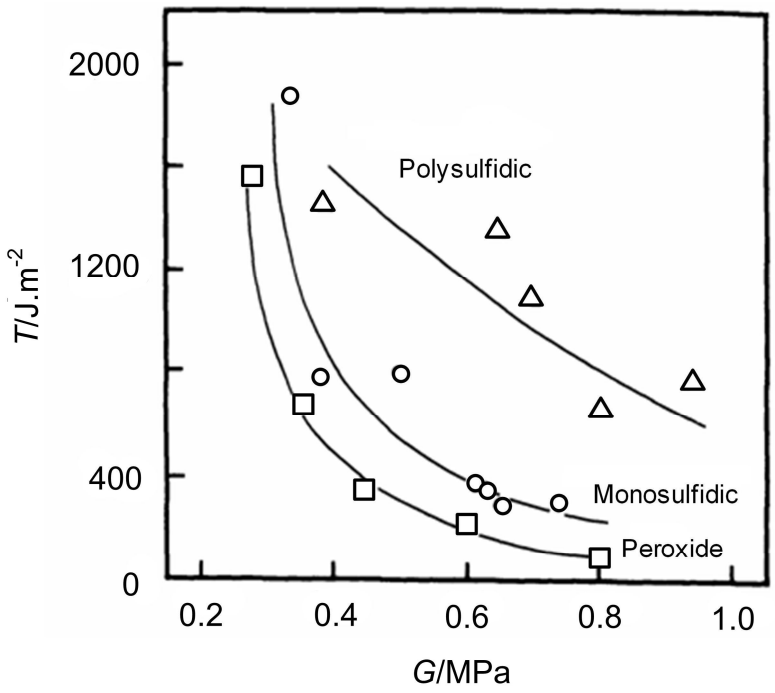

Figure 2.35: The effect of the vulcanizing system and crosslink density on the tearing behaviour for unfilled isomerised NR at a crack growth rate of 10 μm.s^{-1} (Brown et al. 1987).

2.4.9 Dependence of tearing energy on strain crystallisation

Some rubbers such as natural rubber (NR) and polycholoroprene rubber (CR) are strain-crystallisable because they are made up of a regular repeating unit that is capable of producing a certain degree of molecular orientation under strain. The crystallisation induced by extension is temporary and disappears as soon as the straining is removed. The strain crystallisation forms in highly extended regions such as in the crack tip region. No crack propagation occurs in strain crystallising rubber until the stresses is built up sufficiently to produce an abrupt (catastrophic) rupture; see Figure 2.36 (Persson et al. 2005). Styrene-butadiene rubber (SBR) does not exhibit strain crystallisation and therefore is intrinsically inferior to natural rubber in terms of the mechanical properties such as crack growth resistance and tensile properties.

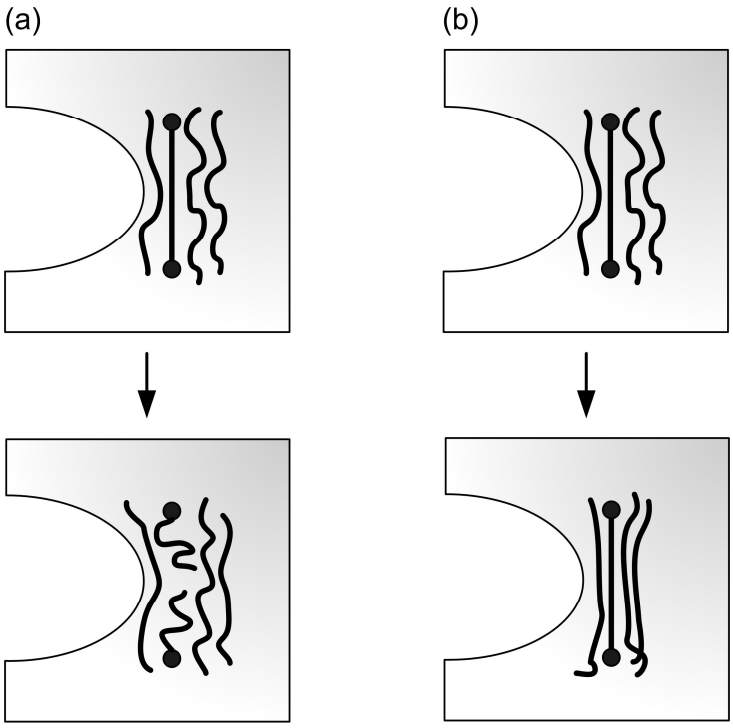

Figure 2.36: The bond-breaking process at a crack tip in a rubber undergoing strain crystallisation (b), and in a rubber where no strain crystallisation can occur (a). Because of the inhomogeneous nature of rubbery materials, the different polymer chains at the crack tip will be stretched to the break-limit at different times. For a rubber which undergoes strain crystallisation (b), the chains in the vicinity of a fully stretched chain will adhere in a commensurate way to the stretched chain, thus strengthening the weakest link. This will result in a strong enhancement in the (average) stress at the crack tip necessary for the onset of crack propagation (Persson et al. 2005).

A study on the morphological feature of the crystallisation around the strained crack tip in natural rubber with a crack length of 0.5 and 1.0 mm by X-diffraction found that a crystallised zone at the crack tip was initially observed at the extension ratio λ in the bulk far removed from the crack tip as relatively low as 1.3. The amount of this region was linearly dependent on the extension ratio and related to the initial cut length as shown in Figure 2.37 and Figure 2.38 respectively (Trabelsi et al. 2002).

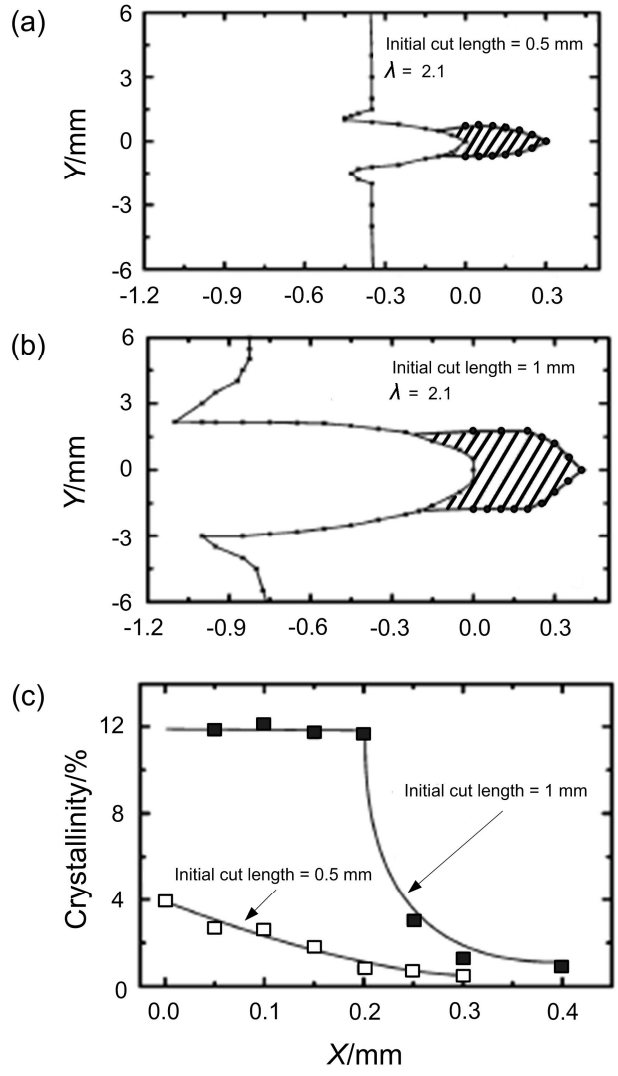

Figure 2.37: Dimensions of the crystalline deformed zones (hatched area) at the crack tip of NR with the crack length of 0.5 mm (a), 1 mm (b), and (c) percentage of crystallinity against the distance from the crack tip *X* along the crack propagation direction for the two specimens in Figure (a) and (b). (Trabelsi et al. 2002).

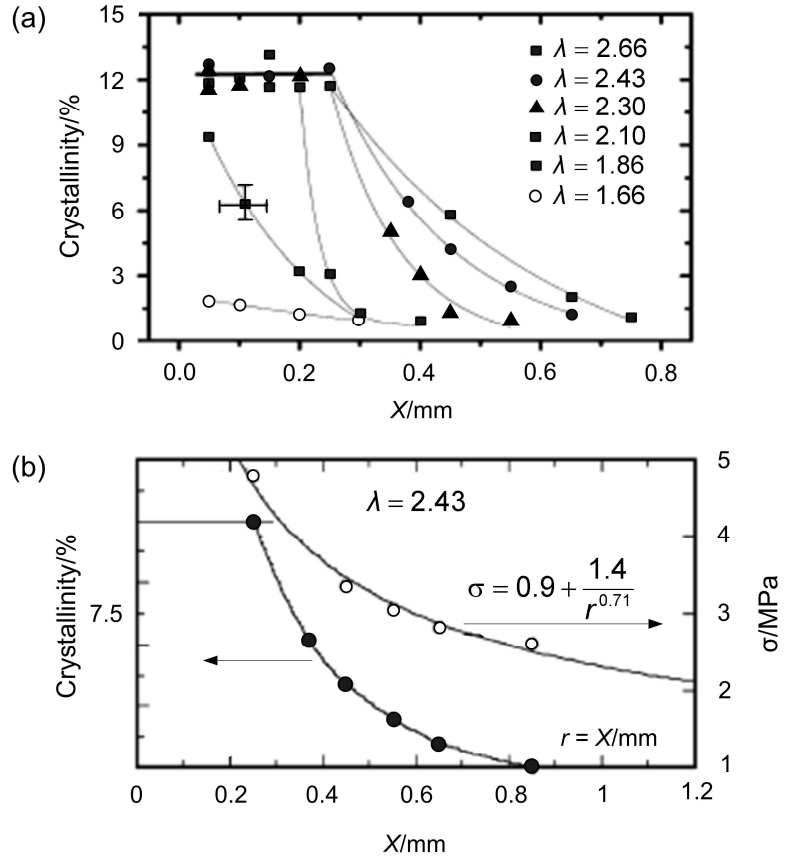

Figure 2.38: (a) The percentage of crystallinity as a function of the distance from the crack tip *X* along the crack propagation direction for various extension ratios and (b) the relationship between the percentage of crystallinity (filled circle) and local stress (plain circle) in the vicinity of the crack tip at λ = 2.43 (Trabelsi et al. 2002).

Interestingly, the formation of the plateau of crystallinity was observed in Figure 2.37 (c) and Figure 2.38 (a). They concluded that this could be associated with a critical cut length and a critical extension ratio.

A recent study on a real-time development of crystalline structures induced by deformation in natural rubber with different degrees of crosslink using simultaneous synchrotron X-ray diffraction revealed that the initial stage of the development of strain crystallisation was almost independent of the network-chain densities and the time for the crystal growth was shorter in the specimen with the higher crosslink density. Additionally, in the stretching process, the lateral crystallite size was smaller in the specimen with the larger crosslink density. From this experiment, the crystallisation model was proposed as shown in Figure 2.39 (Tosaka et al. 2004).

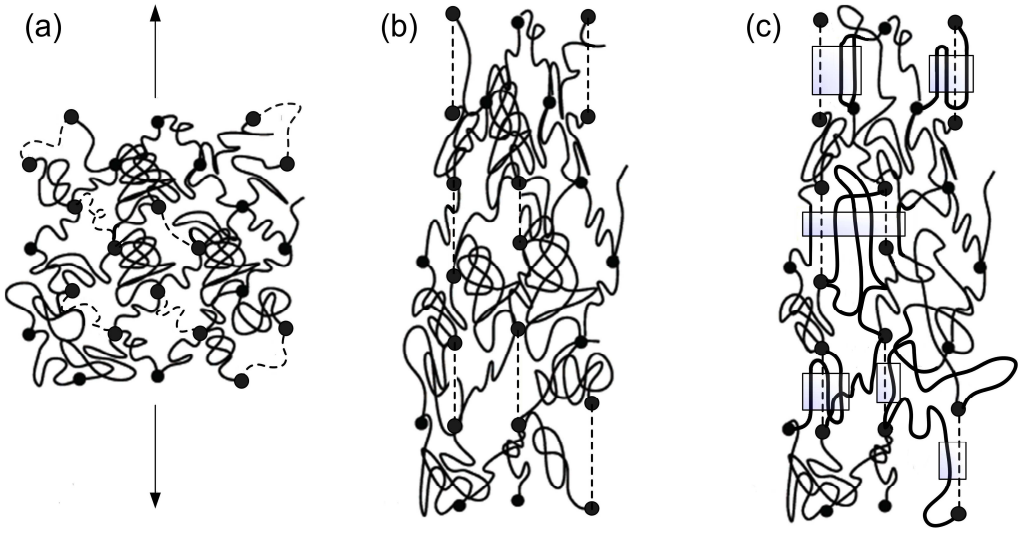

Figure 2.39: Model of nucleation and crystallisation in vulcanised natural rubber. Relatively short chains are drawn as dotted lines. Filled circles represent crosslinks. (a) Before deformation: crosslinks are distributed uniformly. (b) After deformation: short chains are fully stretched. Note that the distribution of crosslinks is no longer uniform to keep many network chains in the random-coil-like state. (c) The fully stretched chains act as nucleus of crystallites (in □). (Adapted fromTosaka et al. 2004).

Gent et al. (1998) investigated the effect of strain induced crystallisation on the tearing energy as a function of tear rate of natural rubber (NR) and synthetic *cis*-1,4-polyisoprene (IR) vulcanised with dicumyl peroxide (DCP). In their experiment, they employed the strip specimens which were modified by adhering two closely-spaced lengths of fibre-reinforced tape to their surfaces so as to constrain the tear path to propagate along the central line and to suppress the extension of the torn portions caused by the tearing force. The investigation was carried out at various tearing rates derived from one half of the crosshead speed. A marked difference in the tearing energy of both materials was observed at the highest tear rate, about 0.1 m/s, as shown in Figure 2.40. They concluded that IR crystallised more slowly than its natural counterpart. This was reflected in a lower tear strength. Moreover, there have been several factors that might be attributed to a reduced degree of crystallisation by straining in IR, namely chain irregularities in the synthetic molecules (Schoenberg et al. 1979), lack of crystal nucleation catalysts such as stearic acid (Gent 1954) and absence of synergistic interactions between fatty acid and an ester group normally found near one end of the NR molecule (Nishiyama et al. 1996).

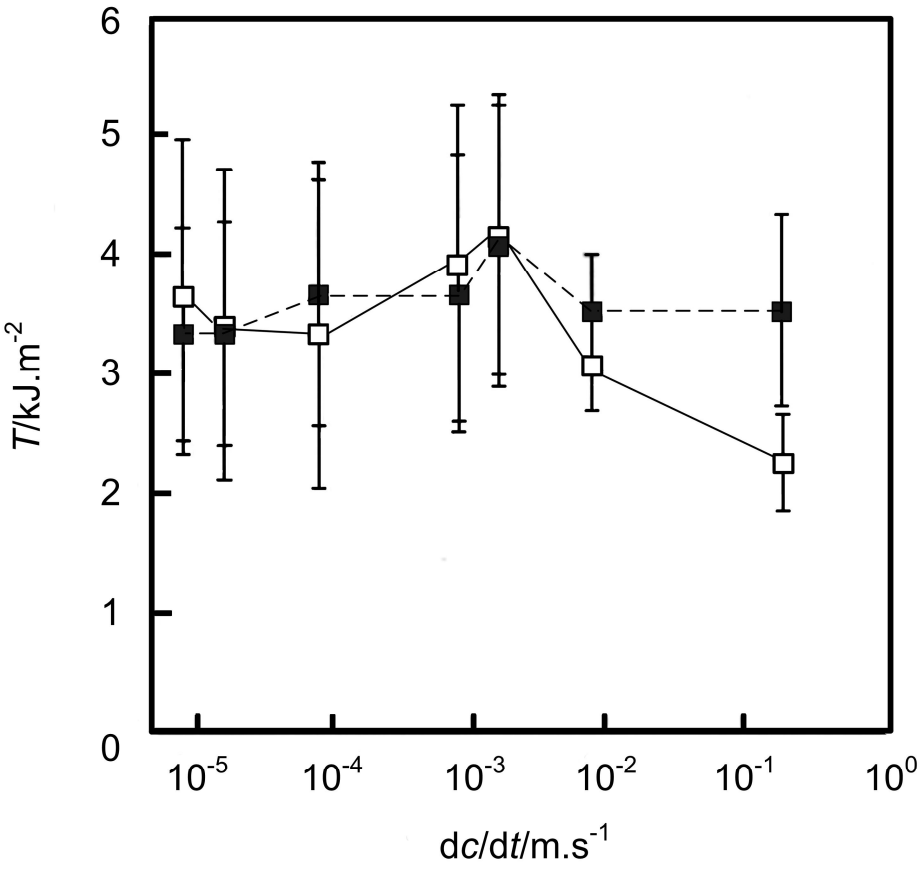

Figure 2.40: Tearing energy at room temperature against rate of crack growth for NR (filled symbols) and IR (open symbols) crosslinked with 2% DCP (Gent et al. 1998).

Persson et al. (2005) proposed the schematic diagram of the tearing energy *T* as a function of the crack tip velocity v_c for strain crystallising and non-strain crystallising rubbers as shown in Figure 2.41.

For non-strain crystallising rubber, the magnitude of *T* depends strongly on the crack tip velocity in a manner which follows the viscoelastic effect. In the case of strain crystallising rubber, the value of *T* falls abruptly over a certain range of the crack tip velocity because there is less time for crystallisation to develop at higher rates of deformation. After passing a minimum, the value of *T* resumes increasing in the same manner as observed in non-strain crystallising rubber.

Obviously, so far, studies on the tearing behaviour of rubber in relation to the rate of tearing have been built on the rate of the crosshead displacement of the test machine and no attention has been paid to experimentally investigate the effect of

the rate of the development of crystallisation on the tear strength of rubber under rapid tearing.

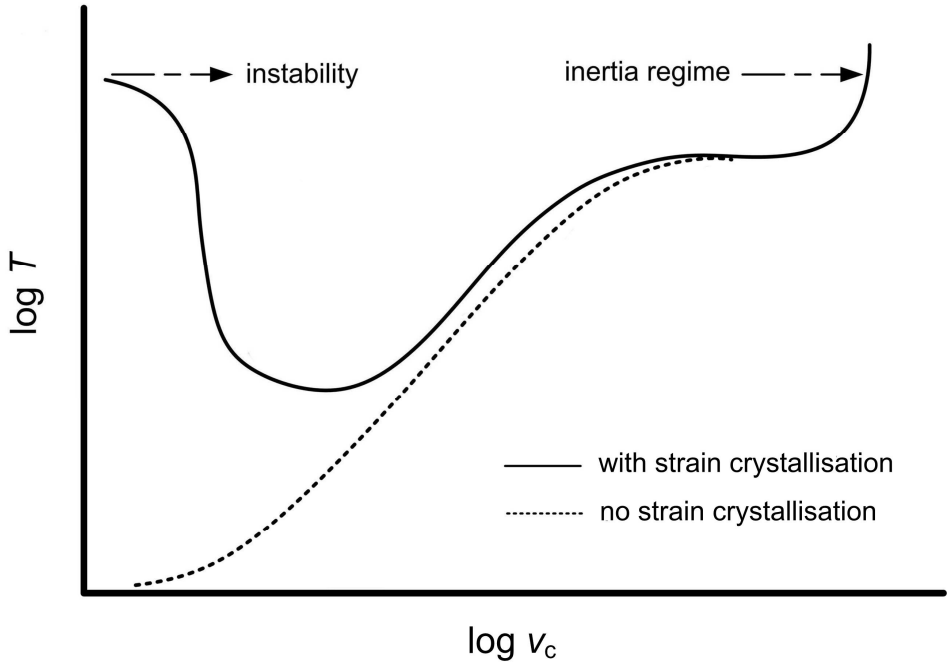

Figure 2.41: Tearing energy *T* as a function of crack tip velocity v_c for a rubber which undergoes no strain crystallisation, and for a rubber which strain crystallises (Persson et al. 2005).

2.5 Rapid fracture in rubber

Although most of the significant information on the fracture of rubber is provided by investigation on macroscopically steady fracture propagation by suitable adjustment of the boundary conditions such as that undertaken by Greensmith and Thomas (1955) in controlling fracture speed and investigating the variation in energy consumption related to the characteristic energy for tearing with the rate of propagation, several studies have also been made on high speed fracture.

Albertoni (1937) utilised an impact tester with a modified pendulum hammer to determine the work done to stretch a rubber ring specimen at high strain rate up to 80 sec^{-1}. In testing, the specimen is extended to a pre-determined elongation by the pendulum which is equipped with an engaging system to engage and release the specimen when the pendulum is near or at the bottom of the fall. The difference in the height, between the point at which the pendulum is dropped and that at the other side of the stroke, is a function of the strain energy to break or stretch the specimen.

Roth and Holt (1935) used an in-house falling weight, as shown in Figure 2.42, to achieve a high strain rates. A ring-shaped specimen was stretched at a non-uniform rate up to 20 sec^{-1} to the point of rupture. The stress-strain curves obtained from the relatively high speed testing is above that for slow speed testing. However, at very high strain, the curves sometimes approach or cross each other. They explained this effect might be due to an increase in the temperature when the rubber is stretched rapidly.

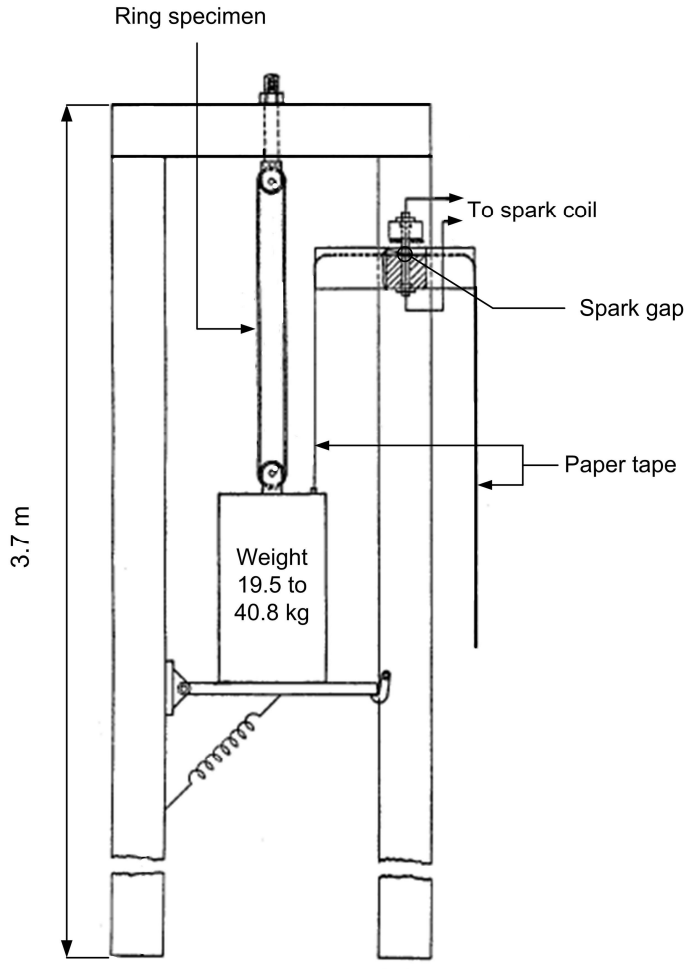

Figure 2.42: A falling weight apparatus. A ring specimen is extended to rupture by the falling weight which is attached to a paper tape being pulled through a spark gap. The distance between the holes in the paper tape, produced by the spark as it passes through the gap, is related to the average speed of the weight (Roth and Holt 1940).

Villars (1950) investigated the tensile properties of various kinds of filled and unfilled vulcanisates stretched at a strain rate between 100-3000 s^{-1} using a pin attached to the circumference of a rotating wheel to strike the middle enlarged part of a dumbbell specimen hanging in the form of a loop. This test was developed

especially to examine the tensile strength of strain crystallising rubbers, the test results tend to decrease to a minimum with increasing strain rate up to about 100 s^{-1} and then finally it rises again.

Mason (1958) examined the tearing behaviour of rubbers at a speed approaching the speed of sound in the rubber sheet. For a high speed fracture to be produced, the rubber specimen, approximately 25 cm long and 1 mm thick, was firmly clamped on its two major edges with an initial grip distance of about 1 cm as shown in Figure 2.43. By increasing this distance uniformly, the specimen could be extended to the required extent in a state of pure shear. Fracture was then introduced by cutting into the material at the centre of a free edge. The progress of the crack accompanied by the propagation of transverse stress wave in material was observed by the use of a high speed camera. On a plot of crack length as a function of time, it was found that for both types of rubber, strain and non-strain crystallising, at a certain crack length prior to the end of the test, the contour of the fracture surface varied with the velocity of fracture propagation.

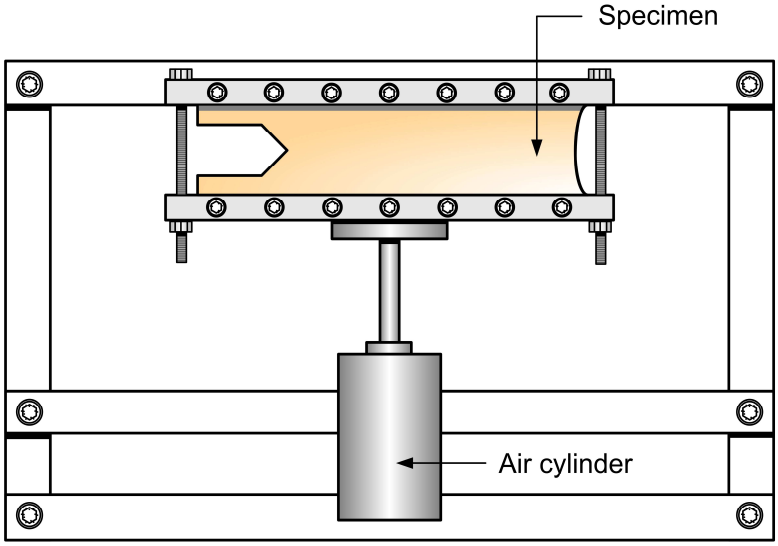

Figure 2.43: Schematic diagram of experimental arrangement for the high speed fracture. (Adapted from Mason 1958).

Greensmith (1960) used a tensometer to study the load-extension curves of filled and unfilled SBR which were extended at various rates from about 0.1 to 2000% per second. In his work, he used a ring specimen that was looped over two small rollers of the tensometer as shown in Figure 2.44. The movement of a main crosshead was powered by a variable speed motor through a chain that was fixed on a pair of

sprocket wheels below the crossheads. The main crosshead was mechanically moved by engaging a pin in the crosshead with the links of the chain. In detecting the deflection of the cantilever spring which was used for measuring the force, a drum camera which was geared to the chain drive was used to record the deflection of the light spot from an optical lever system. Thus, the curve of the force on the ring as a function of the displacement of the crosshead was traced out on the drum camera.

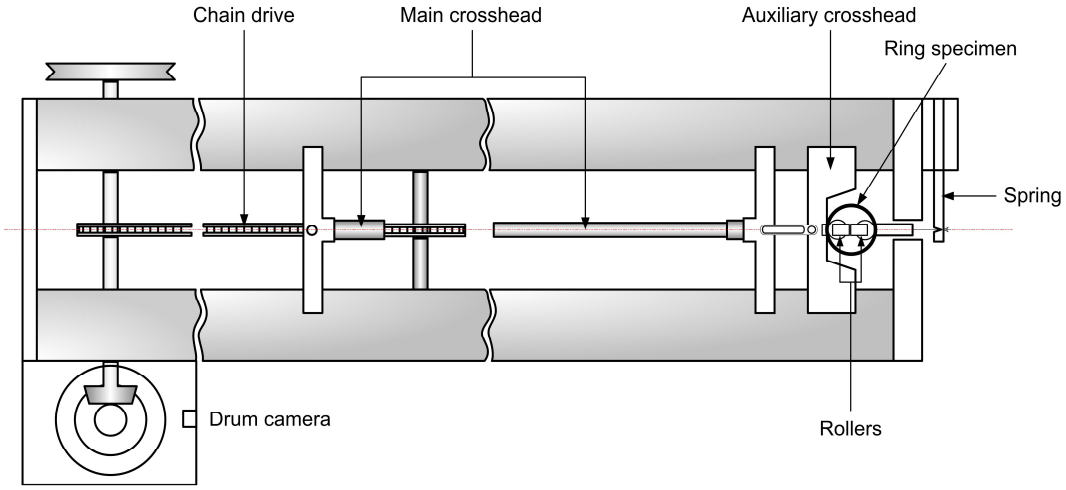

Figure 2.44: Schematic diagram of tensometer. (Adapted from Geensmith 1960).

At the test temperature, he found that the tensile strength of unfilled vulcanisate increased continuously with the rate of extension but the tensile strength of the filled vulcanisate passed through a maximum. These results are shown in Figure 2.45 and Figure 2.46 respectively. He concluded that the effect of the rate of extension on the load-extension curve of the unfilled SBR vulcanisate was as expected from the viscoelastic properties of the material. The occurrence of a maximum in the tensile strength of the filled SBR vulcanisate as the rate of extension was increased indicated that part, at least, of the reinforcing action developed during extension and required a finite time for development and therefore it did not occur at the highest rates of extension. The results for the filled SBR vulcanisate showing that the maximum shifted to higher rates of extension as the temperature was increased, suggested that time required for the development of the reinforcing action decreased as the temperature was increased.

Dannis (1962) developed a different approach using a high speed stress-strain apparatus to measure the strength and elongation of rubber using a falling drop weight down a chimney onto an instrumented specimen carriage.

Stevenson and Thomas (1979) studied the tear behaviour during the bursting of natural rubber balloons under various biaxial strains. Observed retraction (unloading) velocities were consistent with the theoretical predictions based on the static stress-strain curve in biaxial tension. They pointed out that the fracture velocity was determined by the elastic properties of the rubber in a localised region of high strain just around the tip.

Lake et al. (2000) investigated the fracture behaviour of rubbers in the high speed region immediately above a transition region where a change in the nature of fracture occurred using the pre-strained pure shear crack growth and tensile strip (with edge crack) specimens. They found that the fracture energies in this region correlated fairly well with the viscoelastic properties (Figure 2.47), but the potential for strain crystallisation does exist. This is presumably because at the high failure rates, the loading time at the crack tip is insufficient to allow significant crystallisation to occur.

Hoo Fatt and Bekar (2004) studied the tensile properties of unfilled styrene butadiene rubber (SBR) at high speed using a tensile impact apparatus as shown in Figure 2.48 capable of achieving the strain rates ranging from 10-1000 s^{-1}. This apparatus was modified from a Charpy impact tester which was typically used to measure the impact toughness of metals. A pendulum raised to a given height hit a slider bar that connected to two cables. The cables were passed around pulleys and attached to movable guided bases with grips that held opposite ends of the specimen. The tensile force was measured by a load cell at one end of the specimen. The speed of the slider bar was equal to the velocity of the pendulum. From the experiments, they found the three distinct regions of rate-dependent deformation and fracture behaviour of unfilled SBR as shown in Figure 2.49. Region 1, strain rates below 180 s^{-1}, the initial modulus, tensile strength and breaking extension increased as the strain rate increased. Region 2 (between points A and B), between strain rates of 180 and 280 s^{-1}, the initial modulus and tensile strength increased with increasing strain rate but the extension at break decreased with increasing strain rate. Region 3, strain rates greater than 280 s^{-1}, the tensile strength

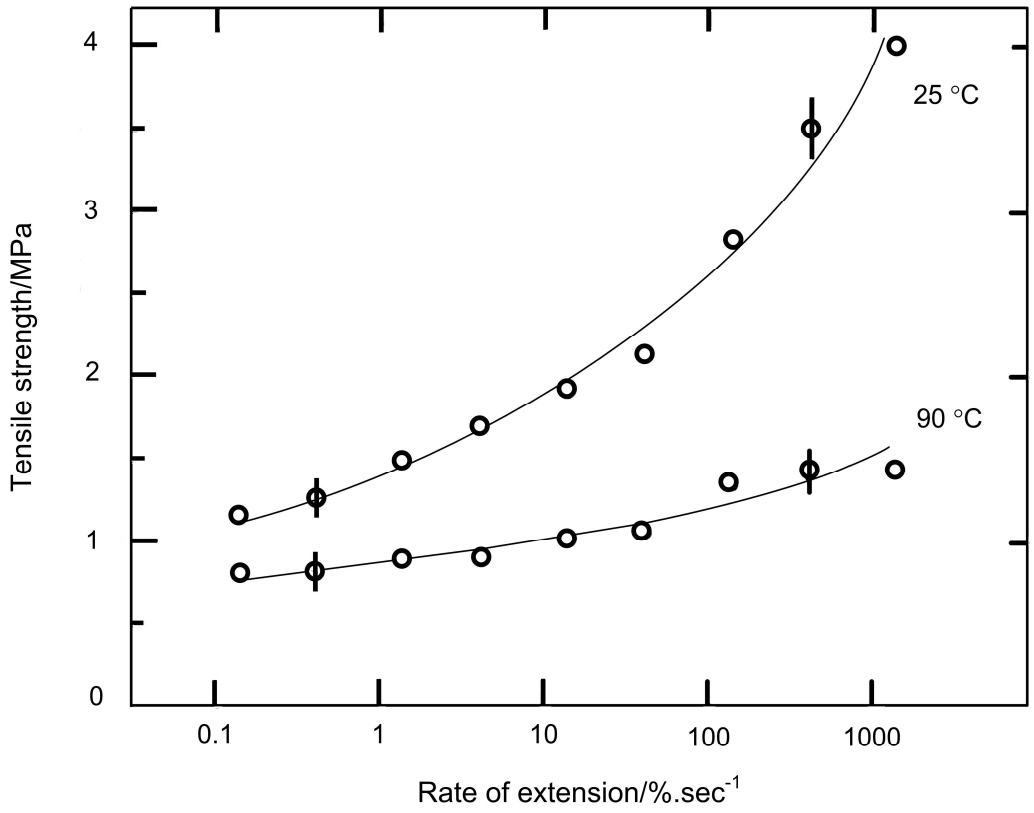

Figure 2.45: Mean values of tensile strength against rate of extension at 25 °C and 90 °C for the unfilled SBR. Vertical bars indicate standard deviation (Geensmith 1960).

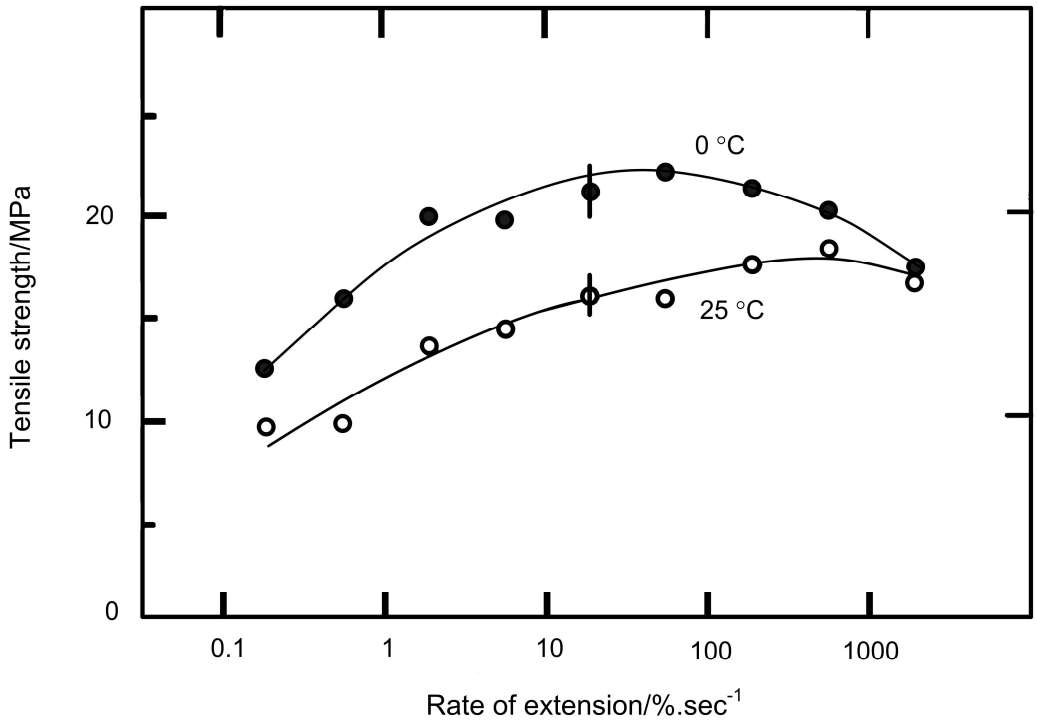

Figure 2.46: Mean values of tensile strength against rate of extension at 0 °C and 25 °C for SBR filled with 50 phr carbon black. Vertical bars indicate standard deviation (Geensmith 1960).

and breaking extension decreased with increasing strain rate while the initial modulus was unchanged. Based on the time scales of the relaxation process regarding the intermolecular slippage accompanying some reversible breaking or

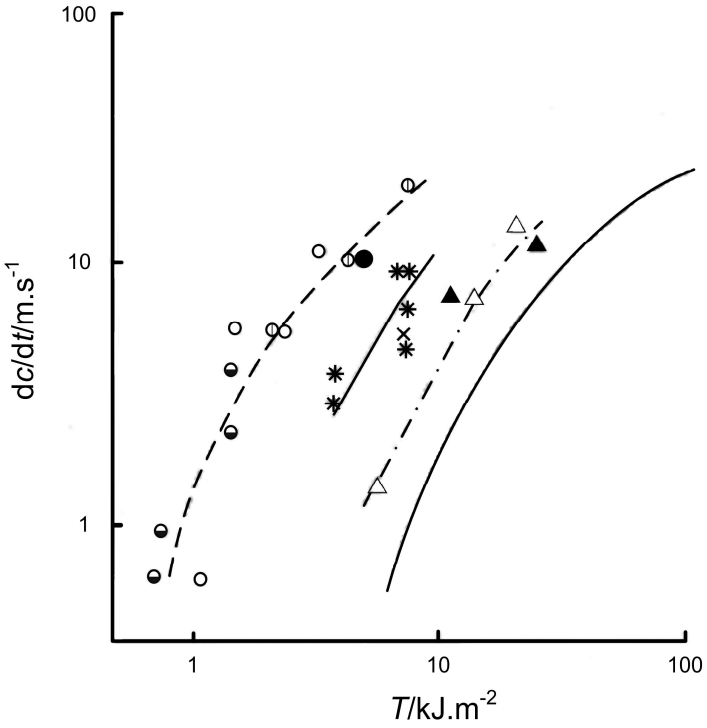

Figure 2.47: Time-dependent crack growth rate d*c*/d*t* plotted against the strain energy release rate *T* in the high speed region for natural rubber (NR) vulcanised with various amounts of dicumyl peroxide (DCP). NR with 1 phr DCP: tensile strip specimens: constant strain rate △; pure shear crack growth specimens: constant strain ▲. NR with 2 phr DCP: tensile strip specimens: constant rate ×; pure shear crack growth specimens: constant rate ∗. NR with 3 phr DCP: tensile strip specimens: constant strain ○, constant rate ϕ; pure shear crack growth specimens: constant strain ●, constant rate ◒. Line for an accelerated-sulphur NR vulcanisate (Lake and Thomas 2000).

swapping of bonds, they concluded that, in Region 1, long-range relaxation involving very slow rearrangement of the convolution with respect to each other was continuously suppressed to occur as the time of the test decreased. In the other words, as the loading rate increases, the time for relaxation processes decreases and some relaxation mechanisms do not occur. In Region 2, none of the long-range relaxation processes occurred during the very short loading times. Region 3, no relaxation existed and deformation could be described by a single stress-extension ratio curve.

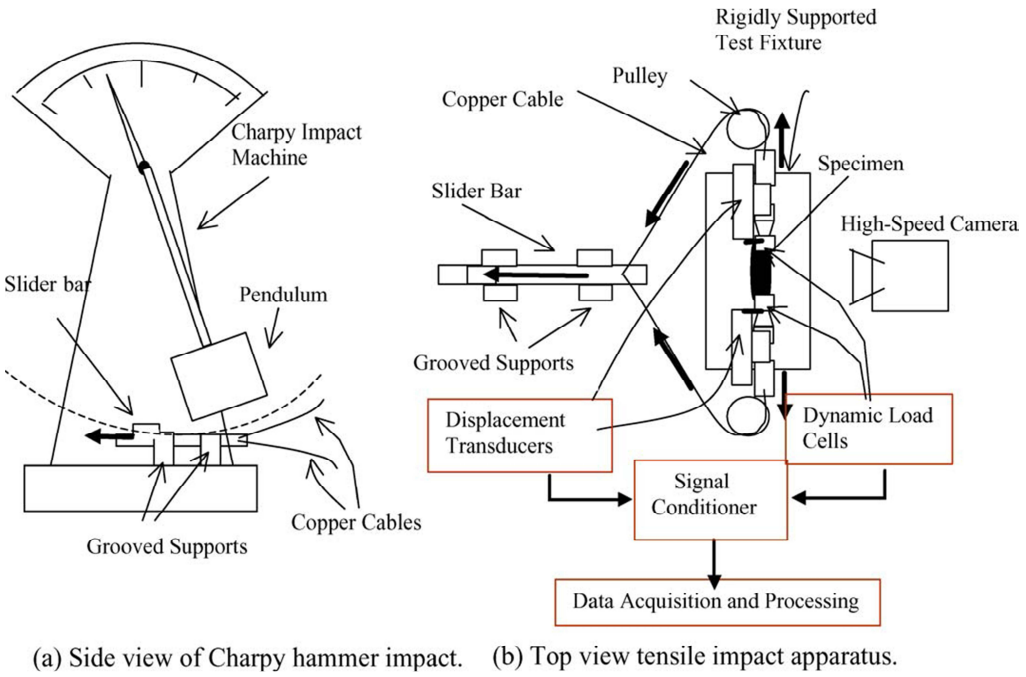

Figure 2.48: Schematic diagram of tensile impact tester (Hoo Fatt and Bekar 2004).

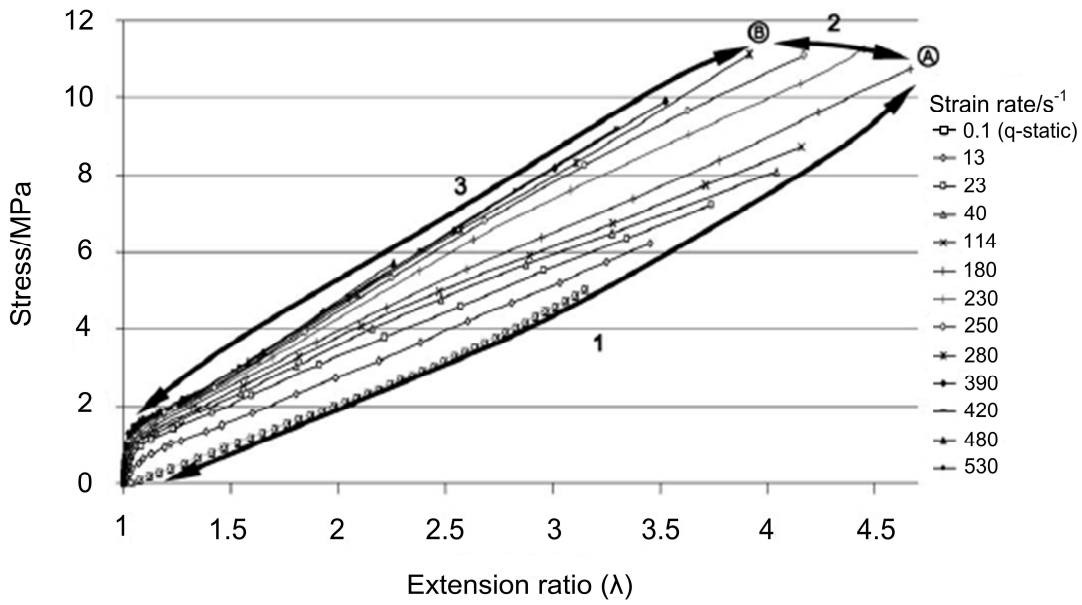

Figure 2.49: Stress-extension ratio curves at various strain rates of the unfilled SBR. Adapted from Hoo Fatt and Bekar (2004).

Roland and coworkers (2007) studied the stress-strain behaviour of an elastomeric polyurea in uniaxial tension test over a wide range of strain rates between 0.06 and 573 s^{-1} employing the different types of test machines, namely a universal testing

machine (Instron testing machine) and in-house test equipment, based on the drop weight, as shown in Figure 2.50. The speed of the shuttles which are attached to the specimen clamps is a function of the speed of an inward movement of the L-levers being activated by the impact bar of the drop weight (100 kg) which is dropped from different heights. The deformation of the test specimen is monitored by a high speed camera at 10^4 frames/sec. The tensile force is measured utilising a strain gauge load cell for conventional tests and a piezoelectric load cell for rapid measurements. Figure 2.51 shows the stress-strain curves of the elastomeric polyurea at the various strain rates. Obviously, the tensile stress increases with the speed of testing. These results correspond to the general viscoelastic behaviour of the material.

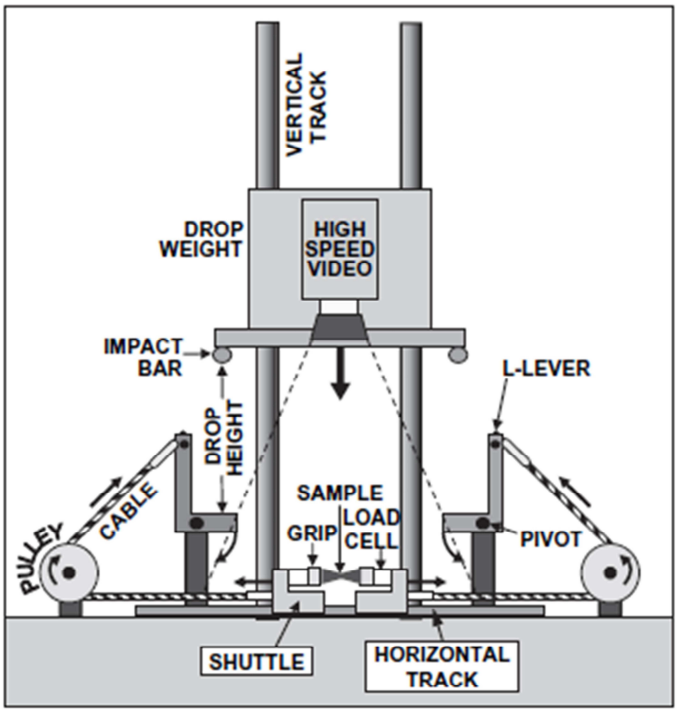

Figure 2.50: Schematic of the high-speed tensile tester (Roland et al. 2007).

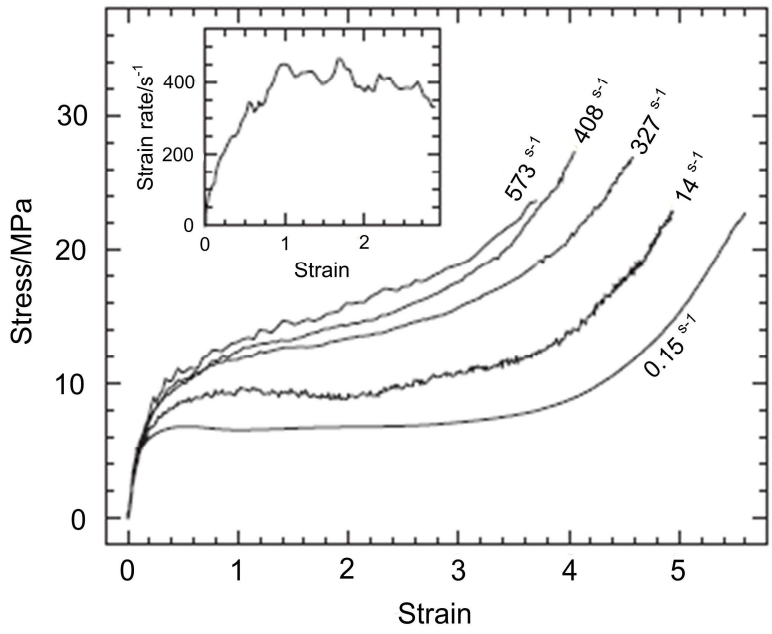

Figure 2.51: Stress-strain curves of the elastomeric polyurea at various strain rates. The inset represents the typical variation of strain rate over the course of a test (Roland et al. 2007).

2.6 Conclusions

Rubber has the unique properties and has a technological importance. It possesses the distinctive characteristics of being soft, highly extensible, and highly elastic and has been applied to many specific applications, namely sealing, vibration and shock absorption, and load bearing applications. Many different types of rubber are commercially available in accordance to their specific applications. The rubber vulcanisates have been assessed in many aspects in order to obtain the parameters to predict their failure behaviour. One of the most important parameters to characterise is the tearing fracture of rubber articles. Typically, the tearing fracture of rubber has been assessed by the relationship between the critical tearing energy and the tearing rate which is a material characteristic and independent of test piece geometry as previously described in the review.

It is widely accepted that tearing in a rubber begins at a flaw in which its localised stress builds up to a critical level under the applied force. This initial process to increase the crack length is typical of all types of rubber material. However, strikingly, the way that the crack propagates, as driven by a release of the elastically stored energy, is a characteristic of the types of rubber. Significant differences arise between rubbers, in particular, between non-strain crystalising and strain

crystallising rubbers. These phenomena have already been studied by many investigators. Unlike the non-strain crystallising rubber, the strain crystallising rubber exhibits an inconsistent rate of crack growth: the rate of crack growth fluctuates between zero rate (stick period) and maximum rate (slip period). This type of crack propagation has also been found in the filled rubber vulcanisates.

From the review, it is clear that all previous work investigating the tearing rate has been based on the speed of the clamp separation with no attention being paid to the process nature of the tearing behaviour of rubber. Some investigators determined the tearing rate by directly measuring the speed of the crack front of a pure shear crack growth specimen using a high speed camera. Obviously, this is still dependent on the detailed types of tearing behaviour as described previously. This framework poses some difficulty when interpreting the test results because this average rate, as obtained, is the tearing rate of a steady tearing behaviour, it is totally inappropriate for measuring unsteady tearing behaviour. As a result, this framework cannot truly elucidate the actual relationship between tearing energy and the onset of unsteady crack growth rate and consequently any measurements made like this are likely to be meaningless. Consequently, this issue raises some challenging questions: what is an actual rate of crack growth?; can we use an average value to represent the rate of crack growth during unsteady tearing behaviour? In this thesis, a novel approach has been introduced to resolve the issue in the interpretation of unsteady tearing behaviour in rubber over a wide range of loading rate and temperatures using different types of rubber. This new concept can be practically applied to investigate the fracture behaviour over a wide range of test rates to assess how the fracture strength encountered in a tire really depends upon the rates of loading at the crack tip.

Chapter 3: Materials and methodology

3.1 Introduction

The aim of this work is to introduce a new approach to investigate the unsteady tearing behaviour which is frequently found in strain crystallising and filled vulcanisates. The purpose of this chapter is to describe the methodologies employed for rubber characterisation, starting with a description of the rubber compounding (section 3.2), followed by basic mechanical (3.3) and dynamic mechanical analysis (3.4). Determination of degree of crosslink density (3.5) and optical characterisation (3.6) of the vulcanisates follow on. Finally, in section 3.7, a new approach to characterise the unsteady tearing is described together with the testing equipment, developed and utilised in this work. The tests were carried out at ambient temperature (23 ± 2 °C), unless otherwise specified.

3.2 Compounding and vulcanisation

Raw rubbers, either natural or synthetic, have viscous liquid-like behaviour which is significantly temperature dependent. They exhibit poor mechanical properties resulting from microscopic slippage between rubber molecular chains that slide past one another. They are generally not suitable for use in engineering applications in this form (Nagdi 1993).

The properties of raw rubber can be considerably enhanced by incorporating additives into the raw rubber. The additives can be fillers which modify the stiffness, damping or tear resistance of the rubber or they can be chemical agents used to promote the formation of crosslinks between polymer chains. This crosslinking process is frequently achieved by a heating process known as vulcanisation. The typical rubber formulations are shown in Table 3.1 and Table 3.2.

Before each compounding process, all the compounding ingredients were weighed within specific tolerances in accordance to ASTM D 3182. The rubber and rubber filler were weighed to within a tolerance of ±1 g and all other ingredients were weighed with a ±0.1 g tolerance. After weighting, all the various rubber additives

were mixed with raw rubber using a two-roll mixing mill as shown in Figure 3.1. The two-roll mixing mill consists of two horizontal, parallel, metal rolls. These rolls turn towards each other with an adjustable gap or nip to allow the rubber to pass through to achieve a high shear mixing. The back roll usually turns at a slightly faster speed than the front roll resulting in increased shear forces. The ratio of the speed between slow and fast row is at 1:1.4. The rubber usually forms a 'band' around the front roll.

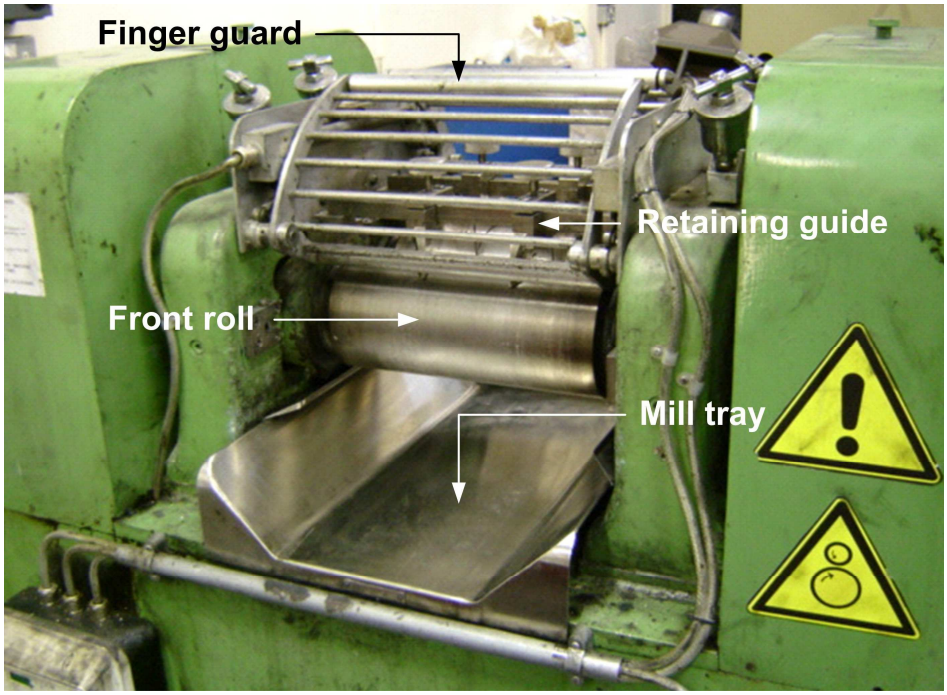

Figure 3.1: Two-roll mixing mill.

The mixing procedures for the rubber compound are described as follows:

1. Set the gap between the rolls to be about 6 mm.

2. Pass the rubber or the carbon black master batch through the gap between the rolls several times until it sheets out sufficiently to cling to the front roll and can be fed back into the gap continuously.

3. Cut the rubber ¾ of the distance across the roll back and forth many times to allow the rubber in the rolling bank above the nip to pass through the rolls and to facilitate the mixing of the entire batch.

4. Add zinc oxide and all other materials, stearic acid and antioxidant, slowly and

evenly across the mill at a uniform rate and then make successive ¾ cuts from alternate ends of the roll to distribute these materials throughout the batch. Do not cut the rubber while free material is evident in the rolling bank or on the milling surface.

5. Open the mill gap slightly and add the accelerator and cut back and forth many times to distribute the material throughout the compound.

6. Check the temperature of the compound to prevent premature vulcanization using a non-contact thermometer before adding the sulphur in the final step. The temperature should be in the range of 70-80 °C.

7. Add sulphur and cut back and forth from the ends of the rolls to facilitate the uniform distribution of the sulphur throughout the batch. Carefully collect materials falling through the nip from a tray and return to the mix.

8. Conclude the mixing cycle by passing the rolled batch endwise through the mill six times with an opening gap between the roll of 0.8 mm to improve the dispersion.

9. Pass the batch four times through the mill at the gap opening of 6 mm, folding it back on itself each time.

10. Cut and remove the finished batch from the mill.

Before vulcanising the rubber compound into test sheets using a compression moulding technique, the vulcanisation characteristic of the sheeted compound, which was conditioned at the room temperature for 1 to 24 hours, was determined using a rotorless curemeter (moving die rheometer MDR 2000) in accordance with ASTM D 5289. A compounded rubber with a mass of approximately 5 g was inserted into a test cavity of the curemeter die, after it was preheated to the specified temperature for 10 minutes. In this measurement, the torque required to oscillate or rotate a lower die, which is proportional to the shear modulus of the test specimen at the test temperature, is recorded as a function of time for 30 minutes. A plot of torque versus time is called the cure curve. This is a characteristic of the rubber compound at the test temperature. Figure 3.2 shows a typical cure curve. The optimum cure times used commonly in industry is called *t* (90). This value is used as it is when 90% of the cure has been completed. The cure however continues as the

compound remains heated immediately upon removal from the mould. This additional heating is presumed to result in an optimum cure in the final cooled test piece. The measured *t* (90) values are given in Table 3.1 and Table 3.2.

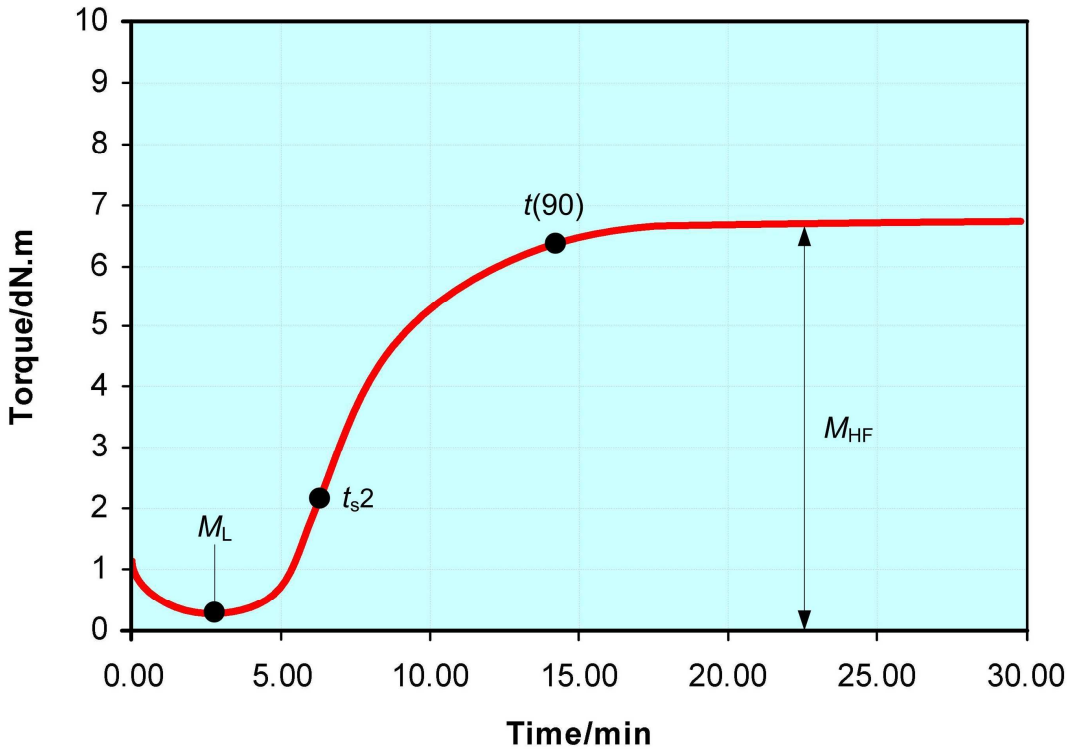

Figure 3.2: A typical cure curve. M_L represents the minimum torque which relates to the processability of the rubber compound. t_s2 denotes the time until a 2 dN.m rise occurs above the minimum which measures the scorch safety time (time to reach the onset of vulcanisation). *t*(90) represents the time required for the rubber compound to reach 90% of the total state of cure. M_{HF} is the maximum torque which relates to the ultimate crosslink density due to the vulcanization process (Dick 2003).

The compounded rubber of each formulation with the known curing time and temperature as previously determined by the cure metre was then cured using a compression mould with six cavities as shown in Figure 3.3. The moulding pressure, about 16 MPa, was applied by a hydraulic hot press. The moulding pressure P_m, which is the pressure exerted on the product in the mould at closure, is determined by

$$P_m = \frac{P_0 A_p}{A_c} \qquad \text{Equation 3.1}$$

where P_0 is the oil pressure which is displayed on the pressure gauge, A_c is the total areas of the mould cavities, and A_p is the area of the press piston

The platens of this machine were electrically heated to a temperature that was maintained by a temperature controller to within ± 2 °C.

The procedure used to manufacture the final flat test sheets is given below:

1. Cut the rubber compound, after storage at an ambient temperature of at least 16 hours and for not more than 96 hours, into the rectangular shapes, whose length corresponds to the milling direction, with a mass of approximately 7 g.

2. Open the compression mould, which has been preheated to the specified temperature of 150 ± 2 °C as verified by a thermocouple which was inserted in the groove of the mould.

3. Insert the unvulcanised pieces into the mould and close the hot press as quickly as possible.

4. Apply and release the moulding pressure three times to get rid of the trapped air.

5. Close and apply the moulding pressure to the mould.

6. Maintain the mould at a pressure of 16 MPa during vulcanisation. The optimum time for vulcanization, as obtained from *t*(90) as measured by the cure meter, is considered to be the period between the instant the pressure is applied fully and the instant the pressure is released.

7. Check the temperature and pressure throughout the moulding cycle, to ensure that both are maintained.

8. Open the mould and remove the rubber sheet from the mould.

9. Condition the vulcanisates at ambient temperature for at least 16 hours and for not more than 96 hours prior to preparation and testing.

3.3 Mechanical analysis

3.3.1 Hardness testing

The hardness of rubber is a measure of the modulus of the material as measured by its resistance to indentation and is expressed as a number with reference to the scale of the instrument employed (Sezna and Vecchio 2003). ASTM standard test method D 2240 describes the procedures for measuring the hardness of rubber using a hardness tester called the Shore durometer. There are a wide range of the scales of Shore durometer, with the Shore A scale being the most appropriate for rubber vulcanisates employed in engineering application, the Shore D scale is applicable to harder rubber compounds such as ebonite, and the Shore O is used for a very soft rubber foam (Sommer and Yeoh 2001). In this work the Shore A scale durometer (Zwick hardness tester) was used to measure the hardness of every moulded test sheet.

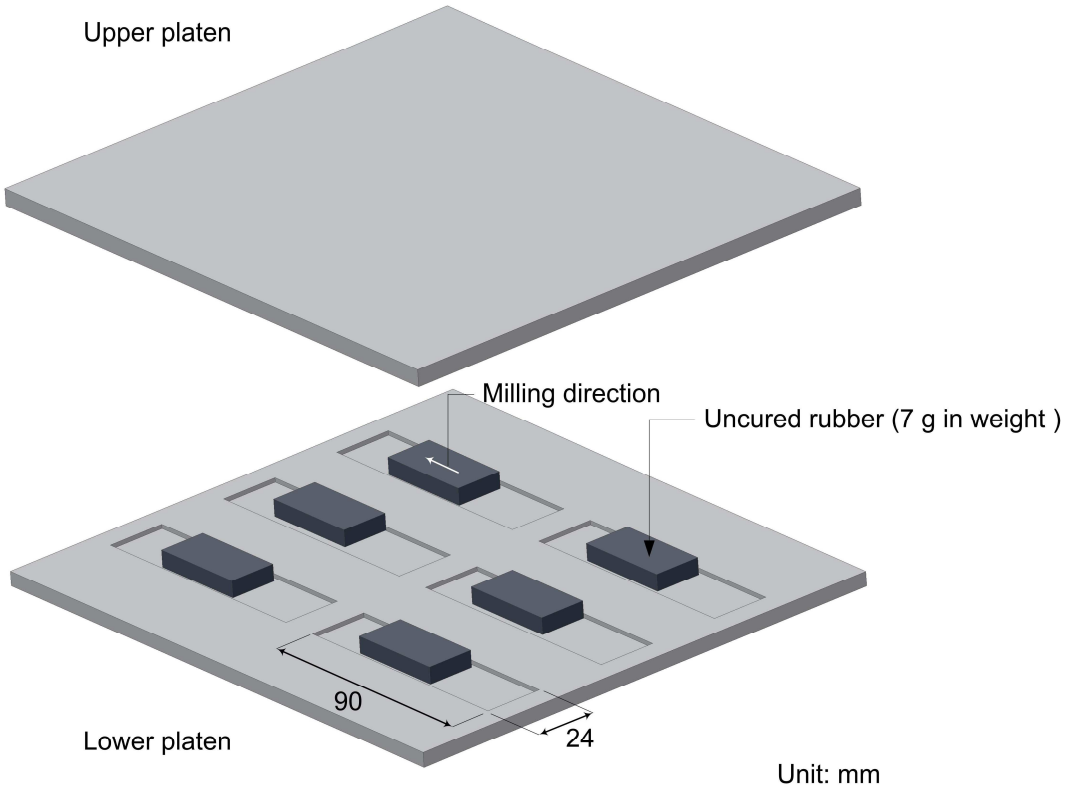

Figure 3.3: The uncured rubber compounds are inserted into the mould cavities.

The procedures for hardness determination are given as:

1. Place the rubber specimens, 24×50×2 mm in size, which were stacked together to obtain the minimum required thickness of 6 mm as required by the standard procedure (ASTM D 2240), on a specimen support and establish a distance of 5-12 mm between the specimen surface and indentor of the hardness tester. This is carried out by vertically adjusting the arm after loosening the locking arm as shown in Figure 3.4.

2. Set preselected contact period using an adjusting knob (Figure 3.4) to read the hardness within 1 second of firm contact with the specimen.

3. Press down a specimen lifting lever to force the specimen support with the specimen against the Shore hardness tester as shown in Figure 3.5.

4. Three repeat measurements were taken per specimen with the mean value taken as the hardness of the compound.

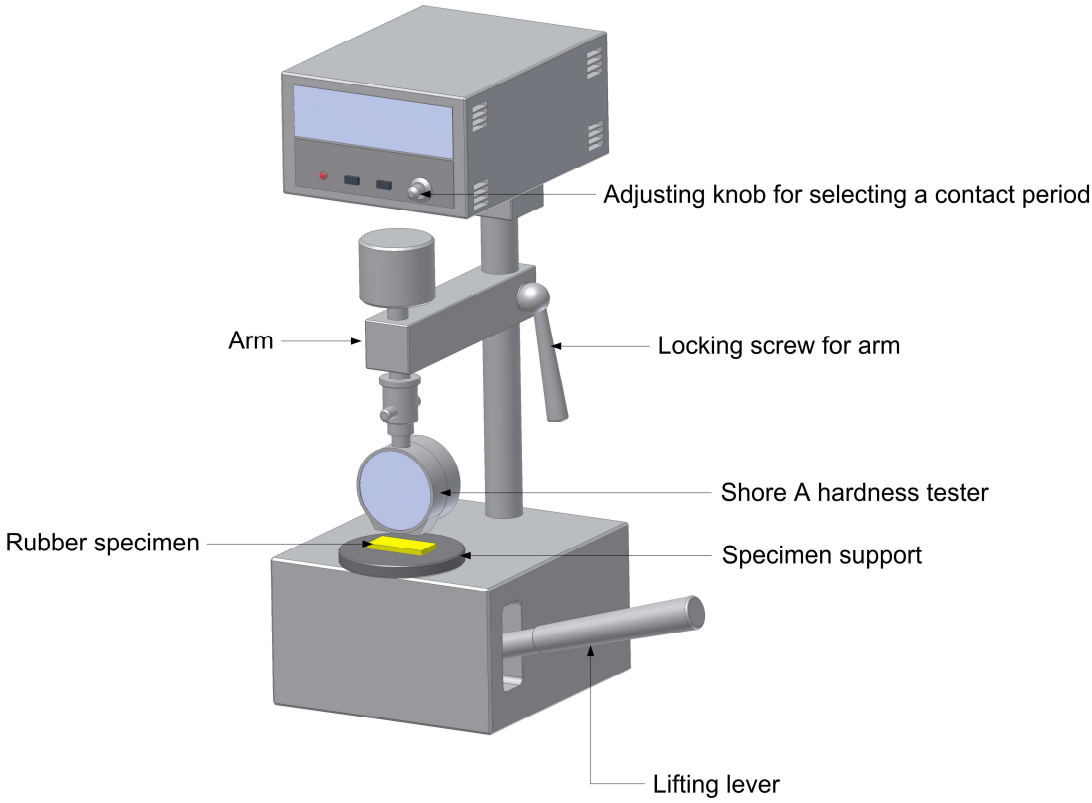

Figure 3.4: Experimental setup for the hardness measurement.

3.3.2 Tensile testing

The measurement of the tensile properties of rubber compound is of importance even though the rubber is seldom utilised in simple extension in service. Tensile tests are useful for the quality control of rubber compounds. In particular, the tensile strength and the elongation at break are very sensitive to changes in manufacturing conditions such as poor vulcanization or a poor dispersion of ingredients during compounding which might include the presence of foreign matter, and the vulcanisation conditions (Smith 1993). In this work, the measurement of the tensile properties of the rubber compounds was carried out in accordance with ASTM D 412 using a dumbbell specimen with the dimensions as shown in Figure 3.6. The dumbbell specimens were stamped from a flat sheet using a cutting die, with the dimensions as specified in Figure 3.6. This was mounted on a hydraulic press as shown in Figure 3.7.

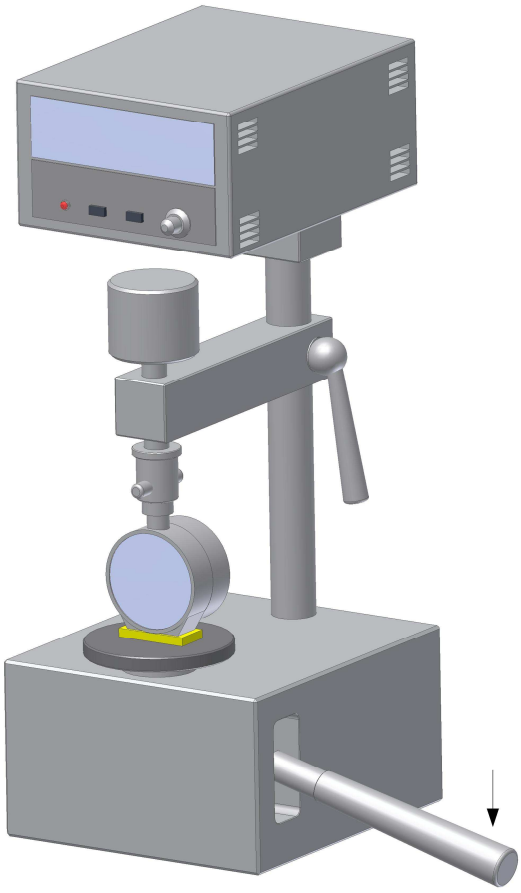

Figure 3.5: The rubber specimen is being pressed against the hardness tester during the measurement.

The procedure for measuring the tensile properties is as follows:

1. Make three thickness measurements: one at the centre and one at each end of the reduced section of the dumbbell specimen, as shown in Figure 3.8, using a dial thickness gauge. The average value of the three measurements is used in calculating the area of the cross-section.

2. Draw clear bench marks at a separation of 20 mm in the reduced portion of the specimen, equidistant from its centre and perpendicular to the longitudinal axis. These marker points were either applied by using black ink on unfilled specimen or applied by using a white correction fluid on carbon black filled specimen.

3. Place the tab ends of dumbbell specimen in the clamps of the Instron universal testing machine (Instron model 5567 equipped with a non-contact extensometre)

with a 1 kN load cell, using care to adjust the specimen symmetrically to distribute tension uniformly over the cross section.

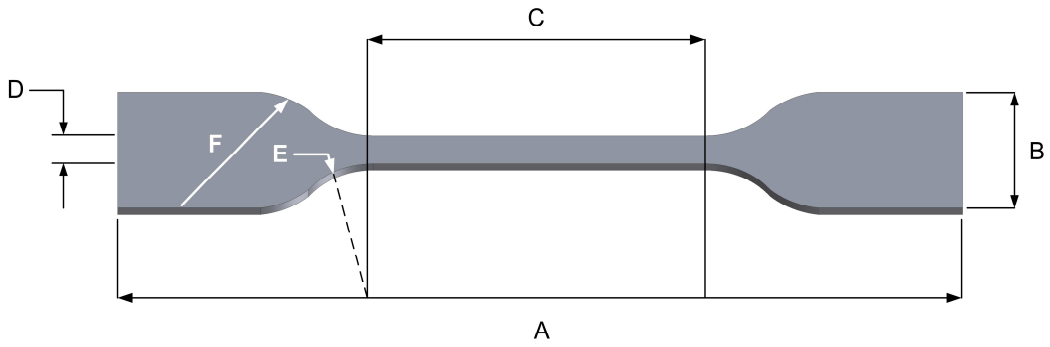

	Dimensions	mm
A	Overall length	70
B	Width of ends	16 ± 1
C	Length of narrow portion	33 ± 2
D	Width of narrow portion	3 ± 0.1
E	Transition radius outside	14 ± 1
F	Transition radius inside	16 ± 2

Figure 3.6: A dumbbell specimen

4. Set up the video (laser) extensometer to track the initial separation of the bench marks placed on the specimen.

5. Start the machine and record continuously the separation of the bench marks and force throughout the test.

6. Three dumbbell specimens were tested for each different material with a speed of 500 mm/min. The tensile strength TS_b is defined as:

$$TS_b = \frac{F_b}{hw_n} \qquad \text{Equation 3.1}$$

where F_b is the force magnitude at rupture, h is the specimen thickness in millimetres, and w_n is the width of the narrow portion of the cutting die in millimetres.

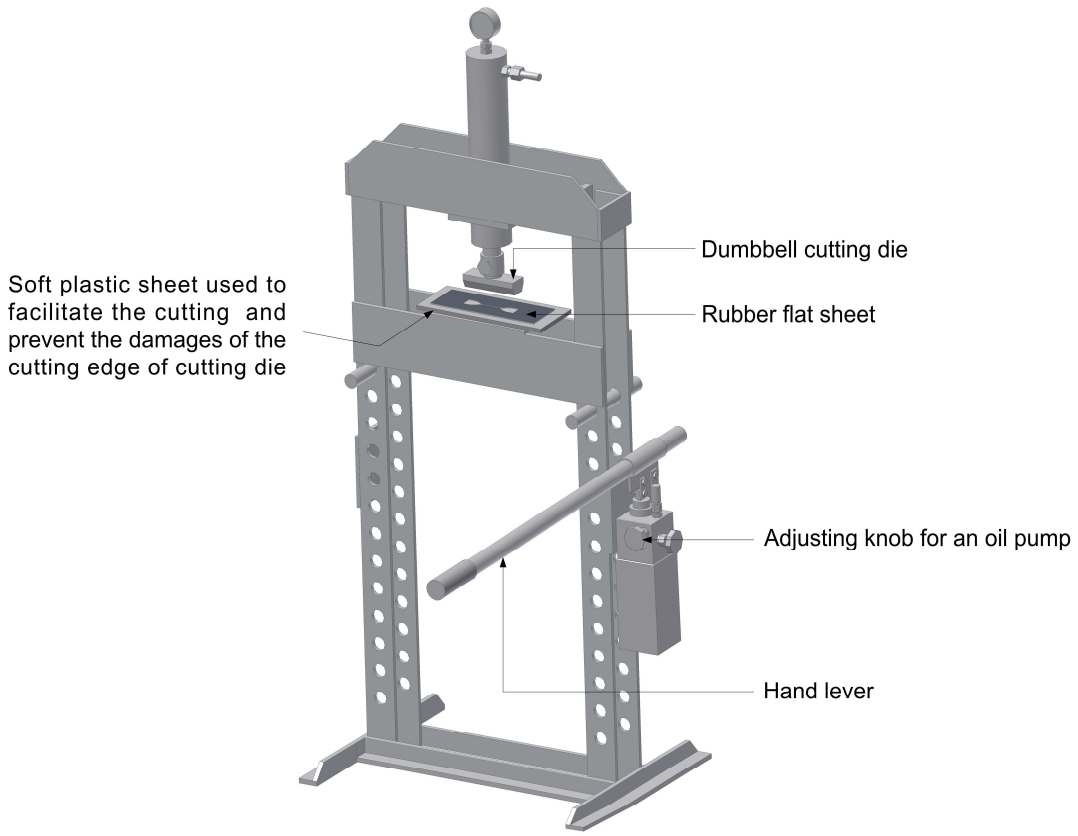

Figure 3.7: A hydraulic press used to stamp out the dumbbell specimen.

The elongation at break e_b, expressed as a percentage, is calculated using the equation

$$e_b = \frac{100(l_b - l_{or})}{l_{or}} \qquad \text{Equation 3.2}$$

where l_{or} is the original distance between the bench marks (20 mm) and l_b is the distance between the bench marks at the point of specimen rupture. The mean values of the tensile strength and elongation at break of the rubber compounds were taken to represent the tensile properties of the compounds. The typical stress-strain curves of unfilled NR and unfilled SBR vulcanisates which were used in this work are shown in Figure 3.9.

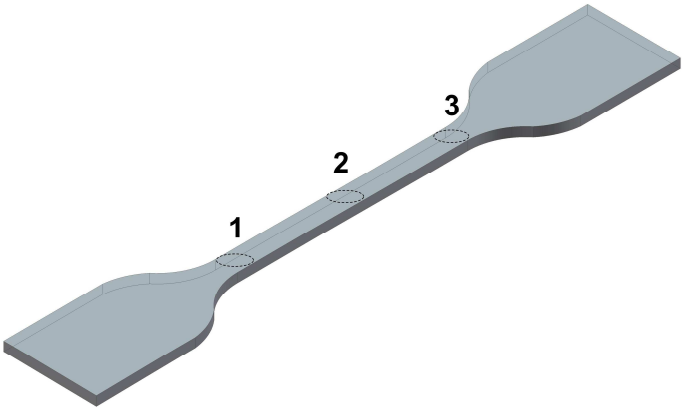

Figure 3.8: The three sections of the dumbbell specimen where the thickness is measured.

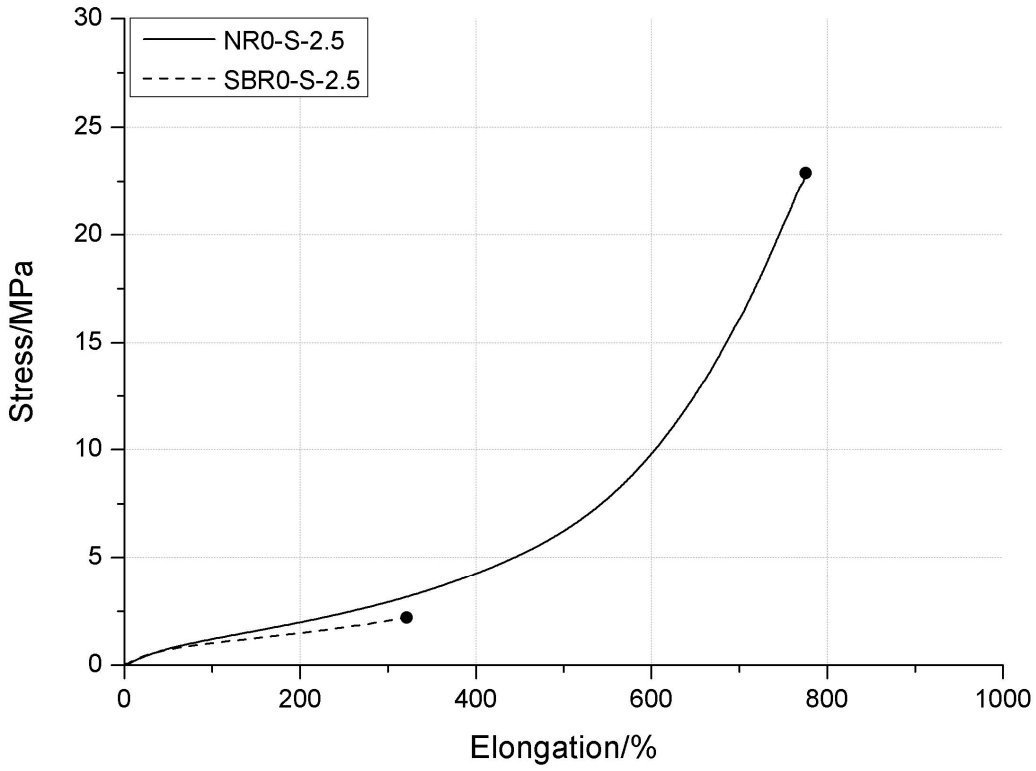

Figure 3.9: Example of typical stress-strain curves of unfilled NR and unfilled SBR which were employed in the work.

3.3.3 Determination of density

The determination of density is an important control of the quality of the rubber compound. The approach used here to determine the density of rubber compound was carried in accordance with BS 903: Part A1. The procedures are given as:

1. Prepare a strip specimen with the dimensions of approximately 10×20×2 mm from the rubber sheet using a sharp blade which was lubricated with soapy water to facilitate the cutting process.

2. Weigh and record the mass of the specimen in air to the nearest 0.1 mg.

3. Place and position a specimen holder on the weighing pan (Figure 3.10).

4. Place a pan straddle on a weighing balance to support the immersion vessel. Care must be taken to ensure that a cut on the side wall of the straddle was properly positioned to allow a hook of the specimen holder to be properly exposed as shown in Figure 3.11.

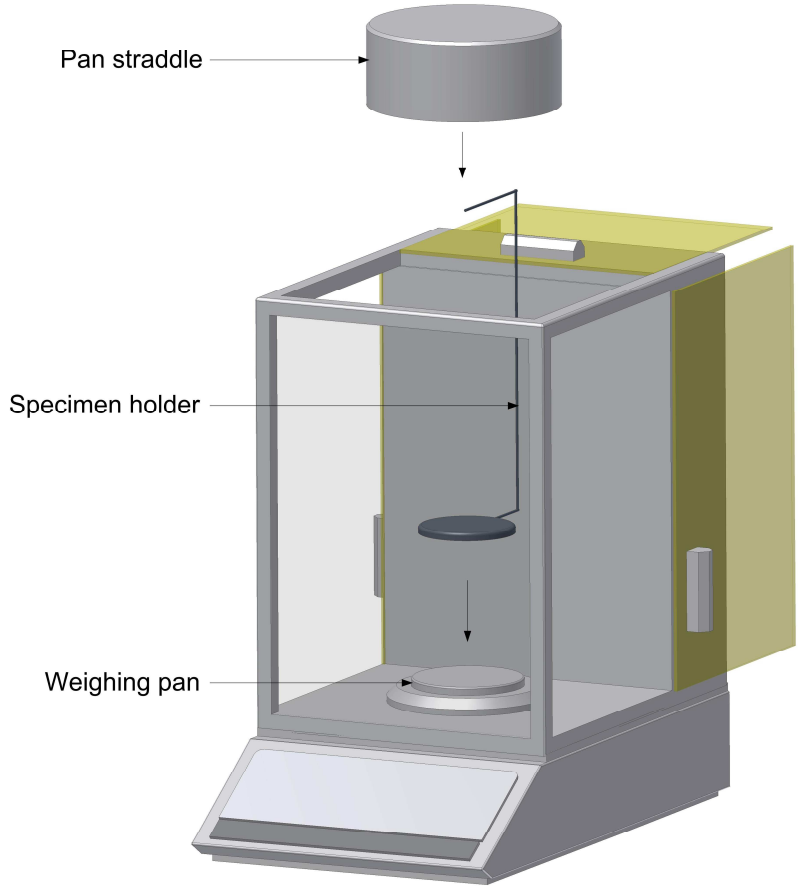

Figure 3.10: Arrangement of the specimen holder.

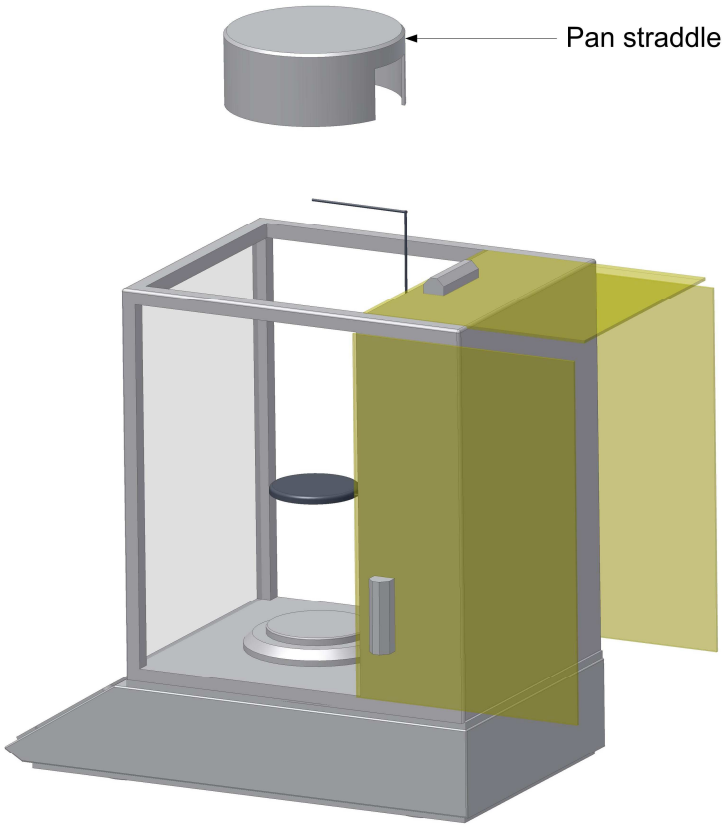

Figure 3.11: Arrangement of the pan straddle with a cut on its side wall which is positioned to facilitate the exposure of the hook of the specimen holder.

5. Place a 250 ml beaker that is filled with approximately 200 ml of distilled water on the pan straddle.

6. Suspend a fine wire from the hook and tare the digital readout of the weighing balance to show zero. Care must be taken to ensure that one end of the filament in the form of loop which is being immersed in the water is suspended about 25 mm above the bottom of the beaker. If a sinker is necessary to be used for specimen having a density less than 1 g/cm^3, the sinker with a mass of approximately 10 g, is attached to the loop of the filament as showed in Figure 3.12.

7. Suspend the specimen from the hook of the specimen holder using the fine wire in step 6 (Figure 3.13) and remove any air bubbles adhering to the specimen by rubbing them with a wire.

8. Determine and record the mass of the specimen in water.

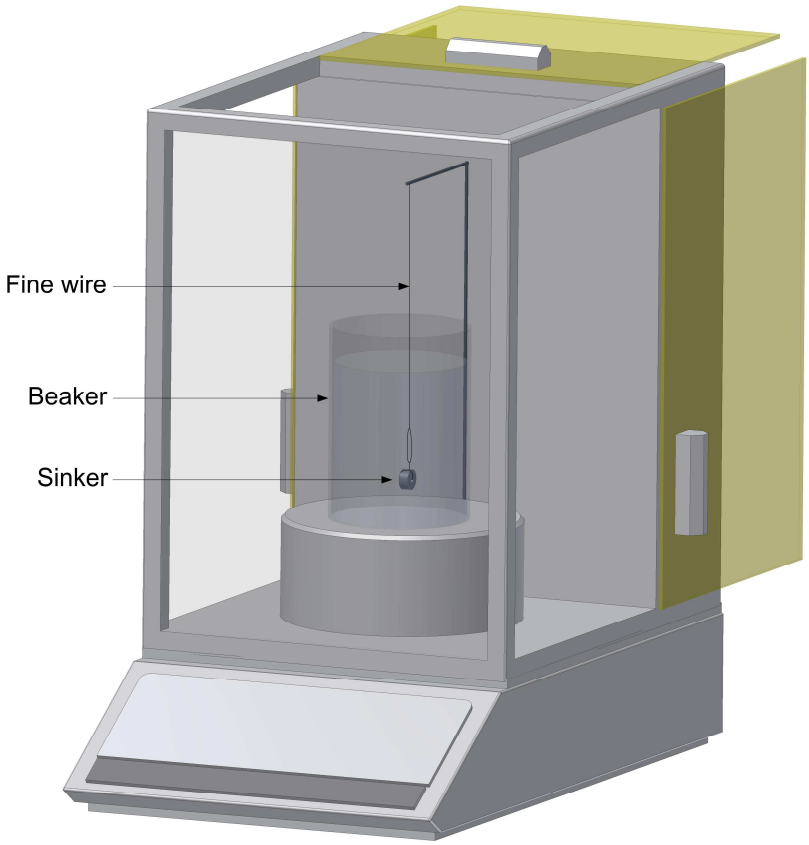

Figure 3.12: A sinker is attached to the supporting filament which is being immersed in water. The sinker will be used in the case of rubber specimen having a density less than 1 g/cm^3 which is typically the case for an unfilled rubber specimen.

9. Calculate the density of rubber specimen ρ, expressed in grams per cubic centimeter, using the formula

$$\rho = \frac{m_1}{m_1 - m_2} \qquad \text{Equation 3.3}$$

where m_1 is the mass of rubber in air and m_2 is the mass of rubber determined by weighing in water. The density of water is taken as 1.00 g/cm^3 for this experiment.

Three measurements were carried out per specimen, with the mean value taken as the density of the compound.

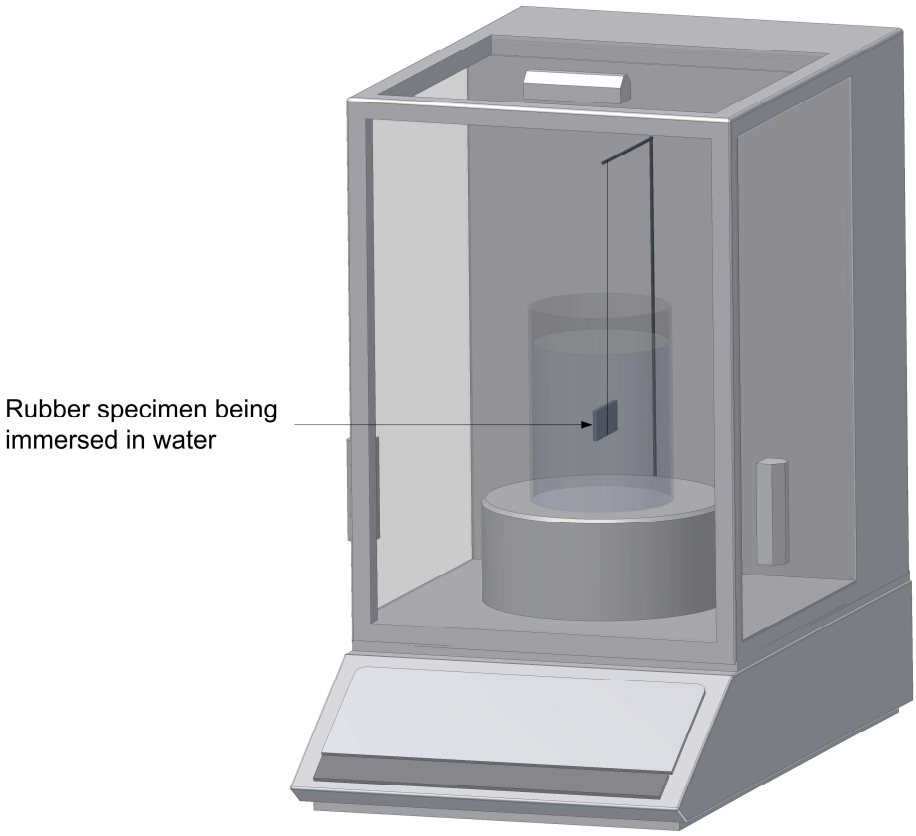

Figure 3.13: Arrangement for the determination of the mass of the specimen in water.

3.4 Dynamic mechanical analysis (DMA)

DMA is extensively employed to identify the transitions in the stiffness and damping of rubber materials as a function of temperature. In an analysis, a specimen is either subjected to a sinusoidal deformation with the measurement of the resultant force or to a dynamic sinusoidal stress with the determination of the resultant deformation. In this work, the DMA technique adopted a tension mode of test using a rectangular specimen with dimensions of approximately: $3 \times 15 \times 1.8$ mm which was mounted in uniaxial tension clamps and subjected to sinusoidal oscillation at a frequency of 1 Hz and an amplitude of 15 μm. The experimental procedure was carried out in accordance with the manufacturer's manual (DMA Q800, TA instruments).

In order to determine the glass transition temperature T_g, the temperature range is varied from -100 °C to 20 °C at a heating rate of 3 °C/min. The glass transition temperature was evaluated from the extrapolated onset temperature, which is the crossover of the inflectional tangent with the tangent determined from temperatures

below the glass transition, obtained from the storage modulus on a log scale against a linear of temperature scale as shown, for example, in Figure 3.14.

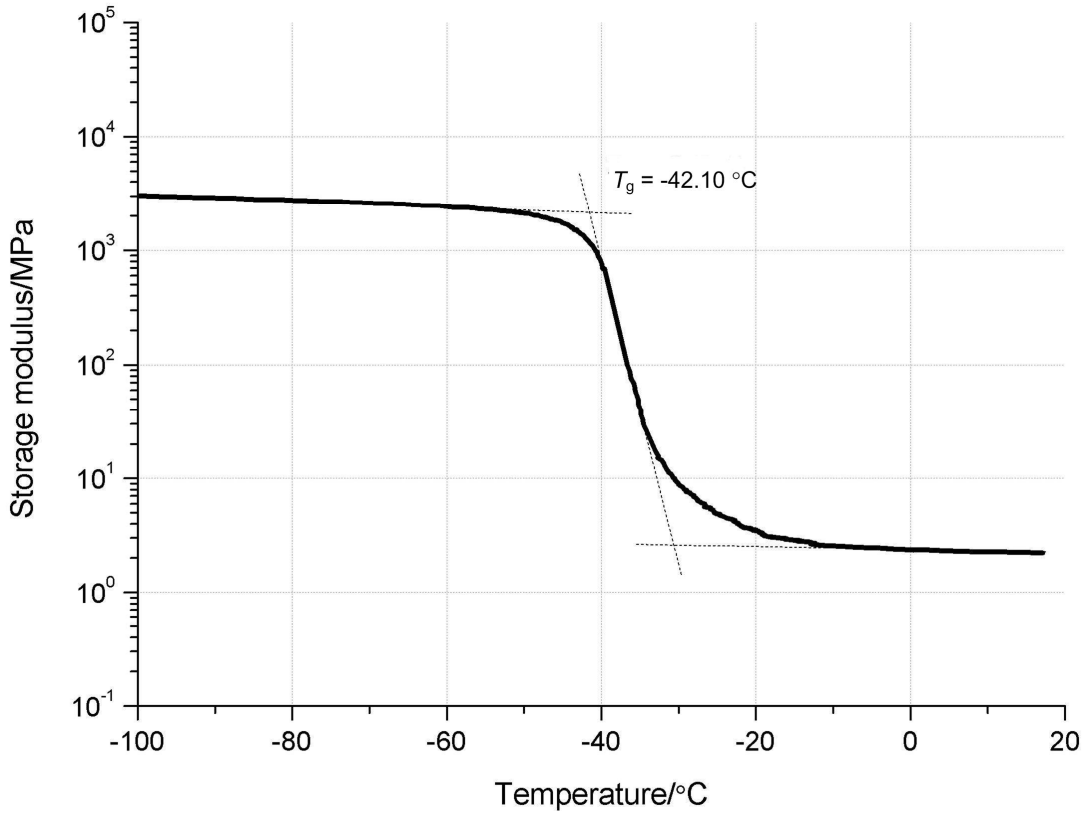

Figure 3.14: Typical DMA graph of an unfilled SBR (SBR0-S-2.5) to determine the glass transition temperature T_g . The T_g is determined from the intersection of two tangents, here which is given as -42.10 °C.

3.5 Determination of crosslink density

Rubber is a material which is typically characterised by a long-range elasticity resulting from the formation of a three-dimensional network of crosslinks which connect the different polymeric chains. Consequently, the properties of rubber are significantly governed by the network structure which is defined by many parameters, including the number of crosslinks, their functionality and distribution, the presence of network defects, and entanglements (Valentin et al. 2008). In this work, both mechanical measurements and equilibrium swelling were employed to assess the crosslink density of the rubber materials.

3.5.1 Determination of crosslink density from stress-strain measurement

The determination of the crosslink density from a stress-strain measurement was carried using a dumbbell specimen as shown in Figure 3.6 which was subjected to the tensile deformation with a testing speed of 5 mm/min using an Instron universal testing machine.

The resulting stress strain curve was fitted between 10% and 66% strain using the Mooney relationship (Mooney 1940):

$$\frac{\sigma}{\lambda - \lambda^{-2}} = C_1 + C_2\lambda^{-1} \qquad \text{Equation 3.4}$$

where σ is the applied engineering stress, λ is the extension ratio, and C_1, C_2 are the Mooney constants. The crosslink density υ is given by:

$$\upsilon = \frac{2C_1}{RT} \qquad \text{Equation 3.5}$$

where R is the gas constant and T is the absolute temperature. C_1 is obtained from the extrapolation from the linear section of a plot of the left hand side of Equation 3.4, which is known as the reduced stress, against the reciprocal of the extension ratio to a *y*-intercept as shown in Figure 3.15.

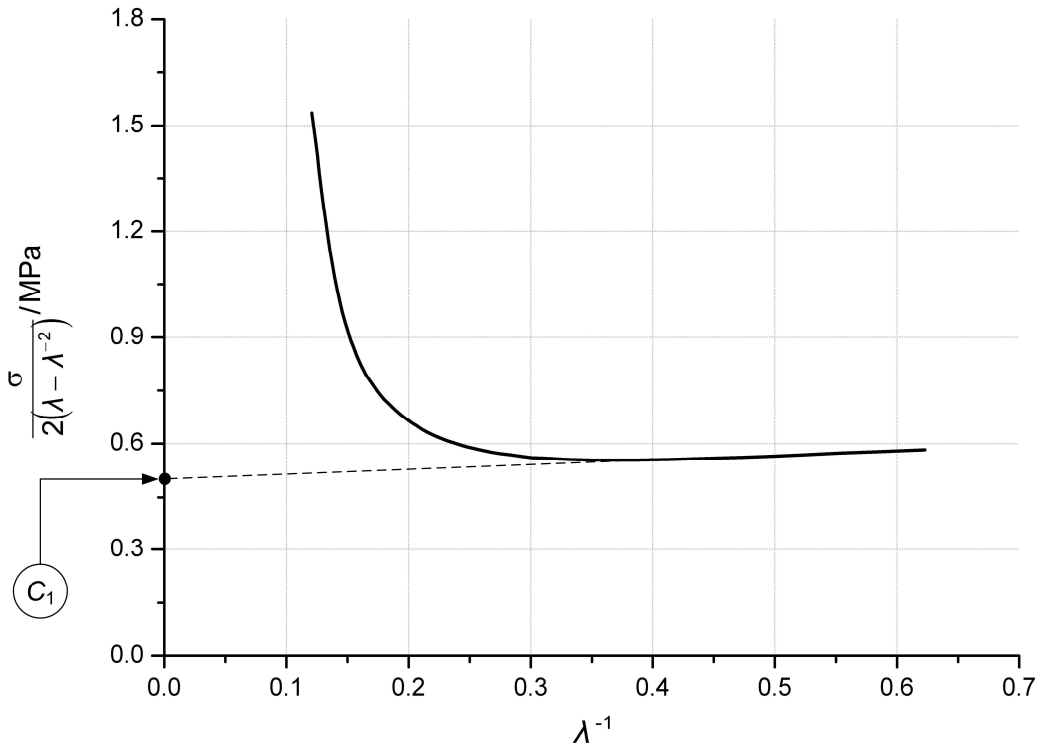

Figure 3.15: Determination of the Mooney constant C_1 from the linear portion of the plot of reduced stress and reciprocal of the extension ratio.

This approach works reasonably well for unfilled rubbers. In the case of filled rubbers, however, it has been suggested that an equilibrium swelling method is more reliable than the former because in the filled rubber a non-affine deformation takes place that gives rise to a stiffening effect which results in the stress-strain behaviour not obeying the Mooney equation and therefore it is difficult to define the value of C_1 on the stress-strain curve (Porter 1967).

3.5.2 Determination of crosslink density using equilibrium swelling

In this work, the rubber specimen was swollen to the equilibrium state (i.e., when the swollen weight became constant) in toluene. Toluene was used as a swelling agent in this study because of its ability to swell rubber to a large extent and due to its low viscosity.

The procedures used for the determination of crosslink density are given below:

1. Cut three specimens, approximately 10 × 10 × 1.8 mm in size, from the vulcanised sheet.

2. Weigh the specimen to the nearest 0.0001 g using an electronic analytical balance.

3. Introduce the specimens into the glass container with the wire sieve which is used to facilitate the contact between the specimens and the solvent in all directions as shown in Figure 3.16.

4. Pour 50 cm^3 of toluene into the glass container and close it properly to prevent the evaporation of the solvent.

5. Allow the specimens to swell at an ambient temperature for 72 h.

6. Remove the specimen from the liquid and dry quickly with a paper towel to remove excess liquid.

7. Place the swollen specimen in a weighing bottle which is closed properly and which is then weighed to the nearest 0.0001 g.

8. Dry the specimens in a vacuum oven at 50 °C until the weight is constant.

9. Weigh the dried specimen to the nearest 0.0001 g and determine the weight of solvent absorbed by the specimen W_s using the data in step 7 and 8.

10. Determine the volume fraction of rubber in the swollen network using the following equation:

$$V_r = \frac{\left[\frac{(W_r - W_f)}{\rho_r}\right]}{\left[\left(\frac{(W_r - W_f)}{\rho_r}\right) + \left(\frac{W_s}{\rho_s}\right)\right]} \qquad \text{Equation 3.6}$$

where W_r and W_s are the weight of dry rubber and the weight of solvent absorbed by the specimen, respectively, W_f is the weight of the filler in the specimen, ρ_r is the density of the rubber compound, and ρ_s is the density of toluene (0.867 $g.cm^{-3}$).

The incorporation of reinforcing filler can suppress the swelling of rubber vulcanisate because the strong interaction of the filler-rubber interface exerts a subtle effect analogous to additional crosslinks in the filled rubber. Therefore, the correction for the effect of the filler-rubber interaction must be determined by the following expression (Kraus 1963):

$$\frac{V_r}{V_{rf}} = 1 - \left[3c\left(1 - V_r^{1/3}\right) + V_r - 1\right]\frac{\phi}{1-\phi} \qquad \textit{Equation 3.7}$$

where V_r is the volume fraction of rubber as determined by Equation 3.6, V_{rf} is the corrected volume fraction of rubber, c is the filler-rubber interaction parameter ($c = 1.17$ for HAF carbon black), and ϕ is the volume fraction of filler.

11. The crosslink density can be determined by the relation (Davies et al. 1994):

$$-\ln(1 - V_{rf}) - V_{rf} - \chi V_{rf}^2 = 2\rho V_0 \upsilon V_{rf}^{1/3} \qquad \text{Equation 3.8}$$

where ρ is the density of the rubber vulcanisate with filler, V_0 the molar volume of the solvent, υ is the crosslink density (including chemical and physical interactions) V_{rf} is the corrected volume fraction of rubber as determined by Equation 3.7, and χ is the polymer solvent interaction parameter. The polymer-solvent interaction parameter χ for the system SBR-toluene and NR-toluene are 0.446 and 0.391 respectively.

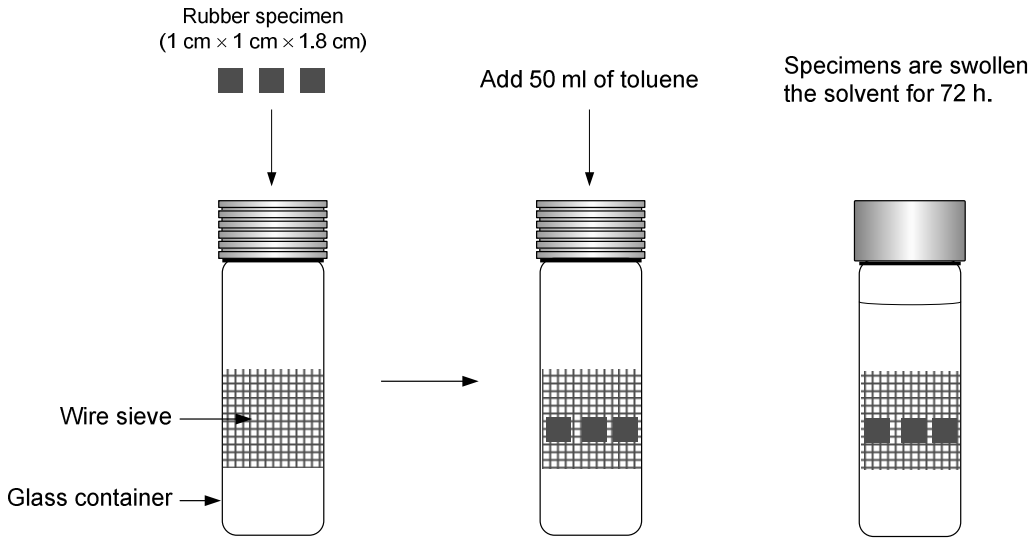

Figure 3.16: Experimental arrangement for equilibrium swelling measurement.

3.6 Examination of fracture surface by scanning electron microscope (SEM)

The imaging process of a SEM is based on the interaction of a high energy (typically 10 kV for rubber specimen) electron beam which is scanned across a surface of the specimen. This creates a number of different signals which relate to the surface of the specimen. The image which is generated represents the strength of these signals as a function of location on the surface. In the experiment, the specimen, 5 × 15 × 2 mm in size was glued on a SEM platform (stub) with an electrically conductive glue. Typically, the rubber specimens are a poor conductor of electricity and a charge rapidly builds up on the specimens when they is bombarded with an electron beam leading to a deflection of the electron beam and thus the distortion of the image quality (Campbell et al. 2000). Therefore, the specimens were coated with a thin layer of gold which is a conductive material as shown in Figure 3.17 before examining their surface.

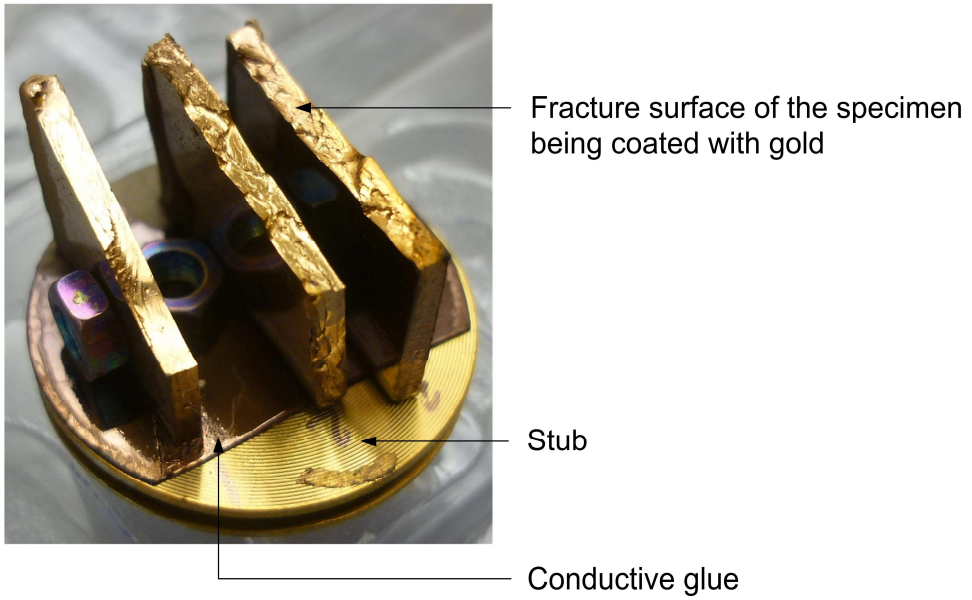

Figure 3.17: Prepared rubber specimens for the SEM measurement.

3.7 Determination of the time derivative of the strain energy release rate $\dot{T}$

In this work, a wide range of testing speeds were employed to investigate the tearing behaviour of rubbers in relation to the strain rate at the crack tip just immediately prior to the propagation of the crack. Consequently, many factors relating to the test methodology and the test equipment needed to be carefully considered in order to obtain reliable test results. In the following section, a brief description of the various techniques is given.

3.7.1 Examination of the response time of the load cell

In this study, two types of load cell were employed, namely a static strain gauge load cell which transforms a mechanically applied load into an electrical signal and a dynamic piezoelectric load cell which generates an electrostatic charge obtained from a built-in piezoelectric material which is proportional to the applied force (Warring and Gibilisco 1985). In order to properly use the load cell to measure the tearing force under the different rates of loading, the response time of both types was assessed.

The response time of the load cell is defined as the time t between the time t_1 at which the given force is applied and the time t_2 at which the output of that applied force becomes stable as shown in Figure 3.18 (a). Response time can also be given as the time t' between the force removal time t_3 and the point t_4 at which the output again becomes stable as shown in Figure 3.18 (b). It may be given in terms of seconds or fractions of second, or sometimes as a percentage of its full value. For example, if the specification states that 95% response time is 3 seconds, it denotes the device takes 3 seconds to reach 95% of its final output value (Elgar 1998). In the examination of the response time of the load cell, a range of standard weights with a known value, as shown in Figure 3.19, were used. With reference to Figure 3.20, after placing the standard weight on the hanger and taring the load reading to zero, the supporting string was quickly cut using sharp scissors to drop the weight. The typical force-time curves of the strain gauge load cell and the piezoelectric load cell obtained from this experimental examination are shown graphically in Figure 3.21 and Figure 3.22. The experiment shows that a static strain gauge load cell has a response rate of about 50 ms and the dynamic piezoelectric load cell has a response rate of about 0.2 ms.

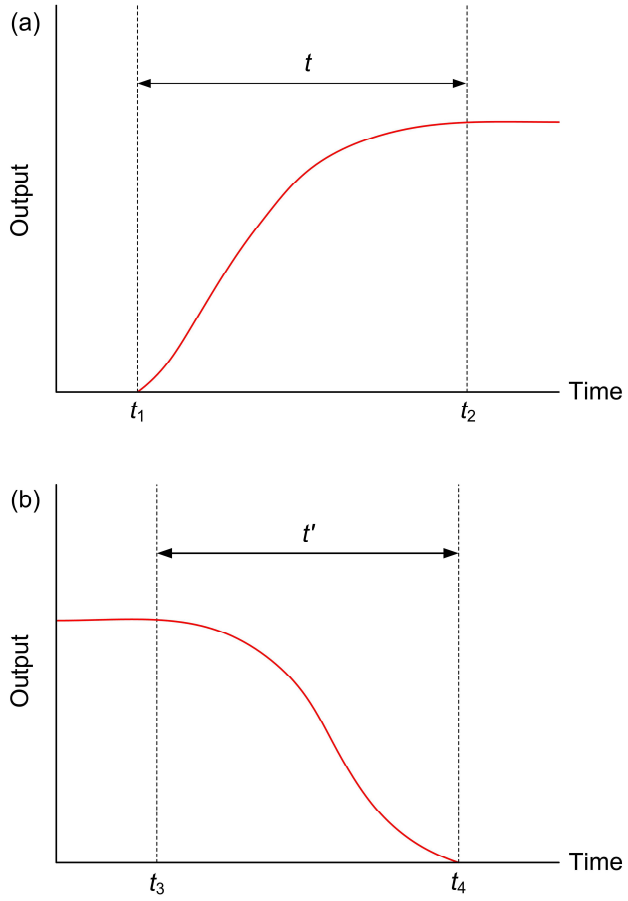

Figure 3.18: Typical graphs represent the response time of the load cell (a) rise time is defined by *t* and (b) decay time is given by *t'*. Adapted from Warring and Gibilisco (1985).

Figure 3.19: Examples of the standard weights which were used to examine the response time of the load cell.

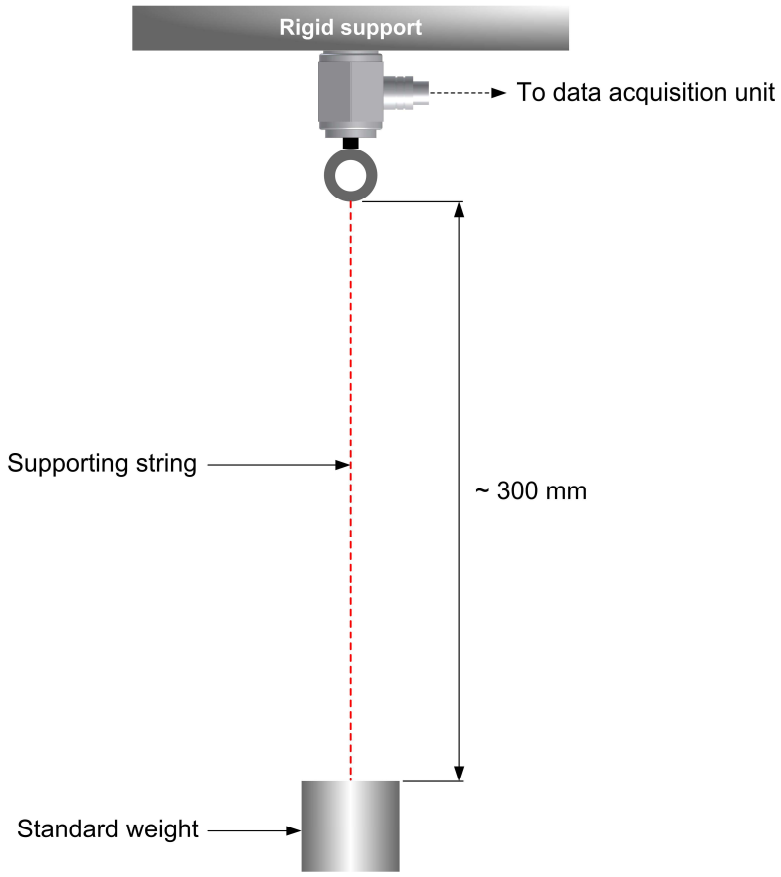

Figure 3.20: Experimental arrangement, for example, to examine the response time of the piezoelectric load cell.

Unlike the strain gauge load cell which an output signal is stable with respect the time, the dynamic piezoelectric load cell shows a drift in the output signal with time due to the charge decay characteristic thus making it unsuitable for a static loading application. Figure 3.23 shows the decay of the output signal of the dynamic piezoelectric load cell as a function of time.

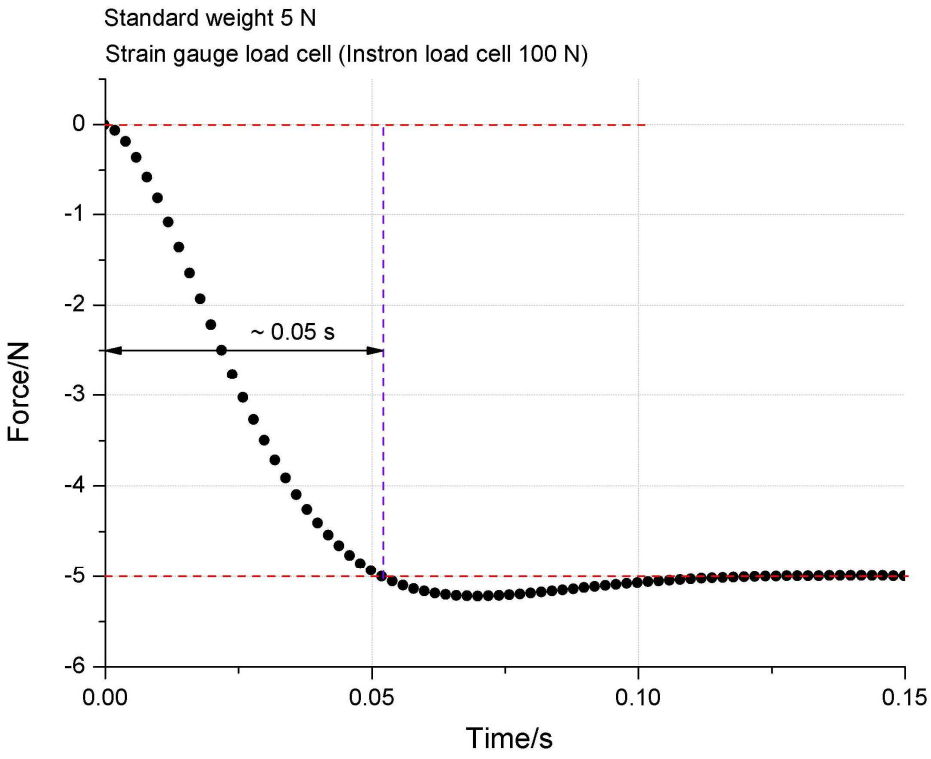

Figure 3.21: Typical force-time curve showing the response rate of the strain gauge load cell after a standard weight of 5 N was instantaneously removed by cutting the supporting string.

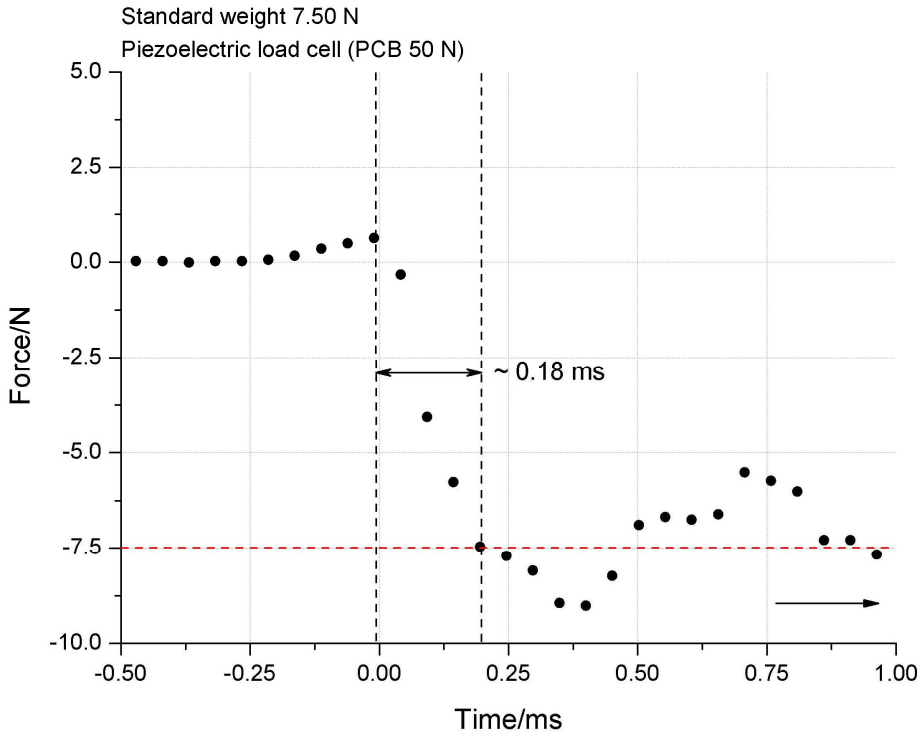

Figure 3.22: Typical force-time curve showing the response rate of the piezoelectric load cell after a standard weight of 7.50 N was instantaneously removed by cutting the supporting string. This plot was obtained from the digital oscilloscope. The output in mV was transformed to force in N.

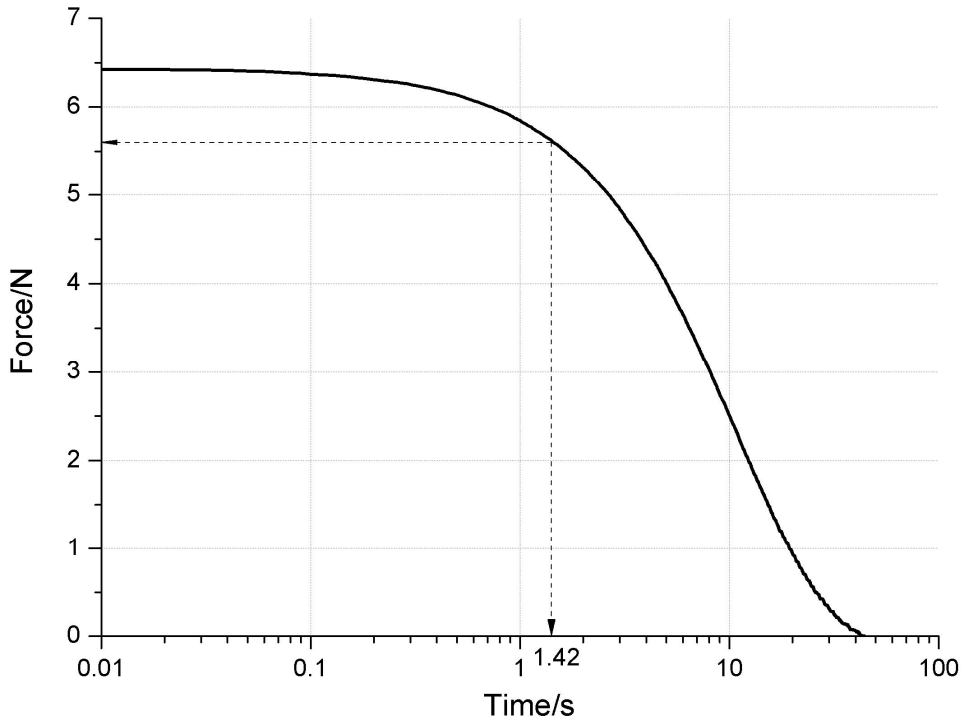

Figure 3.23: Typical signal decline in the output signal of the dynamic piezoelectric load cell. The effective measurement time which is the 10% drop of the measuring signal is about 1.4 s.

3.7.2 Quantification of the time derivative of the strain energy release rate $\dot{T}$

In this work, two types of the test specimen were employed, namely the trouser tear specimen and the pure shear crack growth specimen. The trouser tear specimen was used for most of the testing, with the pure shear crack growth specimen with the clamp separation of 12 mm, 60 mm in length and 10 mm in pre-cut length being utilised for comparison purposes to confirm that the characteristic fracture energy of the rubber at fast rates is still independent of the test piece geometry.

The trouser tear specimen geometry was chosen with the legs kept as short as possible to allow as fast a rate of loading as possible at the crack tip. The sample was 24 mm wide, 30 mm long and roughly 2 mm thick. Each leg of the trouser tear specimen was therefore 12 mm wide and 15 mm long. Approximately 10 mm of the leg of the trouser was clamped in the grip during testing. The cut was introduced to obtain the legs of the specimen by a sharp blade lubricated with soapy water. The resultant sharp razor cut does not represent the geometric profile of the characteristic crack tip. Therefore, prior to each experiment, some small scale manual tearing of the tip was done to introduce a more typical crack tip profile using

an in-house straining device which is equipped with the piezoelectric load cell as shown in Figure 3.24 and Figure 3.25. The specimen was clamped between the grips of the equipment and then the hand wheel was turned to introduce the crack tip profile. The initiation of the crack was identified by the sudden fluctuation of the force as shown on the screen of the data acquisition unit.

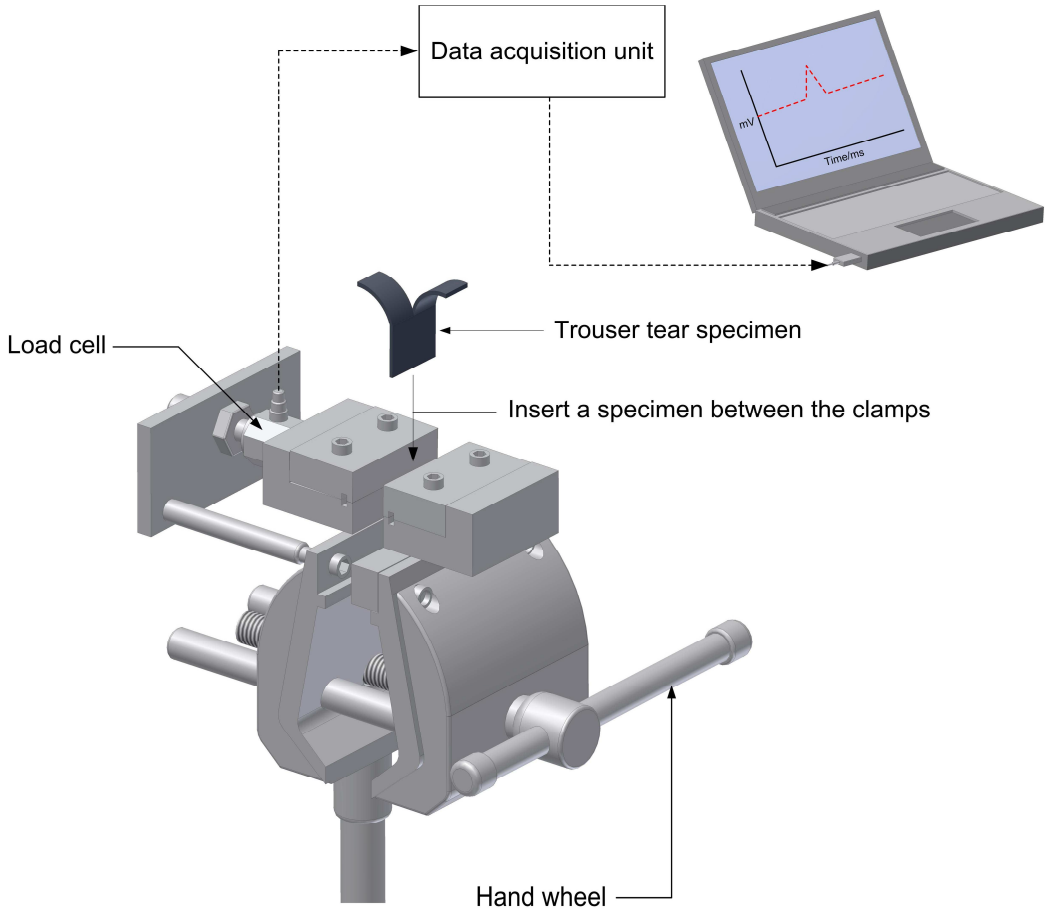

Figure 3.24: Experimental setup for introducing a characteristic crack tip profile of the trouser tear specimen.

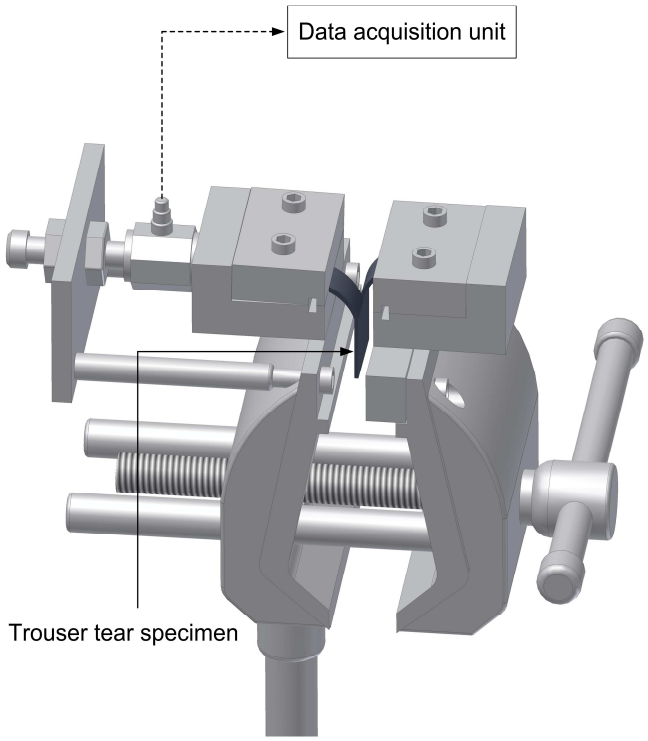

Figure 3.25: The trouser tear specimen was clamped in the straining device prior to extension to introduce a characteristic crack tip profile.

In the early stages of this work, the simple test rig as shown in Figure 3.26 was employed. In Figure 3.26, the specimen was manually pulled after it was firmly attached to the clamps of the test rig. The speed of the loading rate is essentially dependent on the speed and strength used by the operator. The basic concept to determine the strain at the crack tip using the simple test rig was satisfied because the initial part of the tearing force-time curve was used to determine the time derivative of the strain energy release rate. However, to make the procedure much more systematic, another test rig was developed as shown in Figure 3.27. This test rig was equipped with a drop weight in order to increase the speed of the loading rate. The loading rate of the lower clamp was controlled by the drop height of the drop weight which is a function of the length of the string attached to it. However, there were some technical problems due to the significant vibration of the drop weigh as it fell through the guide tube which resulted in a lot of signal noise at the data acquisition unit. Sometimes, the drop weight became trapped inside the guide tube because its vertical position before release was initially distorted by the manual trigger. Therefore, the test rigs were developed further. The third generation facility used a pneumatic test rig as shown in Figure 3.28. In addition, the drop weight test

rig was modified, as shown in Figure 3.31, to accommodate a drop height of up to about 6 m.

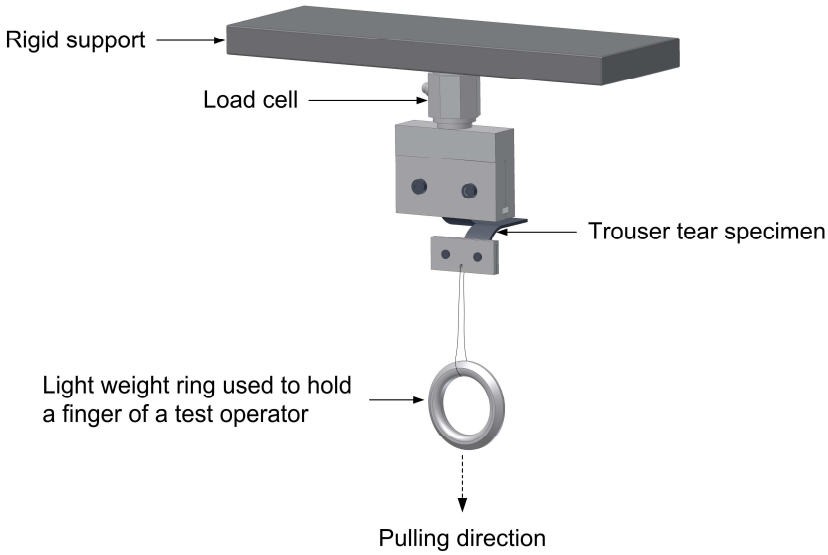

Figure 3.26: The trouser tear specimen being clamped in the straining device before extended to introduce the crack tip profile.

In the pneumatic test rig the speed of the actuator is controlled by the air pressure as regulated through a needle valve. The detail for experimental arrangement for the pneumatic actuator test rig is shown in Figure 3.29 and Figure 3.30. For the drop weight test rig as modified and developed in Figure 3.31, the guide frame is extensible. The dropping system is released by a magnetic trigger using a trigger switch as shown in detail in Figure 3.32.

In this work, tests at elevated temperatures were also carried out. A temperature controlled chamber attached to the Instron universal testing machine was used for relatively low rates of loading on the test specimen. At higher speeds of loading, an in-house heating chamber was developed to attach to the in-house test rigs as shown in Figure 3.33 for the pneumatic test rig and Figure 3.34 for the drop weight apparatus. The in-house heating oven consisted of a main body made from an aluminium cylinder which is wrapped around with the flexible silicon heating material where an insulator is placed on the outside as shown in detail in Figure 3.35. The uniform distribution of the temperature inside the oven is controlled by an air circulating fan.

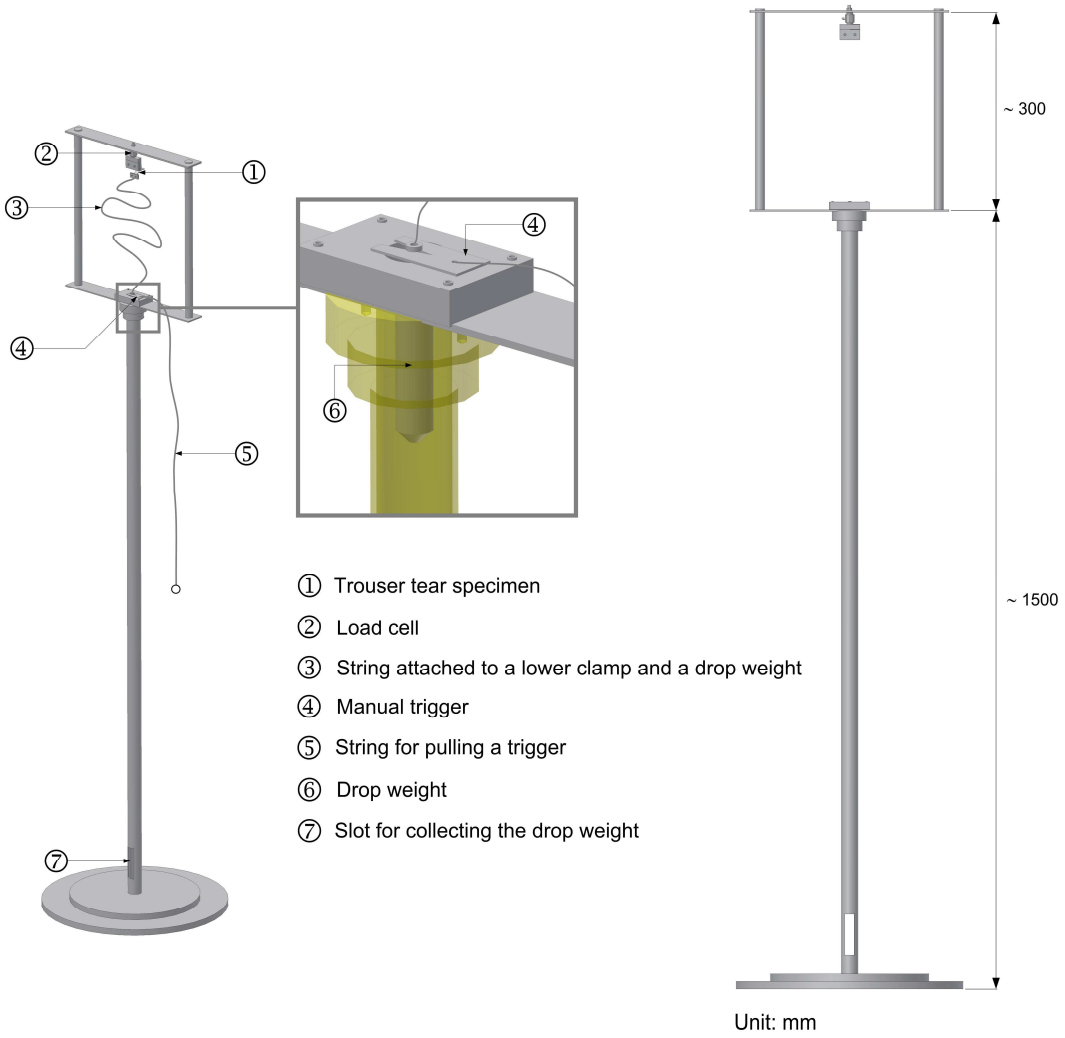

Figure 3.27: A drop weight test rig.

This work required specimens to be torn over at least five orders of magnitude in test rate. Therefore, three different types of test equipment were employed: a screw-driven test machine (Instron testing machine); a pneumatic test rig and a drop-weight test rig as detailed previously.

The point of the onset of tearing for relatively high speed tests was determined from the drop in tearing force at the initial part of the tearing force-time curve, and was independently confirmed using a high speed camera (Fastcam-ultima APX Proton, Model 120k) at 8000 frames/sec at ambient temperature. The time derivative of the strain energy release rate or $\dot{T}$ was experimentally evaluated from the slope of the first peak of the plot of the strain energy release rate against time immediately prior to the first occurrence of any crack extension. Figure 3.36 shows the schematic diagram for determining the time derivative of the strain energy release rate.

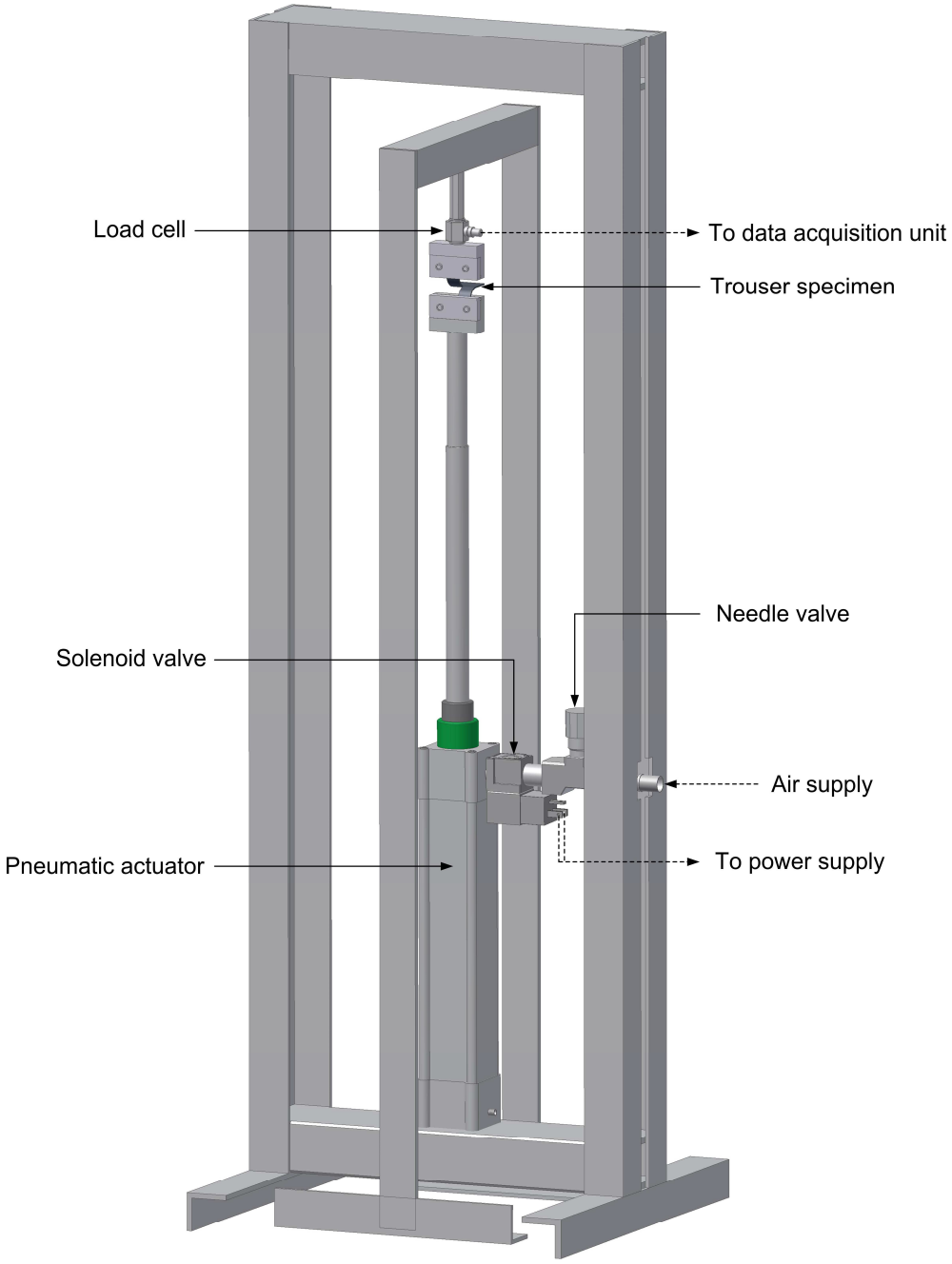

Figure 3.28: A pneumatic test rig.

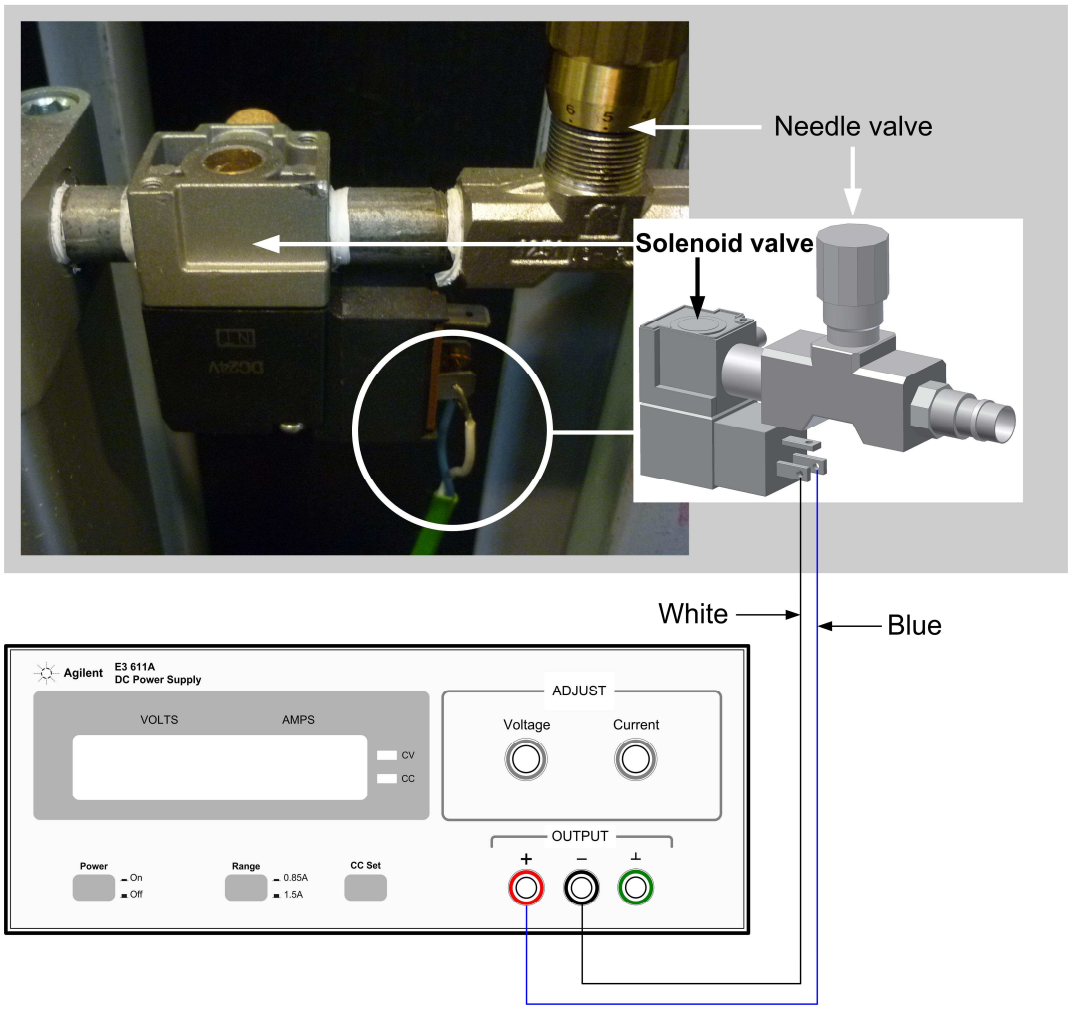

Figure 3.29: Experimental setup representing the connection of the pneumatic test rig to the power supply.

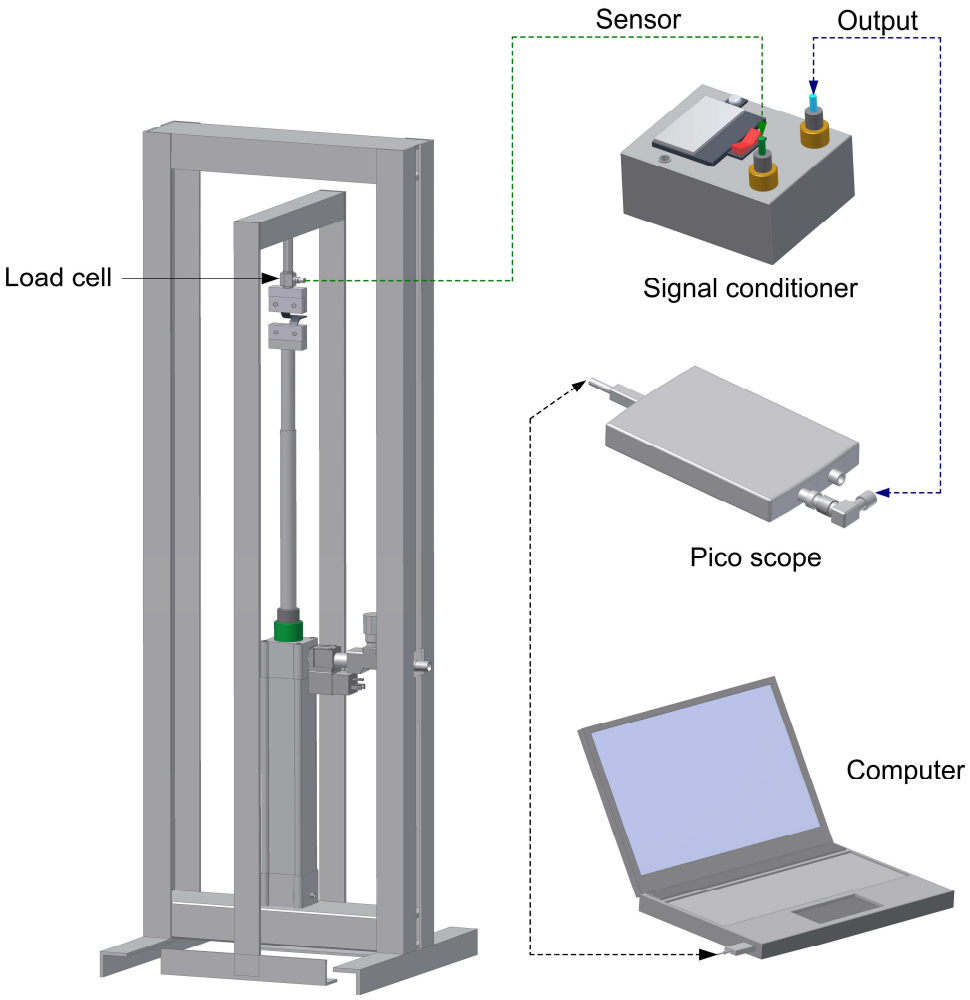

Figure 3.30: Detail of the experimental setup for the pneumatic actuator.

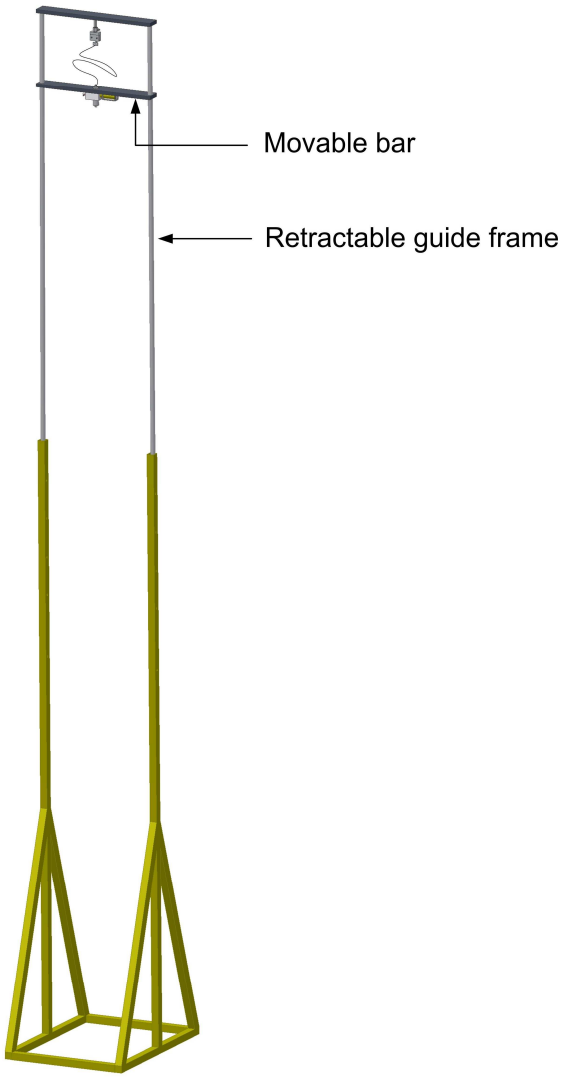

Figure 3.31: The drop weight apparatus used in this work.

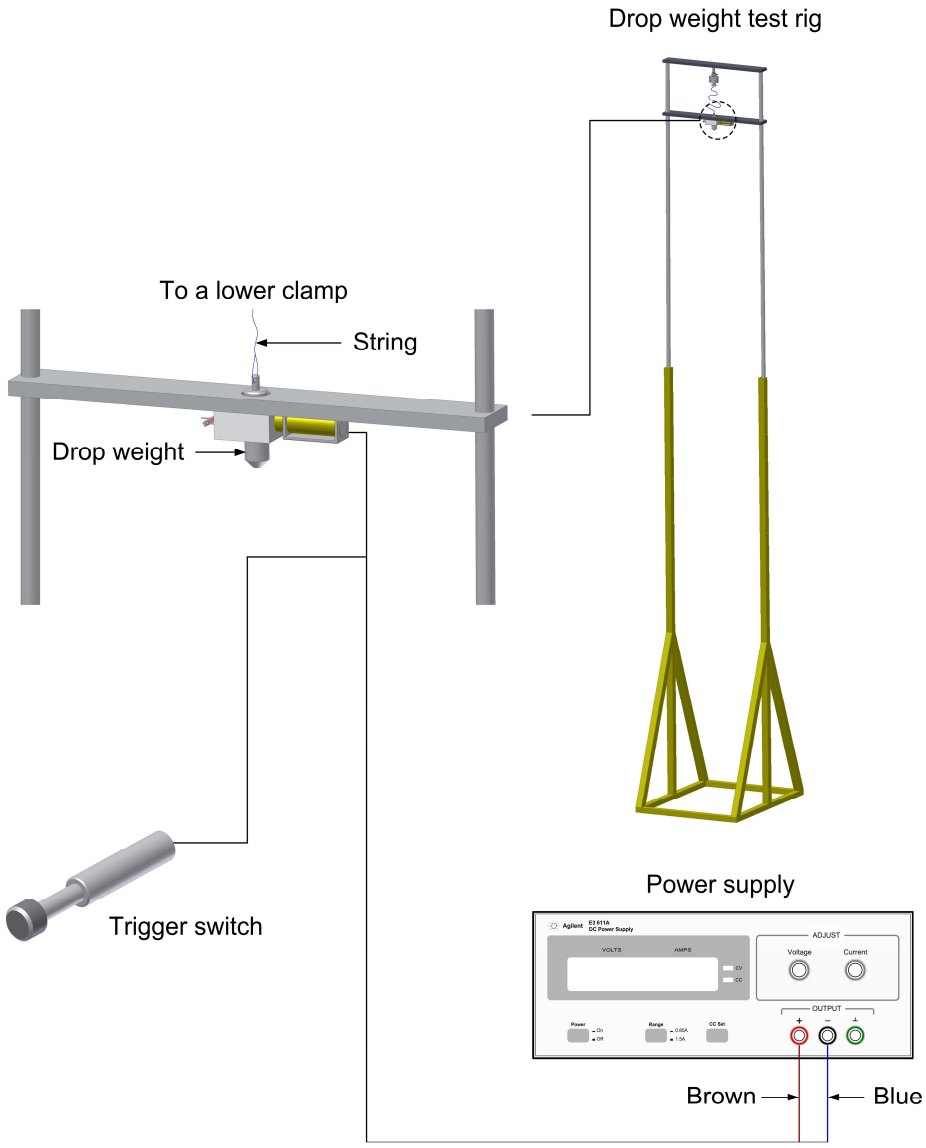

Figure 3.32: The detail for connecting the magnetic trigger switch of the drop weight apparatus to the power supply.

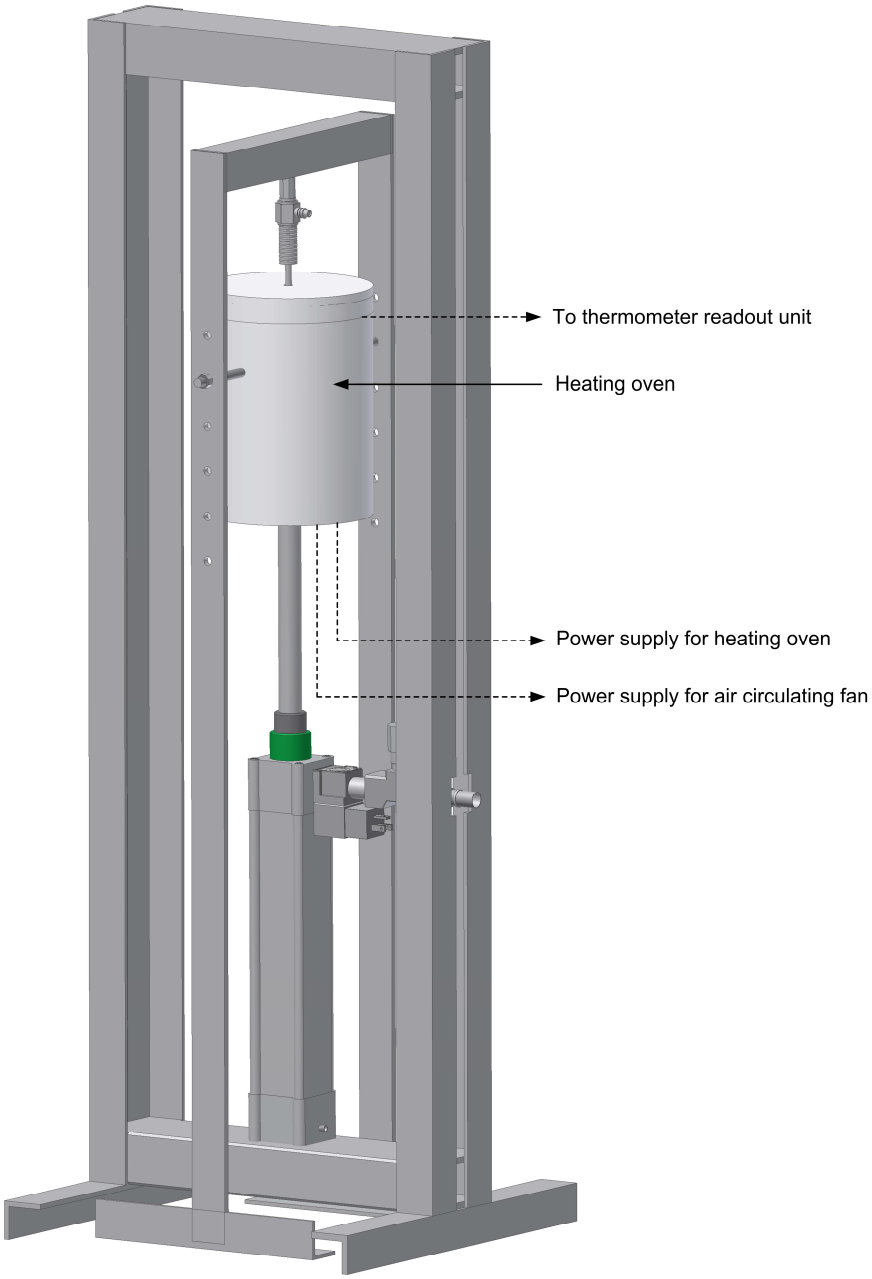

Figure 3.33: The pneumatic test rig is being equipped with the heating chamber.

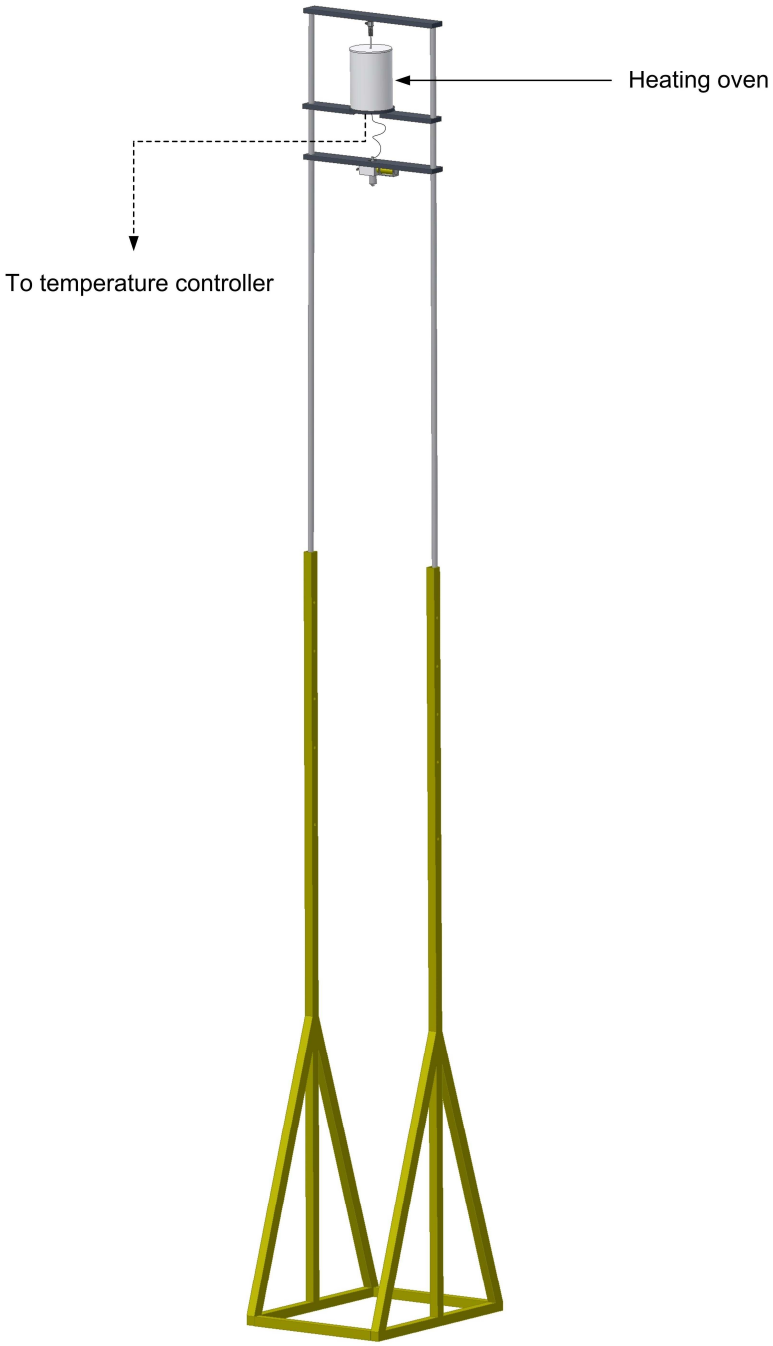

Figure 3.34: The drop weight test rig is being equipped with the heating chamber.

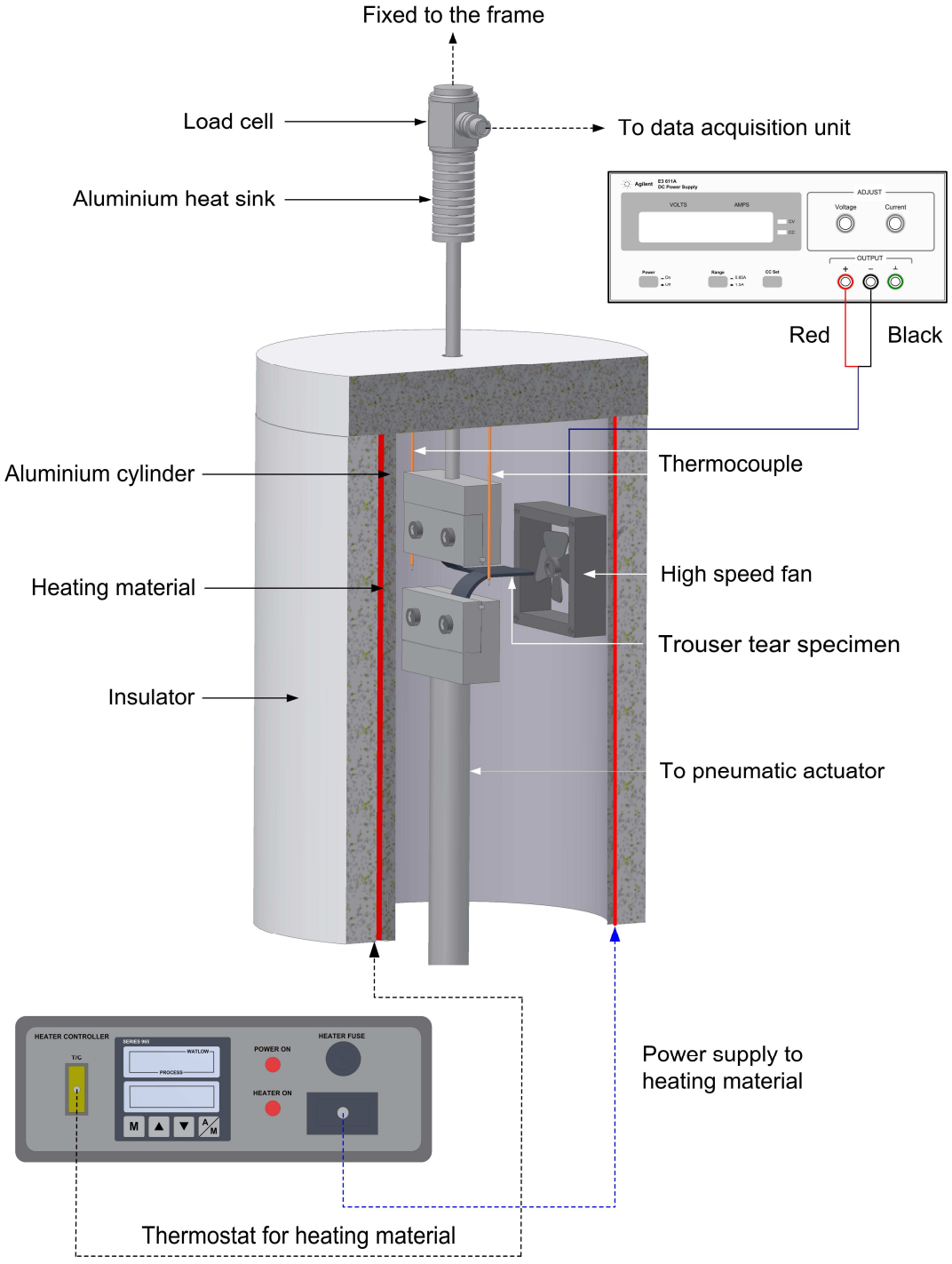

Figure 3.35: Cross-section of the heating oven being equipped with the pneumatic test rig.

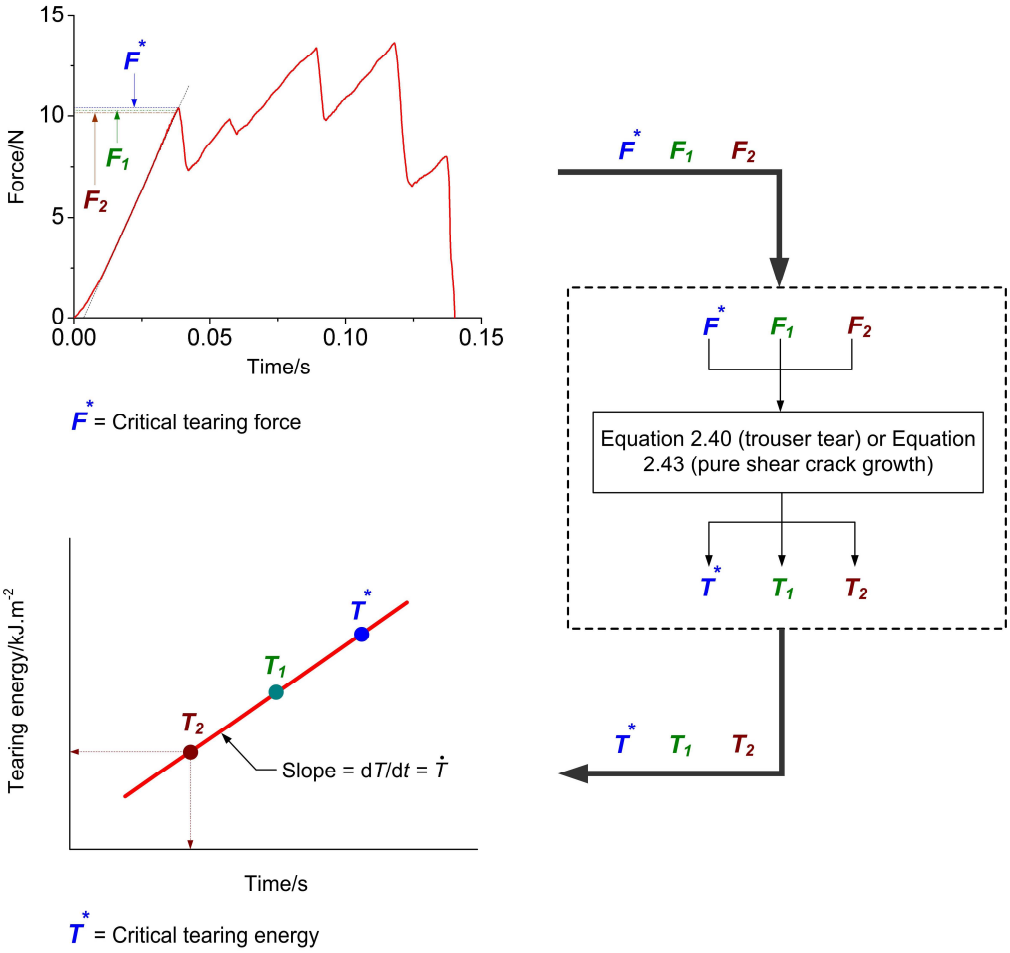

Figure 3.36: Schematic diagram for determining the time derivative of the strain energy release rate $\dot{T}$. The tearing forces as obtained from the force-time curve are transformed to the tearing energies. The $\dot{T}$ is then quantified from the slope of the plot of tearing energy against time.

Table 3.1: Rubber formulations (phr[c]) used in chapter 4 and chapter 6

Ingredients	NR0-S-2.5	NR0-S-7	SBR0-S-2.5	SBR0-S-7	NR50-S-2.5	NR50-S-7	SBR50-S-2.5	SBR50-S-7	NR-P-1	NR-P-3
Natural rubber (SMR CV 60)	100	100	0	0	100	100	0	0	100	100
Styrene butadiene rubber (SBR 1500)	0	0	100	100	0	0	100	100	0	0
Carbon black (HAF N330)	0	0	0	0	50	50	50	50	0	0
Zinc oxide	3	3	3	3	3	3	3	3	0	0
Stearic acid	1	1	1	1	1	1	1	1	0	0
Antioxidant (6PPD[a])	1	1	1	1	1	1	1	1	0	0
Accelerator (CBS[b])	0.75	2.1	0.75	2.1	0.75	2.1	0.75	2.1	0	0
Sulphur	2.5	7	2.5	7	2.5	7	2.5	7	0	0
Peroxide	0	0	0	0	0	0	0	0	1	3
Curing time/min	12	9	27	20	10	8	25	15	42	40
Curing temperature/°C	150	150	150	150	150	150	150	150	150	150
Glass transition temperature/°C	-56	-52	-42	-31	-57	-51	-43	-33	-56	-52
Crosslink density $\times 10^{-4}$/mol.cm^{-3}	0.69	1.37	0.36	1.07	0.79	1.81	0.54	1.29	0.84	2.39
Duromerter hardness/Shore A	40	50	45	55	65	75	65	75	35	50
Tensile strength/MPa	25.4	2.0	2.2	1.7	25.3	9.3	21.9	16	5.3	1.4
Elongation at break/%	750	113	319	63	472	84	292	100	568	70
Density/g.cm^{-3}	0.96	0.98	0.97	1.07	1.15	1.16	1.14	1.17	0.92	0.93

Table 3.2: Rubber formulations (phr[c]) used in chapter 5

Ingredients	NR0-S-2	NR0-S-5	ENR-50-S-2	ENR-50-S-5	BR0-S-2
Natural rubber (SMR CV 60)	100	100	0	0	0
Epoxidised NR (ENR 50)	0	0	100	100	0
Butadiene rubber (JSR BR01)	0	0	0	0	100
Zinc oxide	3	3	3	3	3
Stearic acid	1	1	1	1	1
Antioxidant (6PPD[a])	1	1	1	1	1
Accelerator (CBS[b])	0.6	1.5	0.6	1.5	0.6
Sulphur	2	5	2	5	2
Curing time/min	10	7	14	18	24
Curing temperature/°C	150	150	150	150	150
Glass transition temperature/°C	-56	-52	-14	-12	-90
Crosslink density $\times 10^{-4}$/mol.cm^{-3}	0.38	1.22	0.64	1.32	0.48
Durometer hardness/Shore A	40	50	40	55	40
Tensile strength/MPa	25.7	2.3	25.3	9.5	16.5
Elongation at break/%	750	115	761	325	355
Density/g.cm^{-3}	0.96	0.98	1.05	1.05	0.91

[a]N-(1,3-Dimethylbutyl)-N′-phenyl-p-phenylenediamine.

[b]N-cyclohexyl-2-benzothiazolsulphenamide.

[c]parts by weight per hundred parts of rubber.

Chapter 4: Effect of the rate of strain on tearing in rubber

4.1 Introduction

The relationship between the rate of tearing and the strain energy release rate is a material characteristic that is independent of test piece geometry (Greensmith and Thomas 1955; Thomas 1960). The relationship can, therefore, be characterised by a range of suitable test specimens. One of the most convenient ways to investigate this characteristic relationship is to use the trouser tear specimen. With this type of test specimen, the characteristic tearing behaviour of rubber can be quantitatively investigated. For over half of a century, the characteristic crack propagation rate of rubber has been evaluated using the relation which is a function of the crosshead speed of the testing machine (Greensmith and Thomas 1955; Greensmith 1956; Greensmith et al. 1960).

This approach can be used correctly to characterise the tearing of rubber when the rate is steady as is often observed with an unfilled and non-crystallising rubber such as styrene-butadiene rubber (SBR). During steady tearing, the rate of propagation essentially remains constant once the tearing has commenced. If the crack growth rate dc/dt, which is approximately half of the crosshead speed according to Equation 2.54 as described in chapter 2, has been plotted against time t as shown in Figure 4.1. Obviously, the dc/dt remains constant until the rubber has been completely ruptured. However, for a lot of rubber materials such as a strain-crystallising rubber like natural rubber (NR) or with rubbers filled with reinforcing fillers such as carbon black the rate of tearing is no longer steady. The resulting unsteady tearing behaviour can either be stick slip in nature as shown in Figure 4.2 (a) or even knotty in behaviour as shown in Figure 4.2 (b). Under these unsteady crack growth conditions, an average rate of crack growth determined from the rate of the crosshead displacement is meaningless as it is just an arbitrary average of an unspecified rapid rate of crack growth and a zero rate. The relationship between dc/dt and t obtained from the unsteady tearing also renders the same trend of correlation as that of the steady tearing as shown in Figure 4.2 under this framework. This issue has remained unresolved for nearly 60 years since Rivlin and Thomas (1953) introduced a practical approach to characterise the tearing

behaviour of rubber built up on the energy balance approach. For this reason, the following questions can be raised:

- Is there an alternatively logical approach that is able to characterise the rate of unsteady tearing of rubber without using the rate of clamp separation of the test machine?

- How can the rate during unsteady tearing be measured to create a characteristic crack growth rate which is a combination of the zero rate (a stick process) and the maximum tearing rate (a slip process)?

- Is there possibly a universal approach to characterise the tearing behaviour of rubbers regardless of the type of tearing?

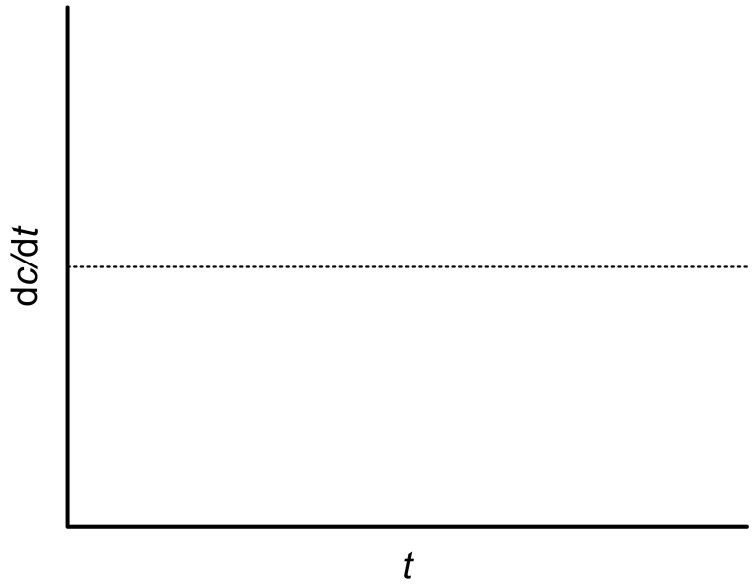

Figure 4.1: A plot of the crack propagation rate d*c*/d*t* against time *t* of the steady tearing behaviour as determined by assuming the rate is constant as indicated by the rate of the clamp separation.

This chapter, based on the publication by Sakulkaew et al. (2010), will address each of these questions whilst developing new approach to characterise and investigate the tearing behaviour of rubber.

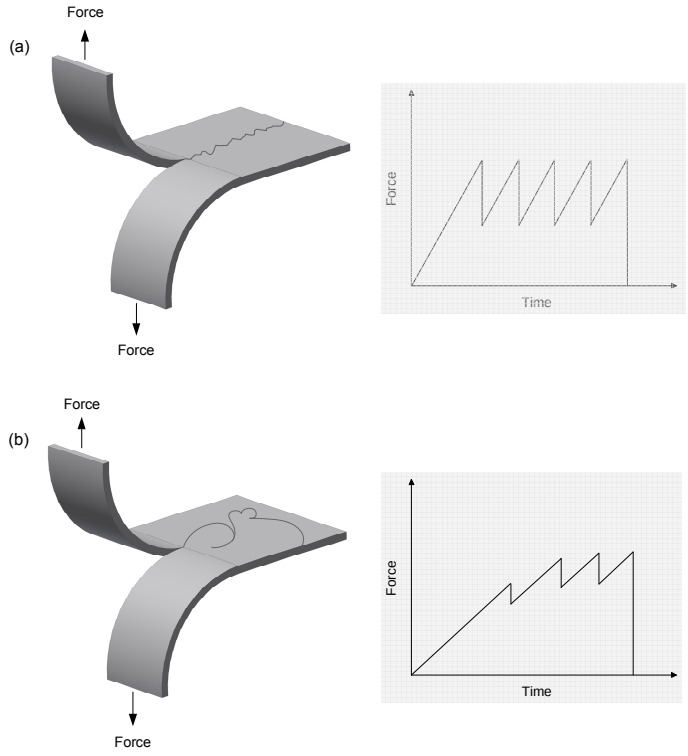

Figure 4.2: Schematic diagram illustrating the plot of tearing force against time of the unsteady tearing behaviour: (a) stick-slip and (b) knotty.

4.2 Theory

For the purpose of this study, it is presumed that the characteristic crack tip diameter *d* does not alter significantly during tearing and thus a measure of the strain energy release rate is proportional to the strain energy at the tip of the crack (Thomas 1955; Greensmith 1956).

$$T \approx dE_t \qquad \text{Equation 4-1}$$

It is possible to take the time derivative of Equation 4-1 to develop the following relationship:

$$\dot{T} \approx d\dot{E}_t \qquad \text{Equation 4-2}$$

Here, $\dot{T}$, which is dT/dt, is the rate of change in the strain energy release rate with time and $\dot{E}$, which is dE_t/dt, is the rate of change of the strain energy with time at the tip of the crack. This equation shows that a measure of the rate of change of strain energy release rate with time can be used as an equivalent measure of the increase in the strain energy at the tip of the crack with time by assuming that the unstrained crack tip diameter d does not change significantly during tearing.

4.3 Results and discussions

The new method, as described in chapter 3, for the first time to characterise the rate of increase in the strain energy at the crack tip just prior to the onset of tearing can be directly measured as the time derivative of the strain energy release rate $\dot{T}$. Figure 4.3 shows the typical tearing process that has been observed in the trouser tear specimen primarily employed in this study. In this chapter, NR, which exhibits strain-induced crystallisation, and SBR, which is a non-crystallising rubber were utilised in order to allow the different contributions from these two characteristic effects to be considered. The experimental results will be divided into 4 phases. The unfilled vulcanisates will be discussed first followed by carbon black-filled compounds. In addition to the sulphur-cured compounds which were mainly used in this study, the peroxide-cured vulcanisates were also utilised which will be discussed in the third phase together with a comparison of the test results obtained from the different test piece geometries: trouser tear and pure shear crack growth specimens. The first materials considered are unfilled NR compounds, which have been observed in the past to have a complicated relationship between the average tearing rate (measured using the average crosshead speed) with strain energy release rate (Greensmith 1956). At first, the material becomes weaker with increasing rate of tearing and then becomes stronger. It has been proposed that the reduction in tear strength is a result of the material being loaded too fast for some aspects of strain-induced crystallisation to fully develop. The subsequent increase in the tearing energy with loading rate has been thought to result from a characteristic increase in the viscoelastic dissipation that arises in a polymer as the rate of loading is increased or if the test temperature is reduced. It is also known that by significantly increasing the crosslink density the kinetics of the strain induced crystallisation are reduced as a result of both more main chain modification as well as a more tightly constrained macromolecular network (Gent 1958). Thus, two

significantly different levels of crosslink density are examined for each of material used in this work.

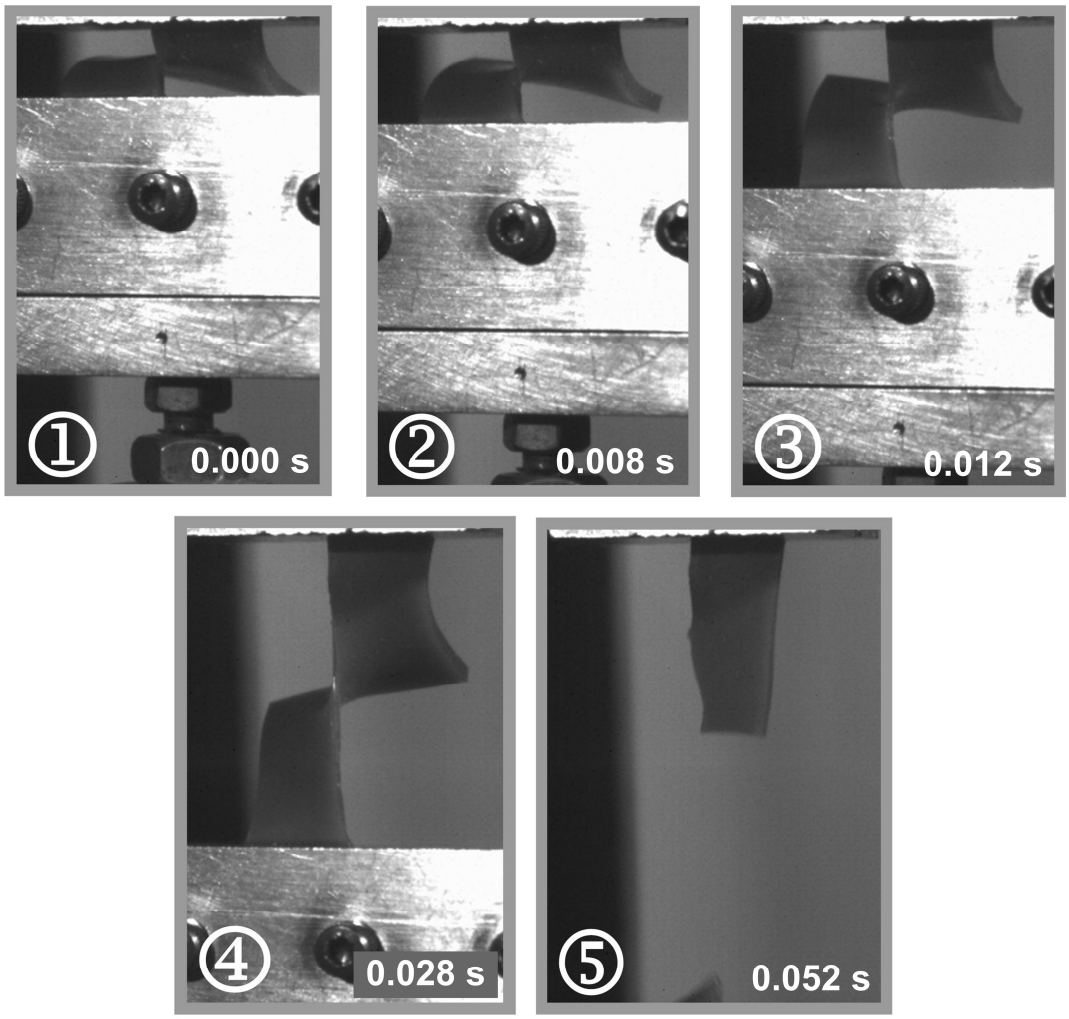

Figure 4.3: Tearing process of the trouser tear specimen which is subjected to a pneumatic actuator. The number ① to ⑤ represent the sequence of events in association with tearing. The onset of tearing is represented by ②. These pictures were captured by a high speed camera with a frame rate of 8000 frames/sec.

The new approach of characterising the critical tearing energy T^* as a function of the rate of change in the strain energy release rate $\dot{T}$ is shown in Figure 4.4 to 4.9 for all the materials tested.

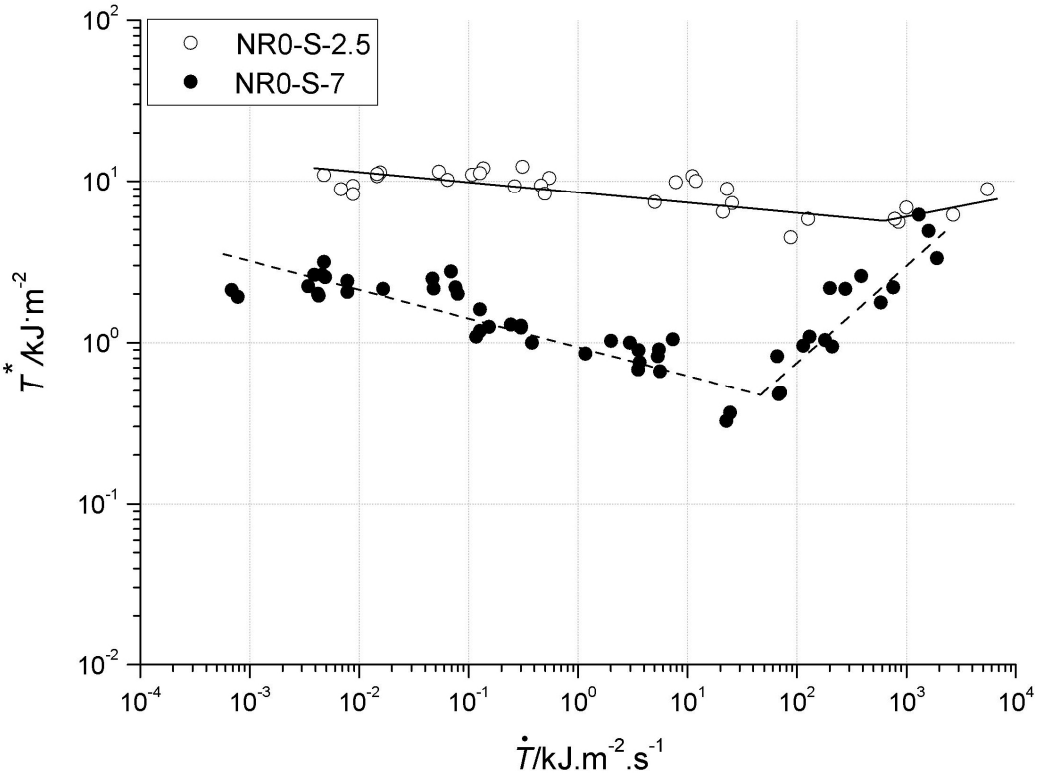

Figure 4.4: Critical tearing energy *T is a function of time derivative of the strain energy release rate $\dot{T}$ of NR vulcanisates with different degrees of crosslink density.**

Figure 4.4 shows the dependence of the critical tearing energy on the rate of testing for the two unfilled NR compounds. The crosslink density of NR0-S-7 is about double that for NR0-S-2.5. The less highly crosslinked compound, NR0-S-2.5, is considerably stronger than the more tightly crosslinked material. This is consistent with the general behaviour reported previously in the literature (Brown et al. 1987). For NR0-S-2.5, there is virtually no dependence of the tearing energy on the rate of testing. There is a very specific rate dependence observed though for NR0-S-7. For this material, the tear strength initially goes down with the magnitude of the strain rate at the tip of the crack and it is seen to increase. The first drop is most likely a result of the suppression of strain-induced crystallisation in the more highly crosslinked material. The increase in the number of crosslinks will have modified the main chains more extensively and it will also inhibit the movement of the polymer chains. Both of these effects are thought likely to reduce the rate of crystal formation

under strain. The critical tear strength reaches a minimum at about 100 $kJ.m^{-2}.s^{-1}$. Above this value, the effects of increased viscoelastic behaviour at the tip of the crack generate an increase in tear strength and, eventually, at the fastest rates the strength approaches that of NR0-S-2.5.

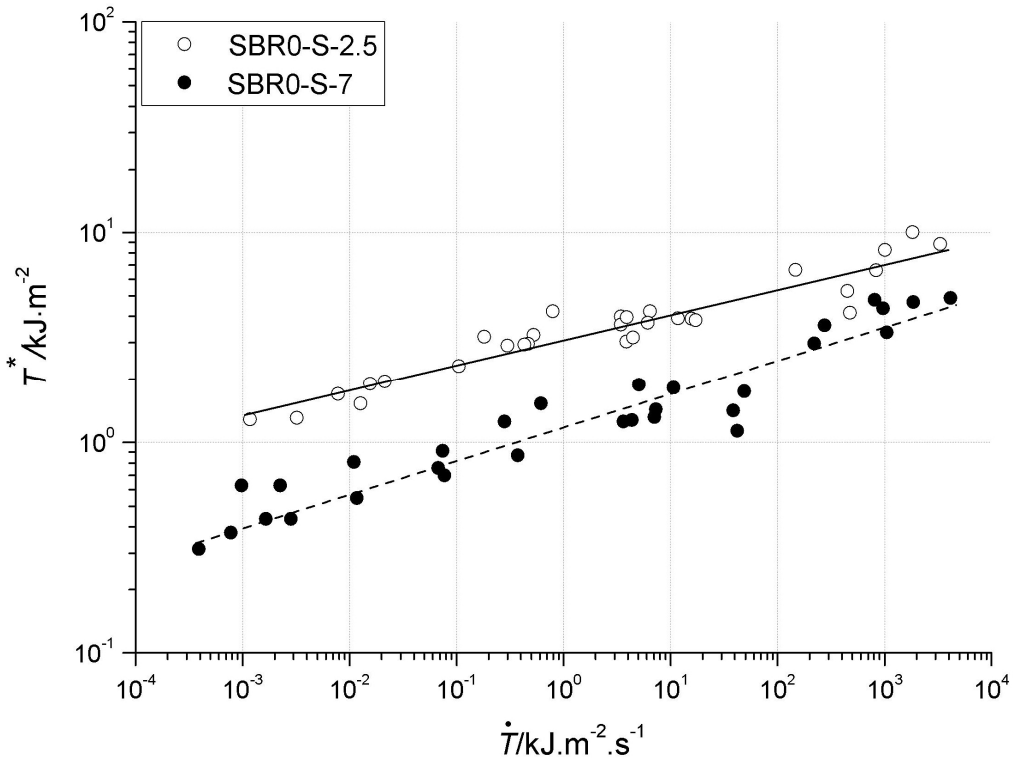

Figure 4.5: Critical tearing energy *T is a function of time derivative of the strain energy release rate $\dot{T}$ of SBR vulcanisates with different degrees of crosslink density.**

The two unfilled SBR compounds are shown in Figure 4.5. As there are both non-strain crystallising rubber, it is clear that the only observable effect is an increase in the tear strength with rate of testing. Both of these materials exhibit steady tear behaviour, so the traditional approach of using a crack growth rate from the crosshead separation would be an acceptable measure of the tear rate. The SBR tear data is plotted here using the new approach only for comparison with NR. The most lightly crosslinked SBR is again much weaker and the increase in viscosity with rate is the reason that both materials become stronger as the rate of testing is increased. The materials are considerably weaker than the unfilled NR compounds.

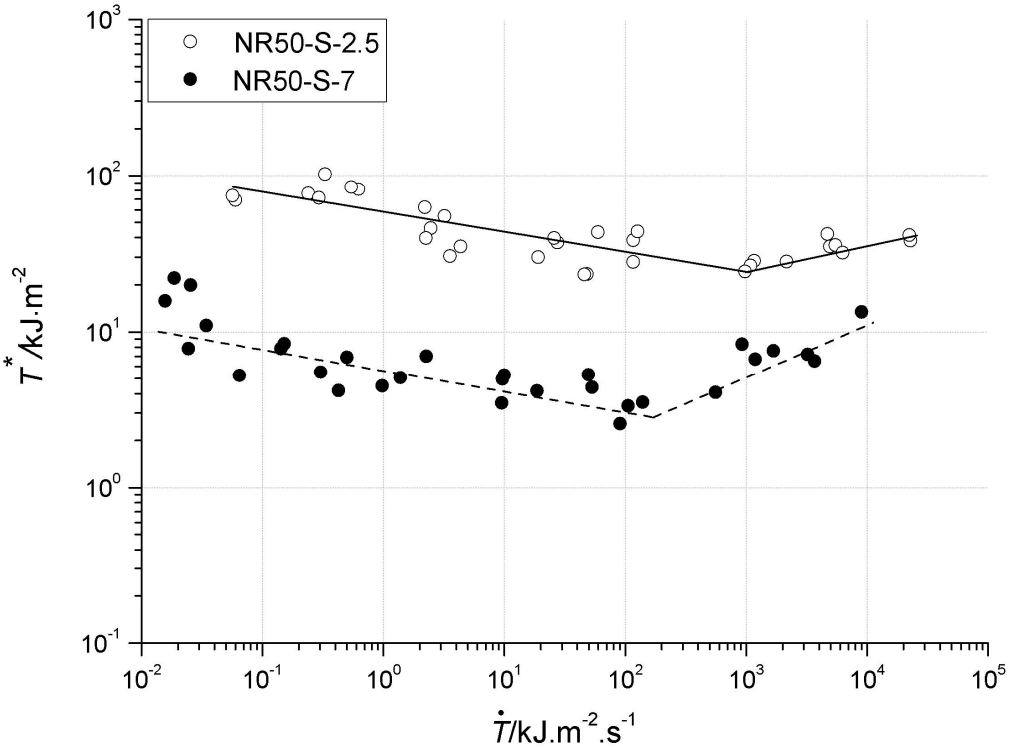

Figure 4.6: Critical tearing energy *T is a function of time derivative of the strain energy release rate $\dot{T}$ of carbon black-filled NR vulcanisates with different degrees of crosslink density.**

The filled NR results are shown in Figure 4.6. Again, the crosslink density of NR50-S-7 is more than double the crosslink density of NR50-S-2.5. The results are broadly similar to those shown in Figure 4.4 for the unfilled NR materials, the most significant difference being that the filler makes both the high and low crosslinked materials more tear resistant. For both levels of crosslink density there is now a consistent reduction in strength with increasing rate as the kinetics of strain induced crystallisation being too low to allow the full development of reinforcing crystals. The higher crosslink density produces a weaker material and, again, it reaches a minimum at 100 kJ.m^{-2}.s^{-1}. For the lower crosslink density, the curve now also passes through a minimum, but this is at a higher tear rate. Above these minima, the rubbers exhibit a strengthening that is a result of the viscoelastic toughening increasing with test speed. It is clear that this new way of examining the fracture behaviour allows the different reinforcing mechanisms to be indentified and examined in more detail than has been previously possible.

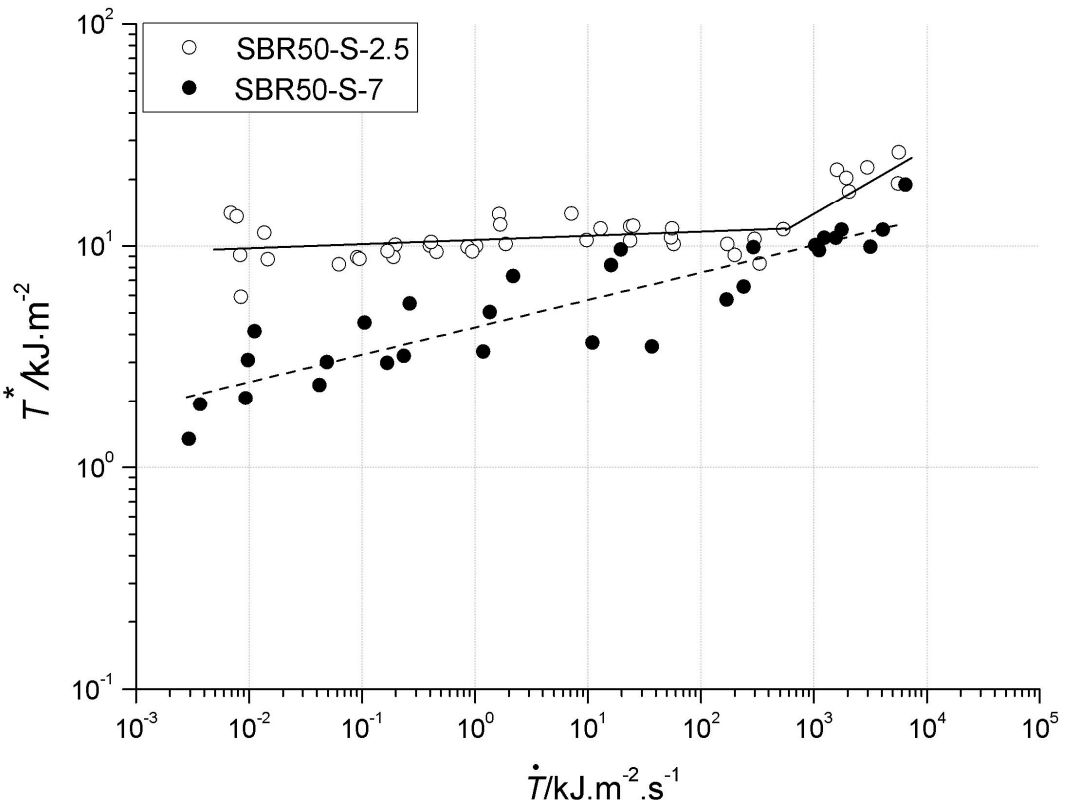

Figure 4.7: Critical tearing energy *T is a function of time derivative of the strain energy release rate $\dot{T}$ of carbon black-filled SBR vulcanisates with different degrees of crosslink density.**

In Figure 4.7, the results for the two filled SBR compounds are shown. Clearly the more highly cross-linked material (SBR50-S-7) exhibits only a characteristic increase in tear strength with rate. SBR50-S-2.5 appears to have two slopes in the behaviour with only a modest increase in tear strength with rate at the lower rates and a faster increase in tear strength with rate at faster rates. It is possible that the technique of presenting the data in this way is identifying an additional effect that counteracts the simple viscoelastic effects alone. These could include for example a kinetic effect related to the rate of formation of the reinforcing structure. Results for the peroxide-cured NR materials are shown in Figure 4.8.

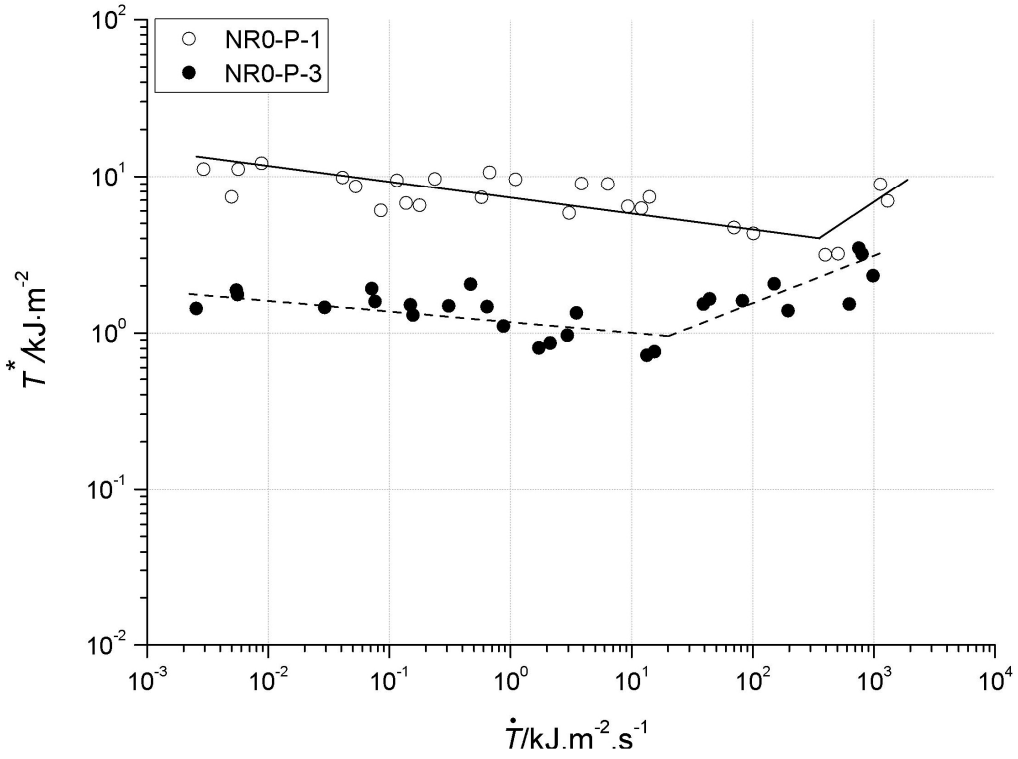

Figure 4.8: Critical tearing energy *T is a function of time derivative of the strain energy release rate $\dot{T}$ of peroxide-cured NR vulcanisates with different degrees of crosslink density.**

It was found that less highly crosslinked compound, NR-P-1 is considerably stronger than the more tightly crosslinked vulcanizate NR-P-3 over the entire range of test rates reported. This trend is similar to that of sulphur-cured vulcanizates.

Additionally, the experiment was also carried out using the pure shear crack growth specimen in order to compare the test results obtained from this type of test piece geometry with those obtained from the trouser tear specimen as shown in Figure 4.9. Figure 4.10 shows the tearing process of the pure shear crack growth specimen.

It is found that there is a good correlation between the trouser tear and pure shear crack growth specimens in terms of the relationship between the critical tearing energy and the time derivative of the strain energy release rate.

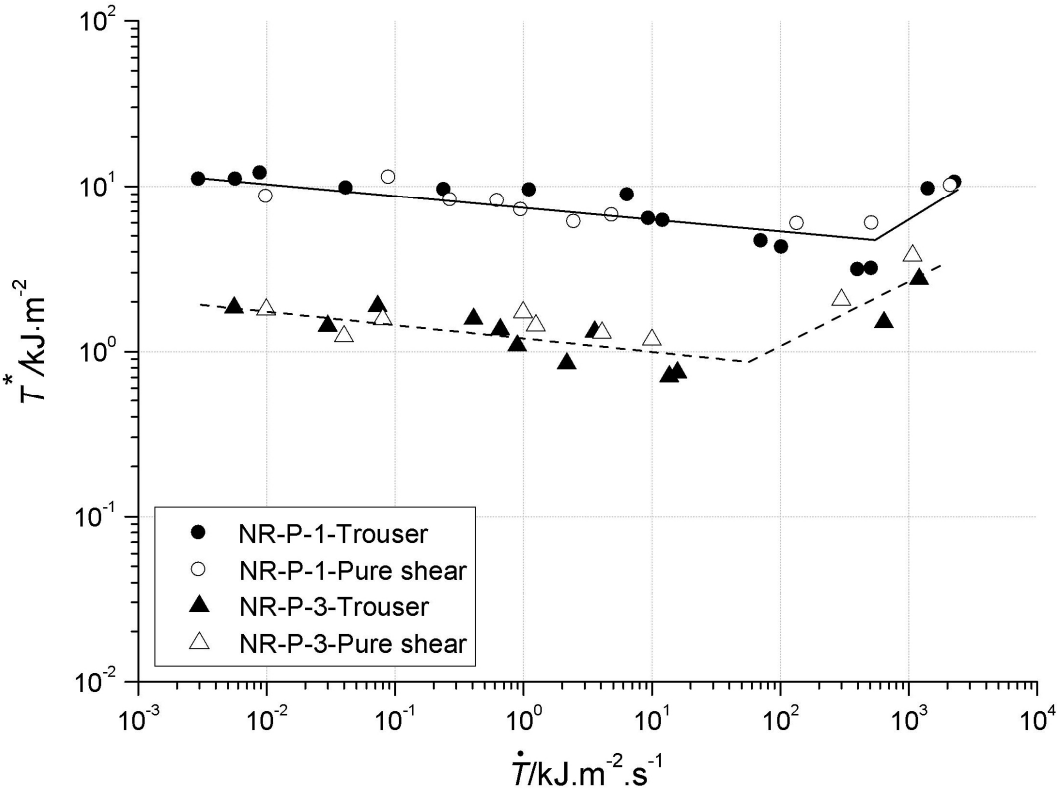

Figure 4.9: Critical tearing energy *T is plotted as function of time derivative of the strain energy release rate $\dot{T}$ of peroxide-cured NR vulcanisates with different degrees of crosslink density obtained form the trouser tear and pure shear crack growth specimens.**

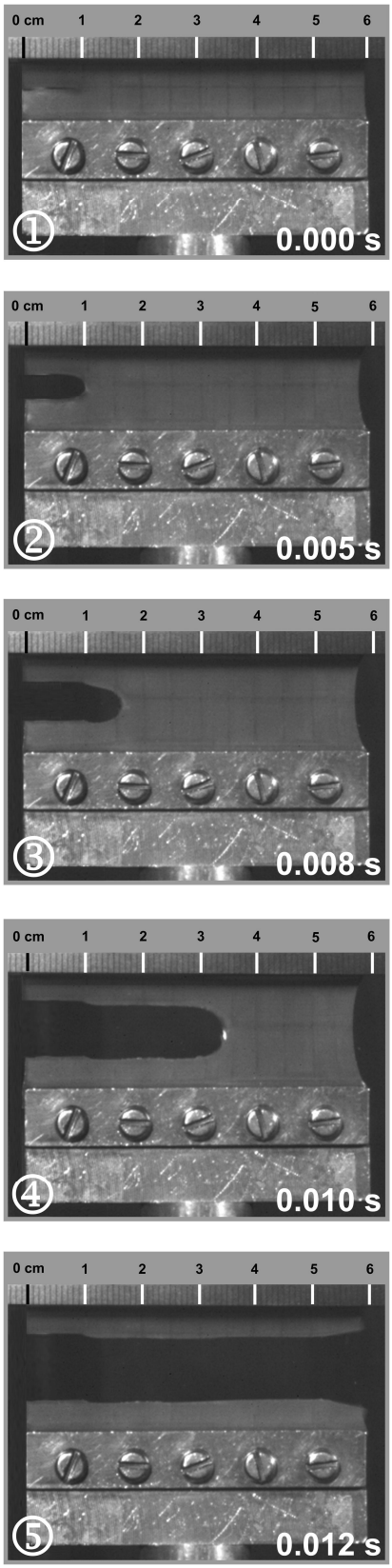

Figure 4.10: Tearing process of the pure shear crack growth specimen. These pictures were captured by a high speed camera with a frame rate of 8000 frames/sec.

4.4 Conclusions

An entirely new approach to characterise the rate of tear and the critical strain energy release rate relationship has been demonstrated. It provides a much clearer way of characterising the rate of strain at the tip of the crack, which is thought to be the main factor when determining the strain energy release rate for the extension of a crack in a rubber sample. The method of using the first derivative with time of the strain energy release rate $\dot{T}$ is easy to measure and can be used to examine all types of non steady tearing such as stick slip or knotty tearing that is observed for a wide range of rubbers.

The method has been applied to different rubbers using a trouser tear test samples and pure shear crack growth specimen over a wide range of fracture rates. The NR samples all exhibit characteristic tearing at the slower rates that represents the failure after the samples have been strain crystallised. At the fastest rates the kinetics of crystallisation were beaten for these materials and the behaviour was that more typically associated with viscoelastic strengthening alone. Unfilled SBR materials were examined for comparison purposes and the technique was useful in identifying the extent of viscoelastic toughening. The filled SBR exhibits non steady tearing and again the technique is suitable to characterise the tear behaviour.

Chapter 5: Examining the effect of temperature on the tearing of rubber

5.1 Introduction

Chapter 4 showed that the relation between the time derivative of the strain energy release rate $\dot{T}$, which is associated with the rate of increase in the strain energy at the crack tip just immediately before the onset of tearing, and the critical tearing energy T^* to propagate the crack allows the effect of the strain-induced crystallisation observed in natural rubber (NR) to be evaluated. In particular, the degree of crosslinking was altered to modify the kinetics of the formation of crystals which are induced by strain. This relation also provides a useful approach in identifying the extent of the viscoelastic toughening in styrene-butadiene rubber (SBR). Additionally, it has been shown that the introduction of the reinforcing filler, such as carbon black, can have a significant effect on the tearing behaviour of rubber. This chapter extends the previous work by examining the effect of elevated temperature on the relation between $\dot{T}$ and T^* using a different range of unfilled rubbers. It is anticipated that this way of analysing the tear behaviour will allow the kinetics of strain crystal formation to be studied.

This chapter is based on a publication by Sakulkaew et al. (2012), and it explores a novel approach to characterise and investigate the tearing behaviour of rubber material over a range of test rates and temperatures.

5.2 Theory

As introduced in chapter 4, it is still presumed that the characteristic crack tip diameter d does not alter significantly during tearing and thus a measure of the strain energy release rate is proportional to the strain energy at the tip of the crack at break (Thomas 1955; Greensmith 1956):

$$T \approx dE_t \qquad \text{Equation 4-1}$$

It is possible to take the time derivative of Equation 4-1 to develop the following relationship:

$$\dot{T} \approx d\dot{E}_t \qquad \text{Equation 4-2}$$

Here, $\dot{T}$, which is dT/dt, is the rate of change in the strain energy release rate with time and $\dot{E}$, which is dE_t/dt, is the rate of change of the strain energy with time at the tip of the crack. Similarly, the rate of strain energy increase at the crack tip can be considered to be a simple relationship with the rate of strain at the crack tip. This equation shows that a measure of the rate of change of strain energy release rate with time can be utilised as an equivalent measure of the increase in strain at the crack tip with time.

To do this, three unfilled strain-crystallising rubbers which exhibit unsteady tearing behaviour were investigated. The first material is again natural rubber which shows a significant drop in the strength as the temperature increases (Thomas and Whittle 1970; Gent at al. 1998). The second material is the epoxidised natural rubber (ENR-50) which is the chemically modified natural rubber with half of the isoprene units being epoxidised. However, it can still undergo some strain crystallisation (Davies et al. 1983). The third material is butadiene rubber (BR) with 95% *cis* content. Butadiene rubber can strain crystallise and shows a similar trend in the drop of strength with the increasing temperature (Gent and Zhang 2001). These materials were crosslinked with sulphur to various degrees of crosslinking with the ratio of the accelerator to sulphur set at 0.3. The higher extent of crosslinking is expected to inhibit crystallisation due to some modification of the main polymer chain.

5.3 Results and discussions

The approach adopted here to characterise unsteady tearing is to plot the measured data in the form of the critical strain energy release rate, T^*, against the rate of change in the energy release rate with time $\dot{T}$. The results are shown in Figures 5.1-5.5 for each of the five rubber compounds investigated as part of this study.

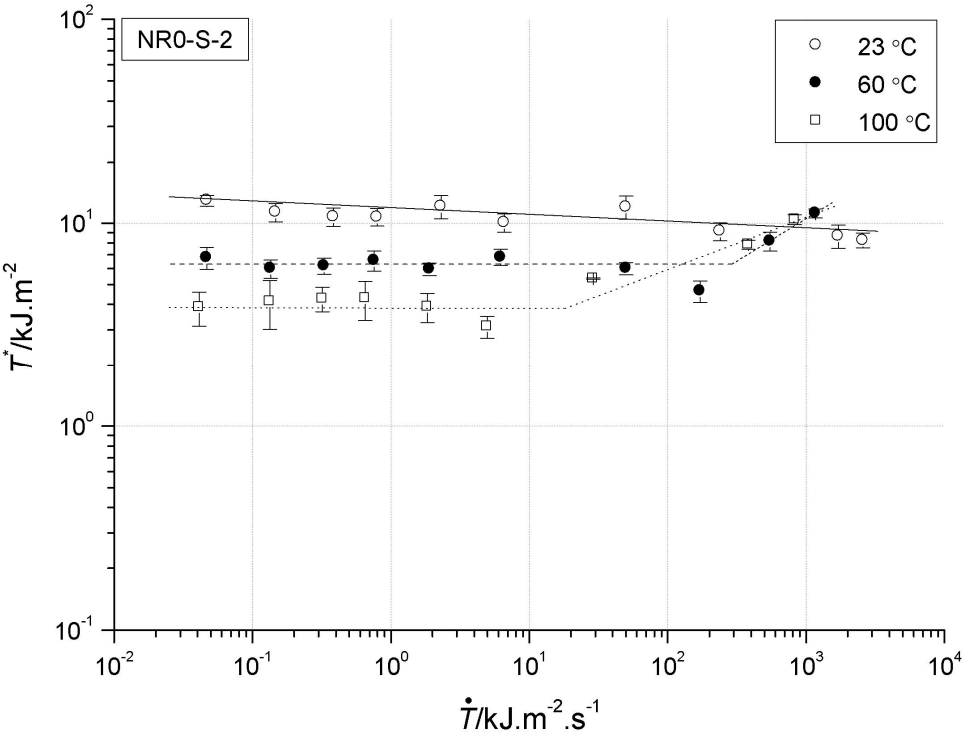

Figure 5.1: Plot of the critical strain energy release rate T^* against $\dot{T}$ of NR0-S-2.

Figure 5.1 shows the dependence of the critical strain energy release rate, T^*, on the rate of change in the strain energy release rate, $\dot{T}$, for the lightly crosslinked natural rubber, NR0-S-2, at three different temperatures over a four order of magnitude change in the test rate. Clearly the increase in temperature has the significant effect of reducing T^*. The increase in temperature takes the rubber further from its glass transition temperature, which can both reduce the amount of visco-elastic toughening as well as reduce the amount or the nature of any strain-induced crystals that can be formed in the region of the crack tip. At 23°C, T^* is surprisingly independent of the rate of loading, $\dot{T}$. If anything, the critical strain energy release rate is slightly reduced with rate. There are two possible explanations for this. The first is that the tearing behaviour is determined essentially by the energy release rate

of the strain-induced crystals and that their energy release rate is almost totally independent of the rate of tearing over this wider range of rates. The second explanation is that any anticipated increase in strain energy release rate from an increase in the viscoelastic behaviour at the faster tearing rates is almost exactly

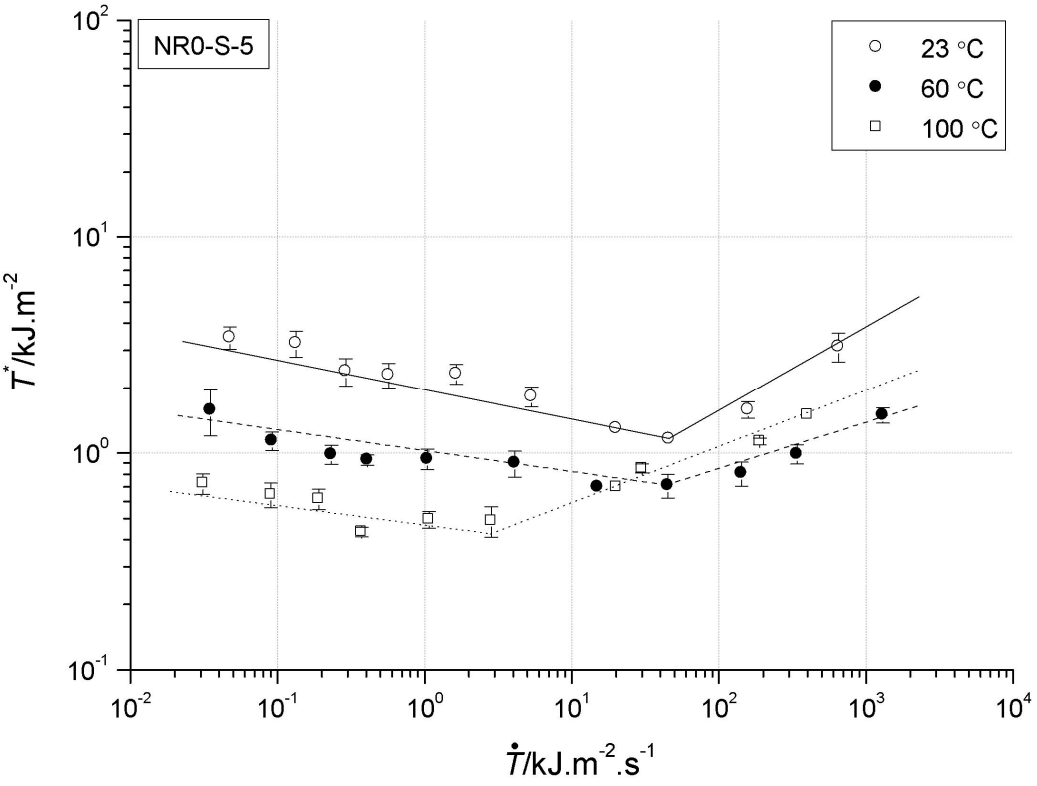

Figure 5.2: Plot of the critical strain energy release rate *T against $\dot{T}$ of NR0-S-5.**

balanced by a reduction in strain energy release rate resulting from a reduction in the toughness due to inhibition of crystallisation by the increased rate of tearing. At the two higher temperatures, the plot of the relation between T^* and $\dot{T}$ shows a break point in the curves. T^* initially goes down slightly with $\dot{T}$ and then it is seen to increase. At 100 °C, the break point appears at a slower rate than is seen at 60°C. Exactly what is taking place at the fastest tearing rates above the break in the curve is hard to determine, but it is likely that the rubber is tearing at a rate too fast to allow the formation of any significant reinforcing strain crystals. This indicates that either the kinetics or the extent of strain-induced crystallisation is temperature dependent. Above the break the tear resistance is, therefore, determined primarily from a consideration of the viscoelastic behaviour of the rubber and it is, therefore, much more tear rate dependent at these faster tearing rates.

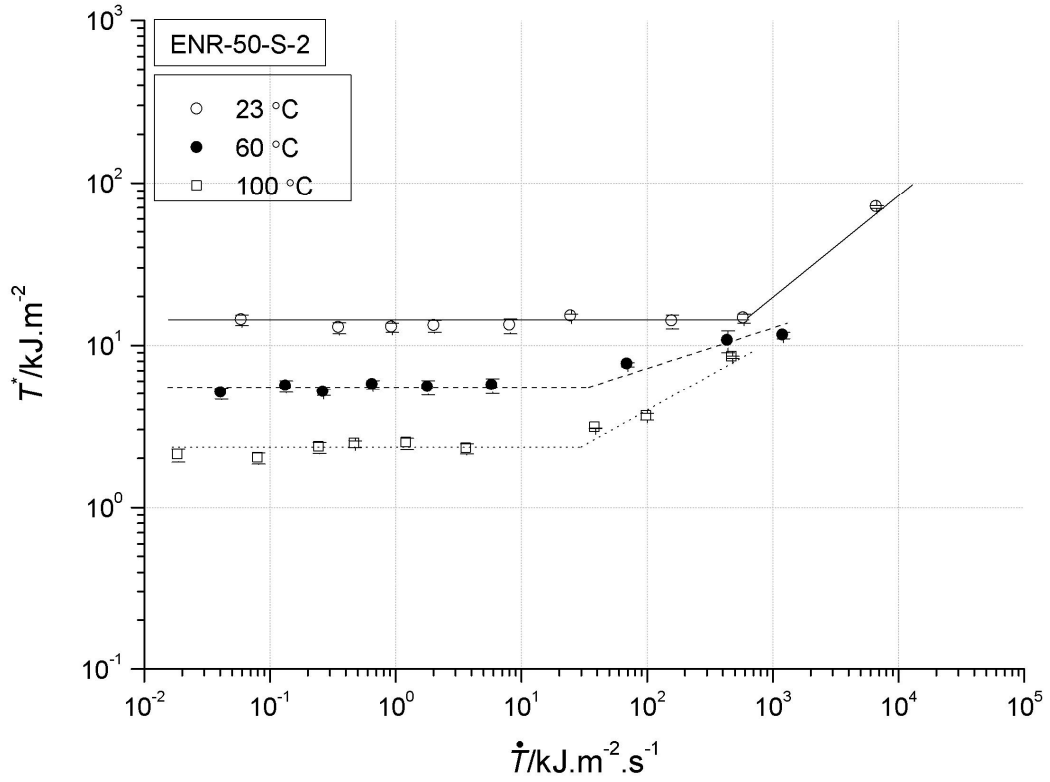

Figure 5.3: Plot of the critical strain energy release rate *T against $\dot{T}$ of ENR-50-S2.**

NR0-S-5 has a crosslink density about twice that of NR0-S-2, as shown in table 3.2. Over the entire range of temperatures and test rates, *T** of NR0-S-5 (shown in Figure 5.2) is significantly lower than those discussed earlier for NR0-S-2. This reduction in *T** results from the rubber being more tightly crosslinked, and hence less viscous and much stiffer in comparison. This is consistent with the general behaviour reported previously in the literature (Brown et al. 1987). The high sulphur content also introduces significant main chain modification in the rubber molecules. This in turn will interfere with the kinetics of crystal formation and the extent of crystal formation. For all three test temperatures, there is a clear reduction in *T** with tearing rate over the range of the slower test rates. In this case, it is proposed that the increase in tear rate results in a reduction in the amount of crystallisation possibly due to the kinetics of crystal formation being relatively slower than the rate of loading used in the tests. Again, there is a break point in the curves above which *T** is significantly increased by increasing the tearing rate. In this fast region, it is again proposed that the crystallisation phenomenon is being suppressed and that the toughness of the material is primarily dependent upon the viscoelastic nature of the rubber. Broadly speaking, the materials rank as expected with temperature, as the further the rubber is from the glass transition temperature the weaker the

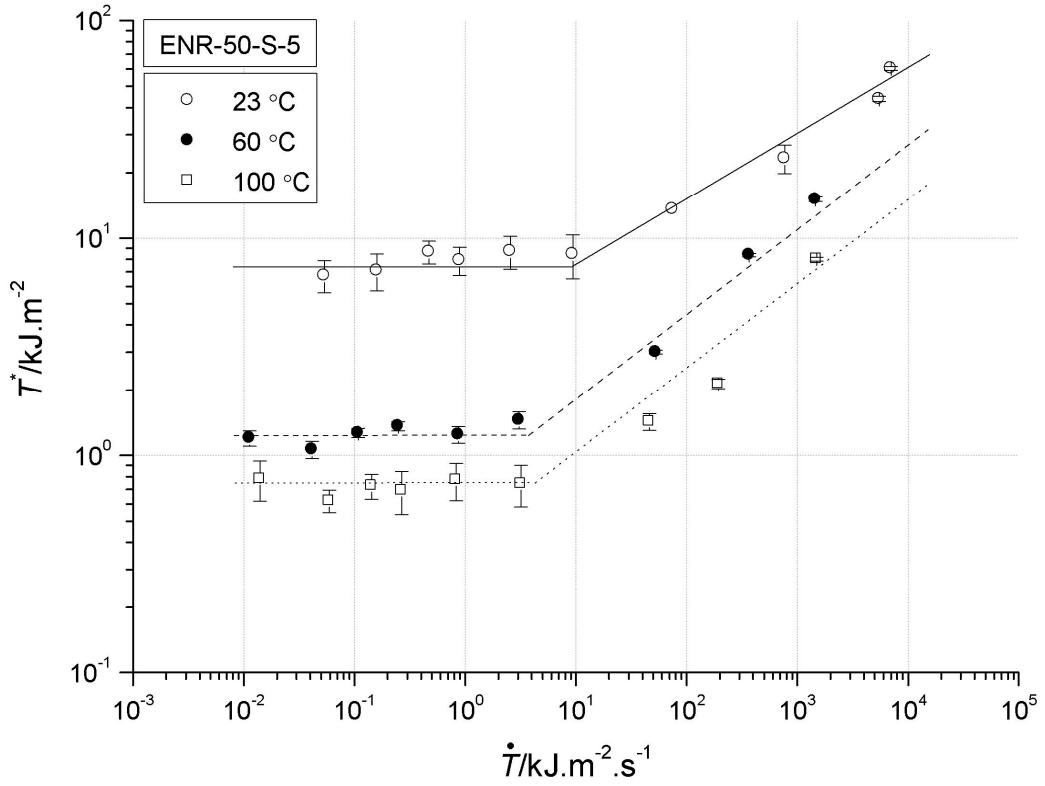

Figure 5.4: Plot of the critical strain energy release rate *T against $\dot{T}$ of ENR-50-S-5.**

material is observed to be. An increase in temperature is again seen to reduce the break point in the curves. This suggests that at higher temperatures, it is harder to crystallise the rubber in the region of the crack tip, and any crystals that are being formed do so to a lesser extent.

The ENR-50 results are shown in Figures 5.3 and 5.4. The epoxidation process is seen to increase the glass transition temperature above that of their NR counterparts. This leads to more energy dissipation being observed than was the case for the corresponding NR compound. Although this material has been chemically modified, it retains its ability to strain crystallise due to the retention of the *cis*-1, 4-stereoregular configuration of NR (Davies et al. 1983). Table 3.2 shows that ENR-50-S-5 has approximately double the crosslink density of ENR-50-S-2. The results are broadly similar to those shown in Figure 5.1 and 5.2 for NR, with a rise in temperature resulting in a reduction in *T**. Again, for all the tests over a wide range of the slower rates of tearing, *T** is remarkably independent of the rate of tearing that is until the break point arises, above which *T** increases dramatically as $\dot{T}$ increases. Below the break point, *T** is again most likely determined from the tear resistance of the crystals, and any expected increase in *T** due to increased viscoelastic

behaviour at the faster rates is again balanced by a presumed similar reduction in crystallisation behaviour with rate. Above the break point, the behaviour is probably being dominated by viscoelastic energy dissipation processes. ENR-50-S-5 is much

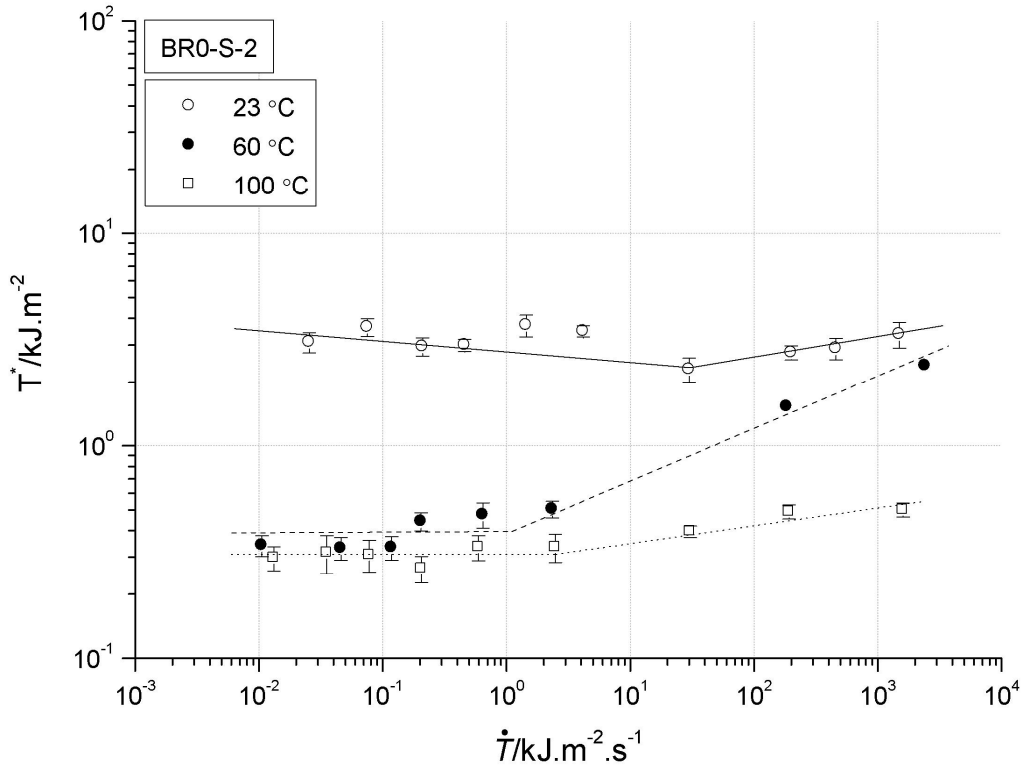

Figure 5.5: Plot of the critical strain energy release rate *T against $\dot{T}$ of BR0-S-2.**

weaker than the less highly crosslinked ENR-50-S-2 compound and the break points are again at slower rates. It is presumed that the higher degree of crosslinking in ENR-50-S-5 again results in modification to the main chain which suppresses the amount of crystal formation in the polymer under strain.

The data for the tearing of the butadiene rubber (BR0-S-2) are shown in Figure 5.5. For BR the glass transition temperature is much lower at -90 °C than the other two rubbers. At each test temperature it is clear that the amount of viscoelastic energy dissipation will be comparably less. This results in reduced *T** when the curves are compared with the other two lightly crosslinked compounds at, for example, room temperature. Butadiene was chosen in this work as it can strain crystallise somewhat at room temperature, but the crystallisation behaviour is significantly suppressed at higher temperatures (Gent and Zhang 2001). This suppression of crystallisation is evident in the weak response of the BR material at the higher temperatures. At 60 °C there is a dramatic rise in *T** with rate but by 100 °C, when

the test is 190 °C above the glass transition temperature, there is hardly any viscoelastic toughening even at the fastest test rates. This weak response at the highest temperature indicates that strain-induced crystallisation and viscoelastic toughening are both effectively removed in BR at 100 °C.

5.4 Conclusions

The conclusions of chapter 4 that using this test approach allows a more detailed understanding of the unsteady tearing behaviour of rubber than was possible in the past, that the reduction in T^* with rate indicates a reduction in strain-induced crystallisation, and that an increase in T^* indicates an increase in the toughness of the rubber due to viscoelastic rate effects have all been confirmed again in this chapter.

In addition to these conclusions it is interesting to note that as expected increasing the temperature reduced the strength of all the materials across the entire range of test rates. This is to be expected as the temperature rise takes the rubber materials further away from the glass transition temperature. In addition, increasing the cross link density produces weaker materials as a result of both reducing crystallisation and by making the materials less viscous. Somewhat unexpectedly though increasing the test temperature has the effect of reducing the tear rate at which the transition from crystallisation dominated toughening to viscoelastic dominated toughening takes place. This was surprising as increasing temperature might have increased the rate at which strain crystals form. This suggests that the amount of crystallisation is reduced at the higher temperature and it is this effect that dominates the transition in the strengthening behaviour.

The expoxidised natural rubber with its highest glass transition temperature showed the most significant effect of both temperature and tearing rate on T^*. The effect of temperature on the butadiene rubber showed that some crystallisation took place a slow rates and at the lower temperatures but by 100 °C crystallisation was totally suppressed and the polymer was sufficiently far from the glass transition temperature that T^* is seen to be virtually independent of tearing rate.

Chapter 6: Elastic-viscous transition in fracture of rubber

6.1 Introduction

The new approach employed to characterise the rate of tearing and the critical strain energy release rate relationship has been demonstrated in chapter 4 and chapter 5 with various rates of loading and temperatures. The approach has been developed for the first time to characterise the rate of increase in the strain energy at the crack tip immediately prior the onset of tearing in rubbers that, in particular, exhibit the unsteady tearing behaviour normally found in the strain crystallising rubber or in filled rubber. It is found that the change of critical strain energy release rate at given value of the time derivative of the strain energy release rate in rubber could be defined as the elastic-viscous transition phenomenon. This transition depends strongly on the balance of elasticity and viscosity of the material in the glass transition temperature and thus two factors: the crosslink density and the viscoelastic energy dissipation of the material governing the phenomenon. Therefore, in this chapter, a new elastic-viscous transition diagram, in association with the rate of change in the strain energy release rate at the tip of the crack, is introduced. This chapter is based on a journal paper has been submitted to Polymer.

6.2 Theory

Tearing energy of rubber material is an inherent failure characteristic independent of geometry and loading. This material characteristic has been derived based on the energy balance approach (Rivlin and Thomas 1953). In fracture process, the strain energy as elastically stored in the rubber which is under the strained state is partly employed to break interatomic bonds to create the new fracture surfaces and it is also partly dissipated in irreversible processes like viscous or viscoelastic flow throughout the material. The greater the increase in the energy dissipation, the higher the strength is. The tearing behaviour of rubber has been usually characterised by the relationship between the tearing rate and the critical strain energy release rate or the critical tearing energy. As described in the chapter 2, the dependence of the tear strength on the tearing rate has been examined by many investigators (Greensmith 1956; Kadir and Thomas 1981; Tsunoda et al. 2000;

Busfield et al. 2002). Interestingly, the tearing phenomenon of rubber material as derived from this interrelation exhibits the three distinctive regimes in relation to the characteristic fracture surfaces.

A similar phenomenon has also been observed in peeling of an adhesive tape (Aubrey and Sherriff 1980; Barquins and Ciccotti 1997), where the three modes of peeling are generated in association with the peeling rate. When the pulling force applied to the tape reaches a critical value, the peeling velocity becomes abruptly higher and an unstable peeling with stick-slip motion starts to emit a characteristic noise. Another similar phenomenon is observed in fractional sliding of an adhesive gel sheet (Baumberger et al. 2002; Yamaguchi et al. 2009). Both phenomena in peeling of the adhesive tape and in frictional sliding of the adhesive gel indicate that the same mechanism may work for these two fracture process. It is also likely to be a similar effect during the tearing of rubber vulcanisates. In frictional sliding of rubber over a wide range of frequencies, when a rigid sphere moves on a rubber surface, two kinds of vibration are produced: a stick-slip motion in the range of 1-20 Hz; and micro-vibrations in the range of 500-1000 Hz. Stick-slip motion, in general, occurs under the condition that the kinetic frictional force is lower than the static frictional force and, in particular, it becomes much greater when the frictional force against sliding velocity relation has a negative slope (Fukahori and Yamazaki 1994). Grosch (1963) introduced the relationship between the coefficient of friction and sliding velocity using WLF superposition treatments which included a maximum in the response. Recently, however, the experimental data show only a positive slope without a clear peak, where the positive slope reduces its angle gradually and reaches a plateau at the highest velocity. Additionally, it has also been seen experimentally that stick-slip motion is imposed at the plateau region and, at lower velocities, the stick-slip motion almost disappears and changes to either Schallamach waves or to smooth sliding (Fukahori and Andrews 1978; Wu-Banouzeta et al. 2007; Fukahori et al. 2008; Fukahori et al. 2010). The surface roughness during tearing results from a secondary crack initiated ahead of the primary crack as shown in Figure 6.1. Secondary fractures occur when the high stresses surrounding primary crack front (a) encounter microscopic stress-raisers (b) or regions of weakness in the path of the crack. If a stress-raiser propagates significantly to a secondary crack (c) before it is overtaken by the primary front, it may join up with the primary crack (d), even though it lies in different plane by shear stresses of the intervening material. Surface roughness is thereby generated. Fukahori and Andrews (1978) also proposed an inverse correlation between the

fracture surface roughness and the mechanical hysteresis of the materials surrounding the propagating crack for various highly deformable polymers as a function of rate, temperature and strain amplitude by the following relation:

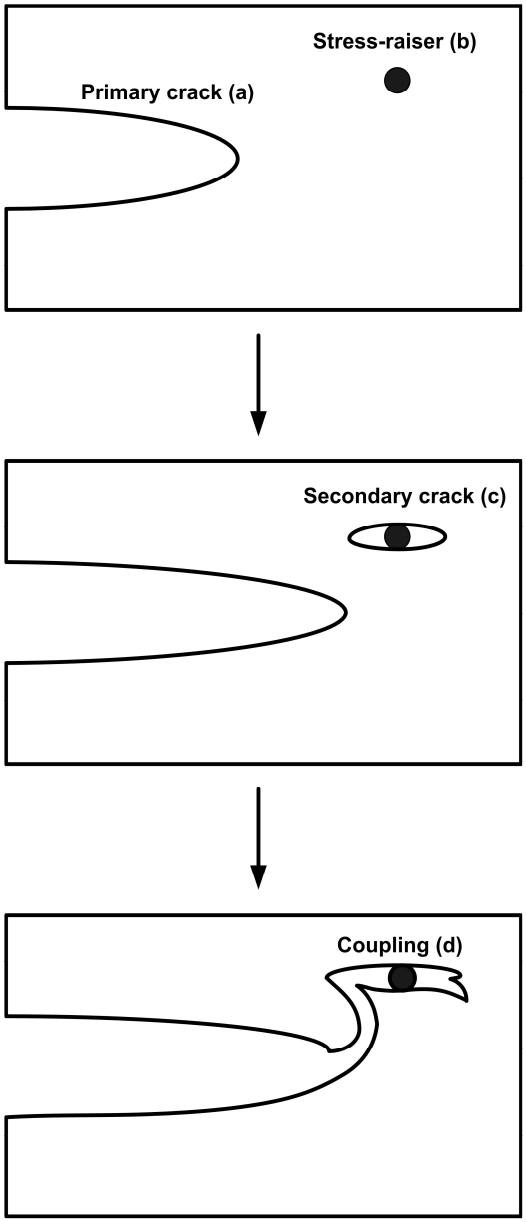

Figure 6.1: Schematic diagram illustrates the deformation of surface roughness by the interconnection of a primary crack front and secondary crack (Fukahori and Andrews 1978).

$$\Delta R = \frac{k}{h} \qquad \text{Equation 6.1}$$

where ΔR is the roughness index which is related to the scale of unevenness in the surface, k is an coefficient, and h is the hysteresis ratio defined as

$$h = \frac{H}{W} \qquad \text{Equation 6.2}$$

where H is the hysteresis energy dissipated in a loading cycle and W is the input strain energy density of deformation up to the point of strain reversal.

The generalised equation of tearing energy of viscoelastic material as proposed by Andrew (1974) can be written in the form

$$T = T_0 \, \Phi (r_c, \text{ temperature}, \varepsilon_0) \qquad \text{Equation 6.3}$$

where T_0 is the threshold tearing energy, Φ is a loss function whose value depends on the crack growth rate r_c, the temperature, and the overall state of strain ε_0 in the material. Fukahori and Andrews (1978) showed that the loss function can be determined in terms of the mechanical hysteresis

$$\Phi = (1 - h)^{-1} \qquad \text{Equation 6.4}$$

where h is the hysteresis ratio. For a specimen with an edge crack, the fracture energy is given by

$$T = 2 k_s W c \qquad \text{Equation 6.5}$$

where k_s is a slowly varying function of strain, W is the elastic strain energy in the simple extension region, and c is the crack length. From the relationship between Equation 6.3, 6.4, and 6.5, it can be seen that the elastic strain energy required to propagate the crack increases with hysteresis ratio of the material.

Under a given strain field surrounding the primary crack, the secondary cracks will occur in a relatively smaller region surrounding the primary crack if h is larger

resulting in a lower degree of roughness. With reference to Figure 6.1, Andrew (1961) showed that the decay of the elastic strain energy W at a point in the stress field around the primary crack is defined by

$$W = \frac{\alpha W_0 c_1}{r} \qquad \text{Equation 6.6}$$

where α is a constant, c_1 is the primary crack length, W_0 is the applied elastic strain energy remote from c_1, and r is the radial distance of the secondary crack length c_2 from the tip of c_1. If W_{crit} is the critical elastic strain energy required to cause the secondary crack length c_2 to grow, then

$$T = 2k_s W_{crit} c_2 \qquad \text{Equation 6.7}$$

The secondary crack will only propagate if it lies within a distance $r = R$ of the primary crack, where R is the maximum vertical displacement of the fracture surface which is directly related to the scale of roughness in the surface, then

$$R = \frac{\alpha W_0 c_1}{W_{crit}} = \frac{c_1 c_2 k_1 W_0}{T} \qquad \text{Equation 6.8}$$

From Equation 6.3, then

$$R = \frac{c_1 c_2 k_1 W_0}{T_0 \Phi} \qquad \text{Equation 6.9}$$

Although R will not be the same as the roughness index ΔR as defined in Equation 6.1, it will be related to it, then

$$\Delta R \cong \frac{c_1 c_2 k_1 W_0}{T_0 \Phi} \qquad \text{Equation 6.10}$$

Equation 6.10 indicates that the secondary crack (larger c_2) that has fully grown up before joining up with the primary crack and the lower hysteresis energy (smaller Φ) form the higher roughness on the fracture surface.

In this chapter, a new concept is introduced to explain the tearing behaviour of rubber by using a newly proposed elastic-viscous transition diagram. The mechanism for the transition phenomenon which is generated at the crack tip is discussed in detail, theoretically and experimentally, from a consideration in the formation of surface roughness together with stick-slip motion produced in the transition zone.

6.3 Results and discussion

6.3.1 Critical tearing energy as a function of crack growth rate in relation to the rate of strain at the crack tip

Figure 6.2 shows the critical strain energy release rate T^* and the time derivative of the strain energy release rate $\dot{T}$ for SBR vulcanizates as shown previously as Figure 4.5 and Figure 4.7 in Chapter 4. SBR0-S-2.5 and SBR0-S-7 are the unfilled vulcanisates. SBR50-S-2.5 and SBR50-S-7 are the carbon black-filled vulcanisates. S-2.5 and S-7 represent the sulphur content in the rubber vulcanisate which is associated with the degree of crosslinking of the compounds with the crosslink density of S-7 being apparently double that of S-2.5 in both unfilled and filled vulcanizates. Although the experimental data are fairly scattered, they show a significant trend of the dependence of T^* and $\dot{T}$. When comparison is made between all the compounds, it is apparent that the compounds, both unfilled and filled, with relatively low crosslink density, SBR0-S-2.5 and SBR50-S-2.5, have a significant

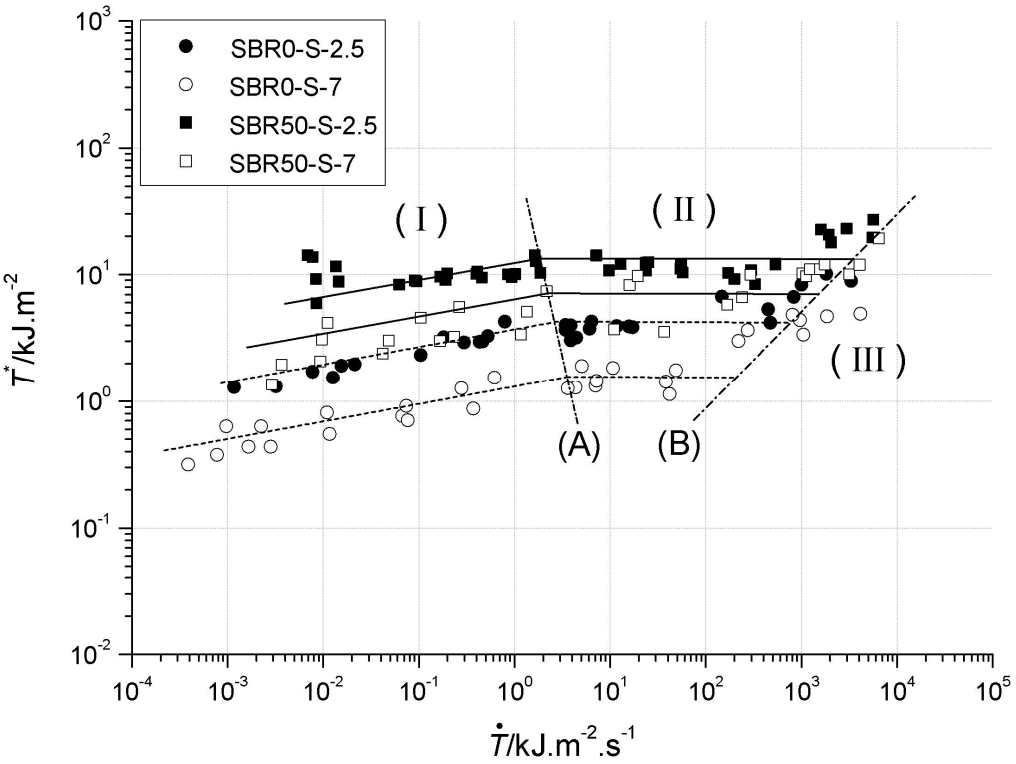

Figure 6.2: Plot of T^* against $\dot{T}$ of SBR vulcanisates.

increase in the tear strength over a wide range of $\dot{T}$. This suggests that lowering the crosslink density and filling with carbon black both create an increase in the viscoelastic energy dissipation of the material and therefore the critical tearing energy increases as suggested by Equation 6.3. It is obvious that the tear fracture behaviour for all the compounds falls into three distinctive regimes in the T^* and $\dot{T}$ relation which can be distinguished by the lines (A) and (B) seen in Figure 6.5. The critical tearing energy increases as a power function of the time derivative of the strain energy release rate up to about 10 $kJ.m^{-2}.s^{-1}$ as shown in Region I and also more than about 10^3 $kJ.m^{-2}.s^{-1}$ as illustrated in Region III. Between these two regions, an almost flat region (Region II) is apparent, where the critical tearing energy is almost constant independent of the strain rate at the crack tip just before the onset of crack propagation.

Figure 6.3 replots the data from Figure 4.4 and Figure 4.6 in Chapter 4 for relationship between T^* and $\dot{T}$ for the NR vulcanisates. NR0-S-2.5 and NR0-S-7 are the unfilled vulcanisates. NR50-S-2.5 and NR50-S-7 are the carbon black-filled vulcanisates. For all the NR compounds almost the same phenomena as shown for the SBR compounds are observed in region (II) and region (III). Between region (I) and (II), however, a new region (IV) appears as a result of a significant increase in the critical tearing energy at the slower test speeds associated with strain-induced crystallisation. Crystallisation, of course, needs enough time for molecules to orientate and thus the effect of crystallisation appears at the relatively lower time derivatives than region (II). More detailed comparison is made between the SBR and NR compounds shown in Figure 6.4 using simply the average lines from Figure 6.2 and Figure 6.3. Both the compounds have the same geometrical features for the region (II) and (III) divided by the lines (A) and (B) and the lines (A′) and (B′), whereas the regions (II) is shifted horizontally towards the higher time derivatives for the NR compounds due to the lower glass transition temperature T_g (195-205 K) relative to the SBR compounds T_g (216-229 K). The effect of the crystallisation, to increase the critical tearing energy, is almost equal over a range of the time derivatives for all the NR compounds. It is emphasized here that the time derivative range for the intermediate zone (II) varies with the critical tearing energy (and hence the viscoelastic energy dissipation), the higher the energy dissipation, the wider the range of the intermediate zone (II), as is discussed in detail later.

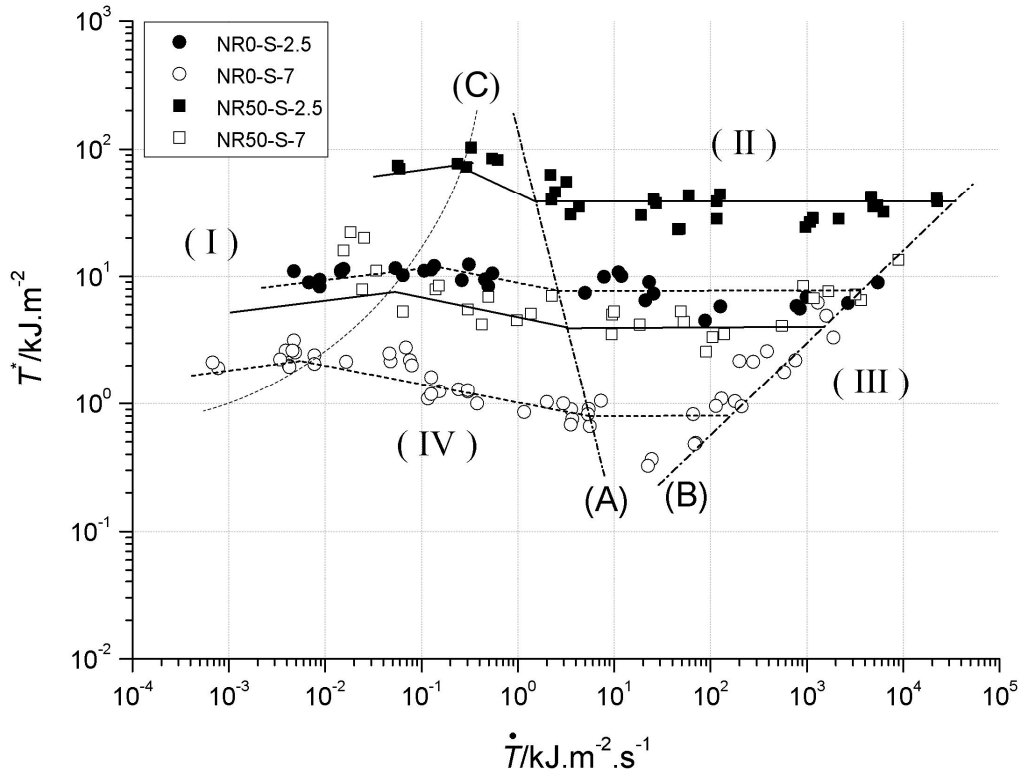

Figure 6.3: Plot of T^* against $\dot{T}$ of NR vulcanisates.

6.3.2 Elastic-viscous transition for tearing fracture of crosslinked and viscoelastic rubbers

Those phenomena shown in Figure 6.2, Figure 6.3, and Figure 6.4 are undoubtedly associated with the established hypothesis in the tearing energy against rate of tear relation proposed in the literature (Greensmith 1956; Kadir and Thomas 1981; Tsunoda et al. 2000). The plot of tearing energy against tearing rate shows how fast the tear propagates at a constant tearing energy or the average relation between both parameters. In comparison with this, the curve shown in this work gives the true relation between the critical strain energy release rate and the crack growth rate at the tip of a crack.

In the physical and mechanical sense, however, both curves are based on the same concept for the propagation of tearing fracture in rubber, when considering the fracture process at the crack tip. To create a new framework lets consider the critical strain energy release rate at the tip of the crack to be T_{tip} and the crack propagation rate R_{tip} to be related to $\dot{T}$ the strain rate at the crack tip.

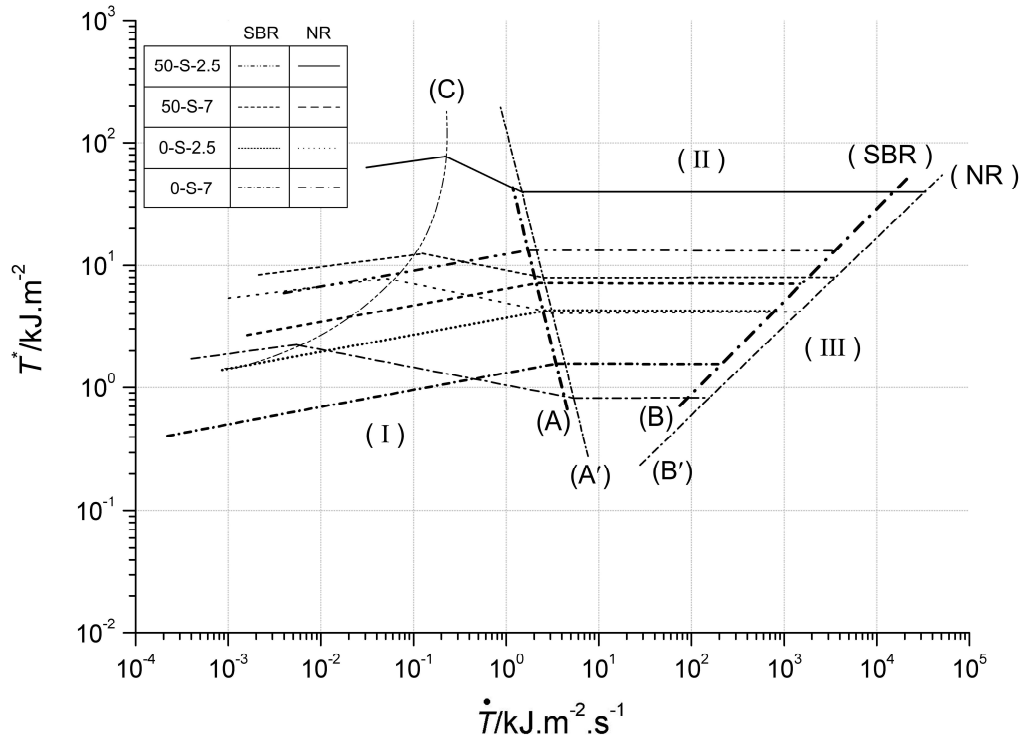

Figure 6.4: Comparison between the SBR and NR vulcanisates using average line induced to Figure 6.2 and Figure 6.3.

Figure 6.2, Figure 6.3, and Figure 6.4 all show common phenomena which characterise the tear fracture of rubber at very high tear rates. First, the abrupt change in critical strain energy release rate as a function of crack growth rate in association with the strain rate at the crack tip just immediately before the crack growth might be defined as the transition phenomenon consisting of three fracture zones. Second, the level of the critical strain energy release rate depends strongly on the viscoelastic energy dissipation of the material and, in addition, the width of the intermediate zone is also related to the amount of energy dissipation. Third, this transition phenomenon is undoubtedly associated with the glass transition temperature of the material. A novel universal concept of an elastic-viscous transition in tearing fracture of crosslinked and viscoelastic rubbers is introduced here to explain this behaviour. Prior to the detailed discussion, the rough image of the elastic-viscous transition is explained with respect to the fracture behaviours as observed in the literatures (Greensmith 1956; Kadir and Thomas 1981; Tsunoda et al. 2000). Figure 6.5 shows the elastic-viscous transition diagram for a crosslinked and viscoelastic (non-crystallising) rubber consisting of three zones of different fracture modes, where a typical crosslinked rubber is shown, for example, as curve (b) in the figure. At relatively low rates, the fracture propagates in a steady and brittle

manner (elastic-brittle fracture zone I) and at relatively high rates fracture also propagates in a steady but more viscous manner (viscous-ductile fracture zone III). Since the rate dependence of strain energy is much greater for energetic viscous behaviour than for entropy elastic behaviour of rubber, the slope in the T_{tip} against R_{tip} relations might be much higher in viscous zone (III) than in elastic zone (I).

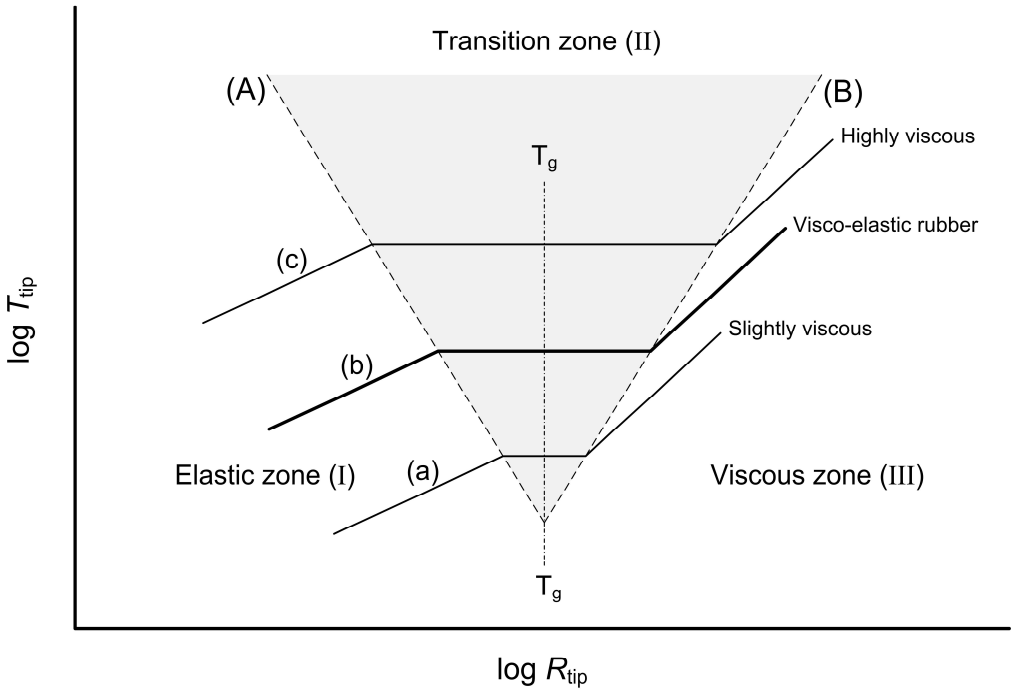

Figure 6.5: Schematic diagram of elastic-viscous transition illustrating the relationship between the critical strain energy release rate and the crack growth rate for a non-crystallising rubber.

Between elastic zone (I) and viscous zone (III), the fracture mode changes from the steady to unsteady response (transition zone II), where fracture proceeds in a stick-slip manner and the average T_{tip} value is almost constant. When the energy dissipation loss increases by filling with carbon black or by decreasing the crosslink density, T_{tip} increases according to Equation 6.3 as shown by the line (c) in Figure 6.5. The influence of the energy dissipation on strain energy release rate works equally over the three zones, resulting in a vertical parallel shifting of the line (b) upwards to the line (c).

Conversely, a decrease in the energy dissipation by increasing the amount of crosslinking and swelling with good solvent or testing at higher temperature shown in the literature (Tsunoda et al. 2000), causes a significant reduction in the magnitude of T_{tip} equally over three fracture zones and hence the line (b) in Figure

6.5 shifts downwards to the line (a). Thus it might be expected that if the material is perfectly elastic (no viscosity), the fracture mode does not change where fracture progresses in a steady brittle manner, independent of rate. In a perfectly viscous material (no cross-links and no entanglements), in contrast, fracture propagates in a perfectly viscous manner, and thus the fracture surface might show very smooth, mirror-like features (Figure 6.10 c).

The unstable transition zone (II) appears around the glass transition temperature. This may be caused by the instantaneous significant change in the modulus of the material in the glass-transition region, and therefore the fracture propagates in an unsteady manner with stick-slip response, sometimes it proceeds very quickly and at other times very slowly depending on the fluctuation in crack growth rate. Thus the rate range of the transition zone, i.e. the flatness of the transition zone (II) shown in Figure 6.5 is governed by the characteristics of the glass transition temperature of the material. More exactly, it is proportional to the profile of the tan δ versus frequency around the glass transition temperature. This provides a rational explanation to the question, why the width of the transition zone changes from wide to narrow when decreasing the viscoelastic energy dissipation and consequently the elastic-viscous transition diagram has a shape like the letter V.

Here the difference between the brittle-ductile transition in plastics and the present elastic-viscous transition in crosslinked rubbers must be considered. The brittle-ductile transition is well observed in some thermosetting resins and thermoplastics, where the brittle fracture occurs without any detectable plastic deformation below the transition temperature in impact strength or fracture toughness. The brittle-ductile transition temperature is dependent on molecular weight and geometry of the specimen (thickness and the length of notch), but scarcely on the viscoelasticity and the glass transition temperature. Although the surface roughness in rubbers, in appearance, also changes from rough to smooth similar to brittle to ductile transition as indicated in the literatures (Greensmith 1956; Kadir and Thomas 1981; Tsunoda et al. 2000), the elastic-viscous transition phenomenon characterised by the intermediate transition zone accompanied with stick-slip motion might be characteristic of crosslinked and viscoelastic rubbers. The suitable number of crosslinks and appropriate viscoelasticity are two major factors establishing this elastic-viscous transition which is observed in rubber materials.

6.3.3 Stick-slip behaviours in the transition zone

Figure 6.6 shows typical force-time curve profiles measured for the three SBR vulcanisates in the three different fracture zones. In elastic zone (I), although rough jaggy patterns are observed, their frequencies are in the range of (1-5) × 10^{-3} Hz and thus these are not recognised normally as a vibration in general experimental conditions. In viscous fracture zone (III), fracture proceeds smoothly without fluctuations similar the ductile fracture generally observed in thermoplastics. In transition zone (II), typical jaggy patterns, known as stick-slip motion are obviously shown, whose frequency changes from 6-8 Hz (SBR50-S-2.5) to 4-5 Hz (SBR0-S-7). Very similar results are observed for three NR compounds in three fracture zones as shown in Figure 6.7, with the frequency being between 8-9 Hz (NR50-S-2.5) and 4-5 Hz (NR0-S-7) in the transition zone (II), the filled compound being double the filled compound.

Stick-slip motion is understood mathematically as follows. Figure 6.8a schematically shows a sliding system of a rigid block with mass M on the surface of rubber track. The rigid block attached to a heavy base with a spring of elastic constant k and a dashpot of damping coefficient c and the track is pulled horizontally at a sliding velocity v. Figure 6.8b indicates the time dependence of tangential force F_t and frictional force F_{fric} driven at a constant velocity v, where the static frictional force F_{static} is constant and the tangential force F_t given by the spring and dashpot system increases almost linearly with time. When the tangential force F_t is lower than F_{static}, the rigid block is adhered to the rubber track and the both move together (stick, OS in Figure 6.8(a, b)). However at the time when the tangential force F_t reaches the static critical frictional force F_{static} the rigid block starts to slide on the surface (slip, SA) where the frictional force changes from static to kinetic and hence the frictional force reduces. When the kinetic frictional force reaches the minimum, the tangential force increases again up to the critical force (stick, AB).

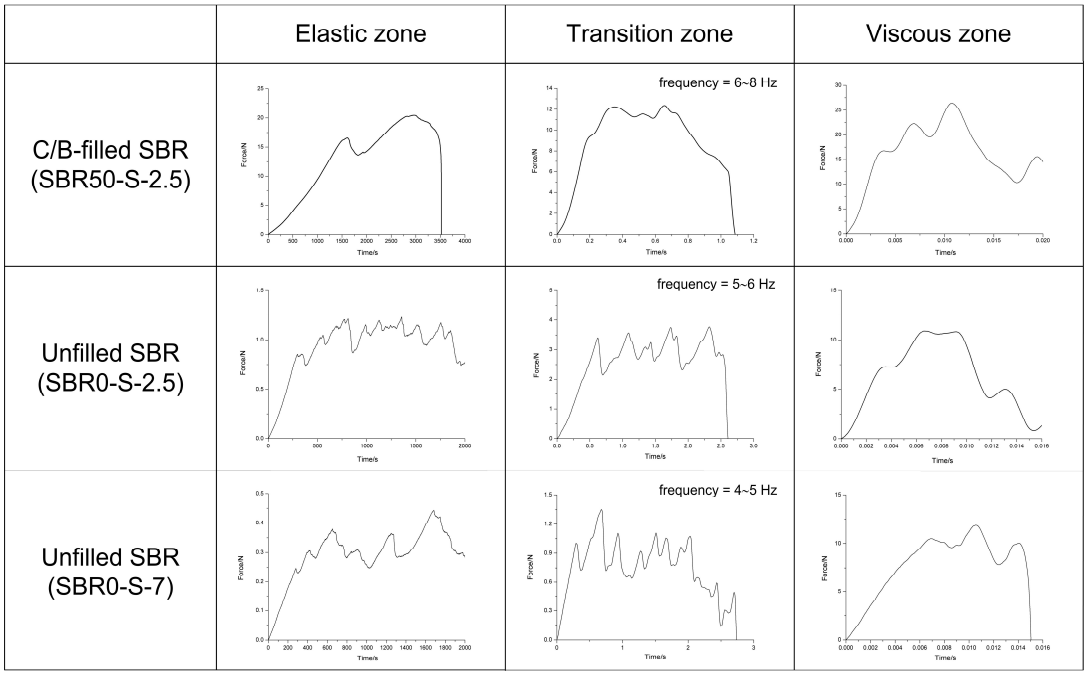

Figure 6.6: Force-time curves for SBR vulcanisates in three fracture zones.

From a mathematical or a computational treatment, it is apparent that the stick-slip motion grows significantly as the mass *M* increases, the stiffness *k* decreases and the damping coefficient *c* decreases (Nakano and Maegawa 2009). According to Moore (1972), although the static frictional force is given by the sum of adhesion component F_{adh} and deformation component F_{def}, the deformation component term could be neglected for the present object. In addition, the adhesion component F_{adh} term is dependent on the viscosity of the material (proportional to the loss angle), thus the static frictional force F_{static} is given as,

$$F_{static} = F_{adh} = k_1 P E' \tan\delta \qquad \text{Equation 6.10}$$

where *P* is the nominal pressure, E' the storage modulus, and k_1 is the coefficient.

In Figure 6.6 and Figure 6.7, the SBR and NR compounds are selected corresponding to the viscoelastic characteristics of the material, the highest viscosities for SBR50-S-2.5 and NR50-S-2.5, the middle viscosities for SBR0-S-2.5 and NR0-S-2.5 and the lowest viscosities for SBR0-S-7 and NR0-S-7. Compiling Figure 6.4 and Figure 6.5 together with Figure 6.6 and Figure 6.7, the transition zone (II) might be explained by using the elastic-viscous transition diagram for tear

fracture of rubber. Firstly, the critical frictional force F_{static} is proportional to tan δ, that is, the frictional force F_t to start sliding with stick-slip motion is higher for the material with a higher viscosity. Consequently, the critical strain energy release rate T_{tip} (proportional to loss function Φ) to start the stick-slip motion in the transition zone (II) is significantly higher for the carbon black-filled rubbers than the highly crosslinked rubbers as shown in Figure 6.4 and Figure 6.5.

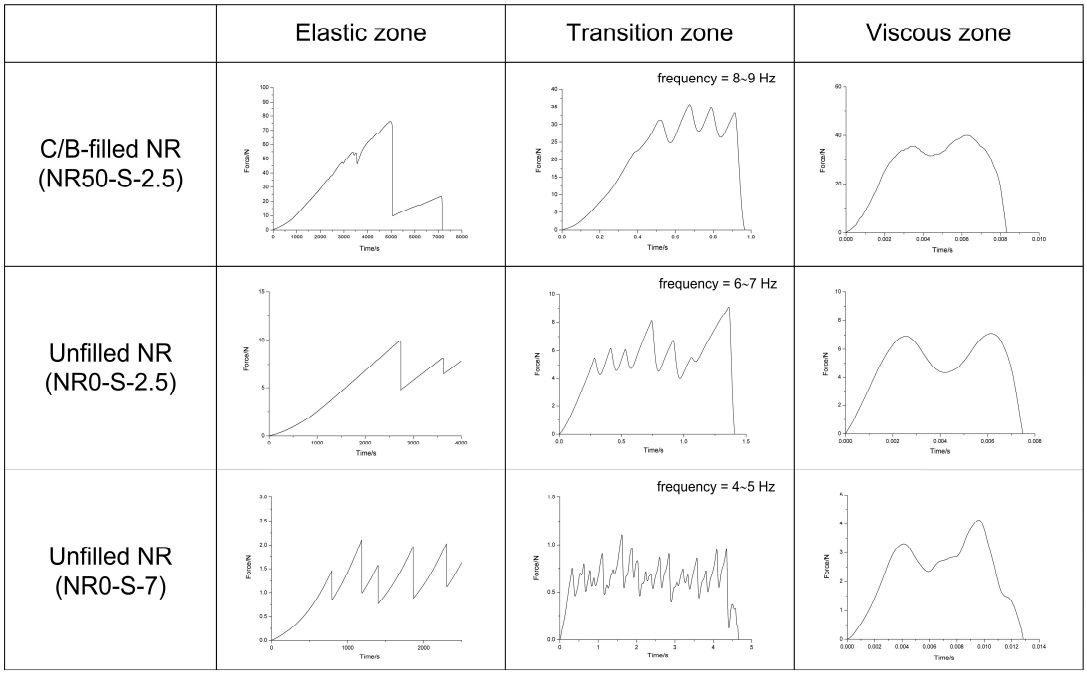

Figure 6.7: Force-time curves for NR vulcanisates in three fracture zones.

Secondly, the flatness of the transition zone (II) in the T_{tip} against crack growth rate T_{tip} relation is characterised directly by the flatness of tan δ versus rate around the glass transition, because the stick-slip motion occurs at the same plateau region as indicated previously (Fukahori and Andrews 1978; Wu-Banouzeta et al. 2007; Fukahori et al. 2008; Fukahori et al. 2010) Payne (1967) showed the effect of filling with carbon black on tan δ as a function of velocity (frequency) given in Figure 6.9. The peak of tan δ decreases with the filler content and therefore it might be assumed that the flatness of the transition zone (II) for stick-slip motion to occur also becomes wider with an increase in the content of carbon black. In contrast, for the highly crosslinked rubbers of low viscosities (together with a swollen rubber or a rubber at a higher temperature (Tsunoda et al. 2000), the flatness of transition zone (II) might be very narrow, because the glass transition phenomenon for such materials may occur abruptly with a very sharp tan δ peak as shown in Figure 6.9.

This may be the reason why the transition zone (II) characterized by the stick-slip motion reveals the V shape profile shown in Figure 6.5.

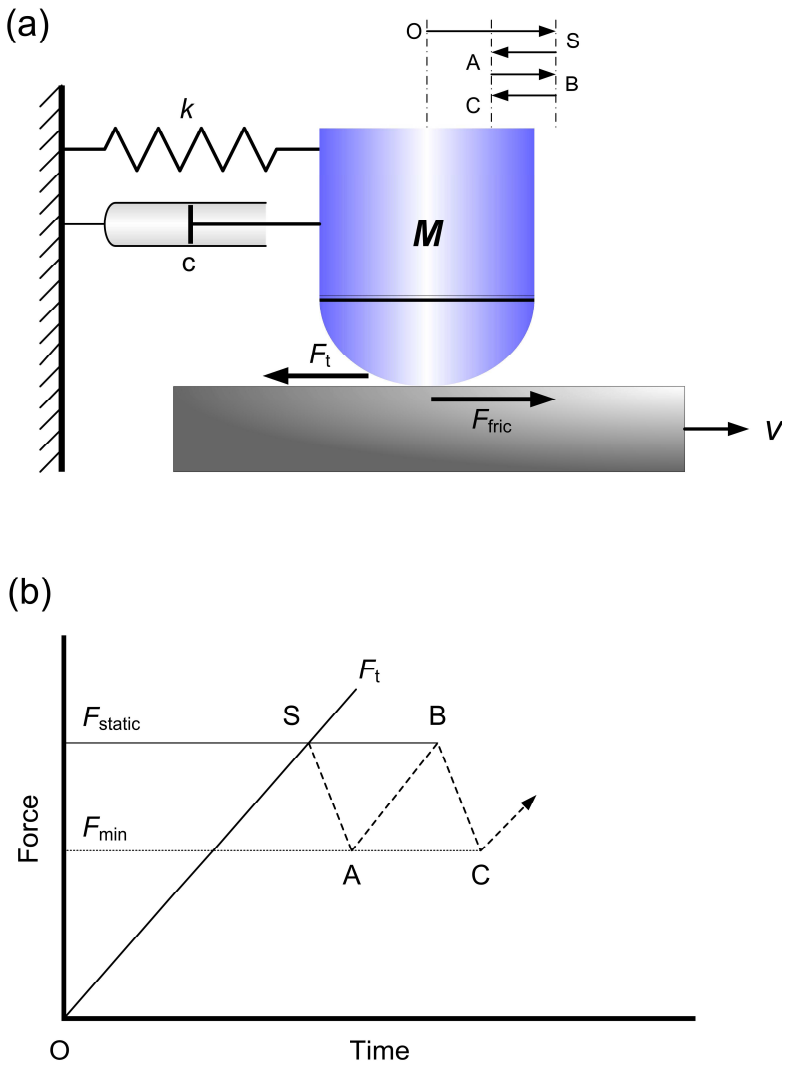

Figure 6.8: Schematic picture illustrating the sliding system of a rigid block on rubber surface (a) and the corresponding force-time diagram (b).

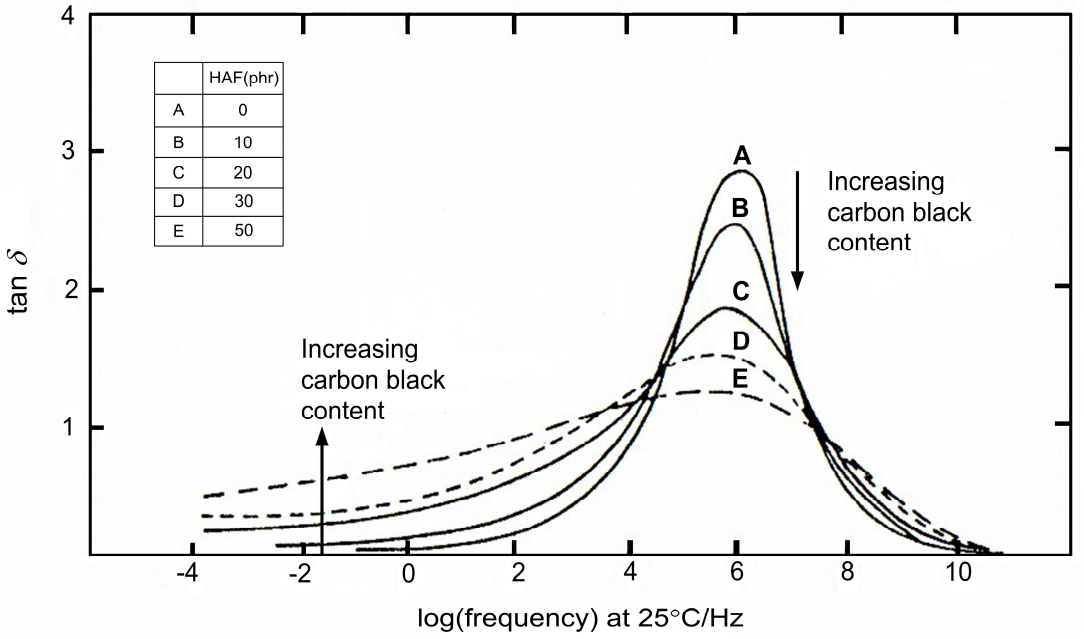

Figure 6.9: Effect of carbon black on tan δ as a function of frequency (Payne 1967).

6.3.4 Formation of the surface roughness in tearing fracture of rubber

In Figure 6.10(a, b, c), the three SBR compounds, SBR0-S-2.5, SBR0-S-7, and SBR50-S-2.5, as observed using SEM in all three fracture zones based on the viscoelastic characteristics of the material. The fracture surface of SBR0-S-7 (Figure 6.10a) are very rough when compared with the other two compounds. Figure 6.10b and Figure 6.10c show SBR0-S-2.5 and SBR50-S-2.5, respectively, indicating that the surface roughness becomes smoother as viscosity increases over all three fracture zones as suggested by Equation 6.10. Roughly estimating the surface roughness ΔR, (the scale of unevenness), may be 40-50μm for SBR0-S-7 (Figure 6.10a), 20-30 μm for SBR0-S-2.5 (Figure 6.10b) and 5-10 μm for SBR50-S-2.5 (Figure 6.10c). The unfilled NR (NR0-S-2.5, Figure 6.11) shows almost the same fracture surface as that for SBR0-S-2.5 (Figure 6.10b) over all three fracture zones, 20-40 μm in the roughness. The surface roughness for unfilled rubbers (Figure 6.10a, Figure 6.10b and Figure 6.11) seems to correspond to a Griffith type crack in rubbery materials (40±20 μm) as indicated by Hamed (1983) and Gent (2005).

Material	Zone	Surface fracture
SBR0-S-7	Elastic rate	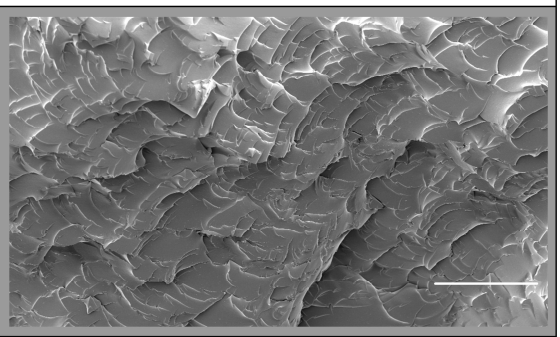
	Transition rate	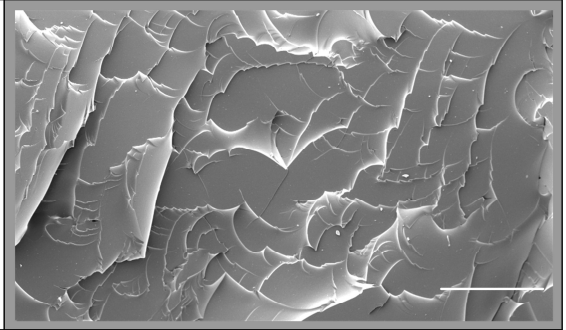
	Viscous rate	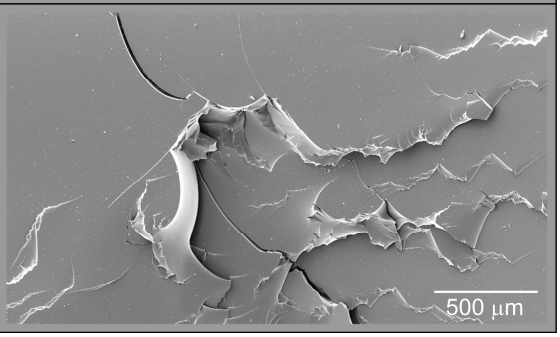

Figure 6.10a: Fracture surface for SBR0-S-7 in three fracture zones, bars and arrows all indicating 500 μm and the direction of fracture, respectively.

Of three fracture zones, the fracture surface has the highest roughness in the elastic zone (I) and the lowest roughness in the viscous zone (III) for all of the compounds. In the case of SBR50-S-2.5 (Figure 6.10c), the fracture surface is very smooth similar to that generally observed in thermoplastic and no difference is seen among the three fracture zones. In other cases (Figure 6.10a, Figure 6.10b and Figure 6.11), although the roughness looks the highest in the elastic zone and the lowest in the viscous zone, the roughness changes monotonically from the elastic to the viscous zone passing through the transition zone. In particular, on the fracture surface of the transition zone, there is no any typical patterns to show the indication the obvious evidence of stick-slip behaviour. Therefore it is very important to

consider what the mechanism for the stick-slip motion, generated in the transition zone, is and this is discussed later.

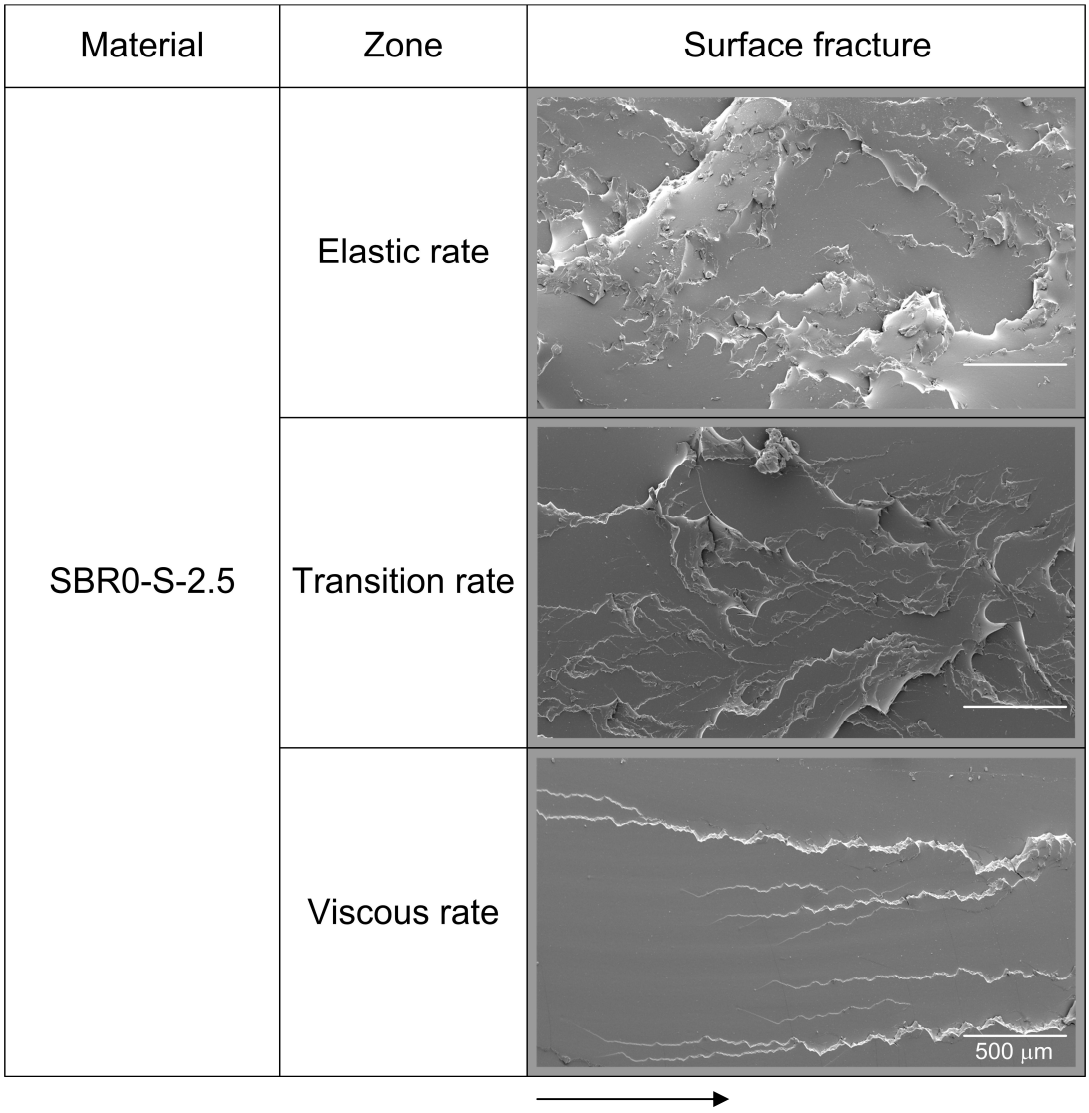

Figure 6.10b: Fracture surface for SBR0-S-2.5 in three fracture zones, bars and arrows all indicating 500 μm and the direction of fracture, respectively.

Figure 6.12 and Figure 6.13 schematically show how the surface roughness would be formed at a large extension for two SBR compounds characterised by the lowest viscosity (SBR0-S-7) and the highest viscosity (SBR50-S-2.5). Figure 6.12a corresponds to the case of SBR0-S-7 (Figure 6.10a). When a primary crack approaches, a numbers of stress raisers have already grown up as large secondary cracks, spread far apart from primary plane of the crack. The secondary cracks are thus torn off at a large extension in shear stress fields and, as a result, long split tangs (chips) are produced that link the secondary cracks to each other. This

procedure forms the longest tangs and hence the highest surface roughness (large ΔR) on the fracture surface as shown in Figure 6.12b.

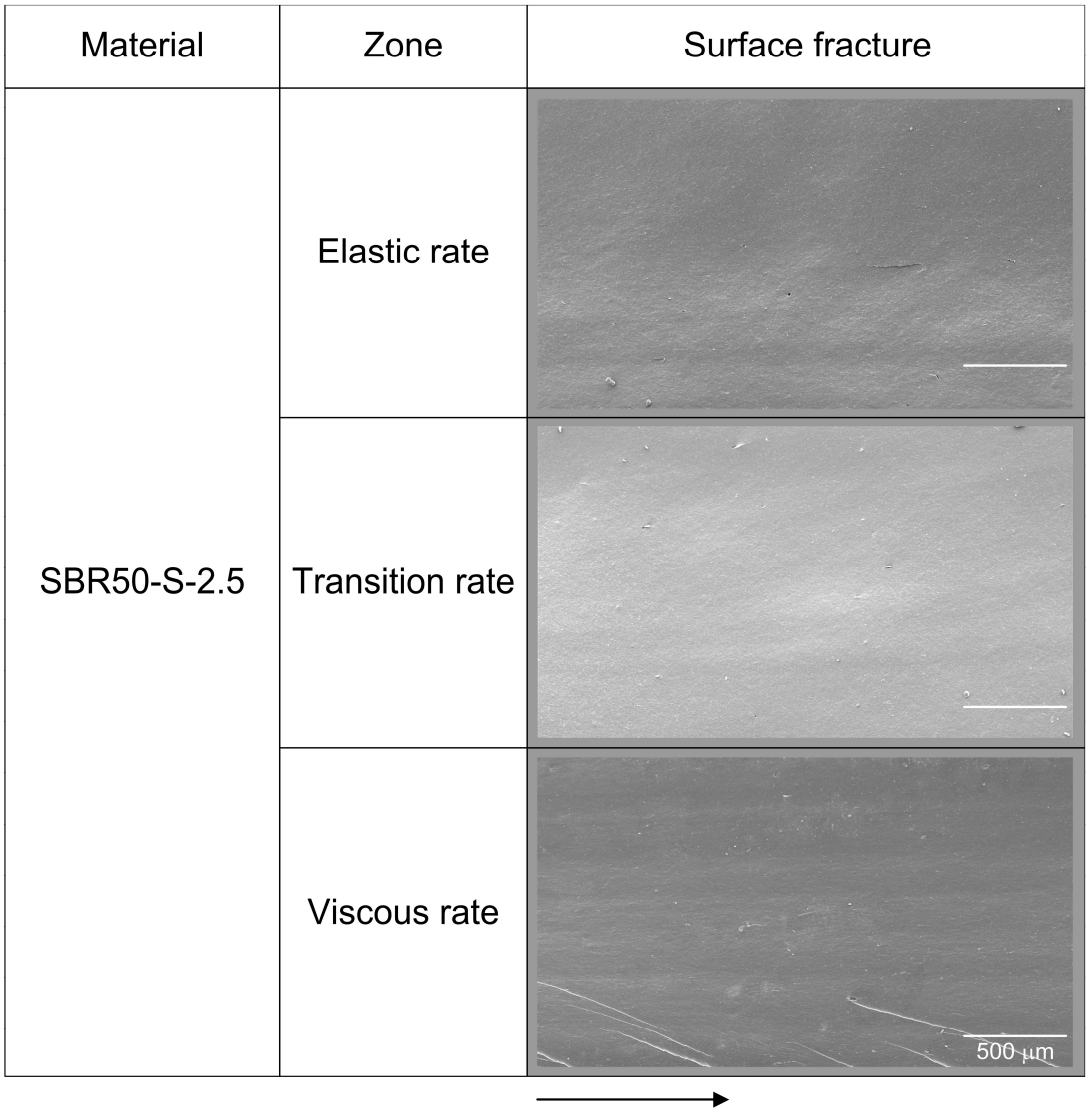

Figure 6.10c: Fracture surface for SBR50-S-2.5 in three fracture zones, bars and arrows all indicating 500 μm and the direction of fracture, respectively.

Conversely in the case of SBR50-S-2.5 (Figure 6.10c), fully developed secondary cracks are only located near the path of the primary crack, thus resulting in the formation of the shortest split tangs and the lowest degree of surface roughness (small ΔR) as shown in Figure 6.13a and Figure 6.13b. This explanation may provide a rational basis for explaining the surface roughness formation in rubbery materials accompanied with the viscoelasticity (and hence the critical strain energy release rate) of the material as suggested by Equation 6.3.

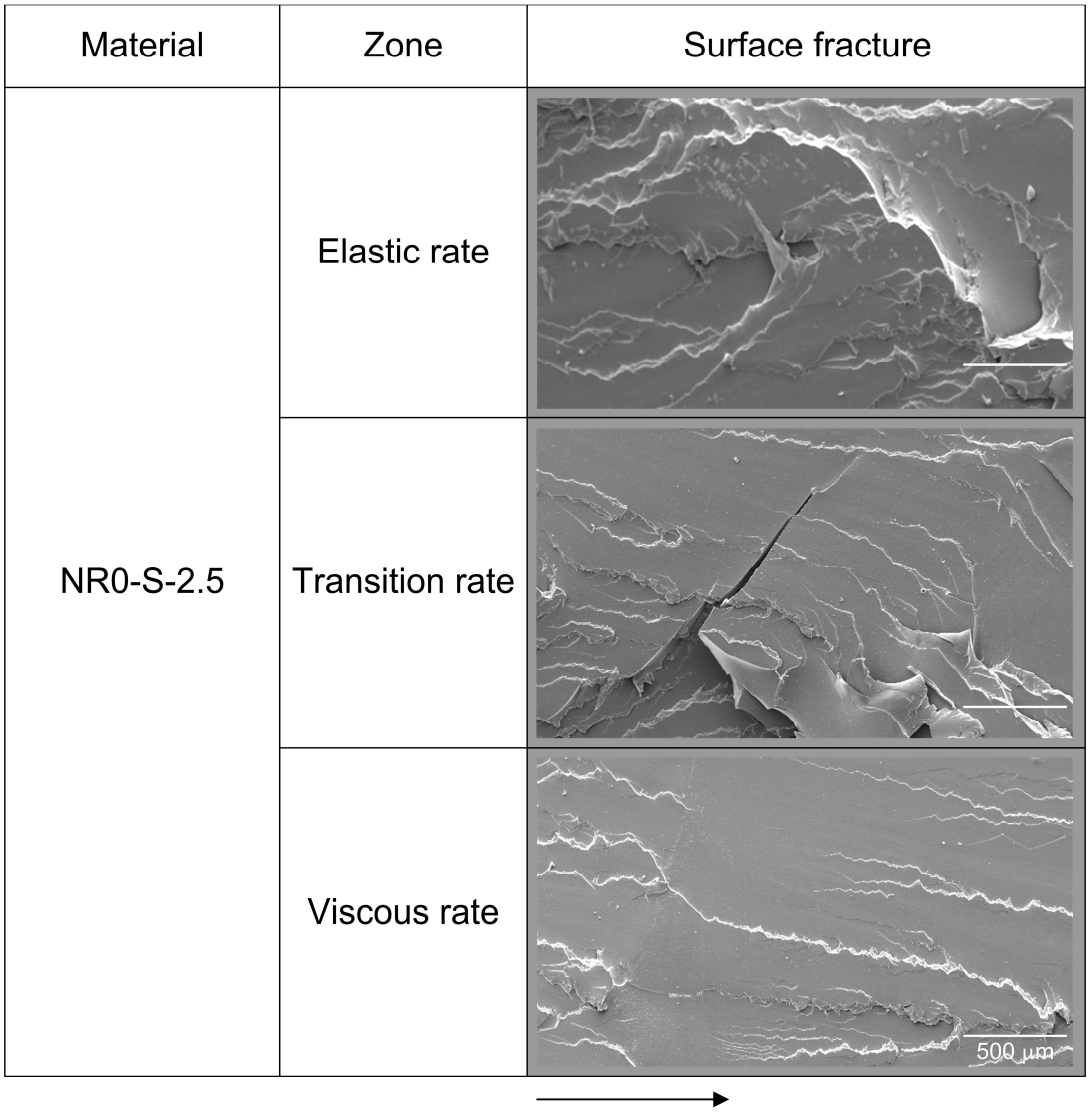

Figure 6.11: Fracture surface for NR0-S-2.5 in three fracture zones, bars and arrows all indicating 500 μm and the direction of fracture, respectively.

6.3.5 Mechanism of the stick-slip response generated at the crack tip

One difficult question remains to be answered. How and why is the stick-slip motion generated at the crack tip during tear fracture? Also is this stick-slip motion related to the phenomenon caused by frictional sliding of rubber? When addressing this question it is important to note that no geometrical traces or marks that show stick-slip fracture or a repetition of a slow and a fast propagation are observed on the fracture surface in the transition zone (II) as shown in Figure 6.10 (a, b, and c) and Figure 6.11.

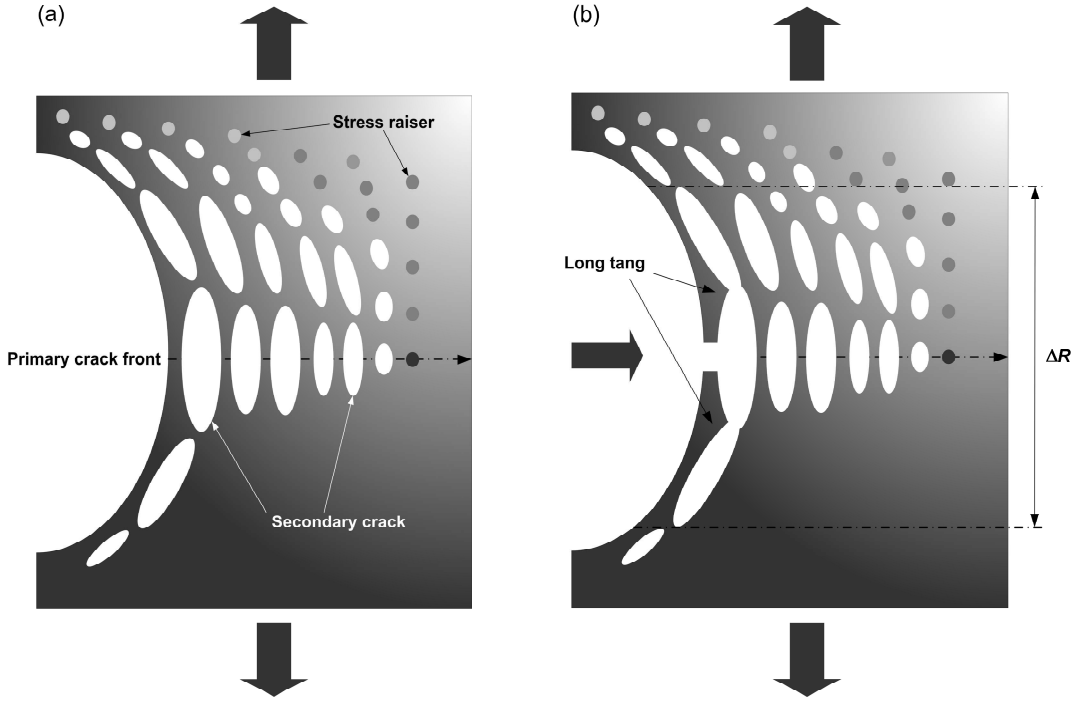

Figure 6.12: Schematic diagram showing the formation for long tang after secondary fracture for SBR0-S-7.

If the force changes from the maximum to the minimum in the force-time plots (Figure 6.6 and Figure 6.7) that directly reflects the tear fracture response and consequently the formation of fracture surface roughness, then striation-like patterns should be left on the fracture surface as is generally observed in the dynamic fatigue fracture of rubbers. Therefore, it might be that the jagged force changes in the force-time plots is generated not during but after the rupture of rubber, independent of the fracture itself and something like frictional sliding seen with stick-slip motion might occur after the breakage of the extended secondary crack at the crack tip.

As seen in Figure 6.12 and Figure 6.13, when a secondary crack is pulled and ultimately torn off at the tip of primary crack, it is divided into two tangs. When the separated tangs shrink by the entropic elastic force, the tangs are compressed at the crack front and start to slide in opposite directions with friction under a shear stress field, similar to the situation shown in Figure 6.8. At that instance, stick-slip motion might be generated depending on such circumstances as velocity, material and geometry. A long tang with a large mass and low viscosity (SBR0-S-7 and NR0-S-7) might generate a significant stick-slip motion with a lower frequency as suggested mathematically (Nakano and Maegawa 2009), whereas a short tang with

a small mass and high viscosity (SBR50-S-2.5 and NR50-S-2.5) generates only a slight stick-slip motion with a higher frequency, as shown in Figure 6.6 and Figure 6.7.

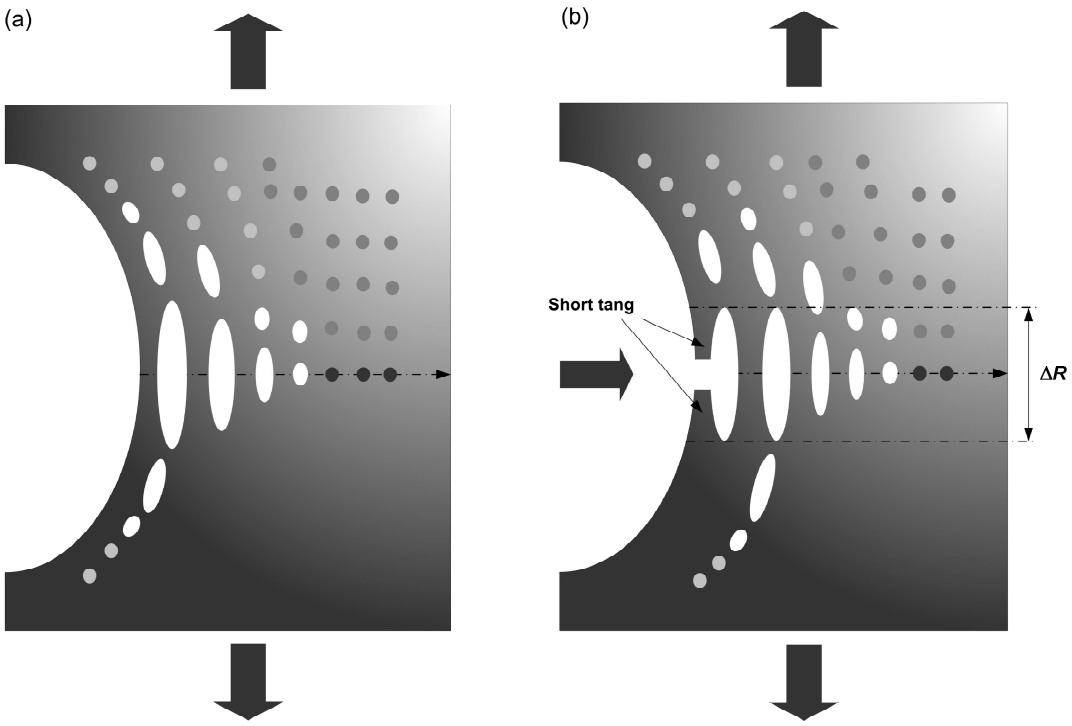

Figure 6.13: Schematic diagram showing the formation for short tang after secondary fracture for SBR50-S-2.5.

Finally, the length of the tangs may reasonably be estimated by assuming that the frequency f of the stick-slip motion observed in Figure 6.6 and Figure 6.7 is represented by the relation, $f = \frac{1}{2\pi}\sqrt{\frac{k}{M}}$ and the elastic constant k is independent of geometry. The length of the tang thus calculated for SBR0-S-7 and NR0-S-7 is four times larger than that for SBR50-S-2.5 and NR50-S-2.5, because the frequency of the stick-slip motion for the latter is about twice as large as the former shown in Figure 6.6 and Figure 6.7. This difference in the length of the tangs for both compounds is clearly shown on the SEM photographs as the fracture surface roughness, 40-50 μm for SBR0-S-7 (Figure 6.10a) and 5-10 μm for SBR50-S-2.5 (Figure 6.10c).

6.4 Conclusions

(1) The relationship between the critical strain energy release rate and the crack growth rate measured here reflects correctly that a true fracture phenomenon occurred at the crack tip, and thus the relation is brought into a universal concept of the elastic-viscous transition represented by an elastic-viscous transition diagram.

(2) The elastic-viscous transition in tear fracture of rubber is essentially a typical phenomenon when the fracture mode changes from brittle to viscous around the glass transition temperature for crosslinked and viscoelastic rubbery materials, depending on the balance of elasticity and viscosity of the material.

(3) The transition zone appears between the elastic and viscous fracture zones at around the glass transition temperature due to its unstable situation in the rate of tearing. For crystallising rubbers the effect of strain-induced crystallisation is added to the diagram as a significant increase of the critical strain energy release rate at slower test speeds.

(4) The elastic-viscous transition diagram is significantly influenced by visco-elasticity of the material. A higher viscosity produces a higher strain energy release rate together with the wider rate range of the transition zone caused by the characteristics of tan δ at the glass transition temperature.

(5) A secondary crack fully grown and torn off at the tip of a primary crack is divided into two tangs of rubber. Longer tangs (and hence higher surface roughness) are formed for the rubber with a lower viscous behaviour and short tangs (lower roughness) for the more viscous rubber.

(6) When two tangs are pulled in opposite directions by the elastic retraction force, the tangs compressed on the rubber surface of the primary crack front slide frictionally with stick-slip motions of 4-8 Hz. A long tang with the large mass and low viscosity yields heavy stick-slip motion of low frequency and a short tang with the small mass and high viscosity provides the slight stick-slip motion at a low frequency in the unstable transition zone.

Chapter 7: Summary and future work

7.1 Summary

This thesis has introduced a new approach to investigate the unsteady crack growth of rubber which is most commonly observed in practice for some unfilled rubbers especially those that are capable of strain induced-crystallisation as well as for filled rubbers. Under this unsteady tearing condition, typically called stick slip or knotty tearing, using a trouser tear specimen, the rate of tearing characteristically fluctuates between a very rapid tearing rate and a zero velocity tearing rate. Consequently, it is very difficult and not clear what actual rate of crack propagation is as the value typically given results from the average rate of a very rapid and zero rates.

This traditional framework assumes the crack propagates steadily in a tearing path located in the middle section between the legs of the trouser tear specimen which is directly proportional to the displacement of the legs of the specimen being clamped by the test machine, the rate of crack growth can be readily determined from the rate of displacement of the clamps of the test machine (Greensmith and Thomas 1955).

This approach works well for the non-strain crystallising rubber, as its tearing behaviour is controlled by a basic tearing process that is primarily viscoelastic in nature, such as styrene-butadiene rubber (SBR) which exhibits a modest fluctuation in the tearing force. However, for a lot of rubbers, namely strain crystallising rubbers and carbon black-filled rubbers, the variation of tearing force is very large and the tearing path tends to deviate from the intended tearing path, especially for carbon black-filled rubbers, due to the local anisotropy at the tip of the crack. These effects invalidate this measurement framework. Many techniques have been utilised to improve and prevent the deviation of the tear from the linear path using a modified trouser tear specimen (Stacer et al. 1985; De and Gent 1998; Hamed and Hiza 2010). Practically, modified trouser tear specimens can inhibit the lateral tear deviation and they help reduce the fluctuation of the tearing force, however, the actual crack growth rate is still difficult to determine under this framework.

In this work, the key approach employed to investigate the unsteady tearing condition is to characterise the rate of increase in the strain energy at the crack tip

just immediately before the onset of tearing. This is measured directly as the time derivative of the strain energy release rate $\dot{T}$. The relation between this and the critical strain energy release rate T^* was examined using a range of different materials with different types of test equipment to produce a wide ranges of loading rates over a wide range of test temperatures.

This new method has been first applied to unfilled and carbon black filled rubber materials with the different degrees of crosslink density in order to modify the main chain structure of the rubber molecule under an ambient test temperature.

For an unfilled strain crystallising rubber, namely, natural rubber (NR) which has been observed in the past to have a complicated relationship between the average rate of tear, as measured using the rate of clamp separation, with the strain energy release rate. The less highly crosslinked compound is considerably stronger than the more tightly crosslinked material. For the former material, there is essentially no dependence of the tearing energy on the rate of loading at the tip of the crack. This was thought from the test being too slow to beat the kinetics of the strain crystallisation. For the tightly crosslinked compound, an interesting rate dependence was observed that the tear strength initially goes down with the loading rate until high speeds are achieved when it is then seen to increase. The first drop is most likely to result of the suppression of strain-induced crystallisation in the more highly crosslinked material. The increase in the number of the crosslinks will have modified the main chain more extensively and it will also inhibit the movement of the molecular chain of the rubber molecule. These effects are thought likely to reduce the rate of the development of crystallisation under strain. For the carbon black-filled NR, the results are broadly similar to those of the unfilled NR. The most significant difference is that the filler makes both crosslinked compounds have a higher tear strength. For both levels of crosslink density, there is a consistent reduction in strength with increasing of loading rate as the kinetics of strain induced crystallisation is too slow to allow the full development of the reinforcing crystals.

For unfilled non-strain crystallising rubber, namely styrene-butadiene rubber (SBR), it is clear that the only observable effect is an increase in the critical strain energy release rate with the rate of loading at the crack tip. This material exhibits steady tearing condition, thus the traditional measure of crack growth rate from the rate of the crosshead displacement would be an acceptable approach to measure the

tearing rate. The most highly crosslinked SBR was again much weaker and the increase in viscosity with the loading rate is the reason for these materials becoming stronger as the rate of testing is increased. For carbon black-filled SBR, clearly the more highly crosslinked compounds exhibit only a characteristic increase in tear strength with the loading rate. The less highly crosslinked SBR compound shows a modest increase in tear strength with the lower loading rate and a faster increase in tear strength with rate at higher rates of loading. It is likely that this technique of representing the data identifies an additional effect that counteracts the basic viscoelastic behaviour alone. This could include a kinetic effect in relation to the rate of the development of a potential reinforcing structure, for instance.

Thus, the novel examination of the tearing behaviour rubber was extended to examine the tearing behaviour of rubber at elevated temperatures, namely, 60°C and 100°C. In the second phase of the work, the three unfilled rubber materials with different levels of crosslink density were employed: natural rubber, epoxidised natural rubber with half of the isoprene units being epoxidised (ENR-50), and polybutadiene rubber (BR). Obviously, for NR, the increase in test temperature has a significant effect of reducing the tear strength. For lightly crosslinked NR at 60°C and 100°C, there is a defection point of the plot between the relation of T^* and $\dot{T}$. At 100°C, the defection point appears at a slower rate of loading at the crack tip than is seen at 60°C. T^* initially goes down slightly with $\dot{T}$ then it is seen to increase. This shows that either the kinetics or the extent of strain induced crystallisation is a function of temperature. Above the deflection point, the tear strength is primarily determined by the viscoelastic behaviour of rubber. The highly crosslinked NR which has a lower viscosity and which is stiffer in comparison with the former NR compound shows an obvious reduction in T^* with the loading rate over the range of the slower rate of loading. It is proposed that the increase in the loading rate results in a reduction in the amount of crystallisation, possibly due to the kinetics of the development of crystal being relatively slower than the rate of loading used in the tests. There is a deflection point in the curves above which T^* is significantly increased by increasing the tearing rate. It is again proposed that the crystallisation phenomenon above this transition is being suppressed and that the toughness of the material is primarily controlled by the viscoelastic nature of the rubber. For ENR-50, the results are broadly similar to those shown for NR with a rise in temperature resulting in a reduction of T^*. The expected increase in tear strength is due to the increased viscoelastic behaviour at the faster rate of loading again balanced by a reduction in crystallisation behaviour with

rate. The effect of temperature on the butadiene rubber shows that some crystallisation takes place the slow rate of loading at the crack tip at the lower temperature but, by 100°C, crystallisation is totally suppressed and the rubber is sufficiently far from the glass transition temperature that T^* is seen to be independent of loading rate.

From the work as mentioned above, it is found that the change of critical strain energy release rate at a given value of the time derivation of the strain energy release rate in rubber could be defined as the elastic-viscous transition phenomenon which is a function of the balance of elastic and viscosity of the material around the glass transition temperature. The extent of transition zone located around the glass transition temperature is primarily governed by the unsteady rate of tearing which is attributed to the molecular arrangement and the viscoelastic nature at the tip of the crack of rubber material.

7.2 Future work

In this thesis, it is found that a new approach which is based on the relation between the critical strain energy release rate and the time derivative of the strain energy release rate has been used successfully to examine a wide range of rubbers both non-strain crystallising rubber and strain crystallising rubber. Additionally, the universal diagram of the elastic-viscous transition in relation to the nature at a tip of the crack has been proposed. It can been seen from the experiments that the extent of crystal structure found in a strain crystallising rubber plays a significant role in controlling the tearing behaviour of rubber when subjected to various rates of loading at the crack tip. The formation of the crystal structure due to strain at the tip of the crack can also give rise to a characteristic fracture surface known as stick-slip behaviour in the rubber literature.

However, it is interesting to know how much of the crystallised structure has been developed at the crack tip to help reinforce the tear strength of the rubber. The suggested approach to quantify this phenomena would be the examination of the temperature change at the crack using an IR thermal imaging camera. This concept is developed based on the knowledge that when rubber crystallises on stretching a significant additional heat is generated due to the formation of crystalline regions in the vicinity of the crack tip. Preliminary results of the suggested experiment are shown in Figure 7.1. From the test results, it is clear that the temperature profile at the tip of the crack can be examined using an IR thermal imaging camera.

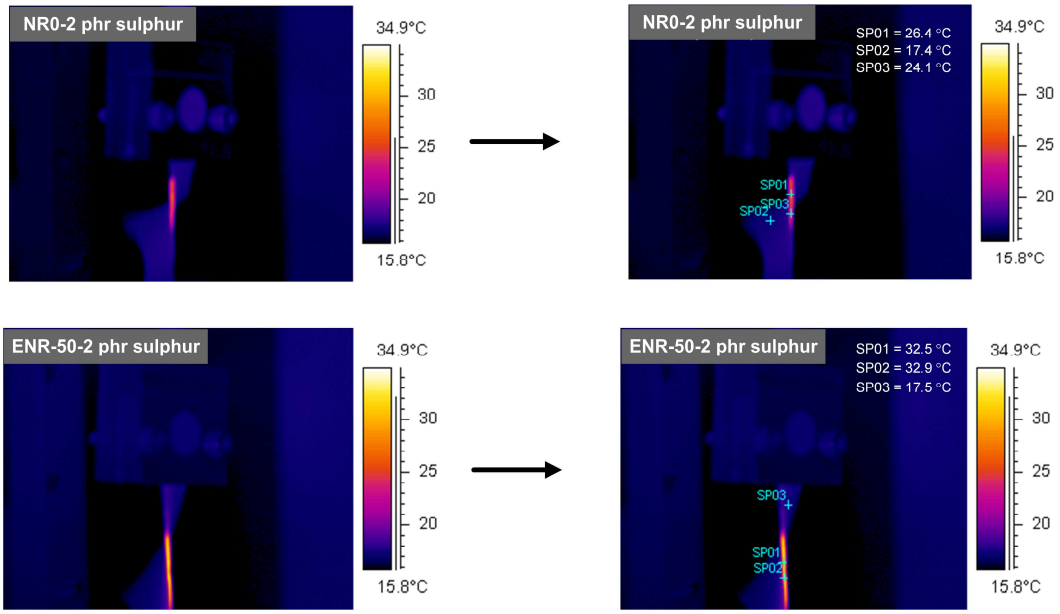

Figure 7.1: The temperature profile at a tip of the crack in a trouser tear specimen as monitored using an IR thermal imaging camera of unfilled natural rubber and an unfilled epoxidised natural rubber (ENR-50) which were loaded rapidly at the crack tip using a pneumatic test rig.

Another potential experiment to quantify the heat associated to the formation of the crystallised structure in rubber material is to use the simple test rig shown in Figure 7.2. The concept of this experiment is to measure the temperature drop as a rubber specimen is retracted and the strain induced crystals melt. To do this dumbbell rubber specimen are prestrained to various elongations which are then conditioned for different periods of time. The rubber specimen is allowed to recover to its original elongation with an instantaneous determination of temperature. The degree of the temperature change between the deformed and the undeformed gives the extent of the formation of the crystallised structure in the rubber compound.

In combination these experiments might help examine the kinetics of crystal formation to help determine the extent of crystallisation during rapid tearing. Having now developed, a framework to measure tear behaviour of any rubber at any rate, the approach could be used to examine the critical features associated with the tearing of say surgical rubber gloves during use or even tyre tread compounds under the types of loading rate encountered during abrasion.

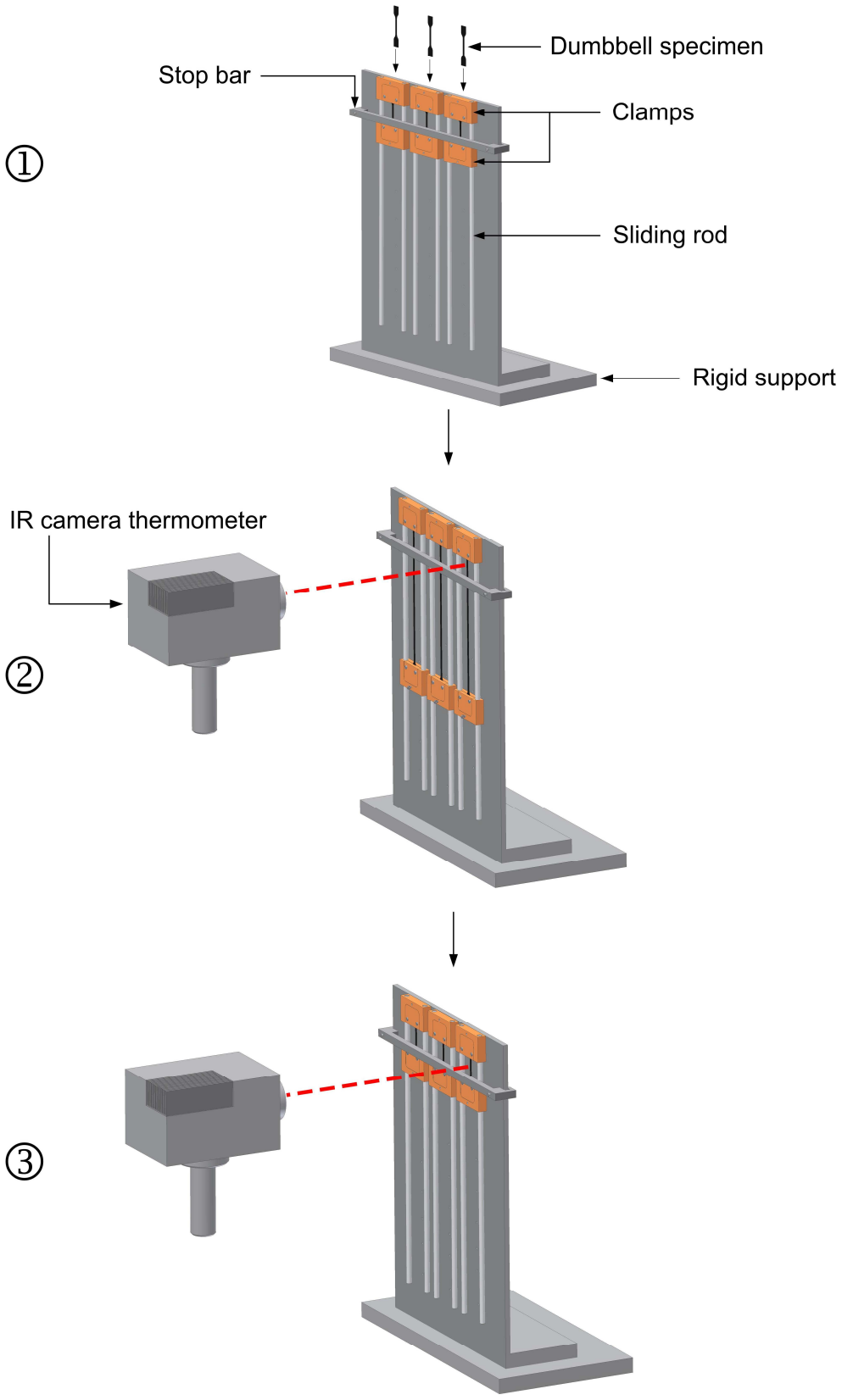

Figure 7.2: A suggested novel experiment for determining the effect of change in temperature in relation to the degree of formation of the crystallisation in rubber after conditioning at the strained state for a given duration at an ambient temperature.

References

Albertoni, G. J. (1937). Impact machine for rubber testing: determining the stress-strain diagram at high speed. *Ind. Eng. Chem. Anal. Ed.*, **9**(1), 30–34.

Andrews, E. H. (1961). Stresses at a crack in an elastomer. *Proc. Phys. Soc.*, **77**, 483-498.

Andrews, E. H. (1974). A generalized theory of fracture mechanics. *J. Mater. Sci.*, **9**(6), 887-894.

Andrews, E. H. and Fukahori, Y. (1977). Generalized fracture mechanics. *J. Mater. Sci.*, **12**(7), 1307-1319.

Andrews, E. H. (1979). Molecular structure and strength of polymers *In:* Andrews, E. H., ed. *Developments in polymer fracture-1.* Essex: Applied Science Publishers Ltd, 1-15.

ASTM (2006) Standard test methods for vulcanized rubber and thermoplastic elastomers—Tension (ASTM D 412-06a). West Conshohocken: ASTM International.

ASTM (2002) Standard test method for rubber property—Durometer hardness (ASTM D 2240-02). West Conshohocken: ASTM International.

ASTM (2006) Standard test method for rubber property—Vulcanization using rotorless cure meters (ASTM D 5289-06). West Conshohocken: ASTM International.

ASTM (2001) Standard practice for rubber-materials, equipment, and procedures for mixing standard compounds and preparing vulcanized sheets (ASTM D 3182-89). West Conshohocken: ASTM International.

ASTM (2002) Standard specification for natural rubber (NR) technical grades (ASTM D 2227-96 (2002)). West Conshohocken: ASTM International.

Aubrey, D. W. and Sherriff, M. J. (1980). Peel adhesion and viscoelasticity of rubber-resin blends. *J. Polym. Sci.: Polym. Chem. Ed.*, **18**, 2597-2608.

Baker, C. S. L. (1988). Modified Natural rubber. *In:* Bhowmick, A. K. and Stephens, H. L., eds. *Handbook of elastomers: New developments and technology.* New York: Marcel Dekker Inc, 61-107.

Barquins, M. and Roberts, A. D. (1986). Rubber friction variation with rate and temperature: Some new observations. *J. Phys. D: Appl. Phys.*, **19**, 547-563.

Barquins, M. and Ciccotti, M. (1997). On the kinetics of peeling of an adhesive tape under a constant imposed load. *Int. J. Adhes. Adhes.*, **17**, 65-68.

Baumberger, T., Caroli, C. and Ronsin, O. (2002). Self-healing slip pulses along a gel/glass interface. *Phys. Rev. Lett.*, **88**(7), 075509.

Brown, P. S., Porter, M. and Thomas, A. G. (1987). Dependence of strength properties on crosslink structure in vulcanized polyisoprenes. *Kautsch Gummi Kunsts.*, **40**, 17.

Brydson, J. A. (1988). *Rubbery materials and their compounds.* Norfolk: Elsevier science publishers Ltd.

BS (1996) Physical testing of rubber: Part A1. Determination of density (BS903: Part A1). London: British Standards Institution.

Burfield, D. R. and Gan, S. N. (1975). Nonoxidative crosslinking reactions in natural rubber. I. Determination of crosslinking groups. *J. Polym. Sci.*, **13**(12), 2725–2734.

Busfield, J. J. C., Tsunoda, K., Davies, C. K. L. and Thomas, A. G. (2002). Contributions of time dependent and cyclic crack growth to the crack growth behavior of non strain-crystallizing elastomers. *Rubber Chem. Technol.*, **75**(4), 643-656.

Busfield, J. J. C., Jha, V., Liang, H., Papadopoulos, I. C. and Thomas, A. G. (2005). Prediction of fatigue crack growth using finite element analysis techniques applied to three dimensional elastomeric components. *Plast. Rubber Comp.*, **34**, 349-356.

Campbell, D., Pethrick, R. A. and White, J. R. (2000). *Polymer characterization: Physical techniques.* Baco Raton: CRS Press.

Cottrell, A. H. (1964). Strong solids. *Proc. R. Soc. Lond. A*, **282**, 2-9.

Dannis, M. L. (1962). Stress-strain testing of rubbers at high rates of elongation. *J. Appl. Polym. Sci.*, **6**(21), 283–296.

Datta, S. (2001). Synthetic Elastomers. *In:* De, S. K. and White, J. M., eds. *Rubber technologist's handbook.* Shropshire: Rapra Technology Limited, 47-86.

Davies, C. K. L., Wolfe, S. V., Gelling, I. R. and Thomas, A. G. (1983). Strain crystallizing in random copolymers produced by epoxidation of *cis* 1,4-polyisoprene. *Polym*., **24**, 107-113.

Davies, C. K. L., Dilip, K. D. and Thomas, A. G. (1994). Characterization of the behaviour of rubber for engineering design purposes. 1. Stress-strain relations. *Rubber Chem. Technol.*, **67**(4), 716-728.

De, D. K. and Gent, A. N. (1996). Tear strength of carbon black filled compounds. *Rubber Chem. Technol.*, **69**(5), 834-850.

De, D. K. and Gent, A. N. (1998). Crack growth in twisted rubber disks. Part II: Experimental results. *Rubber Chem. Technol.*, **71**(1), 84-94.

Dick, J. S. (2003). General test methods. *In:* Dick, J. S., ed. *Basic rubber testing: Selecting methods for a rubber test program*. West Conshohocken: ASTM International.

Eck, L. (1938). Contribution to the history of latex. *Rubber Chem. Technol.*, **11**(3), 482-484.

Eck, L. (1938). The history of rubber. Franz Carl Achard's "Experiments on elastic resin". *Rubber Chem. Technol.*, **11**(4), 653-657.

Elgar, P. (1998). *Sensors for measurement and control.* Dorset: Addison Wesley Longman limited.

Flory, P. J. (1953). *Principles of polymer chemistry*. Ithaca: Cornell University Press.

Fukahori, Y. and Andrews, E. H. (1978). Fracture surface roughness in highly deformable polymers. *J. Mater. Sci.*, **13**(4), 777-785.

Fukahori, Y. and Yamazaki, H. (1994). Mechanism of rubber abrasion. Part I: Abrasion pattern formation in natural rubber vulcanizate. *Wear*, **171**(1-2), 195–202.

Fukahori, F., Liang, H. and Busfield, J. J. C. (2008). Criteria for crack initiation during rubber abrasion. *Wear*, **265**(3-4), 387–395.

Fukahori, Y., Gabriel, P. and Busfield, J. J. C. (2010). How does rubber truly slide between Schallamach waves and stick–slip motion?. *Wear*, **269**(11-12), 854–866.

Gabriel, P. (2010). *Investigation and modelling of rubber friction*. Ph.D. thesis, Queen Mary, University of London.

Gelling, I. R. (1985). Modification of natural rubber latex with peracetic acid. *Rubber Chem. Technol.*, **58**(1), 86-96.

Gent, A. N. (1954). Crystallization and the relaxation of stress in stretched natural rubber vulcanizates. *Trans. Faraday Soc.*, **50**, 521-533.

Gent, A. N. (1958). Crystallization in natural rubber. V. Chemically modified rubber. *J. Polym. Sci.*, **28**, 257–264.

Gent, A. N., Kawahara, S. and Zhao, J. (1998). Crystallization and strength of natural rubber and synthetic *cis*-1,4 polyisoprene. *Rubber Chem. Technol.*, **71**(4), 668-678.

Gent, A. N. (2001). Elasticity. *In:* Gent, A. N., ed. *Engineering with rubber: How to design rubber components*. Munich: Carl Hanser Verlag, 35-71.

Gent, A. N. and Zhang, L. Q. (2001). Strain-induced crystallization and strength of elastomers. I. *cis*-1,4-polybutadiene. *J. Polym. Sci.: Part B: Polym. Phys.*, **39**, 811-817.

Gent, A. N. (2005). Strength of elastomers. *In:* Mark, J. E., Erman, B. and Eirich, F. R. , eds. *Science and technology of rubber.* Burlington: Elsevier Academic Press, 455-495.

Greensmith, H. W. and Thomas, A. G. (1955). Rupture of rubber. III. Determination of tear properties. *J. Polym. Sci.*, **18**, 189-200.

Greensmith, H. W. (1956). Rupture of rubber. IV. Tear properties of vulcanizates containing carbon black. *J. Polym. Sci.*, **21**(98), 175–187.

Greensmith, H. W. (1960). Rupture of rubber. VII. Effect of rate of extension in tensile tests. *J. Appl. Polym. Sci.*, **3**(8), 175–182.

Greensmith, H. W. (1960). Rupture of rubber. VIII. Comparisons of tear and tensile rupture measurements. *J Appl. Polym. Sci.*, **3**, 183-194.

Greensmith, H. W. (1963). Rupture of rubber. X. The change in stored energy on making a small cut in a test piece held in simple extension. *J. Appl. Polym. Sci.*, **7**(3), 993-1002.

Griffith, A. A. (1921). The phenomena of rupture and flow in solids. *Phil. Trans. R. Soc. Lond. A*, **221**, 163-198.

Grosch, K. A. (1963). The Relation between the friction and visco-elastic properties of rubber. *Proc. R. Soc. A*, **274**(1356), 21-39.

Halladay, J. R. (2003). Elastomers as engineering materials. *In:* Vecchio, R. J. D., ed. *Fundamentals of rubber technology*. Akron: Technical consulting services, 27-59.

Hamed, G. R. (1983). Effect of crosslink density on the critical flaw size of a simple elastomer. *Rubber Chem. Technol.*, **56**(1), 244-251.

Hamed, G. R. (2001). Engineering with rubber: How to design rubber components. *In:* Gent, A. N., ed. *Materials and compounds.* 2 ed. Munich: Carl Hanser Verlag, 11-34.

Hamed, G. R. and Hiza, S. (2010). Trouser tearing of a model natural rubber tire belt vulcanizate. Part 1: Effect of rate of tearing. *Rubber Chem. Technol.*, **83**(2), 199-212.

Hauser, E. A. (1938). A contribution to the early history of India-rubber. François Fresneau (1703–1770). *Rubber Chem. Technol.*, **11**(1), 1-4.

Hoo Fatt, M. S. and Bekar, I. (2004). High-speed testing and material modeling of unfilled styrene butadiene vulcanizates at impact rates. *J. Mater. Sci.*, **39**(23), 6885-6899.

Hosler, D., Burkett, S. L. and Tarkanian, M. J. (1999). Prehistoric polymers: Rubber processing in ancient mesoamerica. *Sci.*, **284**, 1988-1991.

ISO (1995) Rubbers and latices—Nomenclature (ISO 1629). Geneva: International Organization for Standardization.

Joule, J. P. (1859). On some thermo-dynamic properties of solids. *Phil. Trans. R. Soc. Lond.*, **149**, 91-131.

Kadir, A. and Thomas, A. G. (1981). Tear behaviour of rubbers over a wide range of rates. *Rubber Chem. Technol.*, **54**(1), 15-23.

Kraus, G. (1963). Swelling of filler-reinforced vulcanizates. *J. Appl. Polym. Sci.*, **7**(3), 861–871.

Lake, G. J. and Thomas, A. G. (1967). The strength of highly elastic materials. *Proc. R. Soc. Lond. A*, **300**, 108-119.

Lake, G. J., Lindley, P. B. and Thomas, A. G. (1969). Fracture mechanics of rubber. *In*: Pratt, P. L., Ed. *The second international conference on fracture.* Brighton: Chapman and Hall.

Lake, G. J. (1995). Fatigue and fracture of elastomers. *Rubber Chem. Technol.*, **68**(3), 435-460.

Lake, G. J., Lawrence, C. C. and Thomas, A. G. (2000). High speed fracture of elastomers: Part I. *Rubber Chem. Technol.*, **73**(5), 801-817.

Lake, G. J. and Thomas, A. G. (2001). Strength *In:* Gent, A. N., ed. *Engineering with rubber: How to design rubber components*. Munich: Carl Hanser Verlag, 99-135.

Loadman, J. (2005). *Tears of the tree: The history of rubber—A modern marvel*. New York: Oxford University Press.

Long, J. C. (2001). The history of rubber—A survey of sources about the history of rubber. *Rubber Chem. Technol.*, **74**(3), 493.

Marckmann, G. and Verron, E. (2006). Comparison of hyperelastic models for rubber-like materials. *Rubber Chem. Technol.*, **79**(5), 835-858.

Mason, P. (1958). High-fracture in rubber. *J. Appl. Phys.*, **29**(8), 1146-1150.

Mathew, N. M. (2001). Natural rubber. *In:* De, S. K., White, J. R., eds. *Rubber technologist's handbook.* Exeter: Rapra Technology Limited, 11-45.

Mooney, M. (1940). A theory of large elastic deformation. *Journal of Applied physics*, **11**, 582-592.

Moore, D. F. (1972). *The friction and lubrication of elastomers.* Oxford: Pergamon.

Morawetz, H. (2000). History of rubber research. *Rubber Chem. Technol.*, **73**(3), 405-426.

Mullins, L. (1959). Determination of degree of crosslinking in natural rubber vulcanizates. Part III. *J. Appl. Polym. Sci.*, **2**(1), 1-7.

Nagdi, K. (1993). *Rubber as an engineering material: Guideline for users.* Munich: Carl Hanser Verlag.

Nakano, K. and Maegawa, S. (2009). Stick-slip in sliding systems with tangential contact compliance. *Tribol. Int.*, **42**(11-12), 1771–1780.

Nishiyama, N., Kakubo, S. K., T., Hwee, E. A. and Tanaka Y. (1996). Original of characteristic properties of natural rubber-synergistic effect of fatty acids on crystallization of *cis*-1,4-polyisoprene: II, mixed and esterified fatty acids in natural rubber. *Rubber Chem. Technol.*, **69**(4), 608-614.

Ownby, D. R. (2002). A history of latex allergy. *J. Allergy Clin. Immunol.*, **110**(2), S27-S32.

Painter, P. C. and Coleman, M. M., (2009). *Essentials of polymer science and engineering.* Lancaster: DEStech Publications, Inc.

Papadopoulos, I. C., Thomas and A. G. and Busfield, J. J. C. (2008). Rate transitions in the fatigue crack growth of elastomers. *J. Appl. Polym. Sci.*, **109**, 1900-1910.

Payne, A. R. (1967). *Use of rubber in engineering.* London: Maclaren and Sons.

Persson, B. N. J., Albohr, O., Heinrich, G. and Ueba, H. (2005). Crack propagation in rubber-like materials. *J. Phys.: Condens. Matter*, **17**, R1071–R1142.

Porter, M. (1967). Structural characterization of filled vulcanizates part 1. Determinations of the concentration of chemical crosslinks in natural rubber vulcanizates containing high abrasion furnace black. *Rubber Chem. Technol.*, **40**(3), 866-882.

Rivlin, R. S. (1948). Large elastic deformations of isotropic materials. I. Fundamental concepts. *Phil. Trans. R. Soc. Lond. A*, **240**, 459-490.

Rivlin, R. S. and Thomas, A. G. (1953). Rupture of rubber. I. Characteristic energy for tearing. *J. Polym. Sci.*, **X**(3), 291-318.

Rivlin, R. S. (1956). Large elastic deformations. *In:* Eirich, F. R., ed. *Rheology: Theory and applications.* New York: Academic Press.

Roland, C. M., Twigg, J. N., Vu, Y. and Mott, P. H. (2007). High strain rate mechanical behavior of polyurea. *Polym.*, **48**, 574-578.

Roth, F. L. and Holt, W. L. (1935). Tensile properties of rubber compounds at high rates of stretch. *J. Res. Natl. Bur. Stand.*, **23**(5), 603-616.

Rubenstein, M. and Colby, R. H. (2003). *Polymer Physics.* Wiltshire: Oxford University Press.

Sakulkaew, K., Thomas, A. G. and Busfield, J. J. C. (2010). The effect of the rate of strain on tearing in rubber. *Polym. testing* **30**, 163-172.

Sakulkaew, K., Thomas, A. G. and Busfield, J. J. C. (2012). The effect of temperature on the tearing of rubber. *Polym. Testing*, In press.

Schoenberg, E., Marsh, H. A., Walters, S. J. and Saltman, W. M. (1979). Polyisoprene. *Rubber Chem. Technol.*, **52**(3), 526-604.

Sekhar, B. C. (1960). Degradation and crosslinking of polyisoprene in Hevea Brasiliensis latex during processing and storage. *J. Polym. Sci.*, **48**(150), 133-137.

Sezna, J. A. and Vecchio, R. J. D. (2003). Testing of rubber. *In:* Vecchio, R. J. D., eds. *Fundamental of rubber technology.* Akron: Technical Consulting Services, 155-193.

Shaw, M. T. and Macknight, W. J. (2005). *Introduction to polymer viscoelasticity.* Hoboken: John Wiley and Sons, Inc.

Sommer, J. G. and Yeoh, O. H. (2001). Tests and specifications. *In:* Gent, A. N., ed. *Engineering with rubber: How to design rubber components* Munich: Carl Hanser Verlag, 307-355.

Sperling, L. H. (2006). *Introduction to physical polymer science.* Hoboken: John Wiley and Sons, Inc.

Stacer, R. G., Yanyo, L. C. and Kelly, F. N. (1985). Observations on the tearing of elatomers. *Rubber Chem. Technol.*, **58**(2), 421-435.

Stevenson, A. and Thomas, A. G. (1979). On the bursting of a balloon. *J. Phys. D: Appl. Phys.*, **12**, 2101-2109.

Subramaniam, A. (1987). Natural rubber. *In:* Morton, M., ed. *Rubber technology.* New York: Van Nostrand Reinhold Company, 179-208.

Thomas, A. G. (1955). Rupture of Rubber. II. The Strain concentration at an incision. *J. Polym. Sci.*, **XVIII**, 177-188.

Thomas, A. G. (1960). Rupture of rubber. VI. Further experiments on the tear criterion. *J. Appl. Polym. Sci.*, **3**, 168-174.

Thomas, A. G. and Whittle, J. M. (1970). Tensile rupture of rubber. *Rubber Chem. Technol.*, **43**(2), 222-228.

Thomas, A. G. (1994). The development of fracture mechanics for elastomers. *Rubber Chem. Technol.*, **67**(3), 50-67.

Tosaka, M., Murakami, S., Poompradub, S., Kohjiya, S., Ikeda, Y., Toki, S., Sics, I. and Hsiao, B.S. (2004). Orientation and crystallization of natural rubber network as revealed by WAXD using synchrotron radiation. *Macromolecules*, **37**(9), 3299-3309.

Trabelsi, S., Albouy, P. A. and Rault, J. (2002). Stress-induced crystallization around a crack tip in natural rubber. *Macromolecules*, **35**(27), 10054-10061.

Treloar, L. R. G. (1944). Stress-strain data for vulcanized rubber under various types of deformation. *Trans. Faraday Soc.*, **40**(2), 59-70.

Treloar, L. R. G. (1975). *The physics of rubber elasticity.* Norfolk: Oxford University Press.

Tsunoda, K., Busfield, J. J. C, Davies, C. K. L. and Thomas, A. G. (2000). Effect of materials variables on the tear behaviour of a non-crystallizing elastomer. *J. Mater. Sci.*, **35**(20), 5187-5198.

Valentin. J. L., Carretero-Gonzalez, J., Mora-Barrantes, I., Chasse, W. And Saalwachter, K. (2008). Uncertainties in the determination of cross-Link density by equilibrium swelling experiments in natural rubber. *Macromolecules*, **41**(3), 4717-4729.

Villars, D. S. (1950). Ultra speed tensile of rubber and synthetic elastomers. *J. Appl. Phys.*, **21**, 565-573.

Vincent, P. I. (1972). A correlation between critical tensile strength and polymer cross-sectional area. *Polym.*, **13**, 558-560.

Warring, R. H. and Gibilisco, S. (1985). *Fundamentals of transducers.* Blue Ridge Summit: Tab books Inc.

Wu-Bavouzeta, F., Clain-Burckbuchlera, J., Buguina, A., De Gennes, P. G. and Brochard-Wyarta, F. (2007). Stick-slip: Wet versus dry. *J. Adhes.*, **83**(8), 761-784

Yamaguchi, T., Ohmata, S. and Doi, M. (2009). Regular to chaotic transition of stick–slip motion in sliding friction of an adhesive gel-sheet. *J. Phys.: Condens. Matter* **21**(20), 1-7.

Yanyo, L. C. (1989). Effect of crosslink type on the fracture of natural rubber vulcanizates. *Inter. J. Fract.*, **39**, 103-111.

Yeoh, O. H. and Fleming, P. D. (1997). A new attempt to reconcile the statistical and phenomenological theories of rubber elasticity. *J. Polym. Sci. Part B: Polym. Phys.*, **35**, 1919-1931.

Young, R. J. and Lovell, P. A. (2011). *Introduction to polymers.* Boca Raton: CRC Press.

Appendix: Refereed journal and conference papers published by the author as part of this thesis

Polymer Testing 30 (2010) 163–172

Contents lists available at ScienceDirect

Polymer Testing

journal homepage: www.elsevier.com/locate/polytest

Test Method

The effect of the rate of strain on tearing in rubber

K. Sakulkaew, A.G. Thomas, J.J.C. Busfield*

Department of Materials, Queen Mary, University of London, Mile End Rd, London E1 4NS, UK

ARTICLE INFO

Article history:
Received 15 October 2010
Accepted 24 November 2010

Keywords:
Rubber
Elastomer
Polymer
Carbon black
Strain induced crystallisation
Tear
Strength
Strain energy release rate
Tearing energy

ABSTRACT

There have been many previous studies on the tearing of rubber materials. The behaviour is typically characterised using a fracture mechanics approach whereby the rubber has a geometrically independent relationship between crack growth rate during tearing versus strain energy release rate. This approach works well under conditions of steady tearing as the crack growth rate is easy to measure. However, this approach is much harder to interpret under conditions where the rubber exhibits discontinuous crack growth behaviour such as knotty tearing or stick slip tearing. Unfortunately, these are the most common tear conditions observed in practice for filled rubbers as well as for some unfilled rubbers, especially those such as natural rubber that are capable of strain induced crystallisation. Under these conditions it is not clear what the actual crack growth rate is as the value typically given results from the average of a very rapid tear rate and a zero velocity tear rate. The approach developed here for the first time is to characterise the rate of increase in the strain energy at the crack tip just immediately before the onset of tearing in a trouser tear test piece. This is measured directly as the time derivative of the strain energy release rate T. In this work the relation between this and the critical strain energy release rate T_{crit} to propagate the tear is examined. Having developed a new technique to characterise the tear behaviour, it is then evaluated using a range of different materials, including both natural rubber (NR) and styrene butadiene rubber (SBR). This allows the effect of the strain induced crystallisation observed in NR to be evaluated. The level of cross linking is varied to modify the kinetics of the strain induced crystal formation, and carbon black is incorporated into some of the NR and SBR compounds. The new technique is seen to provide a useful way of examining the different reinforcing mechanisms exhibited by all these different rubber materials.

1. Introduction

Tearing in rubber is known to initiate from an inherent flaw present in the rubber [1]. When the rubber is stretched, the local stress in the vicinity of a flaw is amplified. Once the local stress reaches a critical level, the rubber tears by extension of the crack (flaw). It has been widely reported that the rate of crack growth in a rubber is determined by a characteristic energy per unit area of the fracture surface created, often known as the tearing energy or the strain energy release rate [2–5]. This is defined as

$$T = -\frac{1}{h}\left(\frac{\partial W}{\partial c}\right)_l \quad (1)$$

where W is the total elastic strain energy stored in a specimen of thickness h measured in the unstrained state and c is the length of a crack. The suffix l denotes that no external work is done at the system boundaries to create new fracture surfaces. In the case of a trouser tear specimen shown in Fig. 1, the tearing energy is given by

* Corresponding author. Tel.: +44 20 7882 8866.
E-mail address: j.busfield@qmul.ac.uk (J.J.C. Busfield).

0142-9418/$ – see front matter © 2010 Elsevier Ltd. All rights reserved.
doi:10.1016/j.polymertesting.2010.11.014

ARTICLE IN PRESS POTE3943_proof ■ 22 September 2012 ■ 1/8

Polymer Testing xxx (2012) 1–8

Contents lists available at SciVerse ScienceDirect

Polymer Testing

journal homepage: www.elsevier.com/locate/polytest

Material properties

The effect of temperature on the tearing of rubber

K. Sakulkaew [a,b], A.G. Thomas [a], J.J.C. Busfield [a,*]

[a] Department of Materials, Queen Mary, University of London, Mile End Road, London E1 4NS, UK
[b] Department of Science Service, Rama VI Road, Bangkok 10400, Thailand

ARTICLE INFO

Article history:
Received 6 July 2012
Accepted 8 September 2012

Keywords:
Rubber
Elastomer
Tear
Fracture
Polymer
Rapid
Natural rubber
Epoxidized natural rubber
Polybutadiene

ABSTRACT

The tearing behaviour of rubber is typically characterised using an energy balance approach where the rubber has a geometrically independent relationship between the crack growth rate and the strain energy release rate. This approach works well during steady tearing, such as that encountered with an unfilled, non-strain crystallising rubber such as styrene butadiene rubber. The rate of tearing is both easy to measure experimentally and to then interpret. However, this approach is made more complicated under conditions where the rubber exhibits unsteady crack growth such as stick slip tearing or knotty tearing, which is often encountered with a strain crystallising rubber such as natural rubber or when reinforcing fillers are used. Under these conditions it is not easy to measure the crack growth rate as the value adopted is usually the average of a very rapid tearing rate and a zero velocity tearing rate. The approach adopted in this study characterises the rate of increase in the strain energy with time, $\dot{T}$, at the crack tip just before the onset of tearing. The relation between this and the critical strain energy release rate T^* for the crack propagation is examined over a wide range of tear rates and temperatures for several different rubber materials, including natural rubber (NR), epoxidized natural rubber with half of the isoprene units being epoxidized (ENR-50) and polybutadiene rubber (BR). It is apparent that the critical strain energy release rate, T^* is surprisingly independent of the rate of strain at the crack tip for the majority of materials and over a wide range of temperatures. Only when tearing has become very rapid do additional viscoelastic mechanisms result in significant toughening of the rubbers.

1. Introduction

Tearing behaviour of rubbers has been extensively investigated in terms of the relationship between the strain energy release rate, which is often referred to as the tearing energy, and the tearing rate [1–4]. The strain energy release rate of a material, T, is the change in the elastic strain energy per unit change in crack surface area. It is defined in the form:

$$T = -\frac{1}{h}\left(\frac{\partial W}{\partial c}\right)_l \quad (1)$$

where W is the total elastic strain energy stored in a specimen of thickness h measured in the unstrained state and c is the crack length. The suffix l denotes that the constrained boundaries of the body do not move and so no external work is done during the propagation of the crack. A value of T can be applied to the specimen containing an incision and the rate of crack growth can be measured experimentally. In the trouser tear test specimen, as shown in Fig. 1, the tearing behaviour of rubber can be primarily classified into two main types: steady or unsteady (sometimes known as stick-slip) [5]. During this test the boundaries move, therefore, the strain energy release rate per unit area of crack growth, T, must also now include an additional term to account for work done associated with the movement of the boundaries during tearing. The resulting expression for the strain energy release rate being given as

* Corresponding author. Tel.: +44 (0) 20 7882 8866.
E-mail address: j.busfield@qmul.ac.uk (J.J.C. Busfield).

0142-9418/$ – see front matter © 2012 Published by Elsevier Ltd.
http://dx.doi.org/10.1016/j.polymertesting.2012.09.002

"Elastic-Viscous Transition in Tear Fracture of Rubbers"

Y. Fukahori, K. Sakulkaew and J.J.C. Busfield

Department of Materials, Queen Mary, University of London
Mile End Road, London, E1 4NS, UK

ABSTRACT

There is a widely reported transition in the relationship between the critical strain energy release rate and a critical crack growth rate during the tearing of rubber materials. This transition is explained here for the first time in terms of an elastic-viscous transition phenomenon. The transition thus characterized depends on the balance of elasticity and viscosity of the material and hence the proximity of the test to the materials' glass transition temperature. Therefore two factors dominate the transition behaviour, the cross-link density and the visco-elastic energy dissipation. A new elastic-viscous transition diagram is introduced to elucidate the mechanism of this phenomenon, where the diagram consists of three zones, each with a different fracture mode. These are an elastic-brittle fracture zone, a viscous-ductile fracture zone and an intermediate transition zone between the elastic and viscous zones. The transition zone characterized by stick-slip motion is caused in mechanics as results from unstable fluctuations of crack growth rate due to the energy dissipation near the glass transition temperature. The mechanism for the transition to be generated at the crack front is investigated both theoretically and experimentally with a consideration of surface roughness formation and stick-slip tear motion together with frictional sliding of the rubber at the crack tip.

KEYWORDS

Elastic-viscous transition, Cross-linked rubber, Viso-elasticity,
Surface roughness formation, Stick-slip motion, Frictional sliding of rubber

(Submitted to POLYMER)

Tire Technology International 2011

Characterization of tearing

behavior of rubber under unsteady tearing conditions

Recent research has resulted in a radical new approach to characterize tear rate and critical strain energy release rate in the examination of non-steady tearing in rubber

by K. Sakulkaew, A. G. Thomas & J. J. C Busfield, Department of Materials, Queen Mary, University of London, UK

Rubber materials are highly deformable, resistant to wear, and have a high coefficient of friction – all of which make rubber the material of choice for tires. However, all materials, including rubber, contain intrinsic flaws. When the rubber is deformed, the local stress in the vicinity of these flaws is raised. The rubber tears if the local stress reaches a critical level. This creates new fracture surfaces within the rubber. It has been well established[1,2,3] that the tearing behavior of rubber can be conveniently described in terms of the relation between the tearing energy or the strain energy release rate T and the rate of tearing r. This relationship is a material characteristic that is independent of the test piece geometry.[2,4,7] The tearing energy is thus defined as the energy required to create the new fracture surface, T:

$$T = -\frac{1}{h}\left(\frac{\partial W}{\partial c}\right)_l$$

where W is the elastically stored energy in the test piece of thickness h, and c is the length of the crack. The suffix l denotes that no external work is done at the system boundaries to create new fracture surfaces. For a trouser tear specimen, shown in Figure 1, the boundaries move and so that the tearing energy is calculated as:

$$T = \frac{2F\ddot{e}}{h} - bW$$

where F is the applied force, h is the specimen thickness, λ is the extension ratio in the legs, b is the total width of the specimen, and W is the elastic stored energy in the legs of the specimen. In the tearing process, a tearing force F applied to the legs produces tearing at the crack tip. The region of each of the legs is essentially in uniaxial extension with a corresponding extension ratio λ. The crack length increases by dc, resulting in an increase in volume in the region of uniaxial in the legs by $2a \bullet h \bullet dc$. The separation l of the clamps of the test machine is increased by $dl = 2\ddot{e}dc$.

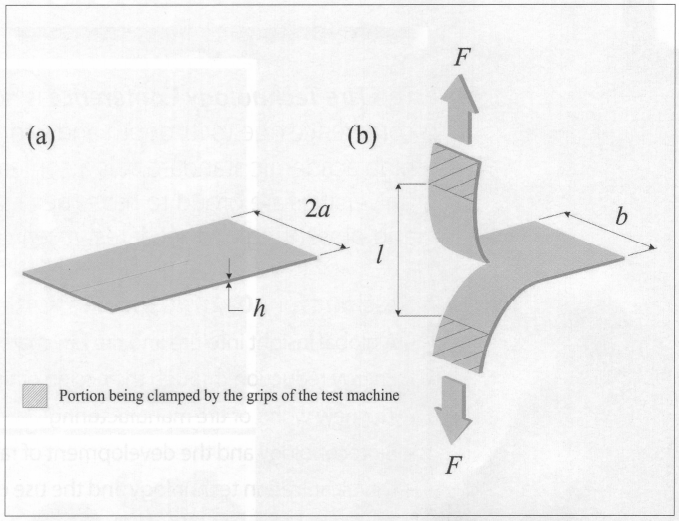

Figure 1: Trouser tear specimen: (a) undeformed; (b) deformed. F represents externally applied force to the legs

If the tearing is smooth and continuous, the average crack growth rate can be determined from the rate of separation of the clamps S by the relation

$$S = \frac{dl}{dt} = \frac{2\ddot{e}dc}{dt}$$

where l is the separation of the clamps, t is the time, and c is the crack length.

This framework can be easily applied to the steady tearing, as shown in Figure 2 (a) and (b) when the tearing rate hardly changes and the relationship between the tearing energy and the crack growth rate can be evaluated to characterize the behavior. However, for many rubber materials the tearing exhibits stick-slip behavior, as shown in Figure 2 (c), or knotty behavior, as shown in Figure 2 (d). Under these conditions the tearing is unsteady and the characteristic rate of crack growth is much harder to measure as it fluctuates between a very rapid rate and a zero rate of crack growth.

Determination of the average crack growth rate based on the crosshead speed is no longer very meaningful. A much more useful quantity to know would be the rate of increase in strain at the crack tip prior to tearing, which can then be related to the critical strain energy release rate for the material. The strain energy release rate T is approximately the product of the size of the unstrained tip diameter of the tear d and the strain energy E integrated around the crack tip at break.[6]

Constitutive Models for Rubber VII – Jerrams & Murphy (eds)
© 2012 Taylor & Francis Group, London, ISBN 978-0-415-68389-0

A new approach to characterize the onset tearing in rubber

K. Sakulkaew, A.G. Thomas & J.J.C Busfield
Department of Materials, Queen Mary, University of London, London, UK

ABSTRACT: Since Rivlin and Thomas (1953) the tearing behaviour of rubber has been characterized using fracture mechanics, whereby the rubber has a geometrically independent relationship between the crack growth rate during tearing versus strain energy release rate. This approach works well under conditions of steady tearing when the crack growth rate is easy to measure. However, this approach is much harder to interpret under conditions where the rubber exhibits discontinuous crack growth behaviour such as knotty tearing or stick slip tearing. This type of tearing often arises for filled rubbers and for rubbers that strain crystallize. The measured crack growth rate is now an average of a very rapid tear rate and a zero velocity tear rate. Sakulkaew et al. (2010) developed a new approach that characterizes the rate of increase in the strain energy at the crack tip just immediately before the onset of tearing in a trouser tear test piece. This is measured directly as the time derivative of the strain energy release rate $\dot{T}$. In this work the critical strain energy release rate T_{crit} to propagate the tear relationship with $\dot{T}$ is examined for a range of natural rubber compounds. The aim being to demonstrate the geometric independence of this relationship to verify that the behaviour measured using a trouser tear test piece produces a similar relationship to that measured using a pure shear tear test piece.

1 INTRODUCTION

Tearing in rubber is known to initiate from an inherent flaw present in the rubber (Gent 2005). When the rubber is stretched, the local stress in the vicinity of a flaw is intensified. Once the local stress reaches a critical level, the rubber tears by extension of the crack. It has been widely reported that the rate of crack growth in rubber is determined by a characteristic energy per unit area of the fracture surface created, often known as the tearing energy or the strain energy release rate (Thomas 1994). This is defined as

$$T = -\frac{1}{h}\left(\frac{\partial W}{\partial c}\right)_l \tag{1}$$

where W is the total elastic strain energy in a specimen of thickness h measured in the unstrained state and c is the length of a crack. The suffix l denotes that no external work is done at the system boundaries to create new crack surfaces. In the case of a trouser tear test piece in Figure 1, the tearing energy is given by

$$T = \frac{2F\lambda}{h} - bW \tag{2}$$

where F is the applied tearing force, h is the specimen thickness, λ is the extension ratio in the legs, b is the total width of the specimen and W is the elastic stored energy in the legs of the specimen far removed from tear. W is determined from integration of a tensile stress-strain curve at a strain that corresponds to the extension ratio in the legs of the specimen at the point

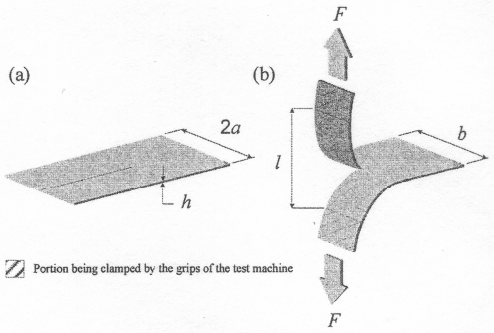

Figure 1. Trouser tear specimen: (a) undeformed; (b) deformed. F denotes the externally applied force to the leg of the specimen.

tearing. The relationship between the rate of tearing and the strain energy release rate is a material characteristic that is independent of test piece geometry (Greensmith and Thomas 1955). In the trouser tear specimen, a tearing force applied to the legs produces tearing at the crack tip. The region of each of the legs is essentially in uniaxial extension with the corresponding extension ratio, λ. The crack length increases by dc which results in an increase in the volume in the region of uniaxial extension in the legs (by $2a \cdot h \cdot dc$). The separation l of the clamps is increased by

$$dl = 2\lambda dc \tag{3}$$